TUM School of Engineering and Design
Department of Civil and Environmental Engineering
Technical University of Munich

Development of a Software Solution for the Use of Slicers for Polymer Materials for Additive Manufacturing with Concretes

David Scheidt

Thesis for the attainment of the academic degree

Master of Science (M.Sc.)

at the Department of Civil and Environmental Engineering of the Technical University of Munich.

Examiner:
Prof. Dr. Oliver Fischer

Supervisor:
M.Sc. Daniel Auer

Submitted:
Munich, 12.06.2025

I hereby declare that this thesis is entirely the result of my own work except where otherwise indicated.
I have only used the resources given in the list of references.

Munich, 12.06.2025 David Scheidt

Danksagung

Ich möchte mich an dieser Stelle ganz herzlich bei Herrn Prof. Dr. Oliver Fischer und meinem Betreuer Daniel Auer für die Chance bedanken mich mit einem meiner Hobbies auch auf wissenschaftlicher Ebene auseinandersetzen zu dürfen. Trotz der Vorerfahrung in Bezug auf 3D-Druck waren Teile dieser Arbeit nicht immer einfach und wären ohne die vielseitige Hilfesbereitschaft, das Vertrauen in meine Arbeit, aber auch die Geduld an mancher Stelle nicht möglich gewesen.
Generell möchte ich mich hier bei meiner gesamten Freundesgruppe bedanken die mich auf diesem Weg begleitet hat und die ich neben unseren gemeinsamen Mittagessen in der Mensa in Zukunft sicher sehr vermissen werde.
Ganz besonderer Dank gilt allerdings einigen Freunden, die ich im Laufe meines Studiums kennengelernen durfte und ohne deren Hilfe ich an mancher Stelle sicher einen anderen Weg eingeschlagen hätte. Dir Leo für die gemeinsamen Abende im Zeichensaal vor den Mathe-Tutorien und deine Unterstützung während meines gesamten Studiums auf die ich mich immer verlassen konnte. Markus für deinen ansteckenden Enthusiasmus, der mich neben deinen Witzen in der Vorlesung durch den kompletten Master getragen hat. Euch Hanna, Sarah und Sofie für die tollen Urlaube und Freizeitaktivitäten die mich immer wieder auf andere Gedanken und neue Ideen gebracht haben.
Abschließend möchte ich mich natürlich auch bei meinen Eltern bedanken, deren Rückhalt auf vielen Ebenen mir dieses Studium erst ermöglicht hat und die mich bei jeder meiner Entscheidungen mit Rat und Zuspruch ermutigt haben weiterzugehen.

Abstract

This thesis investigates the potential of improving the digital planning and fabrication process in robot-assisted concrete-3D-printing at the Technical University of Munich through the automated conversion of slicer outputs into robot-readable KUKA Robot Language (KRL) code. Following an introduction to the fundamentals of additive construction with concrete, the current state of the art is presented, including both the hardware in use and existing software solutions for path generation, control, and visualization.

To address the research question, the developed Python-based program is then introduced. It automatically imports and interprets G-code data from a slicer and translates it into KRL commands for the available robot. At the same time, the system generates a structured 3D-file in Rhinoceros3D that includes layer assignments, line codes, and positional data. This enables transparent control and preparation of the printing process. Parameters such as printing speed, extrusion commands, tool positions, and control signals (e.g., pump control) are processed and consistently transferred into the target language.

The developed program is subsequently tested using a representative application case and evaluated with regard to its functionality, flexibility, and expandability. The results demonstrate that the automated pipeline significantly simplifies the workflow, reduces manual effort, and identifies potential sources of error at an early stage. The thesis concludes with a critical reflection on the system's limitations and an outlook on possible extensions, including the integration of multiple slicers and the digital mapping of the entire process.

Contents

List of Tables

List of Figures

Listings

Abbreviations

A	Activator
A*i*	Rotational Axes (*i*) of Robot
ACDC	Admixture Controlled Digital Casting
AG	Aggregat
AM	Additive Manufacturing
B	Binder
CAD	Computer-Aided Design
CDPR	Cable-Driven Parallel Robot
CLI	Command Line Interface
Cura	Ultimaker Cura (Version 5.8.0)
DOF	Degrees of Freedom
DSC	Digital Casting System
FDM	Fused Deposition Modeling
G-code	Geometric Code
GUI	Graphical User Interface
KRL	KUKA Robot Language
Orca	OrcaSlicer (Version 2.2.0)
OPW	Ortho-Parallel-Wrist
P_{AUX}	Auxiliary Point
Prusa	Prusa Slicer (Version 2.9.2)
Rhino	Rhinoceros 3D (CAD software)
rpm	Revolutions per Minute
SC3DP	Shotcrete 3D-Printing
SDC	Smart Dynamic Casting
SLA	Stereolithography
SLS	Selective Laser Sintering
TCP	Tool Center Point
TUM	Technical University of Munich

1 Introduction

The German Economic Institute identified an annual demand of nearly 373 000 housing units in Germany by the end of 2024. However, since 2021, only around 295 000 units have been completed per year. In Cologne, for instance, newly constructed housing covers only about 40 % of the demand. Especially in major cities such as Berlin, Munich, or Stuttgart, the supply of newly created living space falls significantly short of expectations needed to meet existing demand. [107]
One structural factor contributing to this imbalance is the persistently low productivity growth within the construction industry. According to the German Construction Industry Federation [32], productivity in the German construction sector has exceeded its 1991 reunification benchmark only once (in 1992) and, as of mid-2024, remains approximately 23 % below that level.
While long-term productivity data for Germany as a whole remains limited, international analyses indicate that this is not a nationally isolated phenomenon. According to a study by the consulting firm McKinsey, the U.S. construction sector has recorded an average annual productivity increase of just 0.1 % since 1947, placing it at the bottom of all industrial sectors in terms of long-term productivity growth (see Figure 1.1) [50].

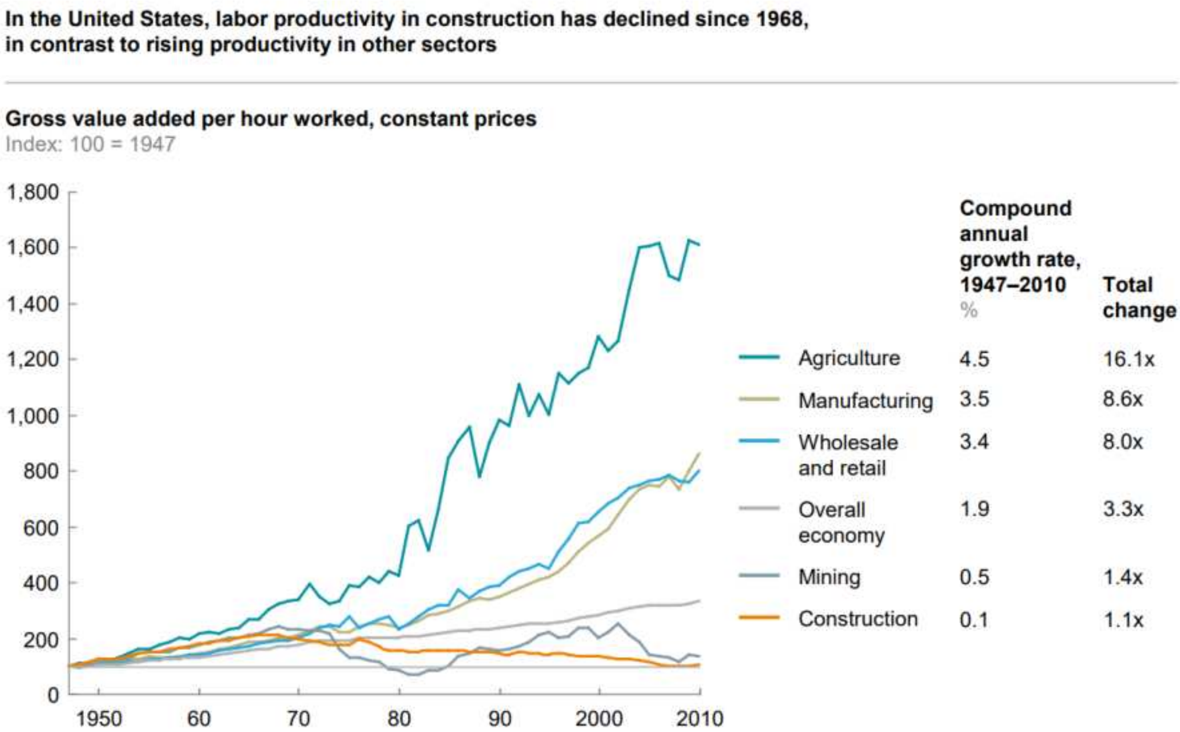

Figure 1.1 Comparison of Productivity Rate for Different Sectors in the US Since 1947

This stagnation not only affects the housing market, as previously discussed, but also contributes to the growing backlog of renovation and maintenance in Germany's infrastructure projects, such as the refurbishment of bridges [17, 37] or the expansion and upkeep of the railway network [22]. In both cases, the average condition of the total stock of infrastructure is now rated only as *"satisfactory"*. Continued operation in these sectors will thus require substantial additional investments and labor for maintenance and renewal in the coming years [13], which must be provided by the construction industry. How, then, can the supply gap in construction services be reduced, or even closed in the future?

When comparing the share of automated labor in the construction sector to other industries, it quickly becomes apparent that manual work still dominates in construction. A 2021 survey conducted by the robotics manufacturer ABB revealed that only about 55 % of the roughly 1900 construction companies surveyed in China, the USA, and Europe integrate robots into their process chains. In contrast, the automotive sector utilizes robotic systems in the value chain in 84 % of the surveyed companies, revealing a gap of approximately 30 %. [3]
Closing this gap could not only help the construction industry overcome the prevailing shortage of skilled labor [3], but also increase productivity rates. However, how can automation technology be effectively integrated into the complex environment of the construction industry, where most projects are unique in both planning and execution?
A promising approach lies in the combination of *additive manufacturing* (AM), also known as *3D-printing*, and concrete construction. In this context, users or companies can incorporate their individual ideas and solutions into an automated manufacturing process. The robot responsible for producing the project can be reprogrammed depending on the requirements, but it is designed to perform the same task, such as the production of waffle slabs or entire building stories in an automated manner (see Figure 1.2).

Figure 1.2 Automated Concrete Wall Construction Using Large-Scale 3D Printing On-Site [18]

By combining various hardware systems and integrating them within a homogeneous software solution, housing units [89] or bridge components [12] could be constructed quickly and efficiently, as demonstrated by the examples mentioned. While 3D-printing has long been part of the repertoire in industries such as aerospace and mechanical engineering, the technology has not yet fully arrived in the construction sector. According to [86], the current market capitalization for 3D-printing within the construction industry is estimated at around 1.9 billion US$ compared to a total additive manufacturing market capitalization of approximately 20 billion US$. However, it should be noted that figures for the construction industry vary significantly depending on the source [74, 101]. Nevertheless, all forecasts clearly indicate that the market is expected to grow strongly, with projected annual growth rates of up to 54 % [86]. As this projection shows, the industry places well-founded hopes in this technological branch.
Therefor also research institutes and universities like the Technical University of Munich (TUM) take part in this development. Through its involvement in the Collaborative Research *Additive Manufacturing in Construction* (AMC TRR 277) of the German Research Foundation [19], TUM is part of a network of institutes aiming to drive innovation in this subfield.

As part of this thesis, an integrative software platform is developed that systematically consolidates the majority of required process steps from the digital 3D model to automated concrete printing. The objective is to represent the workflow in a transparent, comprehensible, and largely automated manner for the user. The tasks range from importing and positioning the geometry, to generating printing paths, and finally to outputting machine-readable control data for a 6-axis industrial robot.
The thesis starts with a brief introduction to the historical, technological, and regulatory foundations of 3D-concrete- printing. Building on this, the current state of the art is presented, followed by a delimitation to relevant system components available at TUM.
Subsequently, the complete process from geometric modeling to slicing and machine execution is analyzed in detail. Existing slicer programs are compared and their functionalities examined more closely. Particular attention is given to adapting an existing open-source slicer originally designed for polymer-based 3D-printing to suit the requirements of concrete printing. The slicer will then be implemented into a whole new program such that it can automatically generate printing paths, interpret process parameters, and produce complete robot programs based on parameterized user input.
In addition, the generated motion data are visually structured in a Rhino file, enabling intuitive digital pre-checks and validation of all boundary conditions. This not only establishes a complete digital process chain, but also contributes to improved accessibility, reproducibility, and automation in robot-assisted construction at TUM.
Finally, a critical reflection on the capabilities and limitations of the developed software is conducted. Potential extensions, such as runtime optimization, user-friendliness, or technological enhancements are discussed, and approaches for future developments are outlined.

2 State of the Art

2.1 Historical Development of Additive Manufacturing Techniques

The origins of additive manufacturing can be traced back to the early 1940s. In 1941, the American entrepreneur and inventor William E. Urschel from Valparaiso, Indiana, filed a patent for his so-called “Urschel Wall Building Machine.” This device was capable of depositing concrete using mechanical guides as “[. . .] solidifiable material into the form of a strip [. . .]” and then using it “as a course or layer in the formation of a wall” [106]. One of the three prototypes built is still on display in Valparaiso, Indiana, USA [105].
After these early developments in concrete, the focus of technological advancements shifted for more than three decades toward polymer-based methods. A significant milestone was reached in 1971, when Wyn Kelly Swainson filed a patent for the curing of thermosetting materials using “radiation beams” [109]. In 1980, Hideo Kodama followed with another patent that laid the groundwork for what is known today as *Stereolithography* (SLA) [33]. Figure 2.1a schematically illustrates how a UV light source is used in SLA technology to harden UV-sensitive resin layer by layer at the intended locations. This process was significantly refined in the following years by Charles Hull, who filed a patent in 1984 for an “apparatus for production of three-dimensional objects by stereolithography,” which was granted in 1986. Just one year later, Hull launched the first commercial 3D printer, the “SLA-1,” through his newly founded company “3D Systems” [2] [10].
In the same year, Carl R. Deckard filed a patent for a powder bed fusion process, which became the foundation for what is now known as *Selective Laser Sintering* (SLS). In this method, layers of plastic or metal powder are applied and selectively fused by a laser (see Figure 2.1b). With the invention of *Fused Deposition Modeling* (FDM) by the couple Scott and Lisa Crump in 1989, the third of today’s three main 3D printing processes was patented [85]. Unlike previous technologies, the object is not formed within a material reservoir; instead, the geometry is extruded layer by layer from a nozzle (see Figure 2.1c). The company Stratasys [87], that emerged from this idea remains, like 3D Systems [2], is still a major player in the industry to this day [94, 54].

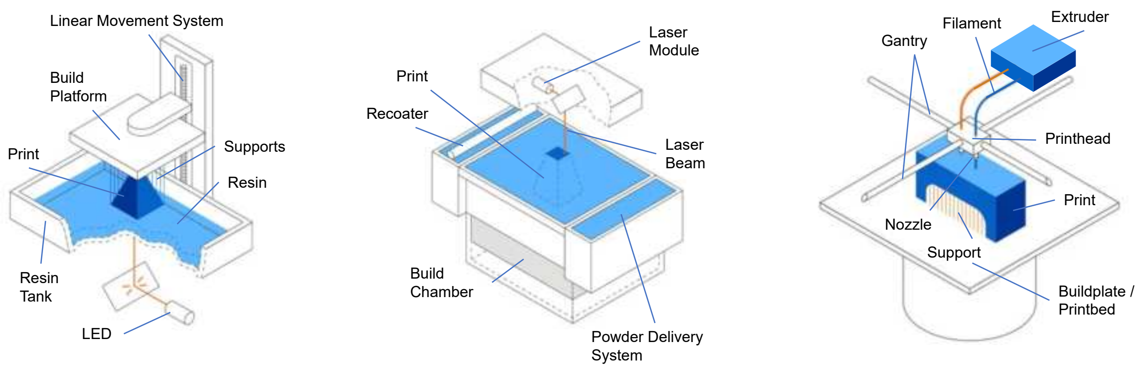

(a) SLA **(b)** SLS **(c)** FDM

Figure 2.1 The Three Basic Methods of 3D Printing Adapted from [30]

With the expiration of the patent held by Scott and Lisa Crump in 2009, the previously tightly regulated technology of FDM became accessible to a broader public. For the first time, numerous companies, research institutions, and private developers were able to design their own FDM-based printing systems and bring them to market without licensing fees or patent-related restrictions. This development played a significant role in making additive manufacturing accessible to a wide user base and in substantially expanding its use beyond industrial applications.
The construction industry, whose productivity growth has been considered below average compared to other sectors since the 1950s as mentioned in the Introduction, also began to recognize the potential of additive manufacturing. 3D-printing not only promises to automate labor-intensive construction processes but also offers new design freedom and the possibility of significantly reducing material usage and construction time.

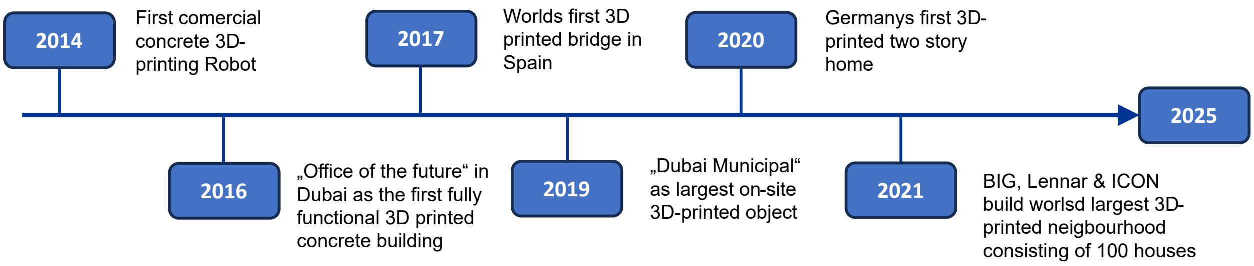

Figure 2.2 Timeline of Significant 3D-Printing Related Projects in Construction Summarized from [54]

From the mid-2010s onward, a continuous increase in 3D-printing-related projects in the construction sector can be observed. Figure 2.2 presents a selection of relevant developments from 2014 onward in chronological order. These include both individual projects and systematic research initiatives. Research groups such as the Collaborative Research Centre *Additive Manufacturing in Construction* (AMC TRR 277), which acts as a joint initiative between the Technical University Braunschweig and the Technical University of Munich funded by the German Research Foundation [19], as well as research teams at ETH Zurich [28] and the *3DCP*-consortium at TU Eindhoven [26] have been driving innovation in this field continuously ever since. The goal is to further develop additive manufacturing methods for use in the construction sector and to make their application economically and sustainably attractive compared to conventional fabrication techniques.

2.2 Normative Classification of Printing Processes

With the increasing use of additive manufacturing processes in the construction industry, the need for a normative framework for the associated terminology and process descriptions also grew. Since 2015, the DIN EN ISO 52900 standard [60] has served as the basis for defining printing-related terminology. In addition, the standard classifies the currently available additive manufacturing processes.
Fundamentally, the standard distinguishes between “single-stage” and “multi-stage” manufacturing processes (see Figure 2.3). Single-stage processes are characterized by the fact that components are produced in a “[...] single operation” both in their “[...] fundamental geometric form” and with their “[...] fundamental material properties.” Actions such as removing formwork or cleaning the surface are considered part of the single-stage process.
In contrast, multi-stage manufacturing processes involve components being produced in “[...] two or more operations.” In this case, the geometric form is first created, and the material properties are subsequently stabilized, for example, through oven sintering or bonding [60].

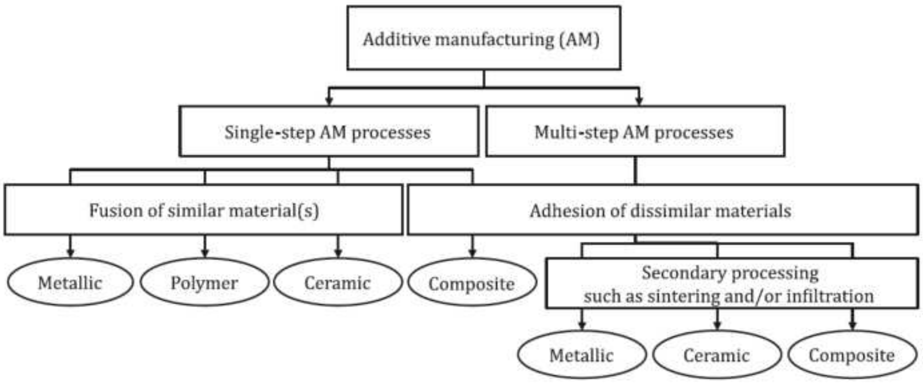

Figure 2.3 Process Principals of Additive Manufacturing According to DIN EN ISO 52900 [60]

2.3 Overview of Additive Manufacturing Methods for Concrete

Since this thesis focuses exclusively on the 3D-printing of concrete, this chapter provides an overview of the current state of the art in this specific field. Other materials addressed by DIN EN ISO52900 are not part of this thesis. Figure2.4 presents an overview of the methods that will be explained in more detail below.
All methods listed therein can be classified as single-stage printing processes according to DIN EN ISO52900 (see Section2.2).

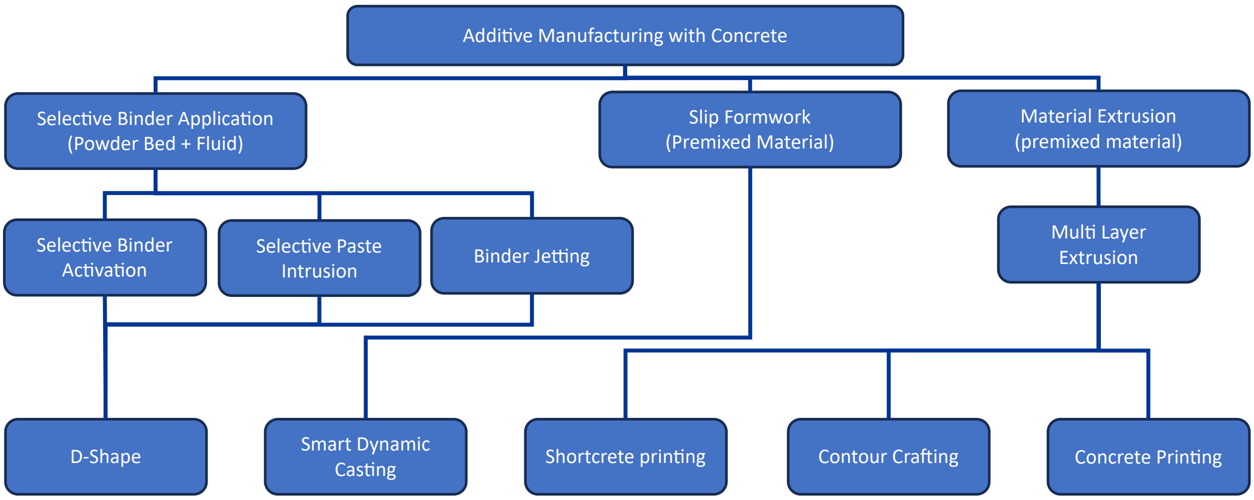

Figure 2.4 Overview on State of the Art Concrete-3D-Printing Methods Adapted from [100] and Adjusted

2.3.1 Selective Binder Application

The fundamental principle behind the method of *Selective Binder Application* is the layer-by-layer bonding of a particle bed through the targeted combination of different materials. In the context of 3D-concrete-printing, the following three components are typically used:

a) an aggregate [AG] (e.g., gravel or sand),

b) a binder [B] (e.g., cement), and

c) an activator [A] (e.g., water).

The manufacturing process is based on the repeated execution of two process steps. Similar to the SLS method presented in Section 2.1, the component is built up layer by layer within a particle bed:

1. application of a uniform layer of unbound particles using a distribution device,
2. selective deposition of a liquid binder via a nozzle onto the regions intended for solidification.

Once the printing process is complete, the printed object can be exposed by removing the unbound particles from the bed [45]. Figure 2.5 shows a schematic representation of the individual process steps.

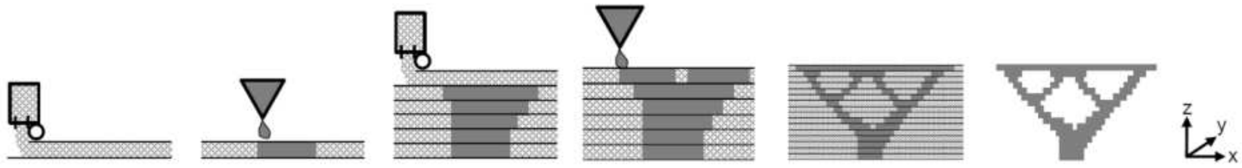

Figure 2.5 Process for Selective Binder Application Taken from [51]

The manufacturing process using *Selective Binder Application* can be further divided into three sub-variants:

Selective Binder Activation

In the method of *Selective Binder Activation*, the printing process is based on a pre-mixed particle bed composed of a fine-grained aggregate (typically with particle diameters < 1 mm, e.g. sand) and a hydraulic binder (e.g. cement). These two components (aggregate [AG] and binder [B]) are homogeneously mixed before the actual printing process and applied as a loose layer at the beginning of each layer.
Targeted activation is then carried out by a local or area-wise application of a liquid, which typically consists of water or a reactive activator solution. This liquid is deposited onto the regions of the particle bed intended for solidification using a nozzle or spray system. The local addition of the activator causes a chemical reaction between the binder and the activator in the treated areas. In the case of cement and water, hydration leads to the formation of a solid structure that binds the particles together in the affected zone. By repeating these steps, the desired geometry is created within the build volume.
Unwetted areas remain unbound and can be removed after the printing process, provided they are not completely enclosed by hardened material. This allows the finished component to be exposed afterwards. The geometric resolution of the process depends primarily on the particle size of the bed and the precision of the activator application [45].

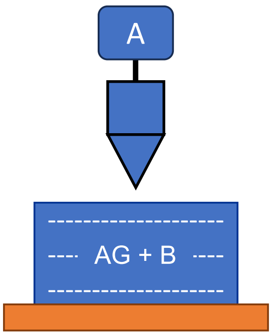

Figure 2.6 Schematic of Selective Binder Activation Adapted from [45]

Selective Paste Intrusion

In contrast to *Selective Binder Activation*, the method of *Selective Paste Intrusion* does not involve mixing the binder into the particle bed in advance. Instead, the binder is combined with the activator, typically as cement paste, and applied directly and selectively through a nozzle. The particle bed usually consists of coarser material such as gravel or coarse sand, with particle sizes of up to 5 mm [45].
The cement paste is specifically applied to the regions designated for solidification and penetrates the pore spaces of the particle bed. Its purpose is to fill the voids between the individual grains completely, thereby creating continuous bonding within the structure. In comparison to *Selective Binder Activation*, this method allows for greater layer thicknesses. This increases the printing speed and makes the method particularly attractive for large-scale applications in the construction sector.
One of the most critical aspects of this process is ensuring that the paste fully infiltrates the particle bed. Only with complete penetration can a homogeneous internal structure and consistent material properties throughout the component be achieved [104].

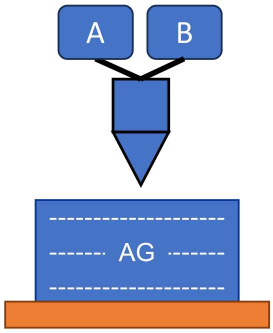

Figure 2.7 Schematic of Selective Paste Intrusion Adapted from [45]

Binder Jetting

Binder Jetting is considered the highest-resolution process currently available within the category of selective binding in powder beds. Unlike the previously described methods, it typically employs a resin–hardener-based binder system [45]. Due to the materials used, this process is not directly associated with concrete-3D-printing. However, it is included here for the sake of completeness.
As with *Selective Binder Activation*, the powder bed in binder jetting consists of a pre-mixed combination of materials. In contrast to that method, the powder bed does not contain the binder itself but rather the activator. The actual binder is applied selectively through a nozzle. The chemical reaction takes place locally at the defined contact points within the powder bed, resulting in the selective bonding of particles, similar to the other previously discussed methods.

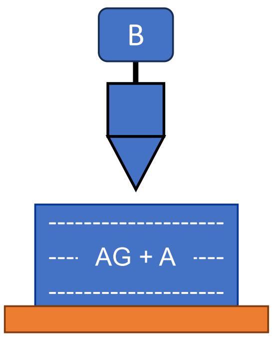

Figure 2.8 Schematic of Binder Jetting Adapted from [45]

Due to the high level of detail achievable, this technology is primarily used in the field of formwork construction, especially for foundry applications. Depending on the geometry of the component, it can offer economic advantages over conventional methods, such as *computerized numerical control milling* (CNC), in terms of both production time and manufacturing costs [104]. For large-scale applications, as commonly found in the construction industry, the technology has so far been used only selectively. This is mainly due to the limited build volume, which currently reaches a maximum of approximately 4 × 2 × 1 meters [81] [79].

D-Shape

An example of integrating the previously described methods into a large-scale application is the so called *D-Shape* process, developed by Enrico Dini in 2008. This system combines the principles of selective binder application with a large build volume of approximately 5 × 5 meters. This setup enables the processing of large-volume objects with layer thicknesses of up to 5 mm [1] and a maximum particle size of up to 20 mm [104].

The printing system is based on a gantry-like frame mounted on four vertically aligned supports. Within this frame, the devices for granulate deposition and selective binder application move parallel to the build surface (see Figure 2.9). This configuration enables the layer-wise fabrication of large-format structures with comparatively high geometric resolution.

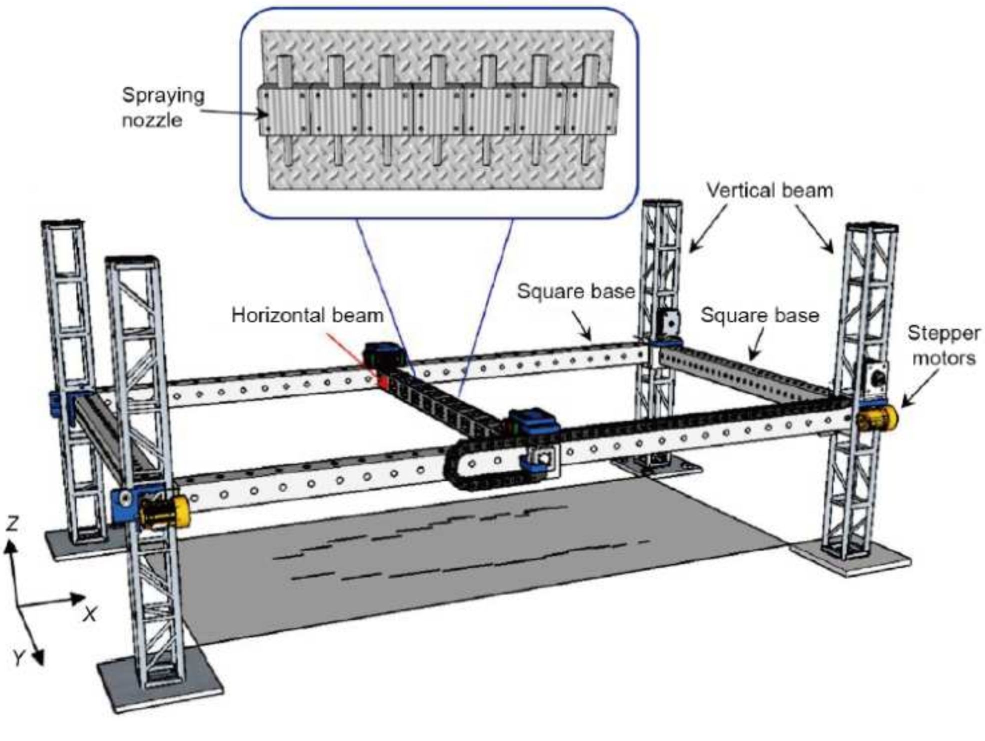

Figure 2.9 Schematic Figure of D-Shape Printer Taken from [46]

2.3.2 Material Depositing Methods

In general, both deposition-based and selective printing processes can be divided into a sequence of individual process steps that are repeated multiple times until the component is fully completed. These recurring steps are schematically illustrated for the deposition-based methods discussed below in Figure 2.10 and can be categorized as follows [51]:

1. Transportation of the build material from the storage system to the printhead,
2. Processing at the printhead and / or extrusion of the material through the nozzle,
3. Deposition of the material, accompanied by its deformation during placement,
4. Deposition of subsequent layers, including the self-weight-induced loading of previously deposited upper layers.

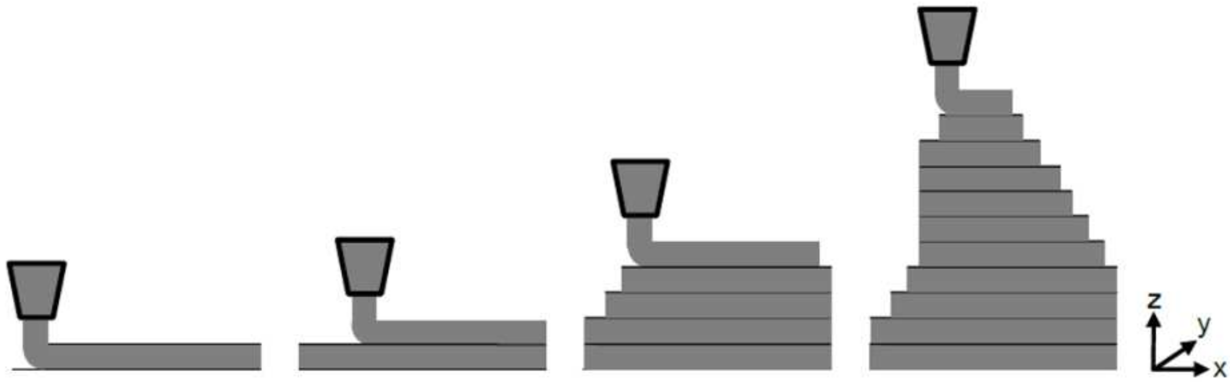

Figure 2.10 Process for Material Deposition Printing Taken from [51]

The so-called deposition-based methods are characterized by a higher material throughput compared to *Selective Binder Application*, which results in significantly shorter printing times for many applications. These properties make them particularly attractive for the fabrication of large-format components with low geometric detail. As a result, these methods have increasingly become a focus of both application and research of 3D-printing in construction [104].
This subfield of concrete-3D-printing can also be further subdivided. The following section presents the three most significant methods currently in use.

Multi Layer Extrusion

One form of deposition-based methods is known as *Multi Layer Extrusion*. This method follows the process principle described in Section 2.3.2 and is fundamentally based on the Fused Deposition Modeling technique developed by Scott and Lisa Crump (see Chapter 2.1).
Multi Layer Extrusion transfers this concept to the processing of concrete and similar materials. The building material is extruded layer by layer through a nozzle and deposited in a stable form on top of the previous layers. Numerous technical variants of this method now exist, differing in terms of material feed, printhead or nozzle configuration, and movement mechanics. The following section provides a closer look at three of the most relevant implementations currently in use.

A) Contour Crafting
In the mid-2010s, Behrokh Khoshnevis from the University of Southern California, in collaboration with NASA, developed a system intended to enable the automated construction of wall structures on the lunar surface. In this method, fresh concrete is conveyed to the nozzle by means of a pump and then deposited layer by layer as a continuous bead. Simultaneously, the outer surface of the printed object is smoothed using an integrated trowel in order to produce a uniform exterior.
After constructing the outer structure, the internal cavity is filled either by injection or by pouring another material [39]. The method is known as *Contour Crafting* and is considered one of the early large-scale applications of multi-layer extrusion.
As a further development of *Contour Crafting*, the so-called *CONPrint3D* method was developed at the Dresden University of Technology. The goal of this technology is to achieve a comparatively high printing speed of up to 10 m/min by increasing the material throughput, allowing for cross-sections of up to 150 × 50 mm² and the use of aggregates with particle sizes of up to 16 mm [100]. A specially designed nozzle enables the direct fabrication of load-bearing wall structures, including integrated reinforcement, within the framework of a continuous on-site printing process.
To realize the required build volume, the printhead is mounted at the end of a boom-like extension on a mobile platform. This configuration makes it possible to construct entire building sections directly on-site, section by section [53].

B) Concrete Printing
The *Concrete Printing* system can be positioned in terms of its application between *Contour Crafting* and the *CONPrint3D* process. With layer heights between 5 and 25 mm and a lower printing speed compared to *CONPrint3D* [46], the method aims to achieve higher resolution and improved geometric precision.
The maximum size of the printed object is limited by the available build volume of the stationary printing system. As a result, the method is particularly suited for serial off-site prefabrication and is primarily used in controlled production environments [100].

C) Shotcrete 3D-Printing
The *Shotcrete 3D-Printing* (SC3DP) method, developed at the Technical University Braunschweig and illustrated schematically in Figure 2.11, represents another robot-assisted technique of additive manufacturing in the field of material extrusion. The method is based on conventional shotcrete technology and combines automated component fabrication with pneumatic material application [100].
The fully mixed fresh concrete is conveyed to the nozzle using a progressive cavity pump. At the nozzle, the material is accelerated by compressed air, which enables the concrete to be applied at high velocity to the target position [40]. This principle allows for rapid construction progress while maintaining high flexibility with regard to both the geometry of the component and the direction of material application. In addition, the process permits the integration of reinforcement elements directly during printing.
To improve surface quality, a targeted smoothing step can be performed after the printing process. This step reduces irregularities and prepares the surface for subsequent construction work [104].

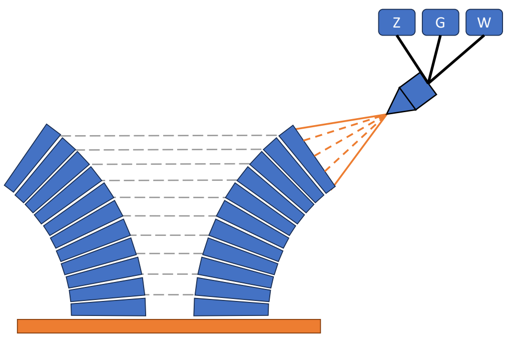

Figure 2.11 Schematic of Shortcrete 3D-Printing Adapted from [40]

2.3.3 Slip Formwork

The field of concrete printing using *Slip Formwork*-techniques, similar to *Multi Layer Extrusion*, can be divided into several distinct technical developments. One of the earliest and most well-known implementations of this principle is the *Smart Dynamic Casting* (SDC) process, developed at ETH Zurich in 2012 [100]. The basic principle of the Slip Formwork process can be described as follows: One or more formwork elements, which are small in dimension compared to the printed structure, are moved, rotated, or locally deformed either continuously or stepwise along the desired component geometry. At the same time, fresh concrete is introduced into the formwork.
Once the previously deposited concrete has sufficiently hardened to support the self-weight of the next section, the formwork is repositioned and the process is repeated [52]. This method enables the fabrication of continuous, geometrically variable concrete structures with high precision, without the need for conventional large-scale formwork systems.

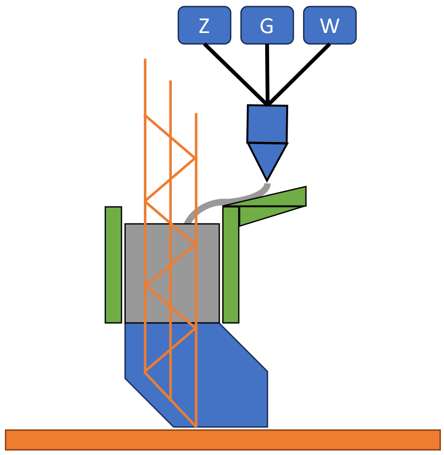

Figure 2.12 Schematic for Slip Formwork 3D-Printing

To reduce the pressure exerted by viscous fresh concrete on the formwork during the construction process, the *Smart Dynamic Casting* system developed at ETH Zurich was further advanced into what is now called the *Digital Casting System* (DCS). By precisely controlling the concrete hydration rate, it becomes possible to adjust the fresh concrete strength to match the construction progress. This enables a significant reduction in the thickness of the formwork elements without compromising the structural stability of the component [44].
Based on this principle, ETH Zurich also developed the process known as *Eggshell with thin printed formwork*. The method uses a thin-walled polymer formwork produced through additive manufacturing. The shell can either be fabricated in advance or printed simultaneously with the concrete casting process, and is then filled with fresh concrete. The concrete mix used, which is referred to as *Set-on-Demand Concrete* hardens rapidly, allowing the system to be self-stabilizing. Because the special concrete places less stress on the formwork, the walls can be made extremely thin (in the referenced example, only 1.5 mm in thickness). The integration of reinforcement elements is also easily achievable with this method.
Another development is the so-called *Admixture Controlled Digital Casting* (ACDC). In this approach, a prefabricated flexible formwork made of PVC or PTFE-glass fiber membrane is used, which is held in shape by a minimal external support structure. The concrete is then filled, depending on the cross section at a rate of up to 2.5 m/h [44].
In contrast to conventional slipforming methods, where the formwork is moved step by step along the printed object, both the *Eggshell* and *Admixture Controlled Digital Casting* methods rely on fully prefabricated formwork. The actual casting process takes place afterward, or in stages, within this fixed form. These approaches open up new design possibilities and allow for high geometric precision while reducing the amount of formwork required.

2.4 Classification of the Printing Process Used

Since numerous ongoing research projects exist in the field of concrete-3D-printing, the methods presented in Chapter 2.3 can only represent a limited portion of the current technological landscape. A more comprehensive and in-depth systematization of the various approaches can be found in the sources cited above [100, 46, 52, 104].

The results presented in this thesis focus exclusively on the method of material extrusion based on the *Concrete Printing* principle. The printing material is assumed to be a pre-mixed mineral-based compound, and the printing process is not designed for multi-material systems as referred to in Chapter 2.3.3 (see Figure 2.13).

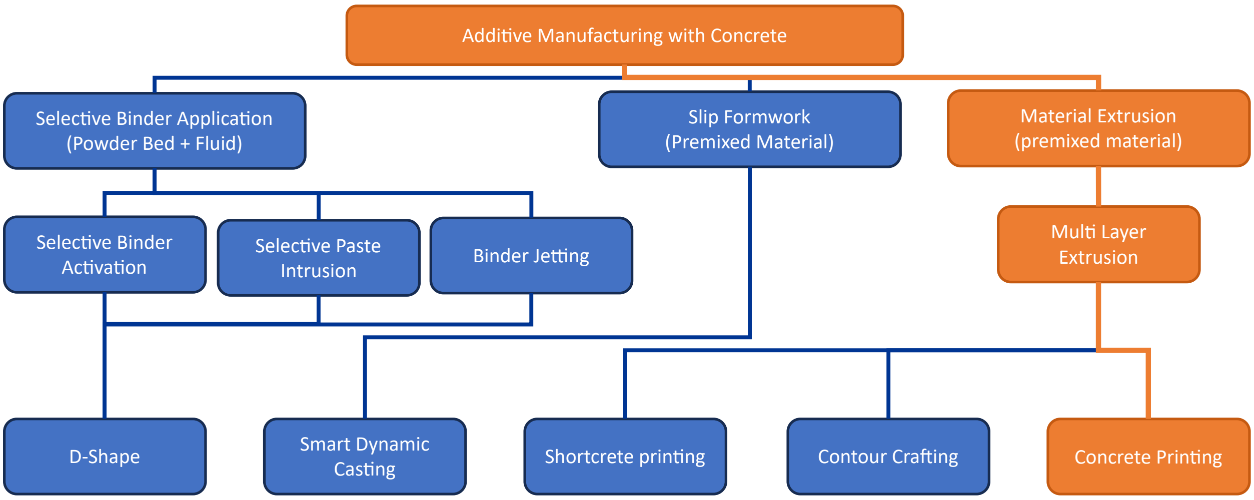

Figure 2.13 Classification of the 3D-Printing Process Discussed in the Existing Processes Adapted from [100]

2.5 Robotic Systems in Additive Manufacturing for Construction

Following the previous chapter's overview of various 3D-concrete-printing methods, this chapter focuses on the robotic hardware used to execute the printing processes. In this thesis, currently employed robotic systems for 3D-printing are classified into two main categories (see Figure 2.14):
Stationary systems remain fixed in position relative to the printed object throughout the entire printing process. As a result, their workspace is limited to the area reachable from their base position. These systems are typically used when the component to be printed can be fully positioned within this workspace.
Mobile systems, by contrast, are capable of moving relative to the printed object either manually or autonomously during the printing process. This movement involves not only the tool unit (end effector) of the robot, but also the relative motion of the entire robotic unit and its components with respect to the object. Consequently, significantly larger components can be fabricated, as the effective workspace of the system is extended by its mobility.

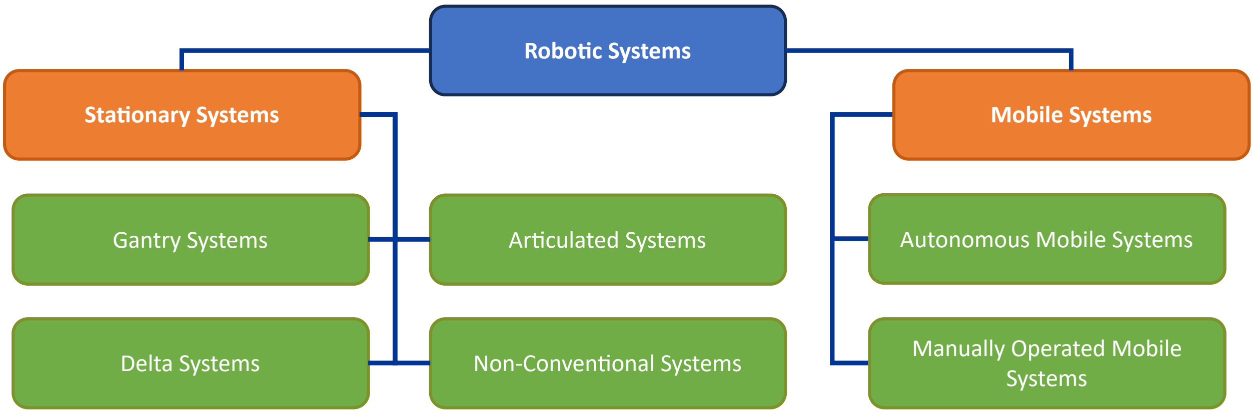

Figure 2.14 Classification of Robotic Systems Used for Concrete-3D-Printing

2.5.1 Stationary Systems

Gantry Systems

So-called *gantry systems* or *portal systems* are based on three linearly movable axes, which are mounted orthogonally to one another. Each axis is responsible for movement along one of the three Cartesian spatial directions (X, Y, Z). As a result, the system is capable of positioning the tool head precisely and independently along each of these directions.
Due to their simple mechanical structure, gantry systems can be adapted to various build volumes. At the same time, they offer high positioning accuracy, making them particularly suitable for large-scale and repeatable applications in additive manufacturing [72]. Because of their simplicity and straightforward kinematics, such systems are already widely in use. Depending on the project requirements, the complexity of the kinematic configuration can be increased, for example by adding a rotational joint around the Z-axis [18, 36].

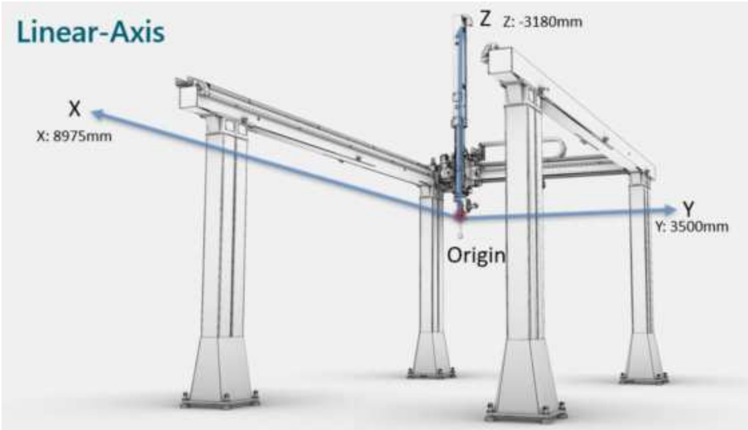

Figure 2.15 Example of a Gantry System Robot with Defined Axis [108]

Delta Systems

Delta systems can be structurally distinguished from conventional gantry systems with relative ease. They consist of two platforms connected by several movable arms. One of these platforms forms the stationary base, while the other acts as the end effector and moves through space relative to the base (see Figure 2.16). Each arm is controlled individually to enable precise relative motion between the platforms.
Although the mechanical structure is significantly more complex than that of Cartesian systems, the delta principle offers the advantage of higher dynamic performance. Since a single motion is distributed across multiple components, each individual component requires less travel. As a result, considerably higher speeds can be achieved. Due to these advantages over gantry systems, manufacturers such as WASP increasingly rely on delta configurations as a basis for concrete-3D-printing [103]. A key disadvantage, however, is the comparatively limited workspace and the greater overall footprint of the system compared to portal systems with an equivalent build volume [8].

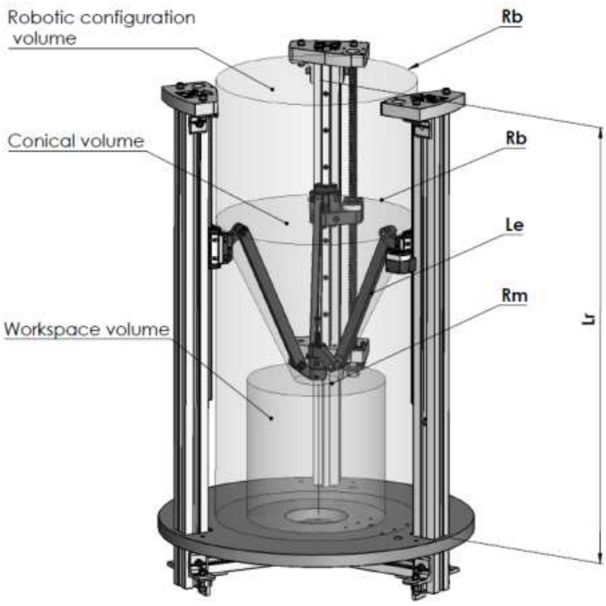

Figure 2.16 Example of a Delta System Robot [8]

Serial Systems

The most versatile form of robotic systems is represented by so-called *serial robots*, also referred to as *articulated robots*. They consist of a serial arrangement of segments connected by joints with varying *Degrees of Freedom* (DOF) [56]. Typically, the foundation of the robotic system, which is also referred to as the *base* is fixed to the reference frame (e.g., the ground) and forms the rotational axis A1, around which the robot can rotate. The other end of the robot arm, known as the *flange*, carries the attached tool, the tip of which forms the robot's *end effector* [99]. The end effector can be oriented and positioned in space depending on the joint configuration and joint limits.
Compared to cartesian systems, the mechanical setup is considerably more complex. However, it also enables significantly greater freedom of movement, particularly with respect to the orientation of the tool relative to the robot base. This capability makes serial robots especially suitable for tasks that require complex, non-linear motion sequences and varying tool orientations. Typical applications include automated painting, welding, or assembly processes involving entire components, such as the joining of car body parts in the automotive industry [64].

Figure 2.17 Example of Serial System Robots Working in Parallel [43]

Non-Conventional Systems

In addition to the commonly used stationary robotic systems described above, a wide range of other, partly highly specialized configurations exists, many of which are already well established in research and development. These include, among others, *continuum robots* [61], *hexapods* or *Stewart platforms* [4], and *Cable-Driven Parallel Robots (CDPRs)* [92].
Such systems are often characterized by unique kinematic properties, a high degree of flexibility, or suitability for specific application areas. However, due to their relatively limited use in large-scale additive manufacturing for construction and the associated practical constraints, they are not discussed in detail in this thesis.

2.5.2 Mobile Systems

In contrast to stationary robotic systems, mobile robots offer significantly greater flexibility and a substantially expanded workspace. Because the entire robot base can be repositioned relative to the reference object, large-scale or segmented printing tasks can be executed step by step using a single system.
However, increased mobility also comes with certain disadvantages. Additional degrees of freedom typically result in reduced positioning accuracy and require greater effort in setting up and calibrating the system. In particular, the precise localization and fixation of the robot during the printing process pose additional technical challenges. Furthermore, all connected systems, such as the pump and mixer, must also be designed for mobility in order to accommodate changes in the position of the printing unit. The payload capacity of the robot is also lower compared to a stationary unit due to limited anchoring possibilities.
The following section presents selected mobile robotic systems that are currently used in the field of concrete-3D-printing.

Manually Operated Mobile Systems

These robots represent a hybrid configuration consisting of a numerically controlled printhead mounted on a semi-automated or manually movable platform.
The system must be positioned at the beginning of each operation. Once one section is completed, it is moved by an operator to a new target position, where it can resume work on the next section. The system is not capable of completing an entire project autonomously once the printing process has begun. Systems such as the "P1" (see Figure 2.18) developed by Putzmeister and further advanced by INSTATIQ [69, 38], or the robotic arm on a movable platform developed by APIS COR [77], fall into this category.

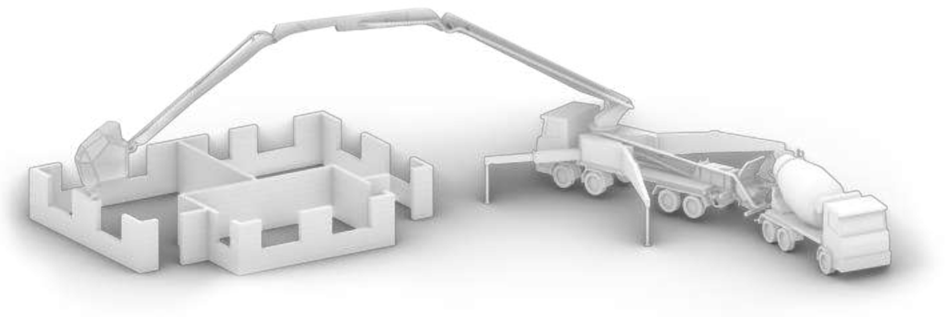

Figure 2.18 Schematic of "INSTATIQ" During Operation [38]

Autonomous Mobile Systems

Fully autonomous robotic systems are capable of independently adjusting their absolute position relative to the component during the printing process without external intervention or input. They navigate the construction site autonomously and are, in principle, capable of completing the entire printing process without continuous human supervision. This would make it possible to fabricate even large-scale components entirely using a single robotic unit.
However, such a level of automation has not yet been fully achieved in the construction industry with the current state of technology. At present, mostly semi-autonomous systems are available in practice. These require manual remeasurement, position adjustment, or external control, as described in the previous section. Nevertheless, research results such as those presented in [88] and [25], along with market-ready robotic systems such as the *Jaibot* by Hilti AG [34] or the *BauBot* by Fischer Holding GmbH & Co. KG [29] demonstrate that this technology offers more than just theoretical potential.

2.6 Specification of the Hardware Used

The software developed in this thesis is specifically tailored to the hardware available at the Technical University of Munich. The following section outlines the relevant specifications and the interaction of the different components during a 3D-printing operation.

2.6.1 Robot

The robotic system used is a *KUKA KR 340 R3300*. This serial industrial robot is equipped with six rotational axes (A1–A6), which are depicted in Figure 2.19b and is designed for applications with high load requirements and an extended working range. The robot itself weighs approximately 2.4 tonnes. Its maximum reach, measured from the robot base (axis A1) to the wrist (axis A5), is 3326 mm. The nominal payload capacity is 340 kg, but it can be increased to up to 418 kg depending on the position of the center of mass of the payload [42].
The repeatability of the robot's positioning is specified according to DIN EN ISO 9283 as ±0.08 mm. Figure 2.19a shows the workspace that can be reached through the rotational motion of joints A2 to A5. This workspace is further extended by the rotation around axis A1 and is approximately spherical around the robot base.

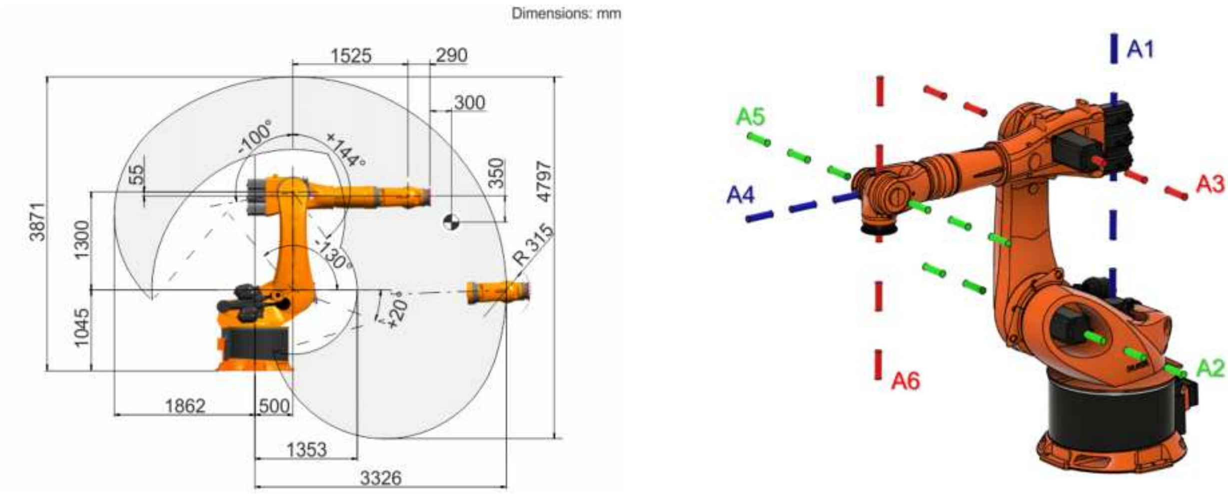

(a) Work Envelope [42]

(b) Axis Definition

Figure 2.19 Technical Data for KUKA KR 340 R3300

At the flange, which forms the end of the KUKA robotic system and includes axis A6, an additional frame with dimensions of approximately 100 × 30 × 30 cm is mounted. In addition to the nozzle of the printhead, this frame supports various measurement and control devices. These include, among others, a camera and a thermal imaging camera, a ring-shaped lighting system for uniform illumination of the printed object, and a contact sensor for the precise detection of the print bed position. The nozzle itself is connected to the material hose via a standardized Whitworth G1/2" thread, allowing for quick replacement and flexible selection of different nozzle geometries. A photograph of the complete tool assembly as used is shown in Figure 2.20.
The nozzle of the printhead defines the so-called *Tool Center Point* (TCP) of the robot, which is the point in space where the trajectory of movement is executed. The printing material is conveyed to the nozzle via the previously mentioned material hose with a nominal diameter of DN25. This hose is routed within the designated empty conduits along the robot arm.

(a) Front View of Tool-Frame Attached to Robot Flange

(b) Side View of Tool-Frame Attached to Robot Flange

Figure 2.20 Picture of Tool Frame in Use

The robot can be operated in two ways. First, manual control is possible using the *smartPAD* provided by KUKA, which features a graphical user interface (GUI). This allows the operator to intuitively and step-by-step move the robot into the desired position.
Second, the robot can be controlled by executing predefined motion sequences through code-based commands. For this purpose, a program written in the manufacturer-specific machine language *KUKA Robot Language* (KRL) is transferred to the robot. A complete KRL program typically consists of two file types, although in some cases all relevant information can be contained within one single file:
The first file is the *.src* file, which contains the actual motion commands and the process logic. The second is the associated *.dat* file, where robot-specific parameters such as tool data, coordinate sets, and internal variables are defined.
To execute motion, the robot is capable of performing a variety of movement types. The three fundamental types of motion are illustrated in Figure 2.21.

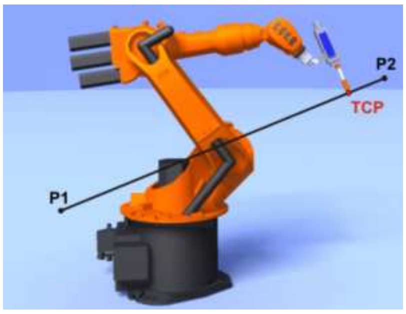

(a) Linear

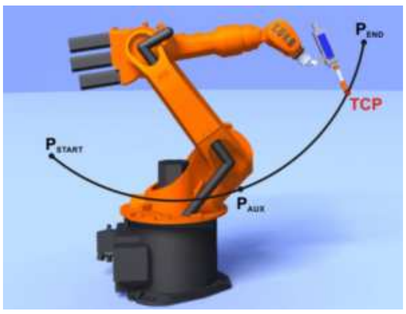

(b) Circular

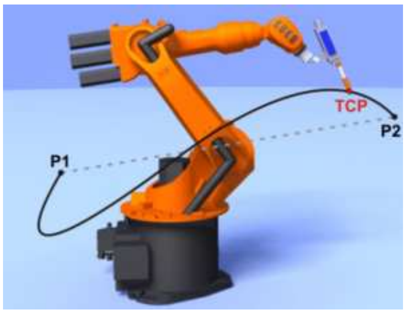

(c) Point to Point

Figure 2.21 Basic Movement Types for KUKA KR 340 R3300 [43]

The visually simplest of these is the so-called *linear motion*, which connects the current tool coordinates to the target point along a straight path. The resulting trajectory represents the shortest distance between the two points and follows this line exactly.
Circular motions require, in addition to the start and end points, a third point, that is known as the *auxiliary point* (P_{AUX}). The robot moves along an arc that passes through all three specified points: the start point, end point, and auxiliary point.
In *point-to-point* motions, as in linear motion, only the start and end points are defined. However, unlike linear motion, the robot calculates a trajectory that reaches the target as quickly as possible. This computation takes into account factors such as the maximum angular velocities of the individual joints, which can be defined in the corresponding *.dat* file. As a result, the actual path is not predictable and may deviate significantly from a straight line between the start and end positions.
In addition to the predefined trajectory, velocity-related parameters can also be transmitted to the robot. These include the translational velocity (in m/s), the angular velocities of the individual axes (in rad/s), the acceleration (i.e., the first time derivative of velocity), and the so-called *jerk* (the second time derivative of velocity), which represents the abrupt change in acceleration (measured in m/s^3) and significantly affects the precision of the robot. These parameters can be defined with high precision for each motion sequence, allowing for targeted control of the robot's dynamic behavior.

2.6.2 Pump

In order to ensure continuous material supply at the nozzle throughout the printing process, fresh concrete is constantly conveyed toward the printhead. For this purpose, a delivery pump of the type *PFT Swing L 400V FU*, manufactured by Knauf PFT GmbH Co. KG, is used. Depending on the configuration of the feed screw and the type of material being conveyed, the pump reaches a maximum delivery rate of 90 liters per minute and is equipped with a storage tank holding 70 liters. It is powered by a 6.05 kW electric motor operating at a variable speed ranging from 146 to 458 revolutions per minute (rpm). The maximum operating pressure is 30 bar, enabling conveying distances of up to 30 meters depending on the material consistency [66]. The pump dimensions are illustrated schematically in Figure 2.22.

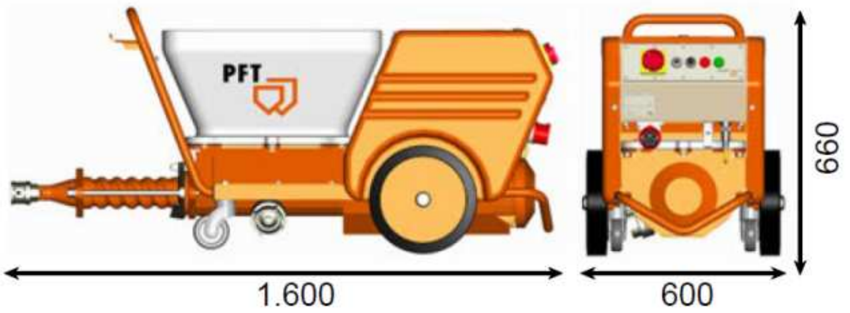

Figure 2.22 Side View and Front View of Pump with Measurements [mm] [66]

The underlying delivery mechanism is based on the principle of a progressive cavity pump. In this system, a metallic rotor with eccentric geometry rotates along a circular path inside an elastic stator. This motion continuously generates sealed conveying chambers that transport the material uniformly from the storage tank to the outlet. The flow rate can be controlled via the motor speed (rpm), which in turn is adjusted by a control signal in the range of 0 to 10 V. This allows for continuous speed variation within the specified range.
This pumping technology enables a low-pulsation material flow with consistent discharge performance, which is particularly beneficial for maintaining uniform print quality in a layer-based 3D-printing processes.

2.6.3 Mixer

Since the capacity of the pump's storage tank is insufficient to ensure continuous material supply, even during low-volume printing processes, additional material feeding during the printing operation is required. For this purpose, a continuous mixer is positioned in close proximity to the pump, supplying fresh material directly into the pump's feed hopper.
The mixer used is a *PFT HM 24* from Knauf PFT GmbH & Co. KG. The unit is equipped with a 3.3 kW electric motor and achieves a mixing output of up to 50 liters per minute at a defined speed of 280 rpm. The dry mortar (cement-based), supplied in bagged form, is continuously mixed with water in the mixer. Therefor water is introduced with a predefined dispense rate via a DN12 connection rated for pressures up to 2.5 bar. Additionally, aggregates with a maximum grain size of up to 6 mm can be processed [65]. This combination of continuous mixing and direct feeding ensures a reliable and uniform material supply, which is a critical factor for maintaining quality and process stability in concrete-3D-printing. A schematic representation of the mixer including rough dimensions is shown in Figure 2.23.

Figure 2.23 Mixer with Measurements Given in [mm] [65]

2.6.4 Print Bed

The print bed consists of two rectangular bolted formwork panels from the MAXIMO series by PERI [31]. The panels have dimensions of 3000 × 1200 mm and 1500 × 1200 mm, respectively, and are rigidly connected on the underside using M24 bolts. The entire print bed is supported by four pairs of height-adjustable feet, which allow for precise leveling of the surface. Each foot is additionally equipped with a load cell, enabling accurate measurement of both the total weight of the print and the weight distribution across the bed.
Any deviations in the bed's position or its parallelism with respect to the robot's nozzle prior to printing can be precisely detected using a contact sensor mounted on the robot's tool frame. These deviations are then compensated internally by the robot system in software. Throughout this thesis, a perfectly positioned print bed is assumed. Figure 2.24 shows the print bed in its assembled state.

Figure 2.24 Print Bed Consisting of PERI MAXIMO Elements (Curvature Due to Lens Distortion)

2.6.5 Overview

Figure 2.25 shows a rendering of the hardware setup used during the printing process. Visible components include the *KUKA KR 340 R3300* with mounted tool frame, the print bed made of formwork panels, the delivery pump, and the continuous mixer used for material supply. This configuration forms the technical basis for the concrete-3D-printing processes investigated in this thesis.
During printing, mineral-based material is first mixed with water in the mixer. Depending on the amount of water added, both the water-to-cement (w/c) ratio or the consistency of the material can be precisely adjusted. The material-specific properties and the exact composition of the concrete mixtures are not considered in detail within the scope of this work.
Once the components are mixed, they are transferred from the mixer to the pump via the discharge pipe. From there, the material is conveyed through a DN25 hose to the nozzle. Through computer-controlled nozzle movement with partially constant speed, consistent beads can be deposited onto the print bed. Layer by layer, the desired object is created.
The objective of this work is to enable a better interaction between the various hardware systems and to provide a software platform that facilitates future printing operations.

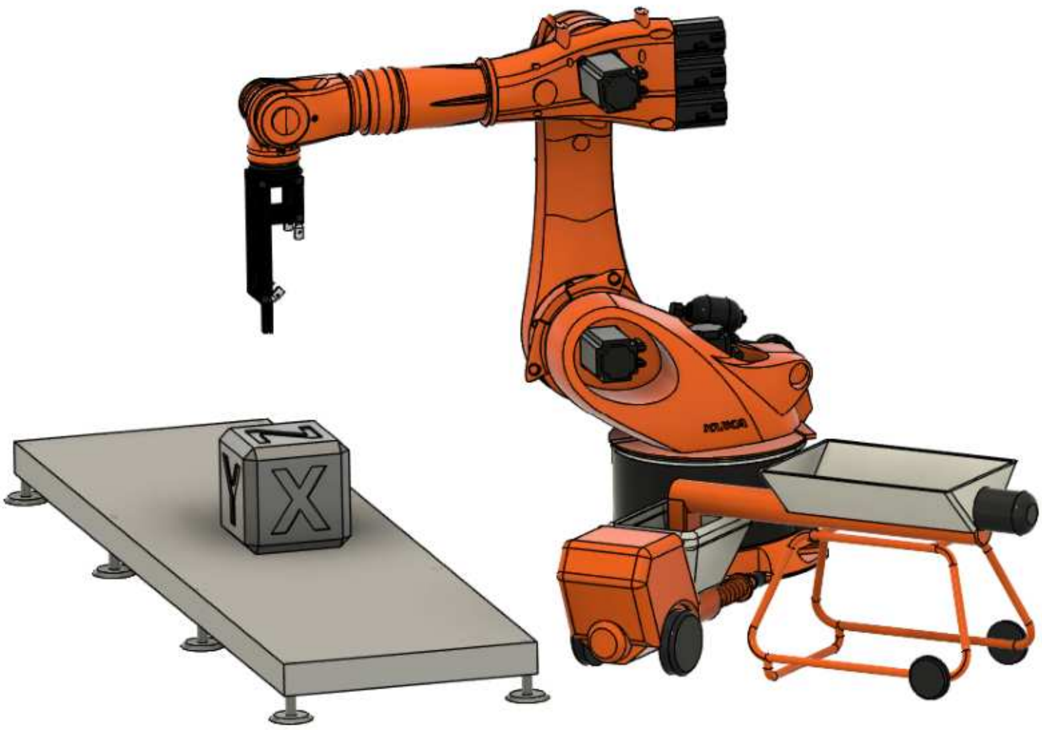

Figure 2.25 Rendering of Robot Cell with Print Related Hardware

3 From Model to Printed Object

3.1 Overview

This chapter traces the complete workflow from digital design to the physical printing of an object, using an exemplary component. The aim is to provide a practical explanation of the essential steps within the additive manufacturing process, ranging from the creation of a 3D model in a CAD environment to the handover to the printer.
A specially designed test object serves as the demonstrator. It combines typical geometric elements such as rectangular contours, circular segments, and a cylindrical recess (see Figure 3.1). Test geometries like this are widely used in 3D-printing, with the complexity of the structure depending on the printing method employed [55]. The illustrated object was created using *Computer Aided Design* (CAD) software [11].
The example shown initially illustrates the process exclusively for polymer-based materials using the Fused Deposition Modeling technique, without yet considering concrete-3D-printing. This method was chosen because, among the three common printing processes (SLA, SLS, and FDM), it is most comparable to concrete printing. A Cartesian 3D printer, such as the gantry printer described in Section 2.5.1, serves as the printing system. The considered objects are processed using planar slicing [57] and printed layer by layer. The terminology and process steps follow the slicing workflow described in [95]. The transfer of these procedures to systems that differ in material and process technology, such as concrete-3D-printing, is addressed in the following chapters.

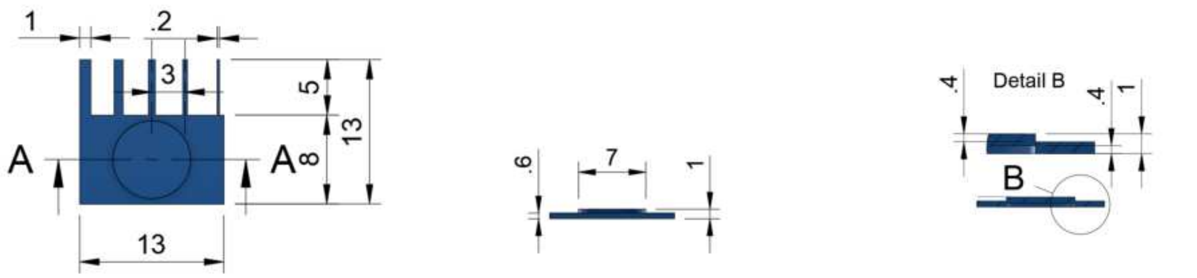

(a) Top view **(b)** Side view **(c)** Section A-A and Detail B

Figure 3.1 Technical Drawing of Test-Object with Measurements in [mm] Made Using Fusion 360 [11]

3.2 Workflow for 3D-Printed Objects

3.2.1 Design Process

The first step on the way to a printed component is the design of a suitable 3D model. Figure 3.2 illustrates the creation process of the test object used in this work.
Starting from a two-dimensional sketch that contains all essential features of the geometry as a projection onto the X-Y-plane, the rectangular base is first extruded. In the next step, the cylindrical extrusion is added, positioned centrally within the rectangular area. Finally, the circular cutout within the base is created using a *cut* operation.
This structure forms the basis for further processing in the slicer creating the required tool path and the subsequent transfer to the printer.

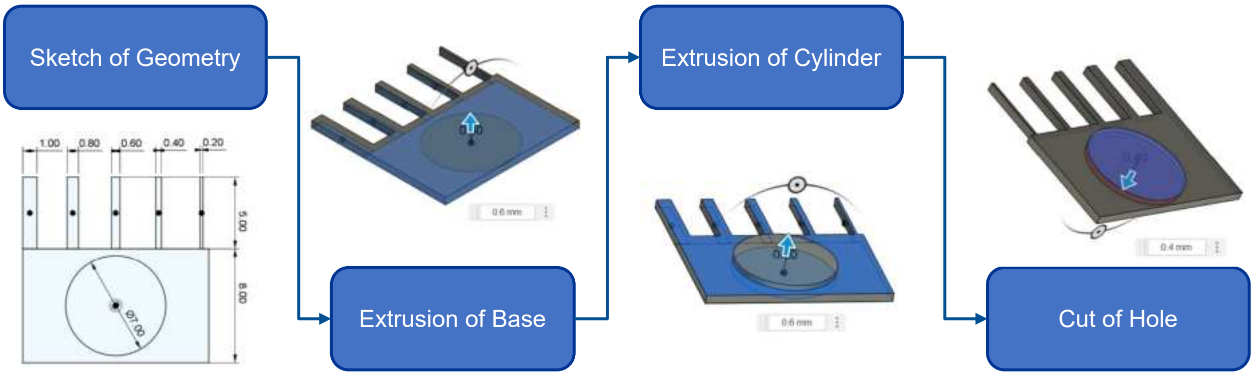

Figure 3.2 Design Process of Test-Object Using Fusion 360 [11]

3.2.2 Slicing Process

Once the digital 3D model has been created, it can be exported in a suitable file format and transferred to a slicer software. Common exchange formats include *.stl*, as well as *.step*, *.obj*, *.dae*, or *.3mf*.
The main task of the slicer is to divide the three-dimensional volume model into a sequence of individual layers. Within each layer, the object is described by line segments that define the motion paths of the printhead. This decomposition into discrete layers and path patterns results in a structured representation that a cartesian 3D printer can interpret and execute layer by layer. As a result, the object is no longer treated as a solid volume but as a superposition of thin, extruded material strands.
The following section provides a detailed examination of this process.

From Solid to Poly-Surface

In order to divide the volume model into individual layers and lines, it is first converted within the slicer into a file format known as the stereolithography file, or *.stl* for short. This format, developed by the aforementioned company 3D Systems [2], describes the object as a hollow geometry based on a triangulated surface mesh. During this conversion, the original solid model is approximated by a network of flat triangular facets. Each of these facets is defined by just three vertices, making triangles the simplest possible planar element for representing flat and angled surfaces. As a result, the volumetric properties of the model are discarded, and its geometry is described exclusively by its outer surfaces.
Figures 3.3a and 3.3b schematically illustrate how a solid body is transformed into such a polygon mesh. In the example shown, a simple cube is approximated using twelve individual triangles. Figure 3.3c shows the actual test object opened as an *.stl* file. It clearly demonstrates that the level of detail in the model is directly related to the number of polygons used: the more complex the geometry, the finer the resulting triangulation.

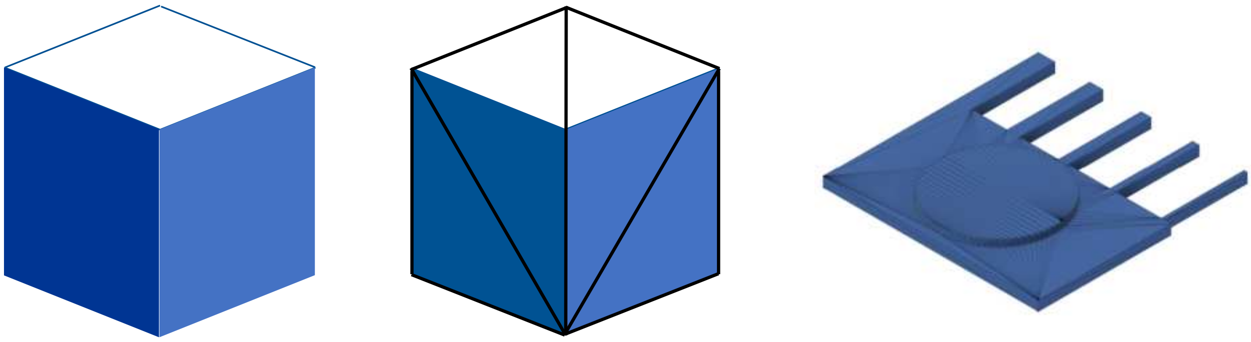

(a) Solid **(b)** .stl Representation **(c)** Test-Object as .stl

Figure 3.3 Object turned from Solid Body to Boundary Representation as .stl

Additionally, it becomes evident that curved structures, such as the cylindrical section of the test object shown above are not represented as exact circular segments, but are instead approximated by a series of straight line segments.
This simplification facilitates the subsequent slicing of the model geometry into planar cross-sections, as each surface is already defined by linear elements.

From Poly-Surface to Print-Path

Since the specific procedures used in slicing can vary significantly depending on the software, settings, and printing strategy, the following section provides only an abstracted representation of the process. Based on the works of [57], [5], and [96], a simplified outline is given of how a 3D model can be converted into a printable path. The actual implementation and sequence may differ between slicers and also depend on parameters such as material type, layer height, or motion strategy.
The first step in converting the mesh geometry into printable tool paths involves assigning mesh facets (polygons) to individual layers. For this purpose, the model is intersected along the Z-axis using a series of cutting planes spaced according to the selected *layer height*. Each of these planes is intersected with the triangular faces of the *.stl* mesh. The goal is to generate a valid line segment from the intersection between each facet and its corresponding plane. This segment will later form part of the closed contour of that layer.
Figure 3.4, adapted from [5], illustrates the geometric configurations that can occur during this intersection. Only configurations 1, 2, and 3 produce valid and usable results, since in these cases the slicing plane intersects exactly two edges of a triangle, thus defining a unique line segment.

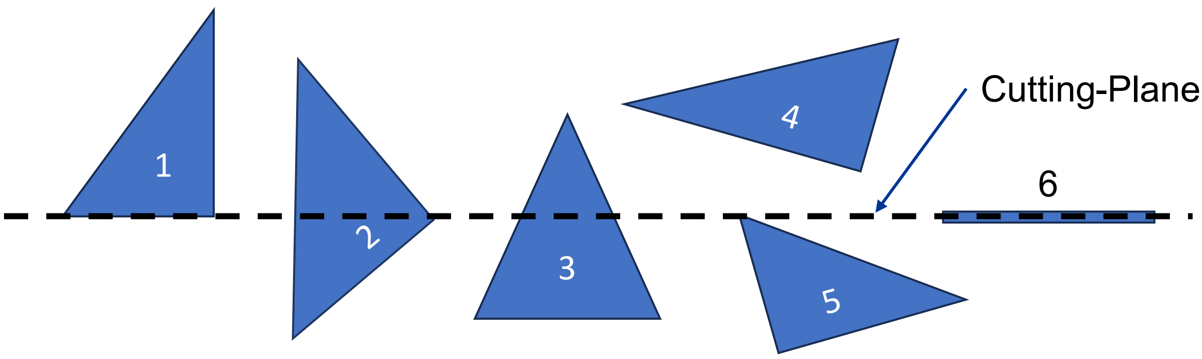

Figure 3.4 Cutting-Plane Intersecting Different Facets of Polygon Mesh [5]

- **Case 4:** The triangle lies entirely outside the current cutting plane and cannot be assigned to this layer.
- **Case 5:** The plane touches only a single vertex of the triangle. As this yields a point coordinate rather than a line segment, the case must be ignored.
- **Case 6:** All three vertices lie in the cutting plane. Although this geometrically defines a face, no unique line segment is created, and thus the case is also discarded.

If a valid intersection is detected, two points can be extracted from the triangle that define the start and end of a line segment. As the entire mesh is processed, multiple partially connected segments are generated. In a subsequent step, these segments are joined to form a continuous path that represents the outer contour of the object at the respective cutting plane height.
Figure 3.5 illustrates the resulting intersection points for *Case 3*. This procedure is then repeated for all required layers. The resulting tool path defines the outer *outer wall* of the object.

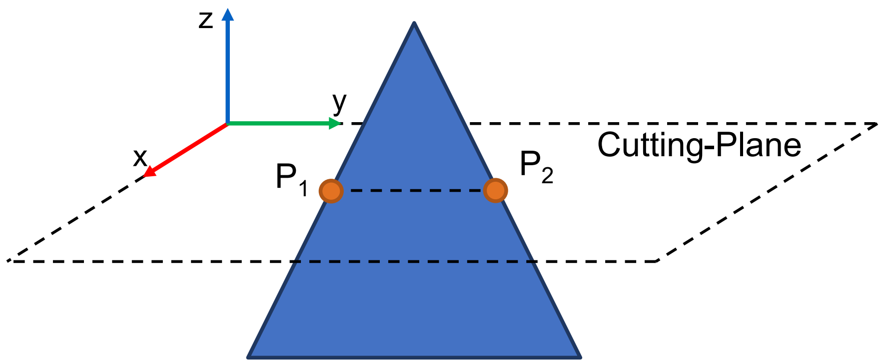

Figure 3.5 Intersection Between Cutting-Plane and Facet Creating Start- and Endpoint of Line Segment [5]

To allow the printhead to move between individual layers, additional connecting paths are required. Along these paths, however, no material is deposited, i.e. no extrusion takes place. Such non-extruding movements are generally referred to as *travel* moves. To ensure an efficient printing process, the travel speed is significantly increased compared to extrusion moves.
When transitioning to a travel move, it is common practice to retract the material away from the nozzle. This is especially true for materials prone to oozing from the nozzle without extrusion commands. This backward motion of the material in the opposite direction of the extrusion is known as *retract* or *retraction*, and it is essential to ensure print quality.
Since the printed object is not intended to consist solely of a hollow outer shell, additional steps are required in the generation of the print path. First, the path representing the *outer wall* can be offset inward by one extrusion width. The resulting additional path is referred to as the *inner wall*.
Because facets that lie exactly in the cutting plane are not considered during slicing, the object must also be closed at the top and bottom. The planes generated in this step are referred to as *surface*, and a further distinction is made depending on their position: the *bottom surface* closes the object in the direction of the print bed, while the *top surface* closes it in the direction of the printhead.
To optimize material usage, the number of wall lines and surface layers can usually be specified explicitly by the user within the slicer. The remaining volume is then filled with the so-called *infill*. This consists of repeated geometric patterns, and its density can be set by the user. Figure 3.6 shows a selection of different infill patterns.

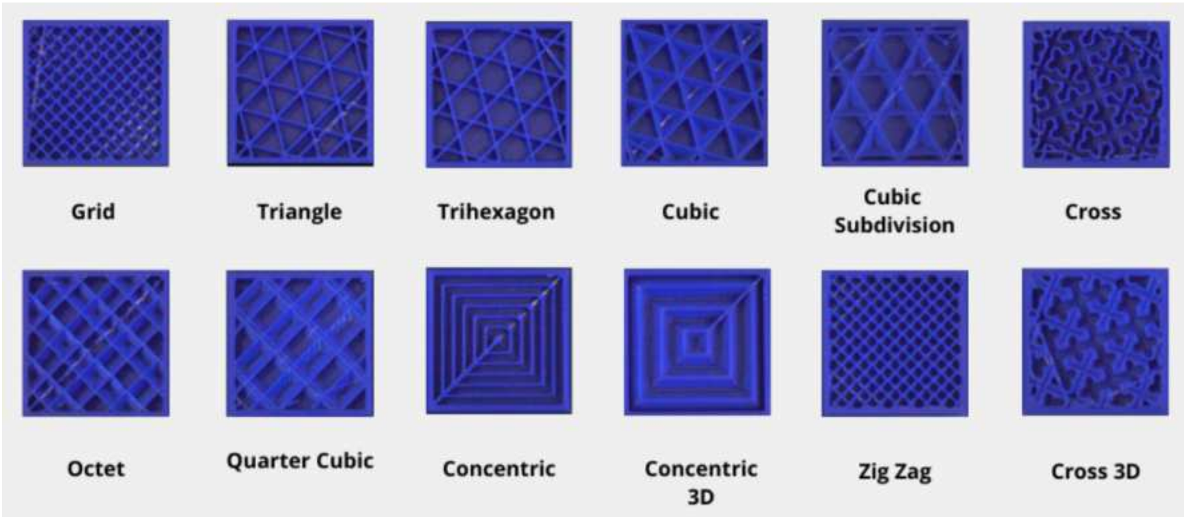

Figure 3.6 Selection of Different Infill Patterns Used in Polymer 3D-Printing [14]

If two distant points within the model need to be connected without any underlying material from previous layers, the resulting line segment is commonly referred to as a *bridge*. When using fast-setting materials, such bridges can span distances that exceed the nozzle diameter many times—sometimes by several hundred times.
However, if the geometry is such that the bridge can no longer support its own weight across the bridges span or would collapse under the weight of subsequent layers, the use of a auxiliary structure becomes necessary. This is known as a *support*. A support structure may be anchored either directly on the print bed or on the object itself and is built up layer by layer until it reaches the critical geometry. After the printing process is complete, the support must be removed in order to obtain the printed object in its intended shape according to the CAD model. Figure 3.7 provides a schematic overview of the various line types using the test object. A corresponding assignment of these line types is given in Table 3.1.

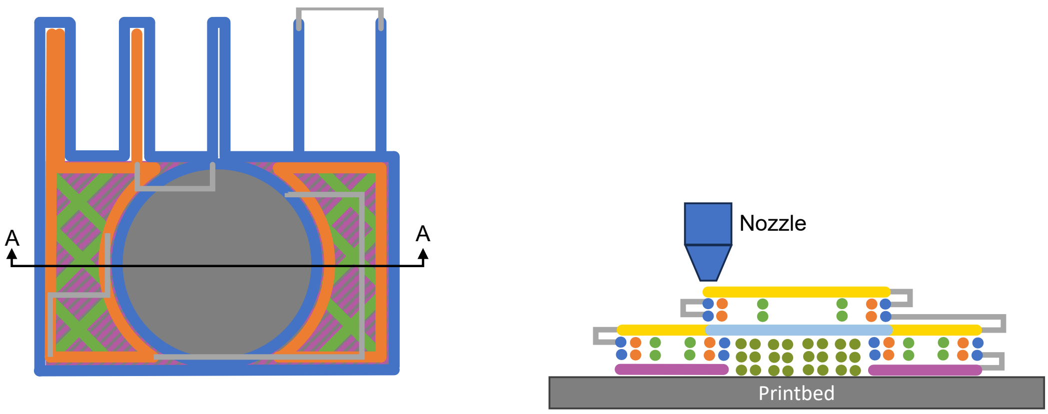

(a) Top View at Z = 0.4 mm (without Support) **(b)** Section A-A form Figure 3.7a (with Support)

Figure 3.7 Overview on Different Linetypes Used After Slicing of the Test-Object

Table 3.1 Color Legend and HEX-Code for the Different Line Types Used in Figure 3.7

Wall Outer	#0065BD	Infill	#A2AD00	Wall Inner	#E37222
Bridge	#5E94D4	Top Surface	#FEDE34	Support	#7D922A
Bottom Surface	#B55CA5	Travel	#999999		

To ensure positional accuracy and geometric fidelity of model and printed part, the adhesion between the printed object and the print bed is of critical importance. For materials with poor bed adhesion, it may be necessary to implement additional measures to prevent detachment during printing. One basic method is to increase the extrusion volume in the first layer, which without changing the nozzle-to-bed distance presses the material more firmly onto the bed surface .
Over time, various alternative techniques have been developed to improve first-layer reliability. Among these, the so-called *skirt*, which represents a closed perimeter around the printed object (see Figure 3.8a) and serves mainly to prime the nozzle by extruding material before the actual print begins. This helps avoid under-extrusion (insufficient material flow) in the initial layer.
The *brim* (see Figure 3.8b), by contrast, is explicitly designed to improve adhesion. It enlarges the contact area of the first layer (*Layer 0*) by adding an outwardly extending edge around the object. After printing, this extra rim is mechanically removed, and the part is usually deburred to eliminate remaining artifacts.
A more robust method is the use of a *raft* (see Figure 3.8c), which slightly lifts the object above the print bed. The gap beneath is filled with a multi-layer structure, forming essentially a platform, that increases the effective contact surface and acts as a bonding interface between bed and object. This helps mitigate issues such as *warping*, which can occur due to uneven material shrinkage during cooling and lead to detachment of lower layers or corner lifting. The raft absorbs these effects, reducing their impact on the final geometry.

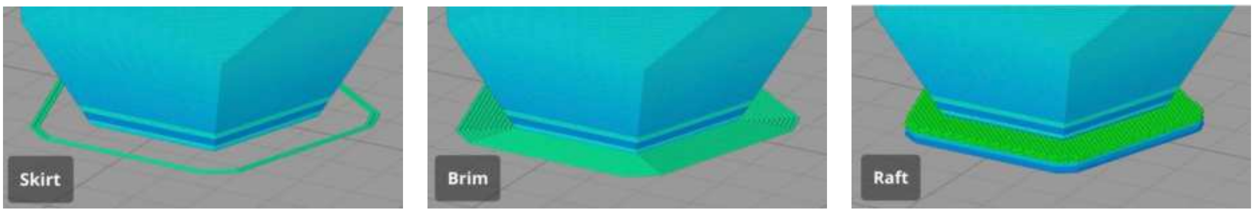

(a) Skirt **(b)** Brim **(c)** Raft

Figure 3.8 Different Bed Adhesion Features Taken from [6]

The line types described above and their respective functions provide a summary of the most commonly used path types in the slicing process. However, depending on the slicer software used, both the terminology and the specific function of individual line types may vary. A more detailed analysis and comparison of different slicer outputs is presented in Chapter 3.2.3.

Machine Code Generated by the Slicer

To make the linear movements defined during the slicing process interpretable for the printer, the coordinate information must be translated into a machine-readable language understood by the printer's firmware interpreter. This is typically achieved by generating commands in the so-called geometric code language (G-code), as specified in the DIN 66025 standard [59].
A typical G-code command includes target coordinates, which are specified using the prefixes X, Y, and Z, each followed by a numerical value. Additionally, movement parameters and command patterns are included. For instance, the F command defines the maximum feed rate in millimeters per minute. The extrusion of material is controlled via the prefix E, whose value specifies the volume of material extruded during the movement, usually given in mm^3.
In addition to these commands, which are referred to as *General Commands* and build the essential base for the printing process the printer must also process instructions for managing hardware components and settings. These are known as *Miscellaneous Commands* and are identified by the prefix M. They are often accompanied by an S parameter, which defines the value to be set.
In Table 3.2, several key G-code commands are presented as examples, along with explanations of how they are interpreted by the firmware *Marlin* [47] used in this thesis.
The listed G-code commands represent a large portion of the input parameters used to control the printer. A comprehensive overview of all commands supported by the *Marlin* firmware can be found in [48].
However, since both the selection and the sequence of these commands are largely determined by the slicing software used, the following section will outline the general structure of a typical G-code output. In addition, key parameters generated by various slicers are compared and discussed.

Table 3.2 Selection of Different G-Code Commands Used with Marlin [47]

Command	Example	Explanation
General Commands (G-Commands)		
G0 – Linear Move	G0 X<pos> Y<pos> Z<pos> F1500	Moves the printhead linearly to the given coordinates at a feed rate of $1500\,\mathrm{mm/min}$. No material is extruded.
G1 – Linear Move + Material Extrusion	G1 X<pos> Y<pos> Z<pos> E3.5 F<val>	Moves linearly to the target while extruding $3.5\,\mathrm{mm}^3$ of material.
G28 – Auto Home	G28 X Y Z	Moves all (or specified [X Y Z]) axes to their endstops to establish the printer's reference (home) position.
G92 – Set Position	G92 E0	Resets the current extruder value to $0\,\mathrm{mm}^3$ without movement.
Miscellaneous Commands (M-Commands)		
M82 – Set Extruder to Absolute Mode	M82 G1 X<pos> Y<pos> Z<pos> E10	Sets the extruder to absolute mode. $E10$ extrudes to $10\,\mathrm{mm}^3$ absolute.
M83 – Set Extruder to Relative Mode	M83 G1 X<pos> Y<pos> Z<pos> E5	Sets the extruder to relative mode. $E5$ adds $5\,\mathrm{mm}^3$ to the current position.
M104 – Set Extruder Temperature	M104 S200	Sets target temperature to $200\,^{\circ}\mathrm{C}$, proceeds immediately without waiting.
M105 – Get Temperature	M105	Requests current nozzle and bed temperatures. Returns values like T:200 /200 B:60 /60.
M106 – Fan On	M106 S128	Turns on the fan at $50\,\%$ speed to cool freshly extruded material.
M107 – Fan Off	M107	Turns off the currently active fan.
M109 – Set Temperature and Wait	M109 S200	Sets the temperature to $200\,^{\circ}\mathrm{C}$ and pauses execution until it is reached.
M201 – Set Max Acceleration	M201 X1000 Y1000 Z500 E<val>	Defines the maximum acceleration $[mm/s^2]$ for each axis during printing moves.
M203 – Set Max Feedrate	M203 X500 Y500 Z100 E<val>	Sets the maximum speed $[mm/s]$ each axis can move.
M204 – Set Acceleration	M204 S400 P<val> T<val> R<val>	Specifies acceleration values for different move types: default (S), printing (P), travel (T), and retract (R).
M205 – Advanced Settings	M205 S<val> B<val> X8.0 Y8.0 Z0.5	Configures advanced motion settings like minimum segment time (B), jerk limits (X/Y/Z), and buffer behavior.

3.2.3 Comparison of Different Slicer Outputs

As an example, the outputs of three widely used slicing programs are compared: *PrusaSlicer* version 2.9.2 [68], and *OrcaSlicer* version 2.2.0 [63], *Ultimaker Cura* version 5.8.0 [97].
The corresponding example files, fully documented in the appendix (see Appendix A), are based on the previously introduced test object. To ensure a consistent basis for comparison, the default print profile for the *Ender 3* printer by Creality [80] was used in all three programs. In each case, the profile is configured for a layer height of 0.2 mm. As a result, the entire test object consists of five layers (Layer 0 to Layer 4). In addition, the following user-defined parameters were adjusted uniformly from each given preset:

Table 3.3 Custom Slicing Parameters Used for Test-Object Generation

Parameter	**Command**	**Description**	**Unit/Type**
Line Width	`0.4`	Width of extruded line	mm
Infill Density	`20`	Percentage of internal part volume to be filled	%
Infill Pattern	`Grid`	Internal fill structure using a grid layout	Pattern
Top Layers	`1`	Number of solid layers at the top	Integer
Bottom Layers	`1`	Number of solid layers at the bottom	Integer
Wall Line Count	`2`	Number of perimeters around the part	Integer
Thin Wall Printing	`true`	Enables printing of features smaller than the nozzle diameter (e.g., 0.2 mm)	Boolean

PrusaSlicer 2.9.2

For the settings used in *PrusaSlicer* (referred to as Prusa hereafter), the estimated print time is two minutes, with approximately 40 % of the movements classified as *travel* (see Figure 3.9c). With a selected filament diameter of 1.75 mm, the total printed volume amounts to 104.16 mm^3, corresponding to a filament length of 0.06 meters. The results generated with Prusa are shown in Figure 3.9.

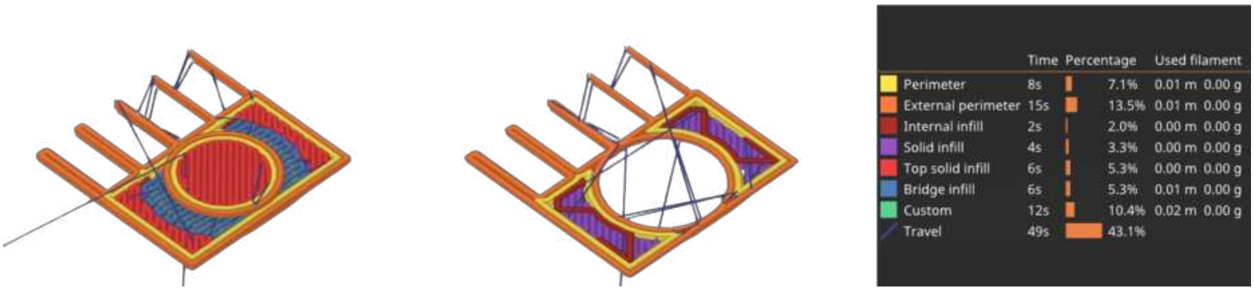

(a) Test Object (Layer 0-4 Active) **(b)** Test Object (Layer 0-1 Active) **(c)** Legend of Different Line Types

Figure 3.9 Slicer Output for Prusa Slicer Version 2.9.2

OrcaSlicer 2.2.0

OrcaSlicer (referred to as Orca hereafter) provides a more detailed breakdown of results. For example, in addition to *retract* movements, it also explicitly lists inverse retractions, during which material is fed back toward the nozzle and refers them as *unretract*. The material consumption is estimated at 0.05 m, while the total print time, including printer preparation, is also estimated at two minutes. Figure 3.10 presents a summary of the Orca graphical user interface.

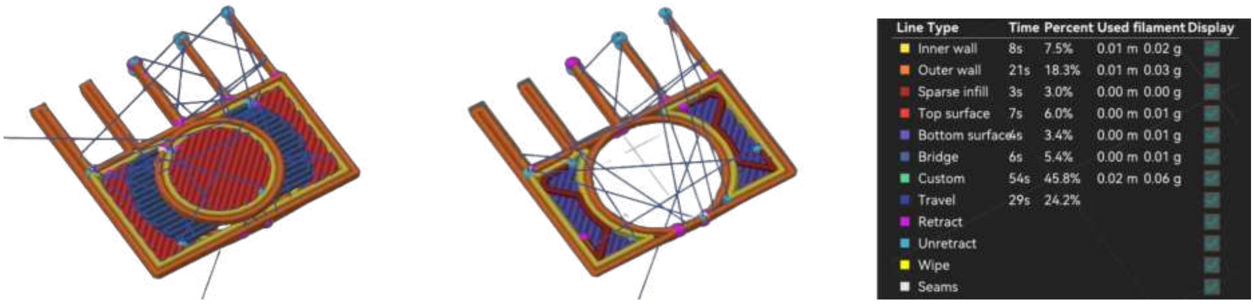

(a) Test Object (Layer 0-4 Active) **(b)** Test Object (Layer 0-1 Active) **(c)** Legend of Different Line Types

Figure 3.10 Slicer Output for Orca Slicer Version 2.2.0

Cura 5.8.0

Ultimaker Cura (referred to as Cura hereafter) estimates the expected print time at one minute, with only about 9 % of that time attributed to *travel* movements. Unlike Prusa, Cura also tracks the time spent on *retractions*, which account for approximately 22% of the total print time. With the same filament diameter of 1.75 mm, Cura estimates a significantly lower material usage of just 0.03 m. All visually accessible results are shown in Figure 3.11.

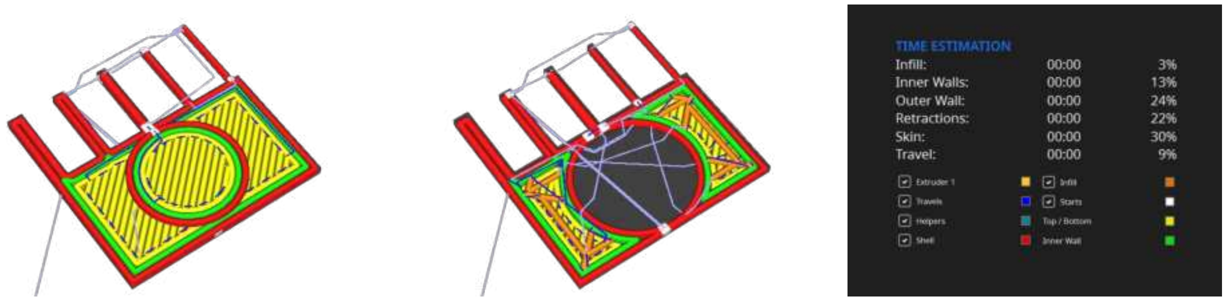

(a) Test Object (Layer 0-4 Active) **(b)** Test Object (Layer 0-1 Active) **(c)** Legend of Different Line Types

Figure 3.11 Slicer Output for Cura Version 5.10.0

3.2.4 G-Code Analysis

Initialization Commands

Based on the G-code files presented in Appendix A, which form the basis of the data discussed earlier, it becomes clear that the generated code is structured into three sections, each highlighted with a distinct background color in the listings. The first part in Appendix A consists of an initialization section, which begins with comments (introduced by a semicolon `;`) related to the respective print object.
In the case of Prusa, this section includes information such as line width (see Listing A.1.1.1, lines 1–11), while Orca also adds data on the number of layers and the object dimensions (see Listing A.2.1.1, lines 1–15). Cura, by contrast, limits itself to object-specific details such as the minimum and maximum dimensions, the selected layer height, and material information including filament diameter and length (see Listing A.3.1.1, lines 1–12).
Following the initial block of general information, Prusa and Orca include a configuration section in which printing parameters are defined using `M200` commands (see Table 3.2). These parameters include, among others, speed limits, accelerations, and so-called jerk values (cf. Chapter 2.6.1). Cura omits explicit parameter constraints at this stage and instead provides a warning system within its graphical user interface . If an incompatible value is entered there, a warning message appears. This happens, provided that the correct printer profile is selected.

In contrast, to both Prusa and Orca, Cura uses this stage to set the target temperatures for the nozzle and heated bed, thereby preparing the printer for the upcoming print process.
Speaking of which, the configuration block is followed in both Prusa and Orca by the command `G90`, which sets the printer's coordinate system to absolute positioning relative to the home position (cf. Table 3.2, command `G28`). This command marks the beginning of the so-called *start G-code*, which can be customized by the user within the slicer. While Cura does not explicitly include the `G90` command, it also defaults to absolute positioning based on the home position. In Cura, the start G-code begins at line 19.
The purpose of the start G-code is to optimally prepare the printer for the actual printing process. This includes, in particular, ensuring that the first layer adheres reliably to the print bed and avoiding print artifacts, which will be discussed in Chapter 3.2.5 caused by excessive or residual material around the nozzle during the heating phase.

Print Commands

As observed, both Prusa and Orca use only the `G1` command for all movements, regardless of whether material is extruded (indicated by an `E<val>` entry within the G-code line). Cura, by contrast, adheres more closely to the formal G-code specification, using `G0` commands for non-extrusion moves and `G1` commands for lines that include material extrusion via `E<val>`. This makes the code much more readable and aids visual understanding.
The printing of the object itself proceeds similarly across all three slicers (see Listings A.1.1.2, A.2.1.2, and A.3.1.2), with only minor differences in the handling of start and end points of travel movements, and in the structure of the infill pattern. The latter shows particularly clear deviations between Cura and the other two slicers (see Figures 3.9b, 3.10b, and 3.11b).
Notable differences are also found in the naming of individual line types, which are indicated prior to each extrusion via the comment prefix `;TYPE:` in the G-code (highlighted in the Appendix A). Each slicer uses its own terminology, offering insight into the internal structuring and segmentation of the generated code.
Table 3.4 provides an overview of all line type designations used in the appendix.

Table 3.4 Line Type Labels Used by Different Slicers

Prusa	Orca	Cura
External perimeter	Outer wall	WALL - OUTER
Perimeter	Inner wall	WALL - INNER
Solid infill	Bottom surface	SKIN
Internal infill	Sparse infill	FILL
Bridge infill	Bridge	
Top solid infill	Top surface	
Custom	Custom	

As shown in Table 3.4, Cura distinguishes between line types in a significantly less differentiated manner than the other two programs. For instance, bridge structures are not explicitly labeled as a distinct line type in Cura but are instead grouped under the general label *SKIN* (see Listing A.3.2.2, line 695 ff.). This umbrella term also includes lines that are identified as *Bottom Surface* or *Top Surface* in Orca and as *Solid infill* or *Top solid infill* in Prusa.
The absence of a *Custom* type in Cura can be attributed to the fact that user-defined G-code sections during initialization are not tagged with a specific line type. Although these custom commands are included in the generated G-code, they are not semantically annotated as they are in Prusa or Orca.

Figure 3.12 provides a graphical illustration of these categorization differences, based on the user interfaces of the three programs.

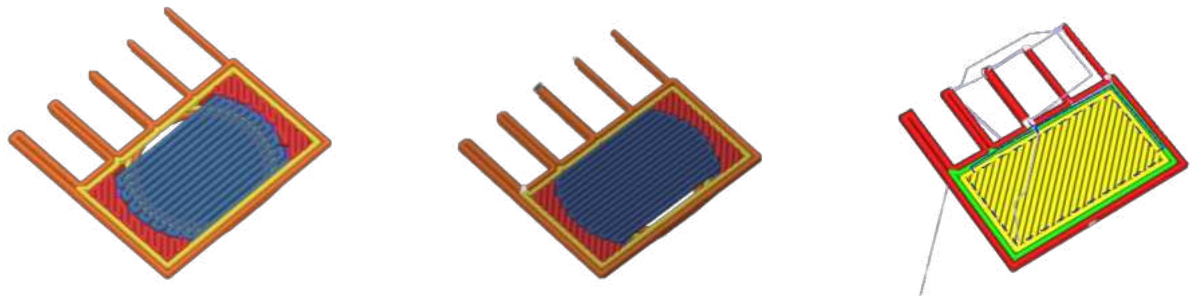

(a) Test Object in Prusa (Layer 0-2 Active)

(b) Test Object in Orca (Layer 0-2 Active)

(c) Test Object in Cura (Layer 0-2 Active)

Figure 3.12 Difference in Line Types Regarding *Bridge* Declaration

During the transition between individual layers, all slicers insert a specific G-code block. In the case of Prusa and Orca, this block can only be partially customized via the printer-specific settings within the slicer. Which could be an issue when adapting the G-code for concrete-3D-printing.
As an example, Table 3.5 presents the layer change G-code as defined in Prusa under the fields *Before layer change G-code* and *After layer change G-code*. The table displays both the user-defined entries within the slicer (left column) and the actual output G-code block (right column), taken from Listing A.1.2.2, lines 433–454.

Table 3.5 Example of G-Code Inserted Before and After Layer Change in PrusaSlicer

Prusa Input	G-Code Output

Before layer change G-Code
`;BEFORE_LAYER_CHANGE`
`G92 E0`
`;layer_z`
 	
After layer change G-Code
`;AFTER_LAYER_CHANGE`
`;layer_z`
	`; LAYER_CHANGE`
	`; Z :0.4`
	`; HEIGHT :0.2`
	`; BEFORE_LAYER_CHANGE`
	`G92 E0`
	`; 0.4`
	
	`G1 E-3.5 F3600`
	`; WIPE_START`
	`G1 F7200`
	`G1 X110.416 Y116.028 E-0.40842`
	`G1 X110.959 Y116.028 E-0.25793`
	`G1 X109.977 Y115.046 E-0.65966`
	`G1 X109.977 Y114.680 E-0.17399`
	`; WIPE_END`
	`G1 Z0.4 F9000`
	`; AFTER_LAYER_CHANGE`
	`; 0.4`
	`G1 Z .4`
	`G1 X115 .779 Y116 .743`
	`G1 E5 F2400`

The command `layer_z` represents a slicer variable that returns the current Z-height within the G-code. The *Before layer change* sequence is then extended by an automatically generated retract command (`G1 E-3.5 F3600`). This initiates an automatic so-called *wipe* sequence, which is intended to remove excess material that may unintentionally ooze from the nozzle.
For this purpose, a series of short retracts and movements in the X-Y plane is executed, during which the adhering material is wiped off inside the part geometry.
Because the retracted material amount (extrusion value `E`) in this sequence is defined relative to the previous position (cf. `G92 E0` in Table 3.5), it must be compensated at the beginning of the new layer. This is achieved by a corresponding extrusion move in the last line of the G-code block shown in Table 3.5, which resets the `E` value relative to its value before the layer change to zero.
Similar sequences can also be observed in Orca (see for example Listing A.2.2.2, lines 478–494). Cura, by contrast, performs the layer change without an automatic in-model nozzle wipe beforehand (see for example Listing A.3.2.2, lines 766–774). This sequence, which consists of the printing of different line types followed by a layer change is repeated cyclically until the object is completed.

Reset Commands

Once printing is complete, all three slicers initiate an end sequence (see Listings A.1.3.3, A.2.3.3, and A.3.3.3). Similar to the start sequence, this section includes commands that can be defined by the user directly within the slicer (for Prusa, see Listing A.1.3.3, lines 1308–1315). During this sequence, the printhead is moved away from the object, and the build plate is positioned in a way that allows for convenient removal of the finished part. In addition, `M`-commands such as `M104` and `M107` are used to disable the nozzle heater and deactivate any running fans.
A large portion of the following code block in Prusa and Orca contains metadata about the parameters used during the slicing process (for Prusa, see Listing A.1.3.3, lines 1316–1691, for Orca see Listing A.2.3.3, lines 1453-1932). Cura, once again, is more restrained in this regard and provides only limited information about the input parameters used.
After the slicer has generated the complete G-code file, the actual fabrication process begins with its interpretation and execution by the printer. The next section therefore focuses on the practical realization of the print path and describes how the object is built up layer by layer.

3.2.5 Print

As briefly outlined in Chapter 2.1, the object is now constructed layer by layer on the print bed based on the generated G-code. Figure 3.13a provides a detailed schematic overview of the components required for this process in an FDM printer.
The raw material is typically supplied as filament on a spool and is continuously fed into the system by the extruder with its subsequent gear assembly. From there, it enters the so-called *hotend assembly*, which consists of two individual components. The task of the latter *hot end* is to heat the filament to the required melting temperature for printing. During this process the temperature is precisely monitored and controlled by an integrated thermistor.
To prevent the melt zone from extending from the hot end toward the *cold end*, cooling fins and an associated fan ensure the targeted dissipation of excess heat. If this heat is not sufficiently removed, a phenomenon known as *heat creep* [73] may occur. In this case, the filament begins to soften prematurely inside the cold end. As a result, the necessary feeding pressure from the extruder gears can no longer be reliably maintained, potentially leading to a nozzle blockage caused by backflow or excess material.

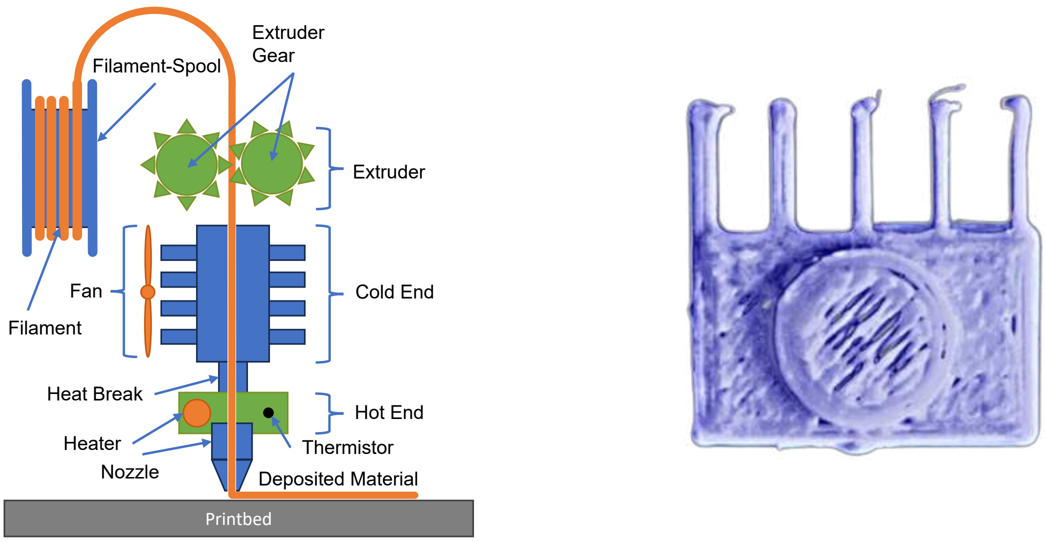

(a) Schematic of Printer Adapted from [21] **(b)** Picture (Post-Processed) of Finished Printed Part

Figure 3.13 Overview on Printer and Printed Part

In addition to the mechanical and thermal influences described in this chapter, a variety of other defects may occur during the printing process. These include insufficient bed adhesion or lifting of the print from the bed (warping), inconsistent layer deposition, under- or over-extrusion, as well as temperature-related issues such as stringing (the formation of fine polymer threads between extrusion stop and start). Figure 3.13b shows the completed print of the test object after removal from the print bed. Visible are, among other things, artifacts caused by extrusion stops on the “fingers” of the object, as well as under-extrusion in the topmost layer of the cylinder. These problems are primarily influenced by the interaction between the hardware used, filament quality, and printing parameters. A comprehensive overview of common FDM-related defects and their remedies can be found, for example, in [67].
A detailed investigation of these aspects is intentionally omitted in this thesis, as the material used may behave totally different from the described thermoplastics. It is henceforth assumed that the printing environment is properly calibrated and that the process is carried out under favorable conditions.
Once printing is successfully completed, the finished object must be detached from the print bed. If support structures have been used, they must be removed in a separate post-processing step. These actions mark the end of the printing process. The printed part is now ready for further post-processing or direct use.

3.2.6 Summary

The processes described in the preceding chapters form the basis for transferring polymer-based FDM printing to mineral materials. Figure 3.14 provides a summary of the entire workflow. Feedback loops may be required between or within individual process steps to ensure an optimal print result.
As shown, the general structure of the slicers is quite similar. This is particularly evident in the case of Prusa and Orca, which can be attributed to the fact that both are based on the same open-source slicing engine: Slic3r [7].
The insights gained in this chapter will now be transferred to the use of concrete as a printing material and applied to the available hardware (cf. Chapter 2.6.1 ff.).
The slicer used as a foundation for this purpose is *Ultimaker Cura*. Despite the slight disadvantages discussed earlier compared to Prusa and Orca, Cura was selected due to its nearly unrestricted configuration capabilities. In particular, parameters such as nozzle diameter and print bed dimensions can be freely defined without constraint. Additionally, the user retains full control over the generation of G-code, such as that shown in Table 3.5. Owing to the increased control over output and the author's prior experience with this slicer, Cura serves as the foundation for the program described in the following chapters.

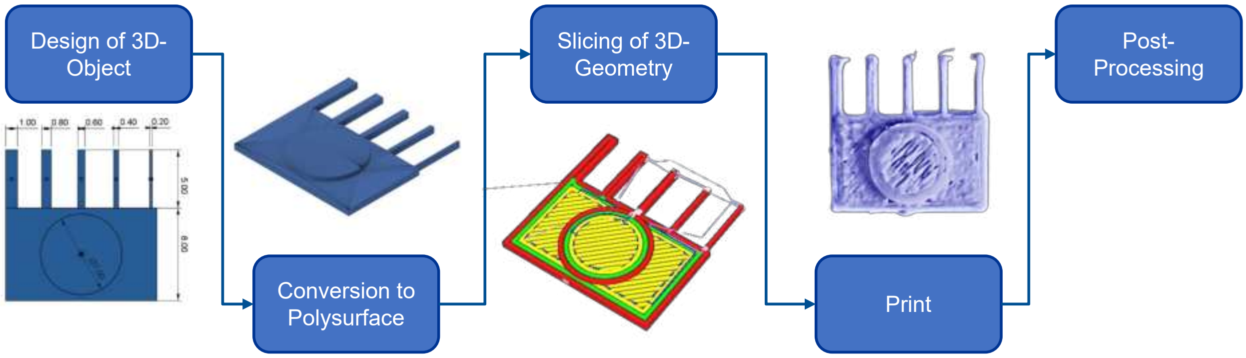

Figure 3.14 Summary of 3D-Printing Process

4 Software Development: Implementation of the Process Chain

4.1 Introduction

This chapter focuses exclusively on the software developed within the scope of this thesis and its individual components. It begins with an overview to provide a basic understanding of the program's architecture and the structure of its subfunctions. Subsequently, the functionality and implementation of the central modules are discussed in detail in the respective sections.
The program itself, along with its full documentation, is freely available via the following GitHub project. The implementation was carried out using *Python* [71] in version 3.12. The project is structured into several packages, each divided into dedicated modules. Within these modules, arguments are processed using functions and classes. A complete list of additional external libraries used for the program is documented in the *requirements.txt* file included in the GitHub repository. To improve code quality and structure, AI-based tools were selectively employed [62]. These tools were used exclusively to improve structure, readability and robustness but were not used for the automated generation of functional program components.
The goal of the software is to integrate various existing software tools and thereby make the relevant information from the FDM slicing process usable for the available KUKA robot, while simultaneously simplifying or automating the process chain up to printing. To achieve this, a user-provided *.stl* file is automatically converted into G-code using established slicer software. Subsequently, the G-code is parsed to extract data relevant to concrete-3D-printing and adapted to the specific hardware. A core feature of the program is the translation of G-code into the machine language used by KUKA (KRL), as well as the code-based control of the extrusion pump. The most important process parameters are then compiled for the user in a summary report in *.docx* format. Finally, a *.3dm* file is generated from the collected data, providing a structured visual representation of all relevant information within Rhinoceros 3D (Rhino) [75].
The slicing process is based on the previously introduced slicer *Ultimaker Cura* [97], version 5.8.0. As discussed in Chapter 3.2.3, Cura produces a less detailed output compared to Prusa and Orca. However, it offers virtually unrestricted configuration options, including print bed dimensions and nozzle diameters, and supports direct execution of the *CuraEngine.exe* via a command line interface (CLI), which handles the slicing process. Further information on this is provided in [98]. This functionality is of central importance for the automation and flexibility of the overall workflow.

4.2 Program Overview

The program is designed primarily as a serial pipeline to convert the G-code generated using Cura into various output files. Figure 4.2 provides an overview of the individual packages and their corresponding modules. The core of the program is the *c3dp_main* function (Concrete-3D-Printing), which coordinates the functionality of all subordinate modules and is responsible for information exchange, data storage, and function calls.
For slicing the current implementation of the program only contains a single package under *slicer*, which handles interaction with the *CuraEngine*. However, due to its modular design, the program is intended to be easily extendable to include additional slicers or functionalities. While this potential is referenced repeatedly throughout the thesis, it is not explored in depth.
The following sections examine the individual components of the packages and folders in greater detail. Each chapter heading indicates the corresponding folder or package to which the described function belongs inside the program. To improve the readability of inputs and code references, the formatting conventions shown in Table 4.1 will be used throughout this thesis to visually distinguish relevant program components and arguments.

Table 4.1 Visualization and Notation Styles Used for Input and Output Formats

Python Code

```python
def example(alpha: int, beta: float) -> None:
    gamma = alpha + beta
    print(f"Sum of {alpha} and {beta} is {gamma}")
```

.json-File

```json
"machine_nozzle_size":
{
        "default_value": 25,
        "type": "float",
        "unit": "mm"
}
```

CLI Output

```
[INFO] This is an example for a CLI Output line
```

Module \ Folder \ Function	*user_input*
File	*printer.def.json*
Argument \ Variable	"default_value"
Section in *setup.json*	"Directory"

At the beginning of each chapter, a progress bar is included to indicate where the content of the upcoming section fits within the overall sequence of the main function. Therefor the color scheme used in all associated flow diagrams follows a consistent logic throughout this thesis. Cells highlighted in green represent input values, while orange cells generally indicate either output values or conditional operations such as *if*-statements. In contrast, cells shaded in blue refer either to packages and folders that contain functional components or to individual functions themselves. Figure 4.1 illustrates a representative progress bar, as used at the beginning of each section in this chapter to indicate which parts of the overall workflow have already been executed and which will be covered next.

Figure 4.1 Progress Bar Referring to Packages in Program

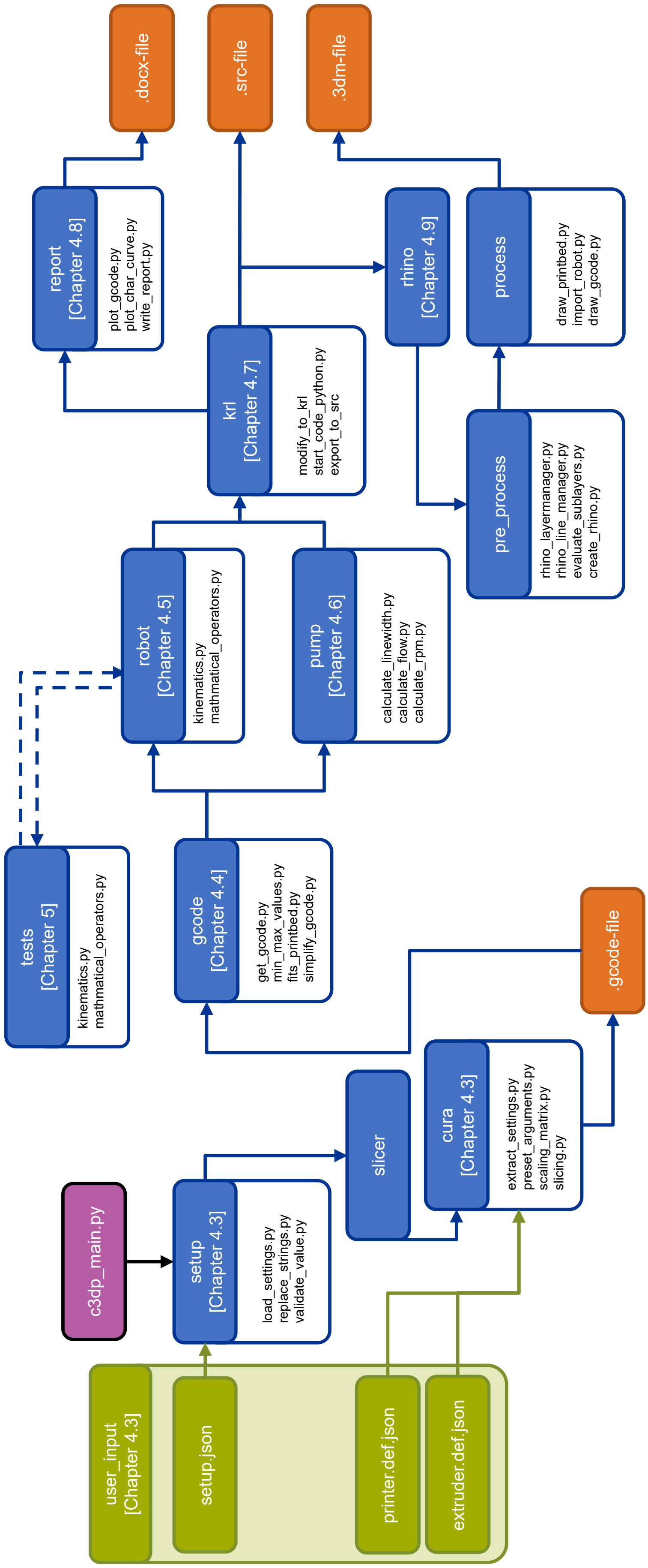

Figure 4.2 Overview of Program with All Implemented Modules and Information on Different Sub-Operations

4.3 Input Parameters [folder: *user_input*]

The user input required for executing the program is organized within the dedicated `user_input` module. This module consists of three *.json* files, which are divided into a general setup file (*setup.json*) and two configuration files required by Cura (*printer.def.json* and *extruder.def.json*).
The following section first focuses on the files relevant for interfacing with Cura.

Figure 4.3 Progress Bar for Chapter 4.3

4.3.1 Cura Setup [file: *printer.def.json* & *extruder.def.json*]

The configuration files required for the slicing process were taken directly from the installation directory of Ultimaker Cura 5.8.0. They contain, in a nested structure, all input parameters necessary for passing information about the printer and extruder to the slicer. The original versions of the duplicates included in the `user_input` folder can be found in the Cura installation directory at the following paths:

1. **Printer:** C:\Program Files\UltiMaker Cura 5.8.0\share\cura\resources\definitions
2. **Extruder:** C:\Program Files\UltiMaker Cura 5.8.0\share\cura\resources\extruders

The described files consist of nested dictionaries that assign a value to each process parameter. The value specified in the `"default_value"` field is used as the input during the slicing process when invoked via the CLI. Listing 4.3.1 provides an example of how an input parameter is defined in the *extruder.def.json* file.

Listing 4.3.1 Section from *extruder.def.json*

```
"machine_nozzle_size":
{
    "default_value": 25,
    "description": "The inner diameter of the nozzle. Chan
       ge this setting when using a non-standard nozzle si
       ze.",
    "label": "Nozzle Diameter",
    "maximum_value_warning": "100",
    "minimum_value": "0.001",
    "settable_per_extruder": true,
    "settable_per_mesh": false,
    "type": "float",
    "unit": "mm"
}
```

The *CuraEngine.exe*, which is used for the slicing process, retrieves only the most deeply nested parameters from the two *.def.json* files. Appendix C and D provide tabular overviews of all supported parameters along with their corresponding input types.
Unfortunately, due to the lack of output data in the generated G-code, it was not possible to retrieve all input parameters from the G-code file in post-processing. As a result, certain inputs are fundamentally excluded from use. These are explicitly marked in Appendix C and D. In addition, some inputs were deliberately fixed to avoid requiring duplicate user entries. Listing B.1 summarizes all such fixed parameters. Most of these variables are defined through user input in *setup.json* and must therefore be sourced from that file. For other fixed values, such as `"ironing_enabled"`, the necessary information could not be retrieved from the G-code and was therefore defined apriori to ensure a smooth process and avoid errors.
When creating new printer profiles or editing existing parameters for the printer or extruder, it is particularly important to ensure that the syntax throughout the entire *def.json* file is correct and that the

value specified under "default_value" matches the data type defined in the "type" field, as these are used in the slicing process as input values. A full validation of all arguments has been deliberately omitted due to the complex structure of the files and the large number of potential error sources. As a result, incorrect, incomplete, or inconsistent entries, as well as missing separators within the Cura specific input files, may lead to faulty execution of the program.
Replacing the existing files in the *user_input* directory with user-specific variants is entirely feasible. In addition to replacement, multiple printer profiles may be stored either in the *user_input* folder or in any other user-defined directory. The only requirement is that the corresponding path to the *printer.def.json* file is correctly specified in *setup.json* under the entry "cura_printer_config_file_path" (see Figure 4.4). Furthermore, the associated extruder file *extruder.def.json* must reside in the same folder and must be correctly referenced in *printer.def.json* under "machine_extruder_trains". An extension to additional slicers would also be possible at this point by adding new packages to the *slicer* directory.

4.3.2 General Setup [file: *setup.json*]

All remaining inputs that are not directly required for slicer operation are defined in *setup.json*. Figure 4.4 provides an overview of the various input parameters located under the *"settings"* section, along with their respective parent sections.
The structure of the *setup.json* file closely mirrors that of *extruder.def.json* and *printer.def.json*. The "Directory" section contains entries for both input and output files and folders. It is important to ensure that the value assigned to "input_name" refers exclusively to an *.stl* file, as this is required to prevent errors in the output. The existence of the specified input file is automatically checked within the main function. Output folders and file paths defined in *setup.json* are created automatically by the program if they do not already exist in the referenced directory.
The largest portion of user input in *setup.json* is found under the "Robot" section. These parameters, along with the entries under "Pump", are discussed in more detail in Chapter 4.5.2 and Chapter 4.6.
The slicer used is defined via the "slicer_name" field within the "Slicer" section. This ensures the correct mapping of line types listed in Chapter 3.2.4. If not developed any further in the future, only the entry "Cura" produces a complete output.
The "Cura" section contains slicer-specific input. Among other things, it specifies the path to the *CuraEngine.exe* file included with Cura 5.8.0. Additionally, the "cura_arguments" field allows arguments from *printer.def.json* and *extruder.def.json* that are normally read by *CuraEngine.exe* to be overwritten. Listing 4.3.2 shows an example input for this parameter.

Listing 4.3.2 Example Input for "cura_arguments" from *setup.json*

```
            "cura_arguments": {
                "description": "Additional arguments to quickly change the
                    settings for CURA slicing. These overwrite the values
                   in the printer and extruder config data",
                "value": {
                    "layer_height_0": "15",
                    "layer_height": "15",
                    "mesh_position_x": "0",
                    "min_wall_line_width": "25",
                    "retraction_enable": "true"
                },
                "type": "dict[str,str]"
```

If one of the input parameters predefined in Listing B.1 is nevertheless specified by the user in *setup.json*, it will be automatically overwritten by the corresponding default value during program execution. In such cases, the program issues a warning message but continues the execution process without interruption. Listing 4.3.3 provides an example of such a warning for the parameter "retraction_enable".

Listing 4.3.3 Console Output from Setup Validation with Error Message

```
[INFO] Validating and updating user arguments...
[INFO] retraction_enable = False from setup.json is valid
[WARNING] Preset value applied for 'retraction_enable': True
[INFO] Starting to slice Test Object.stl
```

The field "`cura_line_types_dict`" is used to group the line type identifiers defined by Cura into a set of uniform categories. This categorization is intended to ensure that adapting the program for use with other slicers does not require fundamental changes to the code structure. A total of eight line type categories are distinguished, of which types 1 through 7 can be explicitly assigned by the user:

1. **surface:** Lines that are coplanar with the object, typically lying within the X–Y plane.
2. **wall_outer:** The outermost, visible perimeter of the object.
3. **wall_inner:** All additional wall lines located within the object interior that are not visible in on the finished part.
4. **infill:** Material used to fill the space between inner and outer walls.
5. **bridge:** Lines that span unsupported regions and would hang freely in the air if support structure is not generated.
6. **curb:** A collective category for all bed-adhesion features, as shown in Figure 3.8.
7. **support:** Support material that is not part of the actual print object.
8. **unknown:** This internal category is not visible to the user. It serves as a fallback for any line types that cannot be matched to a predefined entry in "`cura_line_types_dict`" and is used as the default value during program execution.

The final section of input parameters is labeled "Rhino". All entries in this section directly affect the rendering and output of the *.stl* file as visualized tool paths in the generated *.3dm* file. Details on these inputs are provided in Chapter 4.9.

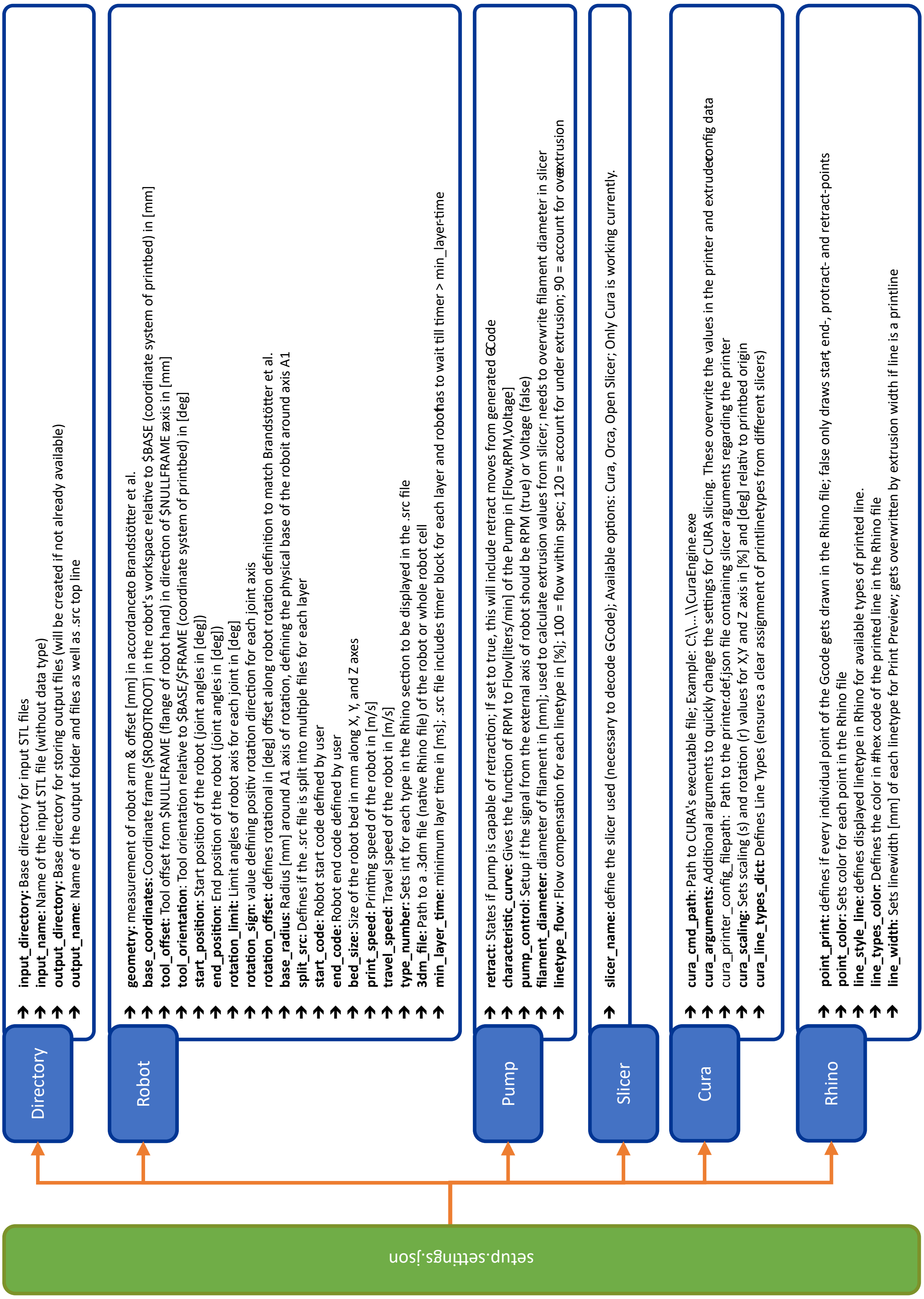

Figure 4.4 Overview of the Different Sections Included in *setup.json* With Descriptions of Each Input Parameter

4.3.3 Validation of User Input [module: *validate_value*]

To prevent potential errors in the *setup.json* file caused by incorrect user input, additional validation functions have been implemented within the `setup` package. As already established for *printer.def.json* and *extruder.def.json*, the data type for each user-defined parameter is explicitly specified within its respective entry. Table 4.2 provides an overview of all supported data types along with illustrative examples.

Table 4.2 Overview of Data Types Used in *setup.json*

Data Type	**Description**	**Example Value**
str	String	`KUKA KR340 R 3300`
int	Integer	`10000`
float	Floating Point Number	`43.99`
bool	Boolean	`false`
dict[str,str]	Dictionary [key = str, value = str]	`{'layer_height_0': '15', 'layer_height': '15', 'infill_li...'}`
dict[str,int]	Dictionary [key = str, value = int]	`{'A1': -1, 'A2': 1, 'A3': 1, 'A4': -1, 'A5': 1, 'A6': -1}`
list[str]	List [value = str]	`[';Printer: ?id?', ';Declarations for RSI']`
dict[str,list[int]]	Dictionary [key = str, value = list of int]	`{'A1': [-185, 185], 'A2': [-130, 20], 'A3': [-100, 144], ...}`
dict[str,list[str]]	Dictionary [key = str, value = list of str]	`{'surface': ['SKIN'], 'wall_outer': ['WALL-OUTER'], ...}`

If input data types inside *setup.json* are nested, simple constructs such as `dict[str, float]` are automatically recognized and recursively passed through the validation function until all input values have been fully checked to match the data type specified. For more complex, deeply nested data types, specific *if*-conditions have been implemented within the `validate_value` module to handle these cases in a targeted manner. When adding new input parameters in the future, this module must be extended accordingly.
If a user entry does not match the expected data type, the program issues a detailed error message pointing directly to the erroneous input location and terminates execution without producing any output. Once the error regarding data type has been corrected, the `main` function can be re-executed. An example of such an error message is shown in Listing 4.3.4.

Listing 4.3.4 Console Output from Setup Validation with Error Message

```
[ERROR] Invalid input in setup.json
[ERROR] Configuration error found
[WARNING] settings.Slicer.slicer_name: Invalid value '1' for type
          'str'
```

4.4 Parsing and Interpretation of G-Code [package: *gcode*]

Figure 4.5 Progress Bar for Chapter 4.4

If the G-code has been generated as described in Chapter 3 and stored in the directory specified by `"output_directory"`, it must subsequently be imported into Python. For this purpose, it is first necessary to determine which parts of the code are of essential relevance. To avoid unintended movements caused by the initialization and reset commands shown in Chapter 3.2.3, the program deliberately omits the code blocks at the beginning and end of the G-code that describe the actual print object. The corresponding user inputs in Cura are part of the fixed user parameters shown in Listing B.1, ensuring that accidental activation is excluded. Furthermore, the relevant fields in the *.def.json* files (see `"machine_start_gcode"`, `"machine_end_gcode"`, `"machine_extruder_start_gcode"` as well as`"machine_extruder_end_gcode"`) can be safely defined as empty strings.
The G-code itself is subsequently imported into Python as a list of strings via the module *`get_gcode`* and then parsed by the module *`min_max_values`* to determine the minimum and maximum coordinates within the list. As the full set of information on position is not always given from the start of the G-code, these serve as initial fallback values for the following module to ensure that complete coordinate information (X, Y, and Z) is available starting from line 1 of the G-code.
Using *regular expressions* (RegEx) and the corresponding Python library [102], the G-code is then analyzed. Listing 4.4.1 shows the relevant lines of code from the *`simplify_gcode`* module. Table 4.3 provides a detailed explanation of the associated search patterns.

Listing 4.4.1 RegEx Pattern Used in *`simplify_gcode`*

```python
    # Step 1: Define regex patterns
    type_pattern = r"(?i)[;$]?TYPE[:\s]*(.+)"
    gcode_pattern = r"(G[01])?(?:\s*F[\d\.]+)?(?:\s*X\s*([-?\d\.]+))
        ?(?:\s*Y\s*([-?\d\.]+))?(?:\s*Z\s*([-?\d\.]+))?(?:\s*E\s*([-?\d
        \.]+))?"
    feedrate_pattern = r"(G[01])\s*F[\d\.]+$"
    g92_pattern = r"G92\s+E0"  # Matches "G92 E0"

    # Step 2: Determine extrusion mode (M82/M83)
    absolute_mode = not any("M83" in line for line in gcode[:300])
```

Table 4.3 Explanation of Regular Expressions Used for Parsing G-Code

Regex Pattern	Explanation of Search Criteria
`type_pattern`	Finds a line containing the word `TYPE`, optionally preceded by `$` or `;`, using `[$;]?`. It is case-insensitive due to `(?i)` and allows colons or whitespace between `TYPE` and its value using `[:\s]*`. The value is captured in `(.+)`.
`gcode_pattern`	Parses G-code motion lines using `(G[01])?` for optional G0/G1 command, followed by optional feedrate `(?:\s*F[\d.]+)?`, and optional coordinates `X`, `Y`, `Z`, and extrusion `E`, each using non-capturing optional groups like `(?:\s*X\s*([-?\d.]+))`.
`feedrate_pattern`	Matches G0/G1 lines that end in a feedrate using `(G[01])\s*F[\d.]+$`. The line must end (`$`) after the feedrate expression, ensuring exclusivity of the match.
`g92_pattern`	Identifies an extrusion reset command `G92 E0` using `G92\s+E0`. Allows one or more spaces between `G92` and `E0` via `\s+`.

As shown in the listing, filtering is based on four distinct character sequences. The first step involves identifying the line type as explained in Chapter 3.2.3. Since all analyzed slicers indicate the type with the prefix `TYPE:`, this string is used as the primary search criterion. The string that follows is stored temporarily under the variable "`type_`" as the current line type.
Next, motion commands are filtered using the pattern "`gcode_pattern`". The relevant lines start with either `G0` or `G1` and represent the general commands that define the desired print path. The type of movement as discussed in Table 3.2 is automatically determined within the function and stored for further use under the variable "`move`". The associated coordinate and extrusion values are grouped and captured using parentheses "(" and ")" in the regular expression and continuously updated in the variables "`current_x`", "`current_y`", and "`current_z`". The value specified under `E`, which indicates the amount of extruded material, is also extracted and stored in the variable "`e_relative`". When interpreting the extrusion value, it is important to consider whether the G-code uses absolute or relative extrusion. This information is derived from the commands `M82` and `M83`, as explained in Table 3.2, and is always specified at the beginning of the G-code file (see Appendix A). The corresponding line is identified using the variable "`absolute_mode`" and is expected to be found within the first 300 lines of G-code (see Listing 4.4.1, Step 2). Based on this, the relative amount of extrusion per segment ("`E_Rel`") can later be calculated precisely (see Chapter 4.6).
As a third criterion, lines that contain only a feedrate value without any accompanying position or extrusion data are identified. Although these lines are not yet processed further, they are already considered in anticipation of a future extension that may incorporate speed information from the slicer.
Finally, the code filters for `G92` commands, which reset the extrusion value to zero. This information enables continuous calculation of the actual amount of material extruded during each linear movement. All other commands found in the G-code, such as temperature settings or fan controls (cf. Table 3.2) are ignored by the program, as they are not required for the subsequent steps. This is either due to the characteristics of the mineral-based material, which does not require as many commands as polymer material, or because the corresponding hardware components (like a part-cooling-fan) are not available or used in the given setup. This selective filtering streamlines data processing and improves the overall runtime of the program.
To ensure that the program remains largely independent of slicer-provided metadata in the G-code, the current layer height ("`Layer_Height`") and the layer number itself ("`Layer`") are determined automatically.
Listing 4.4.2 illustrates how the extracted information is stored as a *dictionary* for each individual line segment. Each new entry related to coordinates or extrusion in the G-Code results in the creation of a new dictionary. All dictionaries are then appended to a list for further processing. This list will be updated and extended during the execution of the program. Chapter 4.7 will discuss what the full set of information looks like before the file that numerically controls the robot is finally generated and exported. Finally, the maximum layer value is retrieved from the last dictionary in the list and stored in a dedicated variable within the `main` function.

Listing 4.4.2 Dictionary Generated for Each New Information Given on Coordinates, Line Type or Extrusion

```
            gcode_entry = {
                "Move": move,
                "X": current_x,
                "Y": current_y,
                "Z": current_z,
                "E_Rel": e_relative if move == "G1" else 0,
                "Layer": current_layer,
                "Type": type_,
                "Layer_Height": layer_height,
            }
```

4.5 Robot Integration and Kinematic Modeling [package: *robot*]

This chapter addresses the integration of the robot into the digital process chain, as well as the underlying kinematic modeling for a specific class of *6-DOF* serial robots. The objective is to implement a class within the program that enables verification of whether all positions contained in the G-code can be reached by the robot defined in *setup.json*.

Figure 4.6 Progress Bar for Chapter 4.5

For this purpose, the underlying coordinate systems are described first, followed by the mathematical foundations of the kinematic modeling. Subsequently, the implementation of the kinematic calculations itself is explained, which forms the basis for the physical execution of the robot's movements.

4.5.1 Coordinate Frames

The robot model used at the TUM is a serial manipulator with a spherical wrist. Since the axes A4 to A6 intersect at a single point, the combined kinematics of these three joints resemble that of a ball joint and are comparable to the human wrist. Figure 4.7 illustrates how the arrangement of axes in this wrist configuration differs from other robotic arm designs. The point of intersection of these three axes plays a crucial role in later simulation steps and is referred to as C_{wrist} in the following.

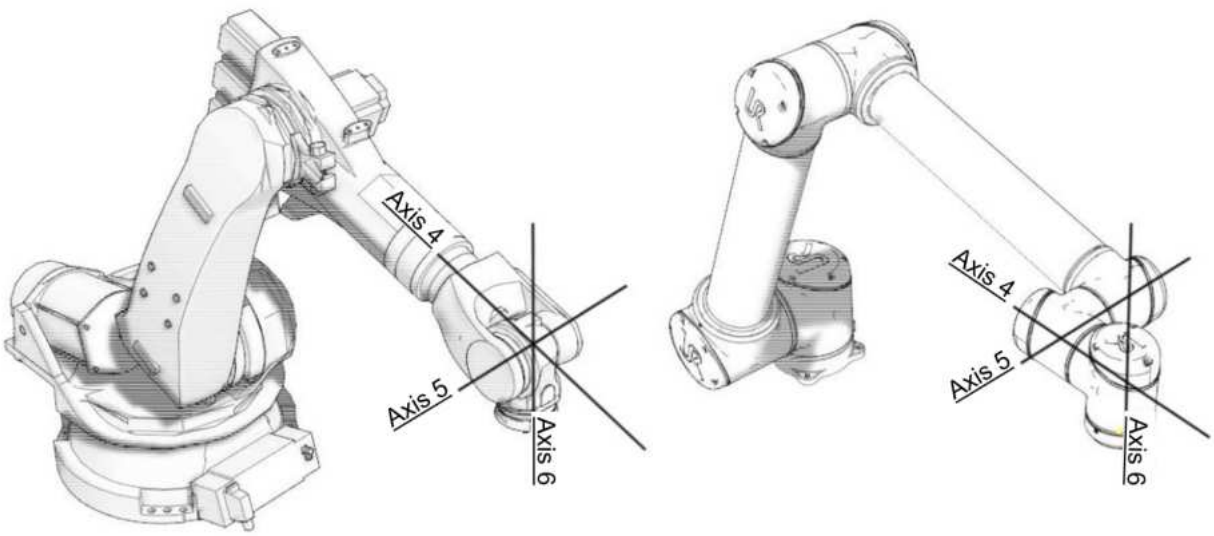

Figure 4.7 Comparison of Spherical and Non-Spherical Wrists for Serial Robots [27]

The coordinate frames of the remaining degrees of freedom (axes A1 to A3) are arranged orthogonally to one another. As a result, they can be transformed into adjacent coordinate systems by rotations of $\pi/2$ about one or more axes. Figure 4.8 illustrates the coordinate systems and axis orientations along the kinematic chain, as positively defined by the manufacturer for the KUKA KR 340 R3300. The Z-axis of each joint always represents the rotational axis (A_i) for the corresponding movement, with the rotation angle θ_i defined as mathematically positive.

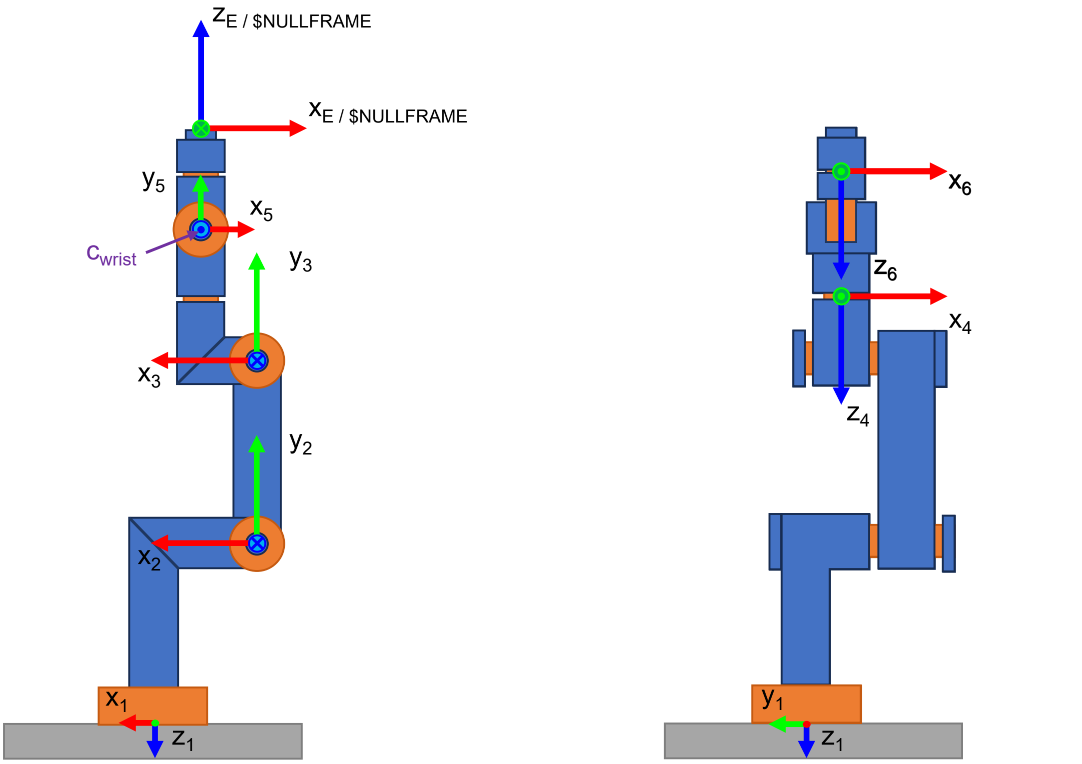

(a) Schematic of Robot in X-Z-Plane of $BASE **(b)** Schematic of Robot in Y-Z-Plane of $BASE

Figure 4.8 Coordinate Systems for Robot Joints of Kuka KR 340 R3300, Adapted from [16].

In addition to the robot-internal coordinate systems shown in Figure 4.8, external objects must also be assigned reference frames to be identified correctly in the following sections. This ensures a clear localization of both the robot relative to the print bed and the printed object relative to the robot. Following the naming conventions used in [41], the following coordinate frames are defined:

- **$BASE:** Origin of the print bed. Both the coordinates of the printed object and the robot's base position and orientation are referenced to this coordinate system.
- **$ROBOTROOT:** Coordinate system coinciding with the origin of axis A1 (cf. Figure 4.8a, 4.8b, axes x_1, y_1, and z_1). This coordinate system defines the robot's reference point relative to the print bed in the X-Y plane. Unlike the orientation shown in Figure 4.8, its Z-axis is defined to point upward.
- **$NULLFRAME:** Coordinate system located at the origin of axis A6; describes the orientation of the flange on the robot arm.
- **$TOOL:** Local coordinate system of the tool mounted on the flange.
- **$FRAME:** Temporary coordinate system of a point on the print path. Its orientation corresponds to that of $BASE, with the respective Z-axes aligned in parallel. When the robot moves to a coordinate, the origins of $NULLFRAME and $TOOL coincide. Moreover, the Z-axis of $TOOL is collinear with that of the currently addressed point, thereby excluding non-planar tool motions relative to the print bed.

Figure 4.9 illustrates the various coordinate systems in their overall context. The coordinate system of $ROBOTROOT is embedded within the robot base and thus not visible. Its orientation is aligned with that of the $BASE coordinate system. For clarity sake, the $TOOL reference frame has been omitted from the visualization; depending on the values specified under `"tool_offset"`, it could, for instance, be located in the extension of $NULLFRAME. Due to the chosen implementation, the $TOOL coordinate system must have the same orientation as $NULLFRAME.

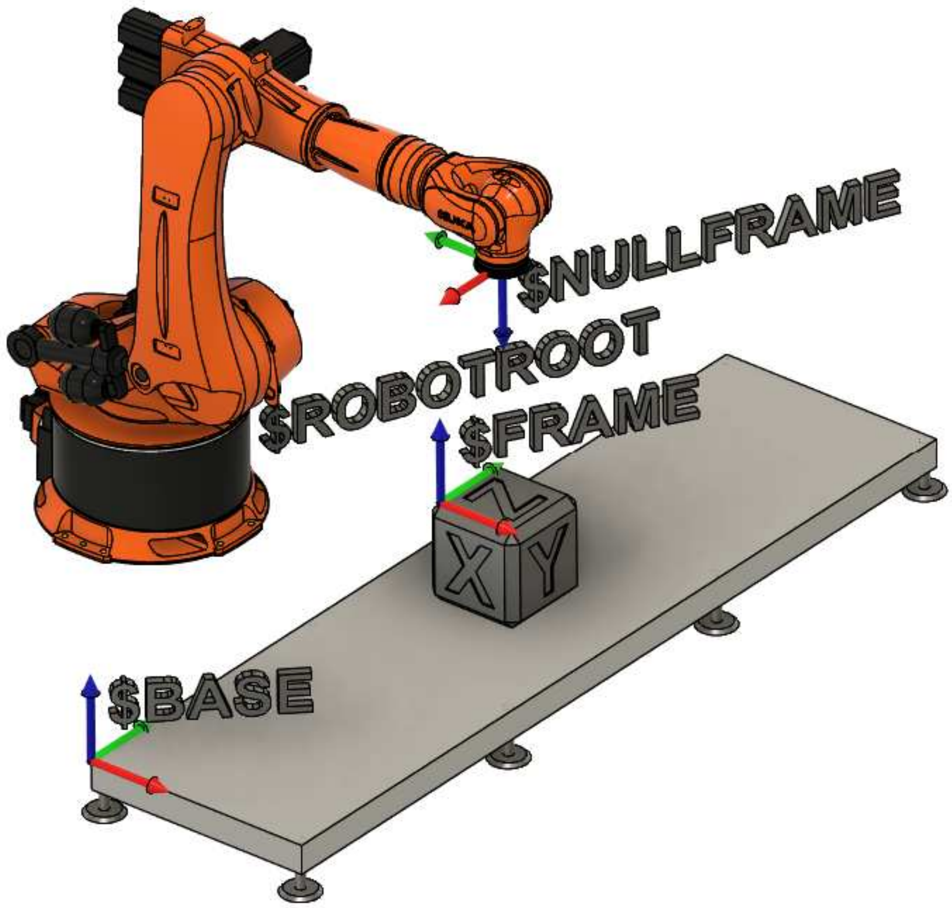

Figure 4.9 Overview of Relevant Coordinate Systems for Robot, Object and Bed Modeled in Fusion 360 [11]

All relevant local coordinate systems as well as the overarching reference frames have thus been described and clearly defined. The following chapter focuses on the required user inputs in *setup.json* that enable the integration of any robot with an identical kinematic structure into the program.

4.5.2 Robot Implementation Using *setup.json* [folder: *user_input*]

The definition of the robot used in the program has been implemented in a fully parametric manner, allowing the integration of various robot types with an identical geometric base structure. This ensures a modular program structure and allows the system to be used flexibly for future configurations or entirely different setups. The section "Robot" in *setup.json* is largely dedicated to this input.
To begin with, the user must specify the position of the robot relative to $BASE. For this purpose, the offset from $BASE to $ROBOTROOT is defined under `"base_coordinates"` in *setup.json*, as well as the rotations around the X, Y, and Z-axis using `"C"`, `"B"`, and `"A"`, respectively, in that order with reference to $BASE. Figure 4.10 schematically illustrates the corresponding dimensions.

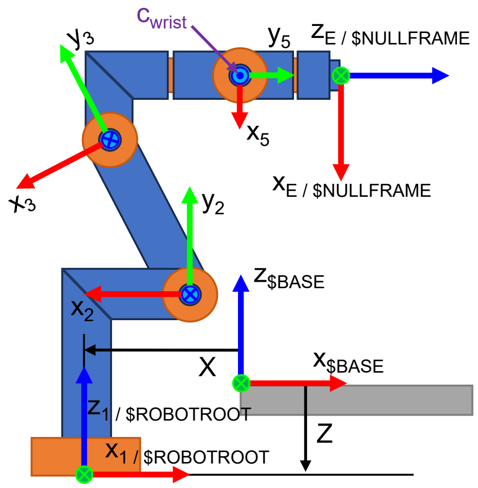

(a) Schematic of Robot Position in X-Z-Plane

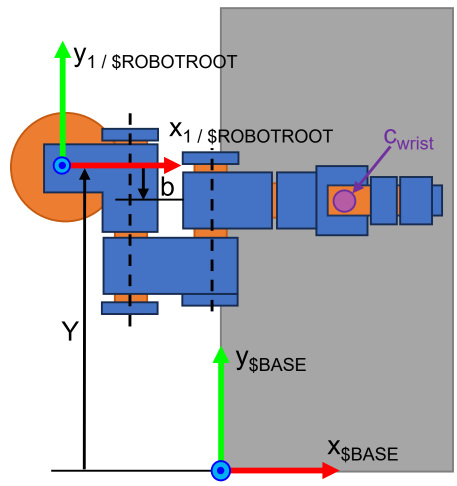

(b) Schematic of Robot Position in X-Y-Plane

Figure 4.10 Overview of `"base_coordinates"` Measurements for *setup.json*

Furthermore, the user must configure the robot's geometry according to the specifications provided by the manufacturer. The corresponding parameters are stored in the `"geometry"` dictionary within *setup.json*. Figure 4.11 illustrates all relevant dimensions in a schematic context.
In addition, the parameter `"base_radius"` defines the radius of the robot base around the Z-axis of $ROBOTROOT. This value is used in later processing steps to detect potential collisions between the robot arm and its own base. Unlike the illustration, the computational assumption takes a conservative approach by extending the base radius along the entire length of "c_1".

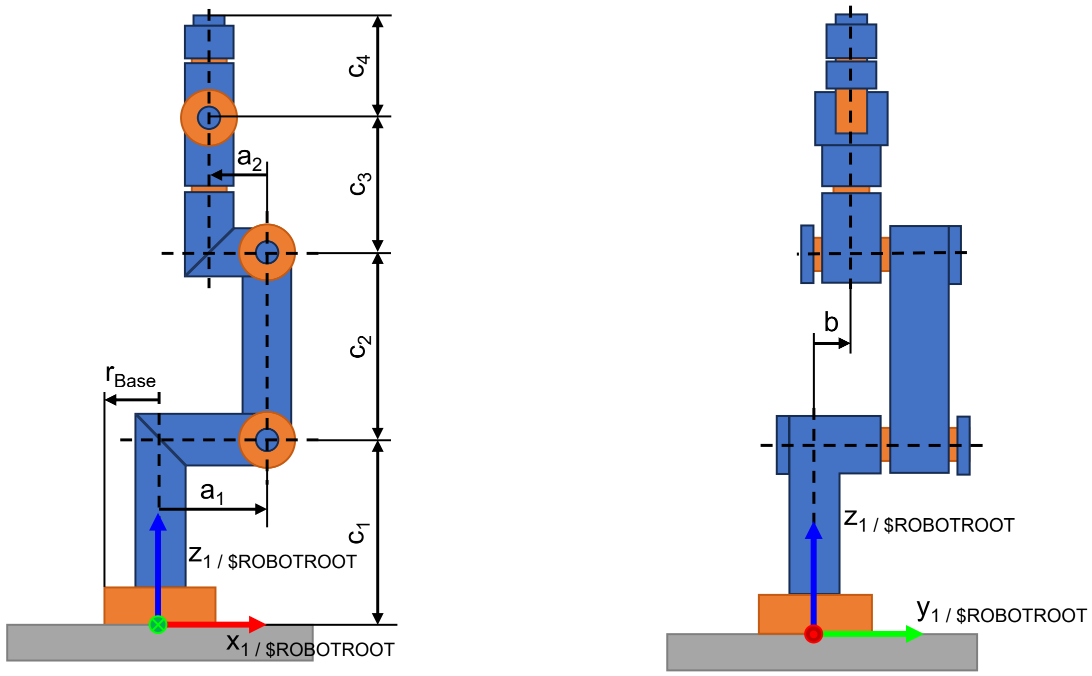

(a) Measurements of Robot in X-Z-Plane

(b) Measurements of Robot in Y-Z-Plane

Figure 4.11 Essential Measurements for Robotic Arm, Adapted from [16].

Besides the geometric properties of the robot arm, the dimensions of the tool head mounted on the robot's flange must also be specified by the user. For this purpose, the offset of the tool relative to the $TOOL coordinate system is defined in millimeters and can be customized using `"tool_offset"` inside *setup.json*. Figure 4.12 illustrates the relevant measurements in both side and top view.

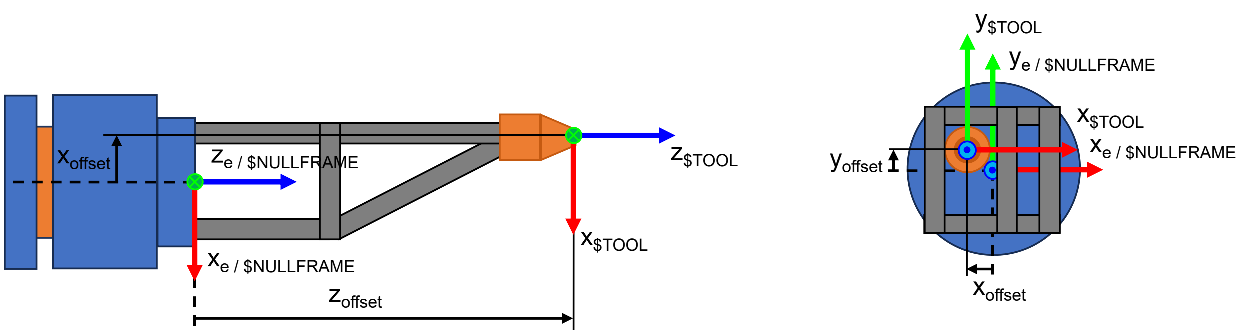

(a) Schematic of Tool-Offset Measurements in X-Z-Plane of Joint 6

(b) Schematic of Tool-Offset Measurements in X-Y-Plane of Joint 6

Figure 4.12 Overview of `"tool_offset"` Measurements for *setup.json*

Since the orientation of the tool relative to the print bed or the printed object must also be specified in addition to its dimensions, this is defined using the parameter `"tool_orientation"`. As previously explained, the orientation is given relative to $BASE as the reference coordinate system and remains constant throughout the printing process. The three parameters `"A"`, `"B"`, and `"C"` represent successive rotations about the Z-, Y-, and X-axes of $BASE, in the specified order.
The rotation is defined as *intrinsic*, meaning that the underlying coordinate system rotates along with each applied transformation. In contrast, an *extrinsic* rotation assumes a fixed coordinate system, where each rotation is applied with respect to the original global axes. Chapter 4.5.3 provides a more detailed explanation of the corresponding mathematical background.

Since the orientation of the coordinate systems of individual robot axes can vary depending on the manufacturers definition, the program must also allow for flexible input in this regard. To still ensure consistent internal processing, the direction of the Z-axis for each joint must be specified using the parameter `"rotation_sign"`. This parameter refers to the reference coordinate systems of each joint as illustrated in Figure 4.13.
The input is provided as a dictionary, in which each axis is assigned a *boolean*-value. A value of `"true"` indicates that the direction of the Z-axis for each joint as defined by the manufacturer corresponds to the reference system shown (cf. Figure 4.13). If the value is `"false"`, the Z-axis is inverted, while the *right-handed* structure of the coordinate system is preserved. Regarding the configuration defined by KUKA for the KR 340 R3300 (see Figure 4.8), this results in the dictionary for `"rotation_sign"` shown in Listing 4.5.1.

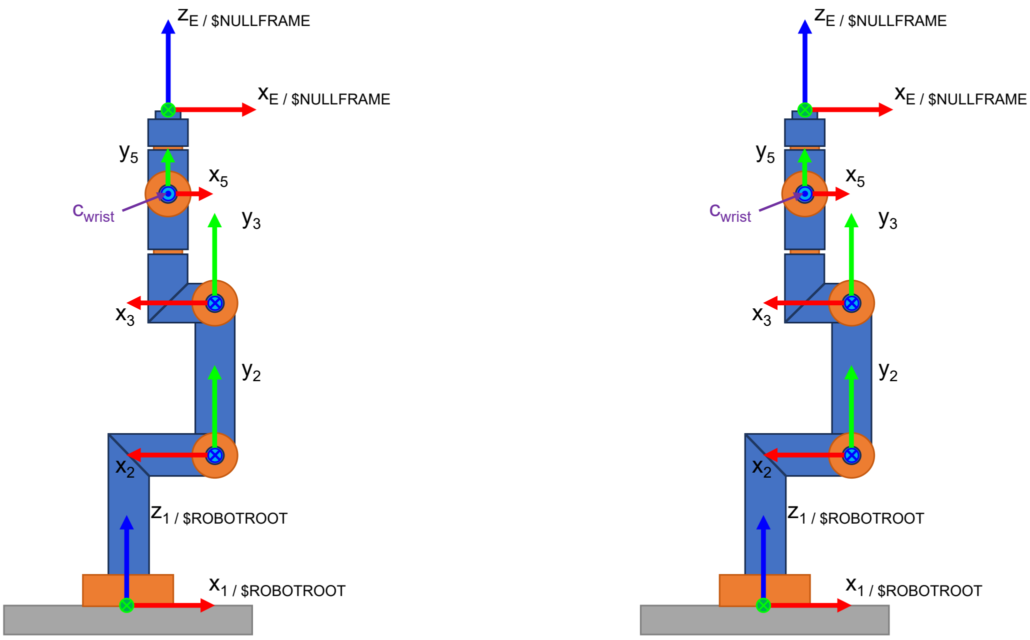

(a) Reference Coordinate Systems and Zero-Position of Robot in X-Z-Plane of $ROBOTROOT

(b) Reference Coordinate Systems and Zero-Position of Robot in X-Z-plane of $ROBOTROOT

Figure 4.13 Orientation of Coordinate Systems for Robotic Arm, according to [16].

To ensure that the robot does not collide with itself during motion execution, manufacturers typically specify limits for the rotational angles of each joint in both the positive and negative directions relative to the joint's zero position (i.e., joint rotation $= 0°$). Since the definition of this zero position can vary between manufacturers, it is necessary to again establish a unified convention within the program. The orientation shown in Figure 4.13 serves as the reference configuration referred to as the zero position, which is consistently used throughout the implementation.
To configure a specific robot, the deviation between the manufacturer's defined zero position and the referenced orientation must be specified. This is done with regard to the coordinate frames given in Figure 2.19b using the parameter `"rotation_offset"` in the *setup.json* file. Following that, the allowable joint angle ranges relative to the robot-specific coordinate systems can be defined using the parameter `"rotation_limit"`. Listing 4.5.1 provides an example of how these parameters are set for the KUKA KR 340 R3300 robot used in this study.

Listing 4.5.1 Example Input to Geometrically Define KUKA KR 340 R3300 Taken from *setup.json*

```
"id": {
    "description": "name of robot",
    "value": "KUKA KR340 R3330",
    "type": "str"
},
"geometry": {
    "description": "measurement of robot arm & offset [mm] in
       accordance to Brandst  tter et. al [https://de.mathwork
       s.com/matlabcentral/fileexchange/48468-inverse-kinemati
       cs-of-serial-robots-with-wrist?s%5C_tid=prof%5C_contrib
       lnk]",
    "value": {"a1": 500, "a2": 55, "b": 0, "c1": 1045, "c2": 1
       300, "c3": 1525, "c4": 290},
    "type": "dict[str,float]"
},
"base_radius": {
    "description": "Radius [mm] around A1 axis of rotation; en
       sures the robot head never intersects with its own base
        (around joint axis A1)",
    "value": 400,
    "type": "float"
},
"tool_offset": {
    "description": "Tool offset from $NULLFRAME (flange of rob
       ot hand) in direction of $NULLFRAME in [mm]; This leads
        to T($NULLFRAME,$TCP) as no rotation is involved",
    "value": {"X": -10.99, "Y": -0.86, "Z": 917.61},
    "type": "dict[str,float]"
},
"tool_orientation": {
    "description": "Tool orientation relative to $BASE/$FRAME
       (coordinate system of printbed) in [deg]; This leads to
        R($BASE/$FRAME,$TCP); A(angle related to Z), B(angle r
       elated to Y), C(angle related to Z)",
    "value": {"A": 0, "B": 0, "C": 180},
    "type": "dict[str,float]"
},
"rotation_sign": {
    "description": "value defining positiv rotation direction
       of axis; true == along z-axis definition, false == agai
       nst z-axis definition",
    "value": {"A1": false, "A2": true, "A3": true, "A4": false
       , "A5": true, "A6": false},
    "type": "dict[str,bool]"
},
"rotation_offset": {
    "description": "defines rotational in [deg] offset along r
       obot rotation definition to match 'Brandst  tter et al.
       '",
    "value": {"A1": 0,"A2": -90,"A3": 0,"A4": 0,"A5": 0,"A6":
       0},
    "type": "dict[str,float]"
},
"rotation_limit": {
    "description": "Limit angles of robot axis for each joint
       in [deg]; valid rotation is between those angles",
    "value": {"A1":[-185, 185], "A2":[-130, 20],"A3": [-100, 1
       44], "A4": [-350, 350],"A5": [-120, 120],"A6": [-350, 3
       50]},
    "type": "dict[str,list[int]]"
},
```

4.5.3 Mathematical Background [module: *mathematical_operators*]

The following section outlines the mathematical principles on which the computational methods for robot kinematics derived by [16] are based upon. Central to this is the definition of a *homogeneous transformation matrix*, which serves as the foundation for describing positions and orientations in general robotic configurations.
The purpose of a homogeneous transformation matrix is to transform a vector defined in a local coordinate system into another, typically global, coordinate system. After the transformation is applied, the vector is no longer expressed relative to its original base frame, but relative to the target frame. This allows for the consistent representation of kinematic chains across multiple coordinate systems.

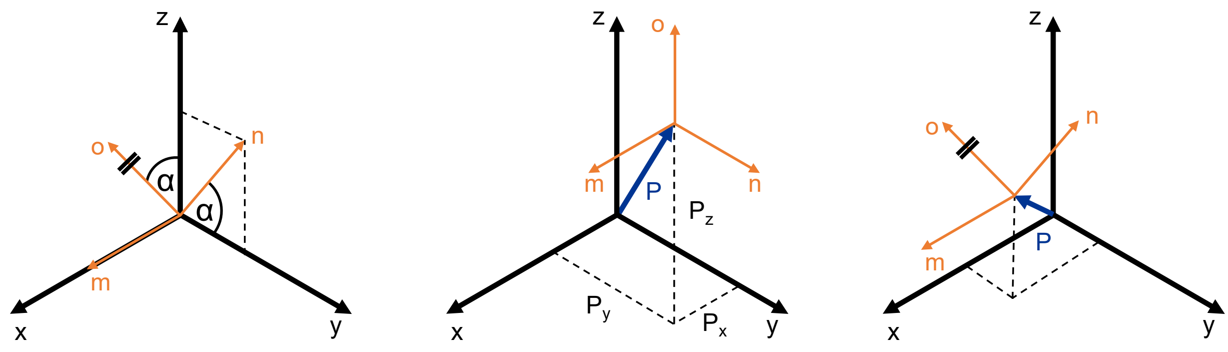

(a) Rotation **(b)** Translation **(c)** Transformation

Figure 4.14 Components of Spacial transformation

A homogeneous transformation matrix consists of two independently defined components (cf. Figure 4.14): a rotation and a translation. The translation describes the displacement of the coordinate origin (cf. Figure 4.14b), while the rotation (cf. Figure 4.14a) alters the orientation of the coordinate axes. In this process, for both rotation as well as translation the orthogonality of the coordinate system is preserved. Each component will be discussed in more detail in the following sections.

Rotation

The rotation consists of three successive partial rotations, each performed about one of the three principal axes of the coordinate system (X, Y, Z). As explained in Chapter 4.5.2, the rotation is carried out *intrinsically* in the present case. Figure 4.15 shows the corresponding rotation matrices for the individual spatial directions. A derivation of these matrices can be found in [35].

$$R_X(\alpha) = \begin{bmatrix} 1 & 0 & 0 \\ 0 & \cos\alpha & -\sin\alpha \\ 0 & \sin\alpha & \cos\alpha \end{bmatrix}$$

(a) Rotation About X-Axis

$$R_Y(\beta) = \begin{bmatrix} \cos\beta & 0 & \sin\beta \\ 0 & 1 & 0 \\ -\sin\beta & 0 & \cos\beta \end{bmatrix}$$

(b) Rotation About Y-Axis

$$R_Z(\gamma) = \begin{bmatrix} \cos\gamma & -\sin\gamma & 0 \\ \sin\gamma & \cos\gamma & 0 \\ 0 & 0 & 1 \end{bmatrix}$$

(c) Rotation About Z-Axis

Figure 4.15 Individual Rotation Matrices

Orientation is often described using the so-called *Euler*-angles, which are typically composed of a sequence of three elemental rotations. These rotations are taken from the principal axes X (*roll*), Y (*pitch*), and Z (*yaw*), and follow specific axis combinations of two of the three axes, such as XYX, XZX, or ZYZ, depending on the chosen convention. The subsequent use of all three rotational axes in this context is known as the *Bryan–Tait* definition [90, 24]. This definition is characterized by

the sequential application of the individual rotations in a specified order, mathematically expressed through the successive multiplication of the corresponding rotation matrices. This convention is used for movement calculation by both KUKA as well as the program itself.
In the case of an intrinsic rotation, the multiplication is carried out from right to left, where the leftmost matrix represents the last rotation to be applied, and the rightmost matrix corresponds to the first. For an XYZ rotation sequence, this means:

$$\mathbf{R}^{\text{intr.}}_{(\alpha,\beta,\gamma)} = R_Z(\gamma) \cdot R_Y(\beta) \cdot R_X(\alpha) \tag{4.1}$$

Rotation about the X-axis is therefore applied first, followed by rotation about the Y-axis and finally about the Z-axis. Each subsequent rotation is performed relative to the already transformed coordinate system.
A key characteristic of this rotational representation is that the order of rotations has a significant effect on the result. Since rotations in three-dimensional space are generally *non-commutative*, the following relation holds, for example:

$$R_X(\alpha) \cdot R_Y(\beta) \neq R_Y(\beta) \cdot R_X(\alpha) \tag{4.2}$$

The orientation of a body after a rotational operation depends significantly on the order in which the individual rotations about the principal axes are executed. Since rotations in three-dimensional space are non-commutative, the same set of angles can lead to different final orientations depending on the sequence in which they are applied. Therefore, the rotation order — for example, in the form of a ZYX or XYZ convention — must always be explicitly specified. Equation 4.3 shows the resulting overall rotation matrix for an intrinsic rotation in XYZ order:

$$\mathbf{R}^{\text{intr.}}_{(\alpha,\beta,\gamma)} = \begin{bmatrix} \cos\beta\cos\gamma & \cos\gamma\sin\alpha\sin\beta - \cos\alpha\sin\gamma & \cos\alpha\cos\gamma\sin\beta + \sin\alpha\sin\gamma \\ \cos\beta\sin\gamma & \cos\alpha\cos\gamma + \sin\alpha\sin\beta\sin\gamma & -\cos\gamma\sin\alpha + \cos\alpha\sin\beta\sin\gamma \\ -\sin\beta & \cos\beta\sin\alpha & \cos\alpha\cos\beta \end{bmatrix} \tag{4.3}$$

In the following, this notation for intrinsic rotations is used in a compact form. Here, A denotes the reference coordinate system in which the angles are defined, and B represents the target coordinate system:

$$\mathbf{R}_{A\to B} = \mathbf{R}^{\text{intr.}}_{(\alpha,\beta,\gamma)} = R_Z(\gamma) \cdot R_Y(\beta) \cdot R_X(\alpha) = \mathbf{R}_{XYZ}\left(\begin{bmatrix} \alpha \\ \beta \\ \gamma \end{bmatrix}\right) \tag{4.4}$$

To apply a rotation to a given vector, it must be multiplied point-wise (i.e., matrix-based) from the left by the previously computed rotation matrix. Equation 4.5 illustrates the structure of this operation using the system shown in Figure 4.14a as an example:

$$\begin{bmatrix} m \\ n \\ o \end{bmatrix} = \underbrace{\begin{bmatrix} R_{11} & R_{12} & R_{13} \\ R_{21} & R_{22} & R_{23} \\ R_{31} & R_{32} & R_{33} \end{bmatrix}}_{\text{Rotationmatrix } R} \cdot \begin{bmatrix} x \\ y \\ z \end{bmatrix} \tag{4.5}$$

In addition to the forward computation of the rotation matrix from given Euler-angles, it is also possible to compute the angle values from an existing rotation matrix. For this purpose, special variants of inverse trigonometric functions are used. Therefor most notably *atan2* is used, which determines both the angle magnitude and the correct quadrant unambiguously.
The following representation shows the corresponding formulas for calculating the two possible sets of solutions for the angles γ, β, and α, based on an XYZ rotation sequence. A detailed derivation can be found in [83].

$$\gamma_1 = -\arcsin(R_{13}) \quad (4.6) \qquad \gamma_2 = \pi - \gamma_1 \quad (4.7)$$

$$\beta_1 = \text{atan2}\left(\frac{R_{12}}{\cos\gamma_1}, \frac{R_{11}}{\cos\gamma_1}\right) \quad (4.8) \qquad \beta_2 = \text{atan2}\left(\frac{R_{12}}{\cos\gamma_2}, \frac{R_{11}}{\cos\gamma_2}\right) \quad (4.9)$$

$$\alpha_1 = \text{atan2}\left(\frac{R_{23}}{\cos\gamma_1}, \frac{R_{33}}{\cos\gamma_1}\right) \quad (4.10) \qquad \alpha_2 = \text{atan2}\left(\frac{R_{23}}{\cos\gamma_2}, \frac{R_{33}}{\cos\gamma_2}\right) \quad (4.11)$$

Since the sine function $\arcsin$ is not injective in the interval $[0; \pi]$, which means that multiple solutions can exist for a given value, more than one angle may correspond to the same function value. Consequently, each of the three Euler-angles has two possible solutions that differ by π (or $180°$), as illustrated in Equation (4.6) and Equation (4.7).
In the implementation of the `mathematical_operators`-module, only the first solution $(\alpha_1, \beta_1, \gamma_1)$ is computed. The second solution, however, is already incorporated in the kinematic calculations (see [16]) and can therefore be disregarded at this point.
A critical limitation of the Euler-angle and Bryon-Tait representation is the potential occurrence of a singularity for certain combinations of angle parameters. Specifically, when the pitch angle reaches $\pm 90°$ (i.e., $\beta = \pm\frac{\pi}{2}$), two of the three rotation axes align, resulting in the loss of one degree of freedom. This phenomenon is known as *Gimbal Lock* and prevents certain orientations from being uniquely defined. In such cases, rotations about the affected axes can cancel each other out, meaning that not all three degrees of freedom can be independently controlled. Figure 4.16 illustrates the loss of a degree of freedom due to overlapping rotation axes in a gimbal system.

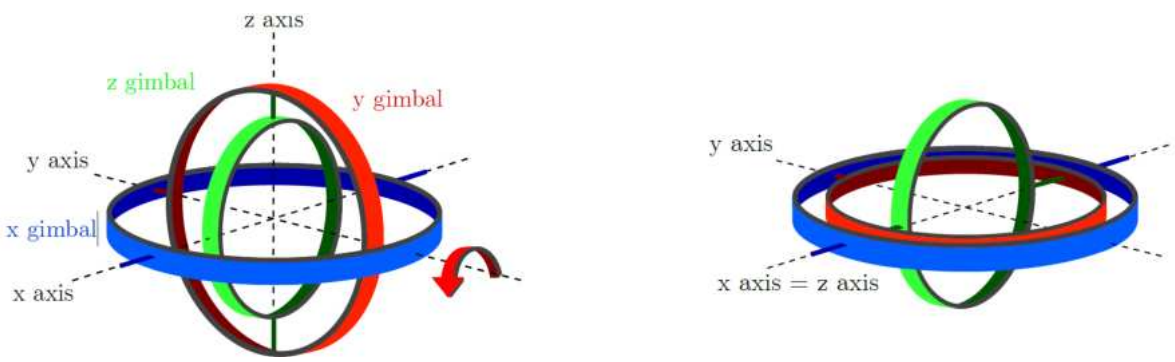

(a) Gimbal System in Base Configuration **(b)** Gimbal System with Gimbal-Lock between X and Z

Figure 4.16 Gimbal and Gimbal-Locked System, Taken from [110]

To counteract this phenomenon during computation of individual angles from a given rotation, it is necessary to explicitly handle this special case. An unambiguous solution is typically achieved by fixing one of the angles to a defined value (e.g., $\alpha = 0$), allowing the remaining two angles to be uniquely determined. The following equations show the solution for special case depicted in Figure 4.16 with $\beta = +\frac{\pi}{2}$.

$$\alpha = 0 \quad (4.12) \qquad \beta = \frac{\pi}{2} \quad (4.13) \qquad \gamma = \text{atan2}(R_{12}, R_{13}) \quad (4.14)$$

Alternatively, the issue of *Gimbal Lock* could be completely avoided by using the so-called *quaternion* representation. A detailed explanation of this approach can be found in [35]. However, since this issue occurs only rarely within the robots kinematics and the solution presented in Equations 4.12 – 4.14 is sufficient for the most relevant cases, the use of the more complex quaternion method is deliberately omitted in this thesis.

Translation

Translation, as illustrated in Figure 4.14b, refers to a pure shift of the origins position for the coordinate system in space. The input quantity required for this operation is the displacement vector $\mathbf{P}$, which specifies both the direction and the magnitude of the translation. It consists of the three displacement components in the X, Y, and Z directions and can be represented as shown in Equation 4.15:

$$\mathbf{P} = \begin{bmatrix} x_A \\ y_A \\ z_A \end{bmatrix} \tag{4.15}$$

To apply a translation to an existing vector $\mathbf{L}$, the corresponding displacement vector $\mathbf{P}$ must be added to it. Equation 4.16 schematically illustrates this operation:

$$\mathbf{L}_{\text{new}} = \mathbf{L} + \mathbf{P} = \begin{bmatrix} L_x \\ L_y \\ L_z \end{bmatrix} + \begin{bmatrix} P_x \\ P_y \\ P_z \end{bmatrix} = \begin{bmatrix} L_{x,new} \\ L_{y,new} \\ L_{z,new} \end{bmatrix} \tag{4.16}$$

Transformation

From the previously explained independent components of rotation (3×3 matrix) and translation (3×1 vector) between two different coordinate systems A and B a combined transformation matrix can be formulated based on the structure of a matrix-vector product, where A represents the base configuration and B the transformed system. However, as shown in Equation 4.17, a direct multiplication with a 3×1 vector is not defined:

$$\underbrace{\begin{bmatrix} R_{3\times3} & t_{3\times1} \end{bmatrix}}_{\text{3×4-Matrix}} \cdot \underbrace{\begin{bmatrix} \mathbf{v}_{3\times1} \end{bmatrix}}_{\text{3×1-Vector}} \quad \text{= not defined} \tag{4.17}$$

To ensure the compatibility of the multiplication, both the transformation matrix $T_{B\to A}$ and the vector are converted into the so-called *homogeneous coordinate space*. For this purpose, the 3×4 matrix is extended by a fourth row $[0 \quad 0 \quad 0 \quad 1]$, and the 3×1 vector is extended by an additional entry with the value 1, resulting in a 4×1 vector. This ensures that the translation component is preserved correctly during the multiplication, while the rotational part remains unchanged. Equation 4.18 shows the structure of the complete multiplication:

$$\underbrace{\begin{bmatrix} R_{11} & R_{12} & R_{13} & t_x \\ R_{21} & R_{22} & R_{23} & t_y \\ R_{31} & R_{32} & R_{33} & t_z \\ 0 & 0 & 0 & 1 \end{bmatrix}}_{\mathbf{T}_{B\to A}} \cdot \underbrace{\begin{bmatrix} x \\ y \\ z \\ 1 \end{bmatrix}}_{\mathbf{L}_A} = \underbrace{\begin{bmatrix} x_{\text{new}} \\ y_{\text{new}} \\ z_{\text{new}} \\ 1 \end{bmatrix}}_{\mathbf{L}_B} \tag{4.18}$$

To transform from system B back to system A, the transformation matrix must be inverted [58]. Since all coordinate systems used are orthonormal, the rotation matrix is orthogonal. In this case, the inverse equals the transpose [58]:

$$\mathbf{T}^{-1} = \mathbf{T}^{\top} \tag{4.19}$$

Transformations across multiple systems are also possible. In this case, the individual matrices can be multiplied. Each matrix links two adjacent coordinate systems. The following relation applies:

$$\mathbf{T}_{B\to A} \cdot \mathbf{T}_{A\to C} = \mathbf{T}_{B\to C} \tag{4.20}$$

This means that a transformation from system C through A into system B can be described by chaining the two individual transformations. The multiplication is always performed from right to left, in accordance with the order of reference systems. This property underlies hierarchical kinematic chains and is applied in the following sections.

4.5.4 Kinematic Modeling [module: *kinematics*]

As described in Chapter 2.6.1, the robot used in this thesis features a kinematic structure with an orthogonal-parallel base (axes A1 – A3) and a spherical wrist (axes A4 – A6). The `kinematics` module is therefore tailored specifically to this geometry. This so-called OPW architecture (**O**rtho-**P**arallel with spherical **W**rist) is characteristic of many industrial 6-DOF serial manipulators.
The basis for the calculations is an analytical solution to the kinematic problem for this robot configuration, as introduced by Brandstötter et al. [16]. Unlike the classical *Denavit–Hartenberg* parameterization [23], which is applicable to arbitrary joint configurations, this approach relies on a compact set of parameters that can be derived directly from the robot's mechanical dimensions. This allows for a more straightforward and robust implementation in the case of these specific robot types.
In general, the kinematic analysis of robotic systems distinguishes between two approaches depending on the given parameters.

1. **Forward Kinematics:** All joint angles (θ_1–θ_6) of the robot are known. The task is to determine the resulting position and orientation of the flange (i. e., $NULLFRAME) or the tool center point (TCP) with respect to the reference frame $ROBOTROOT. For each complete set of joint angles within the joint limits, there exists at most one valid solution.

2. **Inverse Kinematics:** The position and orientation of the TCP in space are given. The goal is to determine the joint angles required to reach this position. Depending on the pose and due to the multiple degrees of freedom of the robot, there may be one, multiple, or no valid solutions for the specified TCP or end-effector configuration.

For both problem types, the analytical method presented in [16] provides closed-form solutions, which are discussed in more detail in the following sections. An overview of the structure of the implemented module is shown in Figure 4.17. The Figure illustrates the contents of the class used to model the robot and outlines the required input and output values

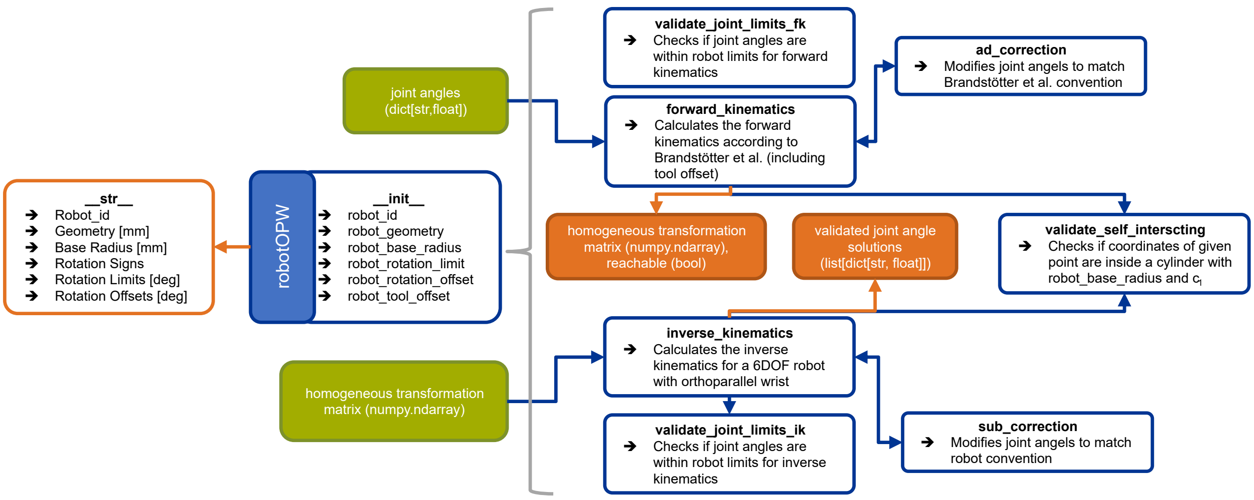

Figure 4.17 Overview of Class `robotOPW` from Module *kinematics* inside Package *robot*

Forward Kinematics

To compute the forward kinematics, the joint angles θ_1 to θ_6 are provided as input parameters. The function first verifies whether these values lie within the joint angle limits defined under "`rotation_limit`". If this condition is not met, the computation is terminated at this point, and an empty array is returned. Otherwise, the angles are transformed to the universal convention as depicted in Figure 4.13 and a complete homogeneous transformation matrix is calculated based on the equations presented in [16], describing the position and orientation of the robot flange relative to the base coordinate system $ROBOTROOT (or coordinate frame 1). A flowchart illustrating the main components of this function is shown in Figure 4.19.
The mathematical expressions required for the calculation are listed in Equations 4.21 to 4.34. These are derived in particular from the geometric relationships depicted in Figures 4.18a and 4.18b.
In the first step, the position-related solution is determined, which uniquely defines the location of the afore mentioned wrist center (C_{wrist}) in space. Once this has been established, the procedure of the program deviates from the method in [16] by introducing a self-collision check with the robot base. If the point C_{wrist} lies within a cylinder defined by the radius specified under "`base_radius`" and extending along the dimension "c_1" of the robot, the computation is likewise terminated.

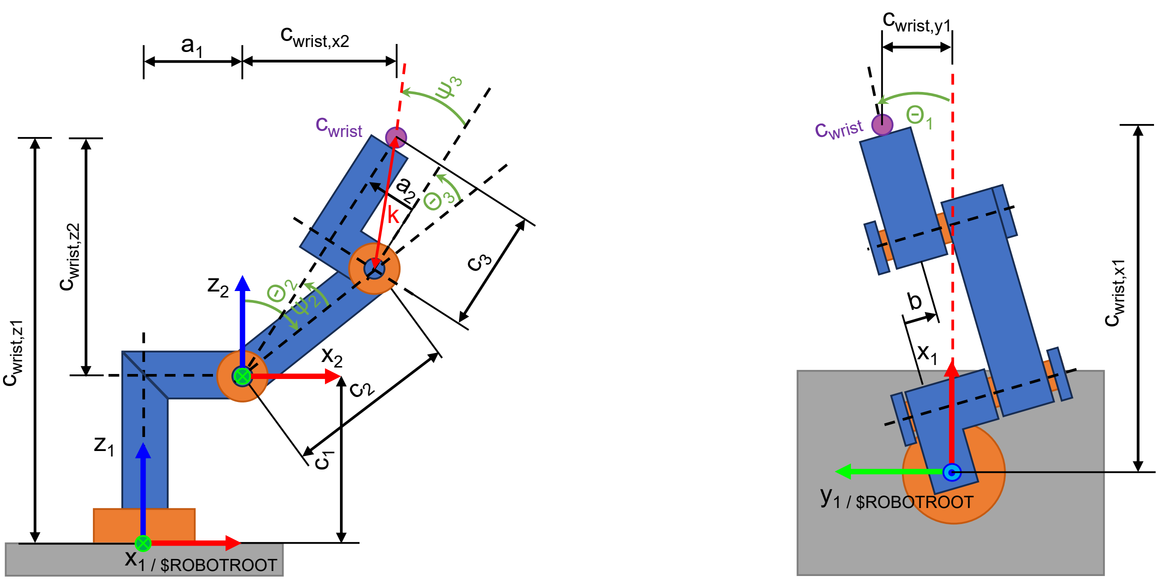

(a) Robot Given in X-Z-Plane Adapted from [16]

(b) Robot Given in X-Y-Plane

Figure 4.18 Necessary Measurements Needed to Determine Position of C_{wirst} wrt. $ROBOTROOT

$$\psi_3 = \arctan\left(\frac{a_2}{c_3}\right) \tag{4.21}$$

$$k = \sqrt{a_2^2 + c_3^2} \tag{4.22}$$

$$c_{wrist,x2} = c_2 \cdot \sin(\theta_2) + k \cdot \sin(\theta_2 + \theta_3 + \psi_3) + a_1 \tag{4.23}$$

$$c_{wrist,y2} = b \tag{4.24}$$

$$c_{wrist,z2} = c_2 \cdot \cos(\theta_2) + k \cdot \cos(\theta_2 + \theta_3 + \psi_3) \tag{4.25}$$

$$c_{wrist,x1} = c_{wrist,x2} \cdot \cos(\theta_1) - c_{wrist,y2} \cdot \sin(\theta_1) \tag{4.26}$$

$$c_{wrist,y1} = c_{wrist,x2} \cdot \sin(\theta_1) + c_{wrist,y2} \cdot \cos(\theta_1) \tag{4.27}$$

$$c_{wrist,z1} = c_{wrist,z2} + c_1 \tag{4.28}$$

Subsequently, the position and orientation of the end-effector are determined based on the location of the wrist center C_{wrist}. To do this, a vector of length "c_4" is added to the position of C_{wrist} in the direction of axis A6 (cf. Figure 4.11). The orientation results from the predefined alignment of axes A4 through A6.
The computation uses the rotation matrix $\mathbf{R}_{\$ROBOTROOT,\ \$NULLFRAME}$, which is calculated as shown in Equation 4.31 and describes the orientation of the end-effector relative to the robot base. In [16], this matrix is denoted as $\mathbf{R}_{0,E}$. By applying this matrix to the vector connecting C_{wrist} and the end-effector, its position in the $ROBOTROOT coordinate system can be determined.
The corresponding mathematical relationships are presented in Equations 4.29 through 4.32.

$$\mathbf{R}_{\$ROBOTROOT \to C_{wrist}} = \mathbf{R}_{A1,\ A2,\ A3}\left(\begin{bmatrix}\theta_1\\ \theta_2\\ \theta_3\end{bmatrix}\right) \tag{4.29}$$

$$\mathbf{R}_{C_{wrist} \to \$NULLFRAME} = \mathbf{R}_{A4,\ A5,\ A6}\left(\begin{bmatrix}\theta_4\\ \theta_5\\ \theta_6\end{bmatrix}\right) \tag{4.30}$$

$$\mathbf{R}_{\$ROBOTROOT \to \$NULLFRAME} = \mathbf{R}_{\$ROBOTROOT \to C_{wrist}} \cdot \mathbf{R}_{C_{wrist} \to \$NULLFRAME} \tag{4.31}$$

$$\mathbf{f} = \begin{bmatrix} c_{wrist,x1} \\ c_{wrist,y1} \\ c_{wrist,z1} \end{bmatrix} + c_4^{\$NULLFRAME} \cdot \mathbf{R}_{\$ROBOTROOT \to \$NULLFRAME} \begin{bmatrix} 0 \\ 0 \\ 1 \end{bmatrix} \tag{4.32}$$

The result from Equation 4.32 describes the position of the robot flange with respect to $ROBOTROOT. For the origin of this coordinate system, again a self-collision check with the robot base is performed.
Since the formulation in [16] does not account for additional tool attachments on the robot, the equation set was extended accordingly. It is assumed that the tool does not exhibit any rotation relative to the coordinate system of the robot flange ($NULLFRAME), and that only a translational offset in the X, Y, or Z direction exists between $NULLFRAME and the TCP. The corresponding input values for this tool offset are extracted from the dictionary under the key `"tool_offset"` (cf. Chapter 4.5.2). As shown in Equation 4.33, this offset can also be computed by multiplying it with $\mathbf{R}_{\$ROBOTROOT \to \$NULLFRAME}$ (referred to as $\mathbf{R}_{0,E}$) and subsequently adding it to the position vector $\mathbf{f}$.

$$\mathbf{t} = \mathbf{f} + \mathbf{R}_{0 \to E} \begin{bmatrix} x_{\texttt{tool\_offset}} \\ y_{\texttt{tool\_offset}} \\ z_{\texttt{tool\_offset}} \end{bmatrix} \tag{4.33}$$

If no self-collision is detected between the TCP and the virtual robot base, the homogeneous transformation matrix $\mathbf{p}$ for the vector $\mathbf{t}$ is constructed. It consists of the rotation matrix $\mathbf{R}_{0,E}$ and the vector $\mathbf{t}$ as the translational component. The resulting matrix describes the position and orientation of the TCP, as determined by the provided joint angles θ_1 through θ_6, relative to the coordinate system $ROBOTROOT (cf. Equation 4.34).

$$\mathbf{p}_{homogeneous,\,\$ROBOTROOT} = \begin{bmatrix} \mathbf{R}_{0 \to E} & \mathbf{t} \\ \mathbf{0}_{1\times 3} & 1 \end{bmatrix} \tag{4.34}$$

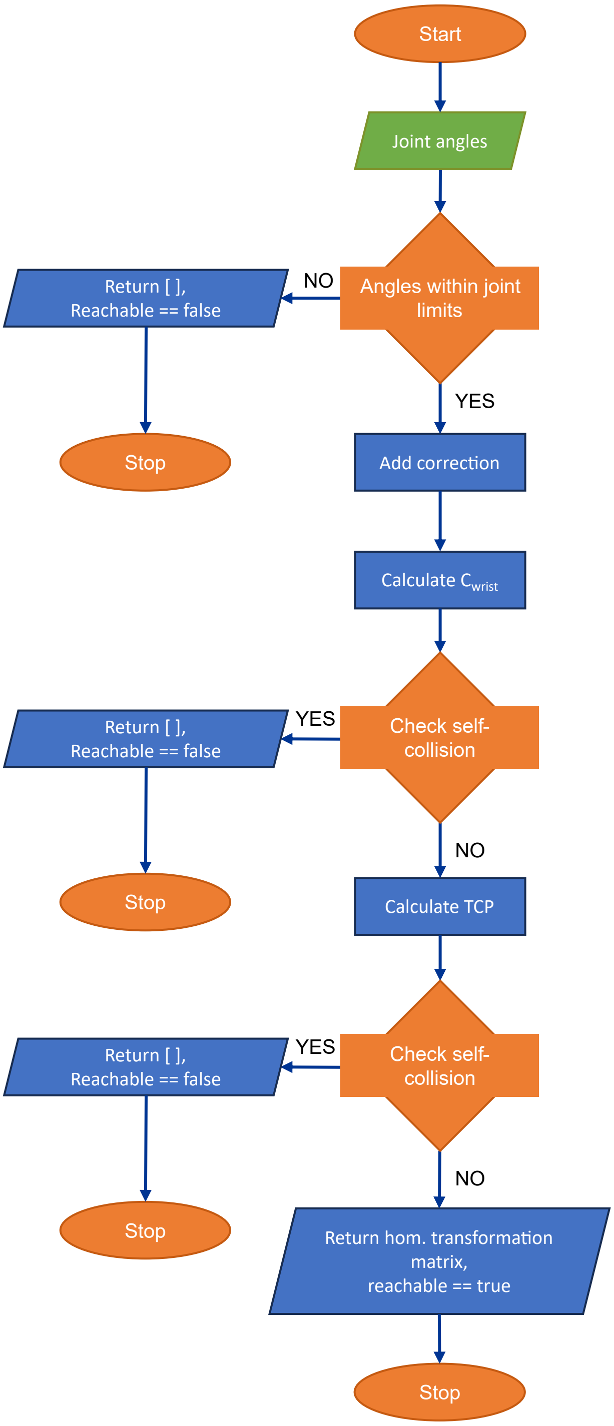

Figure 4.19 Flowchart for `forward_kinematics`-Function Inside `robotOPW`-Class

Inverse Kinematics

For the inverse kinematics, a homogeneous transformation matrix is provided that describes both the orientation and the position of the TCP relative to $ROBOTROOT. Since all joint angles of the robot are apriori unknown, the implementation is considerably more complex compared to the forward kinematics and can yield up to eight individual solutions depending on the arm's configuration (cf. [16]).
To reduce computational effort and improve runtime, all standardizable pre-processing steps are consolidated before passing the homogeneous transformation matrix to *robotOPW*. This includes converting the coordinates defined by the G-code (given relative to $BASE) into the $ROBOTROOT coordinate system. This transformation is possible because all required input values are already known. Figure 4.20 illustrates all relevant coordinate systems given, as well as the transformation matrices that can be derived from the given inputs. The direction of each arrow corresponds to the direction defined by the respective input transformation matrix. As previously explained in Chapter 4.5.1, it is important to note that the origins of $FRAME and the TCP are coincident, while the robot is commanded to move to the point specified by $FRAME.

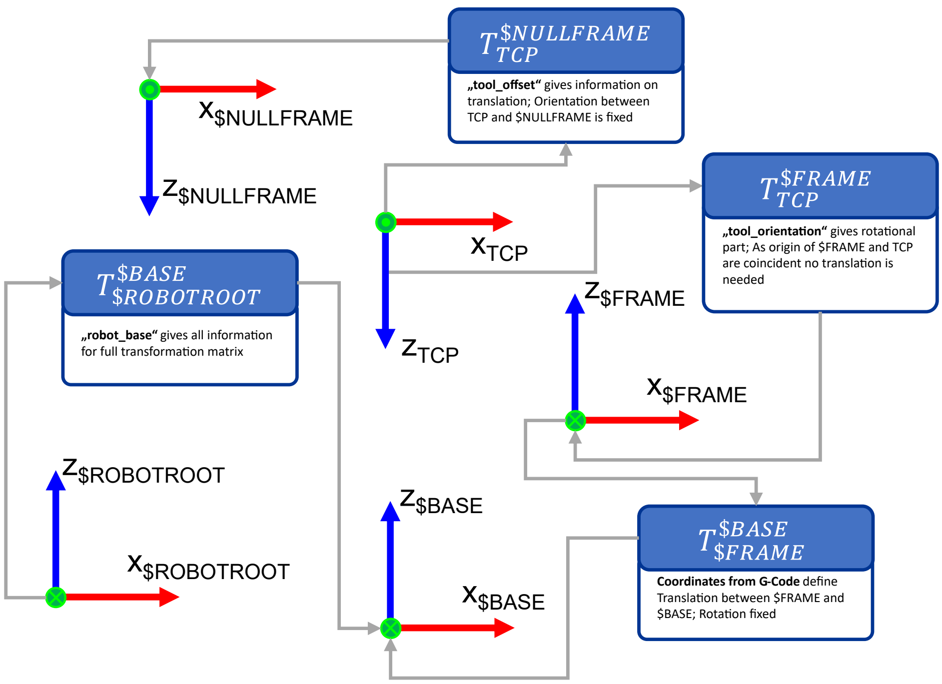

Figure 4.20 Coordinate Frames and Available Transformation Matrices

To construct the homogeneous transformation matrix, the rotational component is first derived. Equations 4.35 to 4.37 illustrate how this rotational part is composed.

$$\mathbf{R}_{\$ROBOTROOT \to \$BASE} = R_{ZYX}\left(\begin{bmatrix} C_{\texttt{base\_coordinates}} \\ B_{\texttt{base\_coordinates}} \\ A_{\texttt{base\_coordinates}} \end{bmatrix}\right) \tag{4.35}$$

$$\mathbf{R}_{TCP \to \$BASE} = R_{ZYX}\left(\begin{bmatrix} C_{\texttt{tool\_orientation}} \\ B_{\texttt{tool\_orientation}} \\ A_{\texttt{tool\_orientation}} \end{bmatrix}\right) \tag{4.36}$$

$$\mathbf{R}_{TCP \to \$ROBOTROOT} = \mathbf{R}^T_{\$BASE \to \$ROBOTROOT} \cdot \mathbf{R}_{TCP \to \$BASE} \tag{4.37}$$

The translational component, which expresses an arbitrary point $(\mathbf{p})$ from $BASE in $ROBOTROOT, can be determined by combining and extending the previously introduced information into a homogeneous transformation matrix using the already introduced extension of $[0 \quad 0 \quad 0 \quad 1]$ in the last row of the matrix:

$$\mathbf{T}_{\$ROBOTROOT \rightarrow \$BASE} = \begin{bmatrix} [\mathbf{R}_{\$ROBOTROOT \rightarrow \$BASE}] & \begin{bmatrix} x_{\texttt{base\_coordinates}} \\ y_{\texttt{base\_coordinates}} \\ z_{\texttt{base\_coordinates}} \end{bmatrix} \\ 0 \quad 0 \quad 0 & 1 \end{bmatrix} \tag{4.38}$$

$$\mathbf{p}^{\$ROBOTROOT} = \mathbf{T}^{\top}_{\$BASE \rightarrow \$ROBOTROOT} \cdot \mathbf{p}^{\$BASE} \tag{4.39}$$

The complete homogeneous transformation matrix for an arbitrary point from the G-code is shown in Equation 4.40. This matrix can now be passed to `robotOPW` to determine all possible joint configurations.

$$\mathbf{p}^{\$ROBOTROOT}_{homogeneous} = \begin{bmatrix} [\mathbf{R}_{TCP \rightarrow \$ROBOTROOT}] & \begin{bmatrix} \mathbf{p}_{x,\ \$ROBOTROOT} \\ \mathbf{p}_{y,\ \$ROBOTROOT} \\ \mathbf{p}_{z,\ \$ROBOTROOT} \end{bmatrix} \\ 0 \quad 0 \quad 0 & 1 \end{bmatrix} \tag{4.40}$$

As described for the forward kinematics, the inverse kinematic was also extended to account for an offset between the $TOOL and $NULLFRAME. To achieve this, the coordinates defined under `"tool_offset"` are first transformed into the $ROBOTROOT frame using $\mathbf{R}_{TCP \rightarrow \$ROBOTROOT}$ (cf. Equation 4.41 and 4.42). The position of C_{wrist} is then determined using Equation 4.43. A check for potential self-collisions of this point as well as compliance with the specified joint limits is also implemented in the program (see Figure 4.21).

$$\texttt{tool\_offset}^{\$ROBOTROOT} = \mathbf{R}_{TCP \rightarrow \$ROBOTROOT} \cdot \begin{bmatrix} x_{\texttt{tool\_offset}} \\ y_{\texttt{tool\_offset}} \\ z_{\texttt{tool\_offset}} \end{bmatrix} \tag{4.41}$$

$$c_4^{\$ROBOTROOT} = c_4^{\$NULLRAME} \cdot \mathbf{R}_{TCP \rightarrow \$ROBOTROOT} \begin{bmatrix} 0 \\ 0 \\ 1 \end{bmatrix} \tag{4.42}$$

$$\mathbf{C}^{\$ROBOTROOT}_{wrist} = \begin{bmatrix} p_{x,\ \$ROBOTROOT} \\ p_{y,\ \$ROBOTROOT} \\ p_{z,\ \$ROBOTROOT} \end{bmatrix} - \begin{bmatrix} x_{\texttt{tool\_offset}} \\ y_{\texttt{tool\_offset}} \\ z_{\texttt{tool\_offset}} \end{bmatrix} + \mathbf{c}_4^{\$ROBOTROOT} \tag{4.43}$$

The remaining steps of the inverse kinematics follow the formulation presented in [16] and are therefore not discussed in detail. However, it should be noted that the formulation provided in [16] does not yield a unique solution in the case of a singularity at $\theta_5 = 0$. In this configuration, the rotation axes of θ_4 and θ_6 become collinear according to the coordinate definition in [16] (see Figure 4.8b). This situation corresponds to the *Gimbal Lock* case described in Chapter 4.5.3.
To still obtain a unique solution whithin the program , the rotation around θ_4 is set to zero, and only θ_6 is used to apply the required orientation. Reference [82] provides an overview of the typical singularity scenarios encountered in 6-DOF serial robots. Other singularities, apart from the so-called *wrist singularity*, in which axes A4 and A6 are collinear are not considered further, as they are not deemed relevant for the printing process with the given robot configuration.
As a result, it is now possible to verify the reachability of all given positions and joint angles. In addition a corresponding validation of the calculations has been conducted and is described in more detail in Chapter 5.1.2.

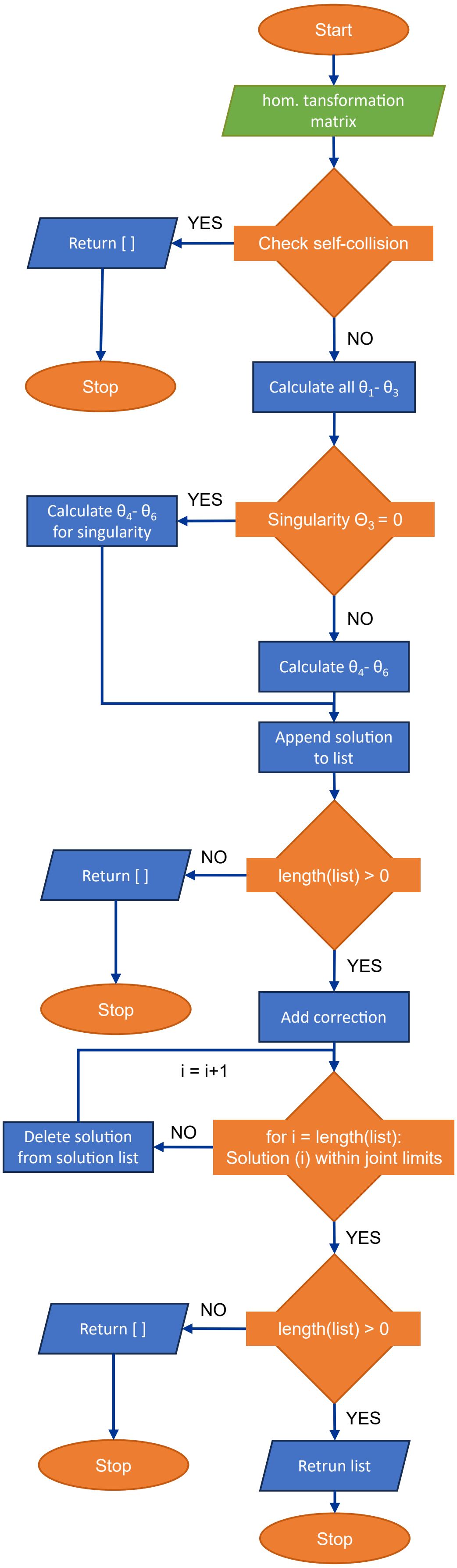

Figure 4.21 Flowchart for *inverse_kinematics*-Function Inside *robotOPW*-Class

4.6 Analysis of Line Geometry and Extrusion Values [package: *pump*]

Figure 4.22 Progress Bar for Chapter 4.6

4.6.1 Calculation of Line Width [module: *calculate_linewidth*]

The objective of this module is to determine the appropriate amount of material for each printing movement, thereby enabling integration of the pump into the process. To achieve this, the effective line width of each segment must first be calculated. This information is essential not only for controlling the extrusion precisely, but also for visualizing the print path in the Rhino model.
Since the line width of individual extrusion movements is not explicitly included in the G-code after slicing, and no geometric data from the associated *.stl* file can be extracted, the actual line width must be reconstructed from the extrusion values (`E`-values) contained in the G-code. Equation 4.44 shows the formula used by Cura to compute the `E`-value, from which the deposited line width can be derived in reverse [20]. As this is a secondary source and no official published formula could be identified, the equation used here was additionally validated through multiple control calculations and found to be plausible.

$$E_{\text{value}} = \frac{h \cdot SF \cdot d_n \cdot l}{\frac{\pi}{4} d_f^2} = \frac{4 \cdot h \cdot SF \cdot d_n \cdot l}{\pi \cdot d_f^2} \tag{4.44}$$

Table 4.4 Definition of Variables Used in Equation 4.44

Symbol	Name	Unit	Input
h	Layer height	mm	calculated
SF	Flow value	–	`"lintype_flow"` from *pump.setup.json*
d_n	Line width	mm	–
l	Segment length	mm	calculated
d_f	Filament diameter	mm	`"filament_diameter"` from *pump.setup.json*
E_{value}	Extrusion value	mm	G-Code input (relative value)

Cura assumes an idealized rectangular geometry for the extruded segment when calculating the material volume. The volume V of the deposited line segment is determined by the product of the layer height h, a scaling factor SF, the line width d_n, and the segment length l, i.e., $V = h \cdot SF \cdot d_n \cdot l$.
To provide this volume during the printing process, Cura advances a filament strand with a known diameter d_f and circular cross-section. The required feed length of the filament is defined in the G-code using the `E`-value. Figure 4.23 illustrates the geometric relationship.

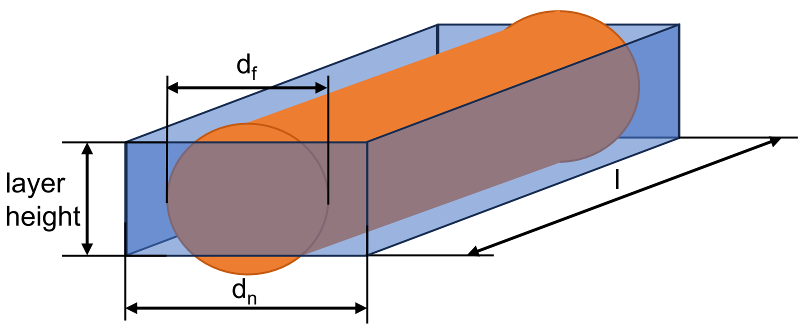

Figure 4.23 Geometry for Filament and Line Segment

The flow rate for each line segment cannot be retroactively extracted from the G-code, but it has already been assigned to a predefined line type via the *setup.json* file. This allows it to be uniquely traced for each line. Since all other parameters are known, the line width d_n remains the only unknown in the equation. The formula can therefore be rearranged to solve for d_n for each line segment.

$$d_n = \frac{E_{\text{value}} \cdot \pi \cdot d_f^2}{4 \cdot h \cdot SF \cdot l} \tag{4.45}$$

The following section explains how the line width calculated in this manner can be translated into commands for controlling the pump.

4.6.2 Calculation for Pump Commands [module: *calculate_flow*, *calculate_rpm*]

Flow [module: *calculate_flow*]

As described in Chapter 2.6.2, the pump serves a role analogous to the extruder of a conventional FDM printer by continuously supplying material to the nozzle throughout the printing process. For this, the volume of an entire line segment is extruded within a defined time interval.
The decisive factor for this is the nozzle's travel speed along the length of the segment (in mm/s), as it directly determines the required volumetric flow rate $\mathbf{q}_{flow}$ of the pump, which is specified in liters per minute. Ideally, the exact local speed profile along each line segment would be known to dynamically adapt the flow rate. However, since the actual travel speed cannot be predicted precisely as it is highly dependent on the orientation as well as prior or following commands, only the target speed specified by the user in the *setup.json* file under `"print_speed"` in m/s is available.
Equation 4.46 shows how this information based on the known parameters is used to calculate the required flow rate in mm^3/s:

$$\mathbf{q}_{\text{flow}}^{[\mathrm{mm}^3/\mathrm{s}]} = d_n^{[\mathrm{mm}]} \cdot h^{[\mathrm{mm}]} \cdot v_{\text{print}}^{[\mathrm{m/s}]} \cdot 1000^{[\mathrm{mm/m}]} \tag{4.46}$$

Conversion of Flow to RPM and Voltage [module: *calculate_rpm*]

Since the pump cannot be directly controlled via a volumetric flow rate, the calculated flow value must be converted into a usable control parameter. For this purpose, the pumps so-called *characteristic curve* is used, which describes the flow rate at the pump outlet as a function of the motor speed (abbreviated as rpm) or the motor voltage (V).
As no characteristic curve has been specified by Knauf PFT GmbH & Co. KG, a linear relationship is assumed for the example input: from 0 rpm at 0 L/min and 0 V up to 458 rpm at 90 L/min and 10 V, which corresponds to the maximum motor input voltage and flow rate of the pump [66].
Alternatively, the user can define a custom pump characteristic curve in the *setup.json* file under `"characteristic_curve"`. The input is provided as a nested list, in which specific support points (defined by [Flow, RPM, Voltage]) along the curve are specified. Listing 4.6.1 shows an example configuration.

Listing 4.6.1 Example Input `"characteristic_curve"` of Pump in *setup.json*

```
"characteristic_curve": {
    "description": "Gives the function of RPM to Flow[liter/min] of the Pump in [Flow,RPM,Voltage]",
    "value": [[10,146,1],[0,0,0],[90,456,10]],
    "type": "list[list[float,float,float]]"
},
```

The discrete points are sorted in ascending order by *rpm* within the module, and the characteristic curve is calculated by mapping discrete points of the flow value from `calculate_flow` and interpolating linearly between two discrete values. The same is done for the given voltage numbers. The result

yields a continuous graph for rpm or voltage, which is then used to automatically control the pump during the printing process.
The user can choose whether the pump is controlled via voltage or rotational speed in the output *.src* file; this selection is also made in *setup.json* under the key `"pump_control"`. The input specified there determines the value later used in the KRL output.
In addition, a velocity limit has been implemented to ensure that the nozzle does not move faster than the pump's maximum delivery rate allows. This is based on Equation 4.46, rearranged to solve for the printing speed v_{print}. The maximum flow rate $\mathbf{q}_{max}$ is used as the upper limit. The calculated speed thus corresponds to the highest permissible feed rate at which the desired line width can still be reliably achieved.
As described in Chapter 3.2.2, transitions between different line types can trigger retraction events, during which material is briefly pulled back to avoid printing artifacts at segment boundaries. However, due to the viscosity of the material used in this context, it is not practical to mechanically retract the material from the nozzle on a regular basis.
Therefore, it is proposed instead to integrate a fast-acting valve between the nozzle and the delivery hose. This valve is mounted on the robot's tool arm and prevents material from oozing during pure travel movements.
In Cura, specific movement patterns arise when switching between `G1` and `G0` commands. These are summarized in Table 4.5.

Table 4.5 Typical G-Code Patterns for FDM-Style Slicing and Printing Using *Ultimaker Cura 5.8.0*

Pattern 1	**E-value**	**Pattern 2**	**E-value**
`G1 Extrusion`	>0	`G1 Extrusion`	>0
`G0 Travel`	<0	`G1 Retract`	<0
`G1 Extrusion`	>0	`G0 Travel`	<0
		`G1 Protract`	$=0$
		`G1 Extrusion`	>0
see Listing A.3.2, Line 266–268 (absolute Mode `M82`)		see Listing A.3.2, Line 72–80 (absolute Mode `M82`)	

The proposed valve can be controlled based on the extrusion values recorded in the *.src* file. If the E-value is less than zero, the valve is closed; if it is zero or greater, the valve is opened. To ensure consistent material flow and to avoid pressure buildup in the pump against a closed valve, both opening and closing should be performed with a slight delay. However, the control and implementation of the valve regulation are not part of this work due to the current lack of suitable hardware on the robot.
In the present setup, the printing process is carried out without retractions. Within Cura, material retractions can be completely disabled. The parameter `"retract"` specified in the *setup.json* file controls the corresponding input passed to Cura.

4.7 Translation to KUKA Robot Language [package: *krl*]

4.7.1 List of Collected Information

Figure 4.24 Progress Bar for Chapter 4.7

Based on the previously determined coordinates, line types, extrusion values, and speeds, a robot-interpretable *.src* file can now be generated. Figure 4.25 illustrates the structure of a single entry in the form of a dictionary of the before mentioned list that contains all information collected throughout the program. Each of these dictionary entries is subsequently converted into an individual KRL code line.

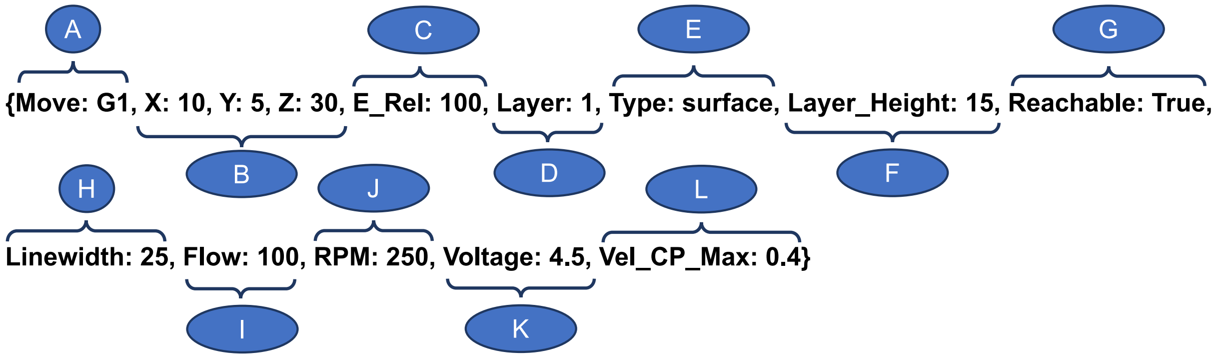

Figure 4.25 Dictionary for Arbitrary G-Code Line Used Inside the Program to Build *.src*-file

Table 4.6 Overview of Parameters Used in Figure 4.25

Symbol	Information	Source
A	Definition of move type (G1, G0)	G-Code [package: g_code]
B	Target coordinates of end point	G-Code [package: g_code]
C	Extrusion value relative to last extrusion	G-Code [package: g_code]
D	Layer number counting from 0	Calculated [package: g_code]
E	Line type of current section (surface, infill, retract, unknown, ...)	Assigned [package: g_code]
F	Current layer height	Calculated [package: g_code]
G	Coordinates reachable for specified robot configuration	Validated [package: robot]
H	Linewidth in mm of current line segment	Calculated [package: pump]
I	Flow related to current line type	Calculated [package: pump]
J	RPM of pump rotor needed to extrude specified line width	Calculated [package: pump]
K	Voltage of pump motor needed to extrude specified line width	Calculated [package: pump]
L	Maximum possible print velocity (depending on pump capability)	Calculated [package: pump]

The program code as a whole is structured analogously to the G-code and divided into three functional sections. The process begins with the initialization phase, during which local variables are declared and assigned, time and progress tracking is started, and return values are set. This is followed by the actual printing phase, in which the path data generated by Cura is translated line by line into KUKA Robot Language and output accordingly. After the printing process is complete, all previously initiated routines are terminated, and the system is returned to a defined initial state, as described in Chapter 3.2.3.

4.7.2 Initialization & Reset of Robot

The initialization and reset sections of the program can largely be configured by the user via the *setup.json* file. Custom code blocks in KRL can be defined under the keys `"start_code"` and `"end_code"`, which are inserted into the resulting *.src* file without additional validation. To avoid redundant entries, for example when specifying print parameters multiple times inside *setup.json*, placeholders can be used. These placeholders are enclosed in question marks (e.g., `?id?`) and reference corresponding keys in the *setup.json* file that contain the actual values (in this case `id`).
If a user-defined placeholder cannot be resolved due to a missing or incorrectly specified key in the *setup.json* file (e.g., `?ip?` instead of `?id?`), the system generates an error message, as shown in Listing 4.7.1, explicitly indicating the invalid entry. As a result, no *.src* file is created. To enable successful output, the error must first be corrected and the program restarted.

Listing 4.7.1 Console Output from *setup replace_strings* with Error Message

```
[ERROR] Key ?ip? inside robot start or end code not found
[WARNING] Key ?ip? not replaced
```

In addition to the manually defined code lines, the module `start_code_python` allows the input of a list of KRL-formatted strings into which dynamic variables from the Python program flow can be integrated. This enables the integration of additional information gathered during program execution into the generated *.src* file. It can be used for example for the automatic inclusion of the maximum number of layers, which was determined at the beginning of the process as described in Chapter 4.4. This information can in turn be used to continuously monitor print progress during execution. The processing of such dynamic content, however, is only possible within the corresponding Python module and cant be accessed from the `setup`-module.
A comparable module for the `"end_code"` section has not yet been implemented, as no practical use case has arisen so far. However, an extension analogous to `start_code_python` could be implemented at any time if needed.

4.7.3 Main Section

The main section of the *.src* file requires the collected information from the G-code (cf. Figure 4.25) to be converted into the format specified by KRL. Figure 4.26 illustrates the structure of a command line that contains all the information necessary for a linear movement.

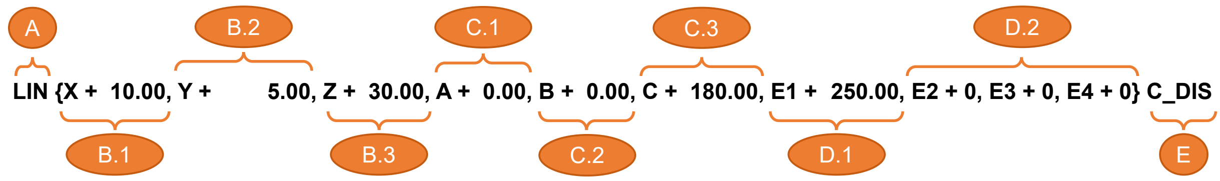

Figure 4.26 Example of KRL-Command for Linear Movement (RPM Used for Pump Control)

Table 4.7 Extended Symbol Overview for KRL Line Definition

Symbol	Information	Source
A	Definition of move type (LIN, CIRC, PTP)	LIN as only G1 or G0 commands occur in G-Code
B.1	Target coordinate of end point in x-direction	see B in Figure 4.25
B.2	Target coordinate of end point in y-direction	see B in Figure 4.25
B.3	Target coordinate of end point in z-direction	see B in Figure 4.25
C.1	Orientation of flange in relation to base coordinate system for z-axis of flange	set via `"tool_orientation"` ["A"]
C.2	Orientation of flange in relation to base coordinate system for y-axis of flange	set via `"tool_orientation"` ["B"]
C.3	Orientation of flange in relation to base coordinate system for x-axis of flange	set via `"tool_orientation"` ["C"]
D.1	Information for external axis of robot (here E1 gives information on extruded material along line and valve position)	see J or K in Figure 4.25
D.2	Unused external axis of robot (always set to 0)	Fixed value [package: pump]
E	Point is approximated to give a more continuous motion between points	mostly set to C_DIS

The commands in the *.src* file are formatted so that the decimal places of all numerical values are precisely aligned in vertical columns within the output file. To achieve this, the maximum character length for each numerical category is determined from the entire G-code in order to efficiently define the output field width. Subsequently, all values are rounded to a predefined number of decimal places, formatted with the appropriate sign, and right-aligned within their respective fields. This structure not only improves readability but also facilitates the targeted editing of individual values, for instance by column-wise selection and replacement.
In addition to the movement commands, the currently active line type is also output. The type designation stored under *E* in Figure 4.25 is converted into an integer value using the mapping defined in *setup.json* under `"type_number"`. This value is output at the beginning of each new line type and can be linked to a already implemented variable of the KUKA system, allowing the current line type to be displayed on the *smartPAD* user interface of the robot. In addition to the line type, the print speed is also specified at the start of each segment category. Although not yet implemented, defining individual speeds for different line types could be considered in the future. This would allow for optimized printing. As an example reducing speed for visually exposed segments like *surface* or *outer wall* could improve overall print quality. Since travel movements are not constrained by the pump's maximum flow rate, an independent speed setting is already implemented and can be specified via `"travel_speed"` in *setup.json*. Listing 4.7.2 illustrates an example output incorporating the afore mentioned features.

Listing 4.7.2 Example for Movement Command and Line Type Annotation Used in *.src*-Output

```
LIN {X +  586.97, Y +  2255.91, Z +   60.00, A +  0.00, B +  0.00,
    C +  180.00, E1 +  5.00, E2 + 0, E3 + 0, E4 + 0} C_DIS
LIN {X +  587.00, Y +  2257.18, Z +   60.00, A +  0.00, B +  0.00,
    C +  180.00, E1 +  5.00, E2 + 0, E3 + 0, E4 + 0} C_DIS

PATH_TYPE = 0
$VEL.CP=0.500
LIN {X +  587.00, Y +  2257.18, Z +   75.00, A +  0.00, B +  0.00,
    C +  180.00, E1 +  0.00, E2 + 0, E3 + 0, E4 + 0} C_DIS
LIN {X +  599.60, Y +  2257.18, Z +   75.00, A +  0.00, B +  0.00,
    C +  180.00, E1 +  0.00, E2 + 0, E3 + 0, E4 + 0} C_DIS
```

Furthermore, the generated *.src* file includes a timer that controls the minimum layer time. This timer is reset at the beginning of each new layer. If the robot reaches the end of the current layer before the time specified under `"min_layer_time"` in *setup.json* has elapsed, the system waits until the target time is reached. Since all *travel*-movements at the end of a layer are still assigned to that layer and every layer necessarily ends with such a movement, it is ensured that the valve mounted on the tool arm receives a command to close. This reliably prevents any unintended material discharge from the nozzle. Listing 4.7.3 illustrates the process using an example *.src* file.

Listing 4.7.3 Example for Layer Timer and Minimum Layer Time Implemented for *.src*-Output

```
LAYER = 0
$TIMER_STOP[4] = FALSE ; start layer timer

PATH_TYPE = 4 ; line type as int
$VEL.CP=0.133 ; velocity in m/s
[...]
WAIT FOR $TIMER[4] > 10000 ; time in ms

$TIMER_STOP[4] = TRUE ; stop layer timer
$TIMER[4] = 0 ; reset layer timer

LAYER = 1 ;layer change
$TIMER_STOP[4] = FALSE ; start layer timer
```

4.8 Print Report [package: *report*]

To provide a compact summary of the most relevant print parameters after successful execution of the program and in particular to allow the user to visually verify the position of the printed object on the print bed a report is automatically generated using the libraries *python-docx* [84], *scipy* [78], and *matplotlib* [49].

Figure 4.27 Progress Bar for Chapter 4.8

This report summarizes the key parameters of the print job and includes graphical evaluations of the characteristic pump curve and the printed object. The report is based on a predefined *.docx* template included in the program. Keys within the template are automatically replaced with the corresponding values, and the final file is saved in the output directory.
The report is structured into the following main sections:

- **Print section:** This section contains information about the processed geometry, including the file name, estimated volume, and the calculated weight of the print based on the extruded filament volume and a specific weight of 21 KN/m^3. It also lists the overall object dimensions in all spatial directions as well as the minimum and maximum coordinates on the print bed, allowing for a quick plausibility check of the object placement.
- **Robot section:** This part lists the robot parameters used in the process. It includes the model designation, the base geometry in OPW format, and the tool offset and orientation. Additionally, the absolute position of the robot ($ROBOTROOT) relative to the print bed ($BASE) is given.
- **Printbed section:** This section provides the defined dimensions of the print bed along with the coordinates of the object's placement in the workspace.
- **Print parameter section:** This part lists the specified print and travel speeds, as well as the mapping of G-code line types. It provides a quick overview that helps with orientation inside the generated *.src* file.
- **Pump section:** This section specifies the pump control setup used during printing. It indicates whether retraction was enabled and whether the pump is controlled via rpm or voltage. The configured flow rates for each line type are listed as a percentage of the nominal flow rate.

The clear structure of the report is intended to facilitate the review of all relevant parameters before starting the print and to ensure quick documentation of the selected settings. On the next page an example report generated for the test object using a scaling factor of 8000 percent is provided.

REPORT

Print:

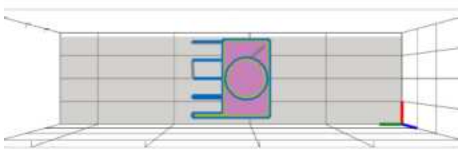

Filename:	Slicer Test v3.stl
Estimated weight [kg]:	72.636
Estimated volume [liter]:	34.589
Measurements [mm]:	[1015.0, 1019.566, 75.0]
Coordinates [mm]:	
Xmin: 92.5	Xmax: 1107.5
Ymin: 1742.5	Ymax: 2762.066
Zmin: 0	Zmax: 75.0

Robot:

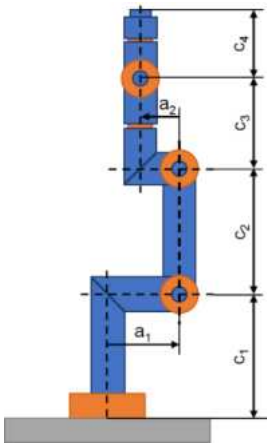

ID:	KUKA KR340 R3330		
Geometry [mm]:	{'a1': 500, 'a2': 55, 'b': 0, 'c1': 1045, 'c2': 1300, 'c3': 1525, 'c4': 290}		
Tool Offset [mm]:	{'X': -10.99, 'Y': -0.86, 'Z': 917.61}		
Tool Orientation [deg]:	{'A': 0, 'B': 0, 'C': 180}		
Printbed [mm]:	{'X': 1200, 'Y': 4500, 'Z': 2000}		
Location [to Printbed in mm]:	{'X': -1460.9, 'Y': 2237.66, 'Z': -268.5, 'A': 0, 'B': 0.0, 'C': 0.0}		
Set Print Speed [m/s]:	0.35	**Travel Speed [m/s]:**	0.5
Line Type Dictionary:	**Minimum Layer Time [sec]:**	10.0	

Protract	-2	**Travel**	0	**Wall outer**	1	**Surface**	7	**Bridge**	5	**Support**	7
Retract	-1			**Wall inner**	2	**Infill**	4	**Curb**	6	**Unknown**	99

Pump:

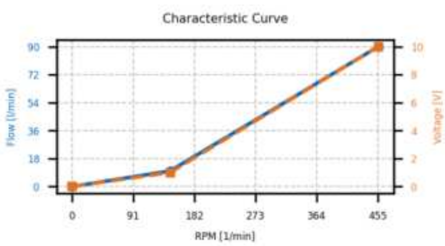

Retract	activated		
Pump cotrol:	RPM		
Flow [%]:			
Wall Outer:	100	**Infill:**	100
Wall Inner:	100	**Bridge:**	100
Surface:	100	**Curb:**	100
Unknown:	100		

4.9 Output in Rhino [package: *rhino*]

In addition to the compact overview provided by the generated report, all collected information is also visualized in a Rhinoceros3D file (*.3dm*). The objective is to allow for a layer-by-layer inspection of the printing process, analogous to the graphical representation used in slicer programs. This includes the visualization of attributes such as print speed, line width and the reachability of individual points.

Figure 4.28 Progress Bar for Chapter 4.9

Therefor a Rhino file is first prepared with a suitable layer structure. Subsequently, the individual line segments are inserted into the corresponding layers and sub-layers. The following sections explain the complete process from raw data preparation to the finished Rhino model.

4.9.1 Setup of Rhinoceros3D File [sub-package: *pre_process*]

The first step consists of creating a template file in the specified output folder before any geometric data is added. The program systematically processes the following three steps:

1. **Creation of an empty *.3dm* file:** Using the *rhinoinside* library [9], an empty Rhino file is generated, accessing a local installation of Rhinoceros3D.
2. **Definition of custom line types:** To allow full control over the graphical representation of motion and print paths, specific line types are generated within the file. These enable the visual differentiation between different printing and travel operations.
3. **Construction of the layer and sublayer structure:** In addition to the three main layers (*toolpath*, *printbed*, *robot*), the structure within the *toolpath* layer is further subdivided. Sublayers are first created for each print layer, within which further sublayers for the individual line segments are added. This hierarchical structure allows the print process to be visualized step-by-step in Rhino by toggling the visibility of individual layers. Figure 4.29 schematically illustrates the layer structure.

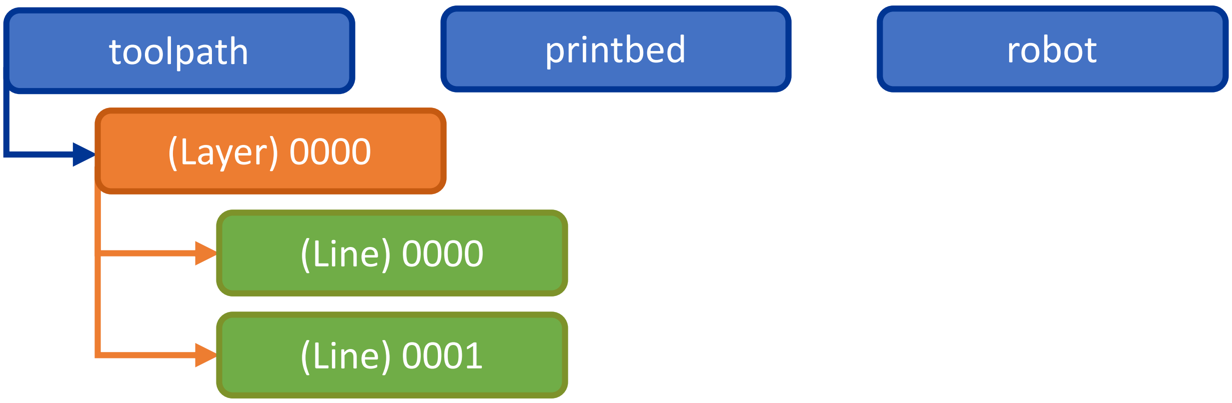

Figure 4.29 Schematic of Layer and Sublayer Structure Inside *.3dm*-file

4.9.2 Write Information to Rhino File [sub-package: *process*]

Preparation of the Rhino File [module: *import_robot*, *draw_printbed*]

Once the basic structure of the Rhino file has been created, the corresponding geometries can be added. To obtain a detailed digital representation of the entire hardware setup during the printing process, it is possible to import existing *.3dm* files of the robot cell. These files are referenced via the parameter `"3dm_file"` in the *setup.json* and are automatically imported when the Rhino file is created.

The imported geometry is then shifted by the displacement defined under `"base_coordinates"`, relative to the origin ($BASE) of the Rhino file. No rotation is applied. Therefore, the robot base ($ROBOTROOT) must already lie at the origin of the imported geometry, and its coordinate system must be aligned parallel to the orientation of the print bed's coordinate system $BASE.

Only the following geometry types are processed: points, curves, lines, B-reps, and meshes. Other entity types are ignored or may lead to errors.

In addition, the print bed is generated as a solid object based on the specified dimensions, with a fixed thickness of 15 cm in the negative Z-direction. It is placed at the origin of the global coordinate system, with its surface lying in the X-Y plane.

Figure 4.30 shows the resulting viewport in Rhino after completion of these initialization steps.

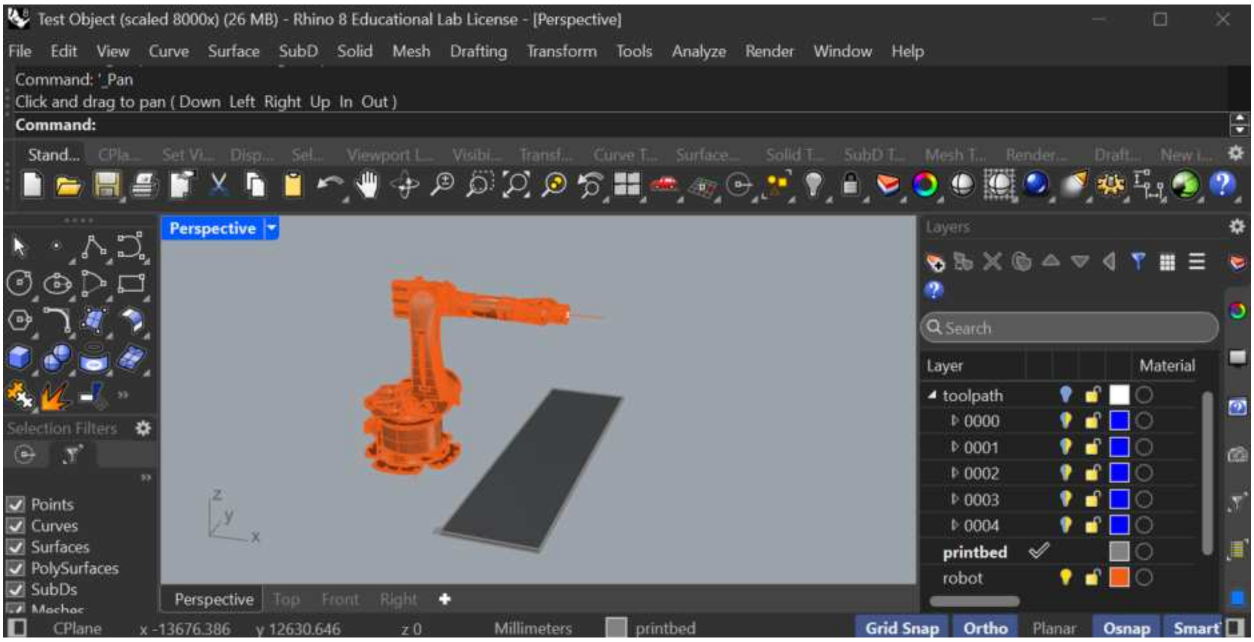

Figure 4.30 Overview of Rhino-File After Initialization

Visualisation of Tool Path [module: ***extend_gcode, draw_gcode***]

After the basic structure of the Rhino file has been created, the generated print paths are transferred and visualised using two central modules:

1. **Numbering of lines and points:** Since a separate polyline is created for each line type (*travel*, *wall_outer*, *infill*, etc.), a new polyline must be started whenever the type changes within a print layer. The endpoint of the previous polyline is therefor duplicated and used as the start point of the new one. This task, along with the continuous numbering of lines and points within each layer, is handled by the `extend_gcode` module.

2. **Transfer of points and lines into the Rhino file:** The prepared and numbered points and line segments are transferred into the designated sublayers within the parent layer `toolpath`. This task is performed by the `draw_gcode` module.

In addition to importing the line geometries, the `draw_gcode` module highlights specific points using color to mark particular events during the printing process:

- **beginning:** Starting point of the entire print process (set via `"start_position"` in *setup.json*).
- **end:** Final point of the entire print process (defined by `"end_position"` in *setup.json*).
- **retract:** Point where material extrusion is paused for a travel move.
- **protract:** Point where material extrusion resumes for a new extrusion move.
- **start:** Starting point of a line segment.
- **stop:** Endpoint of a line segment.

Color assignments are defined via the `"point_color"` entry in the *setup.json* file. Points marked as "unreachable" (see Figure 4.25, section G) are always displayed in black, regardless of the configuration. The same applies to lines with unknown or erroneous types. This ensures that critical conditions remain clearly visible.
Four predefined line styles (*solid*, *dashed*, *dotted*, *dash_dotted*) are available for line visualization. The mapping to motion types is specified in `"line_style_line"` within the *setup.json* file.
To generate a three-dimensional representation of the object geometry, each line is assigned its calculated width (see Chapter 4.6.1). In Rhino, this is implemented using the so-called *Print Width*, which is displayed when *Print View* is activated [command: `PrintDisplay: (State = On)`]. Each line is rendered as a solid with a circular cross-section.
The actual geometry of the extruded lines (e.g., rectangular or elliptical, defined by line width and layer height) is not reproduced exactly as the line-segments represent the path of the nozzle tip and lie not within the center of each line segment. This leads to a slightly idealized representation and minor inaccuracies in the vertical dimensions of the segments. This design choice was made deliberately to reduce computational effort and memory usage. For the reason given, there is a vertical offset of half the layer height between layer 0 and the print bed. Figure 4.31 illustrates the described characteristics.

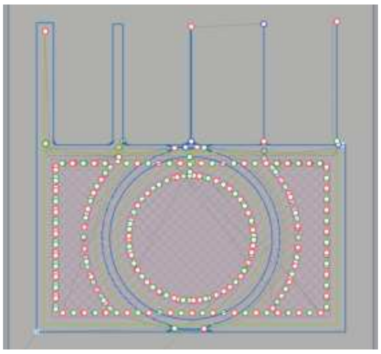

(a) Top View of Test-Object in "View Port"

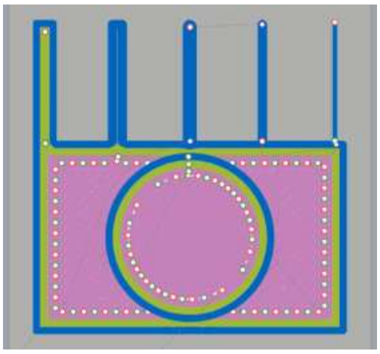

(b) Top View of Test-Object in "Print View"

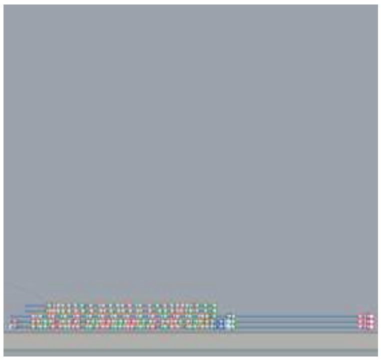

(c) Side View with Gap Between Print Bed and Printed Line

Figure 4.31 Visualization of test object in Rhinoceros3D

In addition to their visual properties, all line and point objects are assigned name attributes that document their unique identification within the printing process. A continuous four-digit numbering system is used, starting at zero for each category:

- For lines: `Layer` / `Line number` / `Segment number`
  (e.g., 0002/0007/0003 → Layer 3, 8th line within the layer, 4th segment).
- For points: `Layer` / `Line number` / `Point number`
  (e.g., 0004/0016/0001 → Layer 5, 17th line within the layer, 1st point).

Note that if `"point_print"` is set to `"false"` in the *setup.json* file, only the previously listed point types are displayed visually to maintain clarity in the file. These are labeled as point 0000 and 0001. Intervening points are not counted. If this setting is changed to `true`, all contact points of individual line segments are additionally marked with colors.
Moreover, all line and point objects receive additional text attributes that store metadata such as local print speed, line width, or the extruded material volume. These attributes are intended to assist the user in conducting a detailed analysis in case a fault diagnosis on the physical print object becomes necessary. Figure 4.32 illustrates an example of the embedded information for line and point objects.

(a) Example of Text Attributes Used for Points

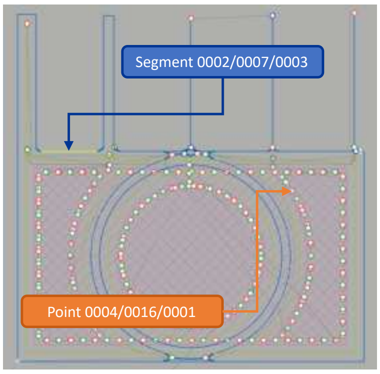

(b) Reference for Specified Point and Line on Test-Object

(c) Example of Text Attributes Used for Lines

Figure 4.32 Attributes Used for Labeling in Rhinoceros3D

This completes the creation of the digital model. Figure 4.33 shows the full Rhino interface as it is presented to the user after successful program execution. In order to react to incorrect inputs during execution and to ensure the robustness of the process, additional safety mechanisms have been implemented. The explanation of these mechanisms is the subject of the following chapter.

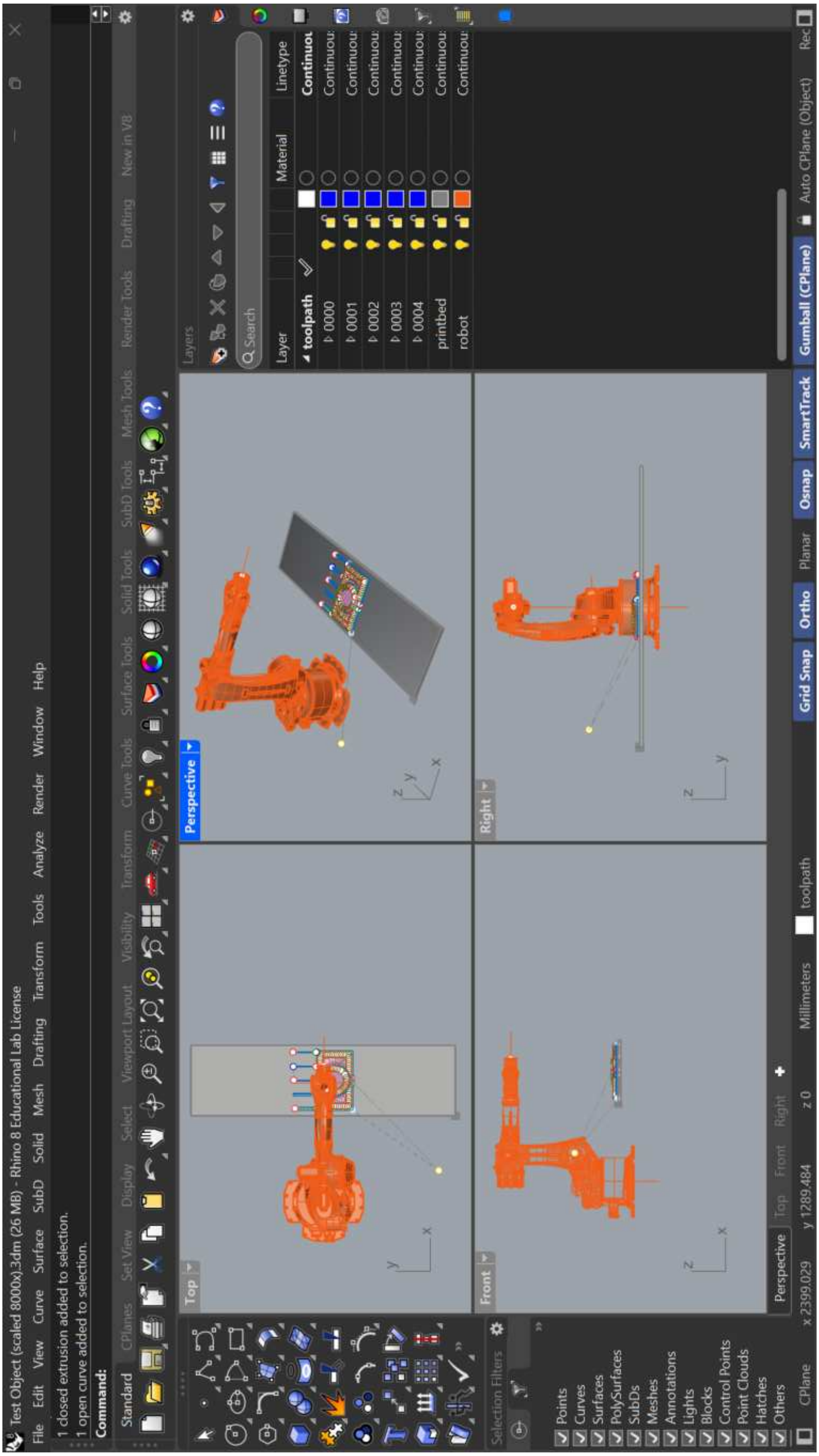

Figure 4.33 Screenshot of Rhinoceros3D Interface with Test Object Sliced and Visualized (beginning & end [yellow], start [green], stop [red])

4.10 Implementation of Safety Mechanisms

In addition to the safety features already described within the individual packages and modules, there are cross-system checks designed to ensure that no invalid files or outputs are generated. The following sections describe the most important functions in detail. The flowchart presented in Figures 4.35 to 4.37 provides an overview of the process flow within the `main`-function including all essential safety features.

4.10.1 Program Abort Errors [*main*-function]

In general, a complete termination of the program has been avoided wherever possible. However, there are four specific cases in which a controlled and defined abort of the program is executed.

- **Invalid input in *setup.json*:** To ensure that no erroneous KUKA code (*.src* file) is generated, the program terminates if a value in the *setup.json* file does not match the specified type defined in the corresponding `"type"` field.
- **File or directory not found:** If an error occurs while attempting to locate a specified file or folder the program is terminated, as no data would be available for further processing. This feature may be activated either due to a typographical error or a non-existent path.
- **Slicer or *.stl* file not found:** If either the slicer engine (for example, *CuraEngine.exe*) or the specified *.stl* file cannot be located at the given path, the program will abort. The process cannot proceed without these essential components.
- **No usable data in the *.gcode* file:** If the generated *.gcode* file does not contain any printable information after slicing, the program will be terminated. This may occur if the geometry of the object is too small relative to the defined print settings, such that no tool paths are generated.

4.10.2 Check Object Size [package: *g_code*; module: *fits_printbed*]

Since the *CuraEngine.exe* does not verify whether the object generated from the *.stl* file fits within the print bed defined in the *printer.def.json*, a separate validation is performed in the `fits_printbed` module. The goal is to ensure that the entire object lies within the specified build volume. Figure 4.34 illustrates the three possible scenarios that are evaluated in the following.

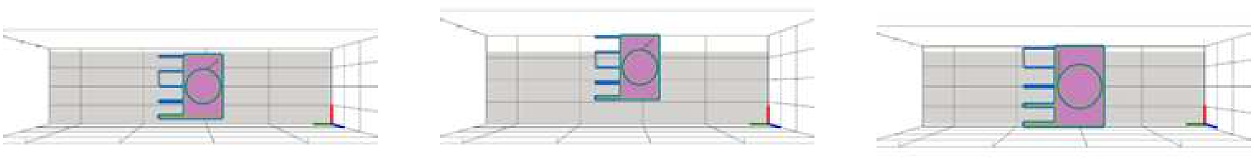

(a) Test-Object (scaled 8000 %) Fitted on Print Bed

(b) Test-Object (scaled 8000 %) Not Located Correctly

(c) Test-Object (scaled 10000 %) Not Fitting Print Bed

Figure 4.34 Test Object (Scaled) on Print Bed in Top View (Taken from Report)

The verification is based on the following input parameters:

- **bed_size:** (b_i) specifies the dimensions of the print bed in the X, Y, and Z directions.
- **min_values:** defines the minimum coordinates of the object.
- **max_values:** defines the maximum coordinates of the object.

First, the length of the object in each spatial direction X, Y, Z (hereinafter referred to as i) is calculated:

$$\Delta i = i_{\text{max}} - i_{\text{min}}, \tag{4.47}$$

The object only fits on the print bed if the following conditions are met in all spatial directions:

$$\Delta i \leq b_i \tag{4.48}$$

If any of these conditions are violated, the object is classified as too large.
Next, a position check is performed to verify whether the object lies within the limits of the print bed:

$$0 \leq i_{\text{min}} \quad \text{and} \quad i_{\text{max}} \leq b_i \tag{4.49}$$

If these positioning conditions are not satisfied, a necessary shift is calculated. The required displacement Δp is determined for each spatial direction as:

$$\Delta p_i = \max(0, -i_{\text{min}}) + \max(0, i_{\text{max}} - b_i) \tag{4.50}$$

Full print approval is only granted if both the dimension check according to Equation (4.48) and the position check according to Equation (4.49) are successfully completed. If this is not the case, one of the two error codes shown in Listings 4.10.1 and 4.10.2 is issued.

Listing 4.10.1 Example of CLI Error Code for Badlly Located Print (See Figure 4.34b)

```
[ERROR] Object not located fully on the printbed; shift at least
        {'dx': -207.5, 'dy': 0, 'dz': 0}
[WARNING] .src file not generated due to invalid location of
   object       or object not fitting on printbed
```

Listing 4.10.2 Example of CLI Error Code for Objects Larger than Printbed (See Figure 4.34c)

```
[ERROR] Object doesn't fit printbed in given orientation
[WARNING] .src file not generated due to invalid location of
   object       or object not fitting on printbed
```

4.10.3 Deactivate Outputs [*main*-function]

If the internal program switch `"src"` is set to `"false"` during execution (see Figure 4.35 to 4.38), the output of the *.src* file is suppressed. The following conditions can trigger this switch:

- **Invalid key in *setup.json*:** If a key specified within `"start_code"` or `"end_code"` does not exist in *setup.json*, the *.src* output will be skipped. Since the key could not be resolved, the *.src* file would be incomplete and corrupted.
- **Object not fully placed on the print bed:** If it is detected, as described in Chapter 4.10.2, that the object lies outside the defined boundaries of the print bed or is simply to large to fit the print bed, the generation of the *.src* file is also suppressed.
- **Kinematics check failed:** If it is determined that the joint angles for the defined start or end position are not within the limits specified under `"joint_limits"`, or if the start position leads to a collision with the robot base, no *.src* file will be created. The same applies if no solution can be found for any of the positions extracted from the G-code using inverse kinematics.

This ensures that only robot control files are generated that have passed all relevant validation steps and meet all defined requirements.
In addition to the validation of input and output parameters, verifying the correctness of the program implementation itself is a crucial step. This topic is addressed in the following chapter.

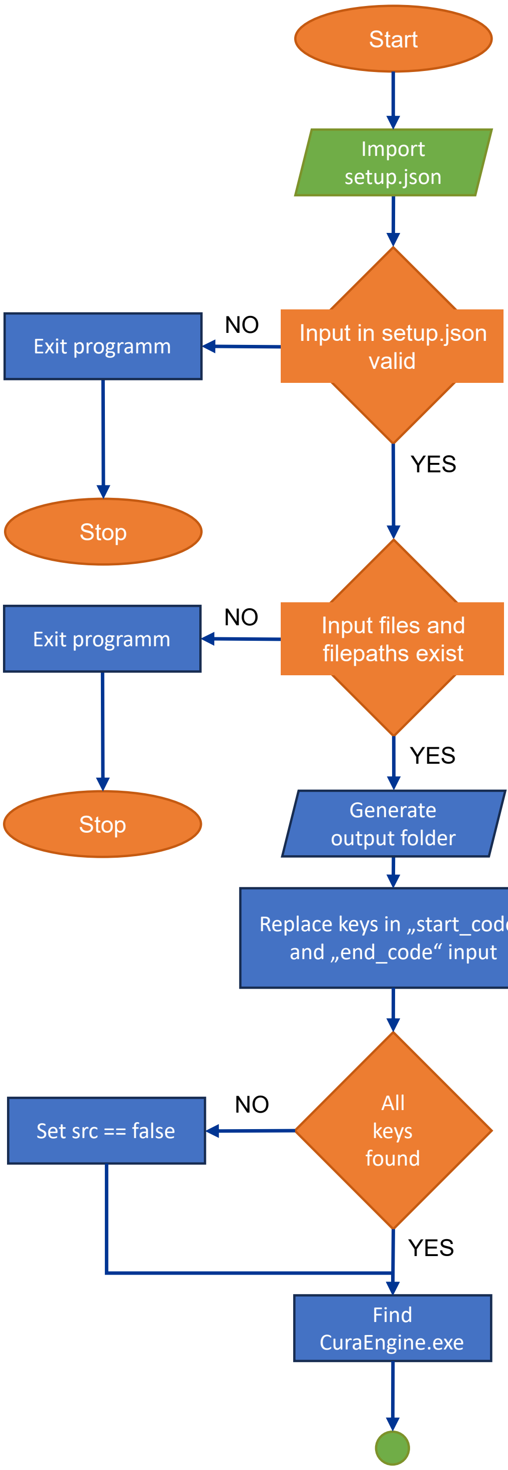

Figure 4.35 Flowchart of *main*-Function (Part 1)

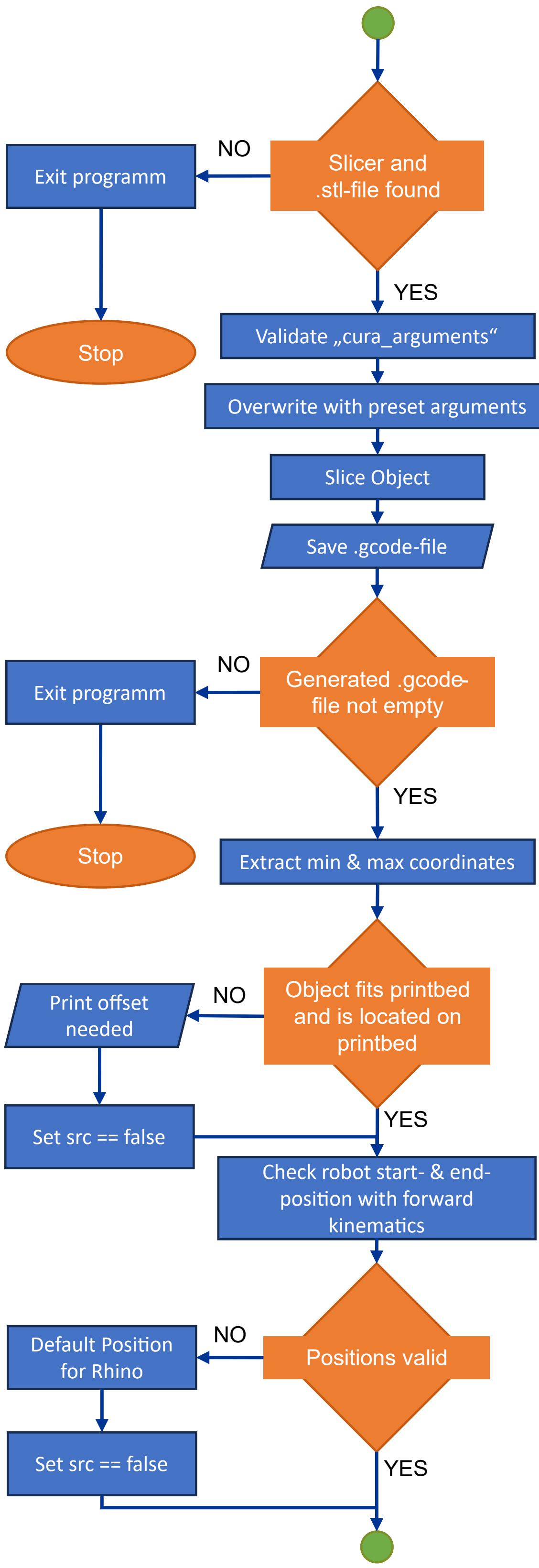

Figure 4.36 Flowchart of *main*-Function (Part 2)

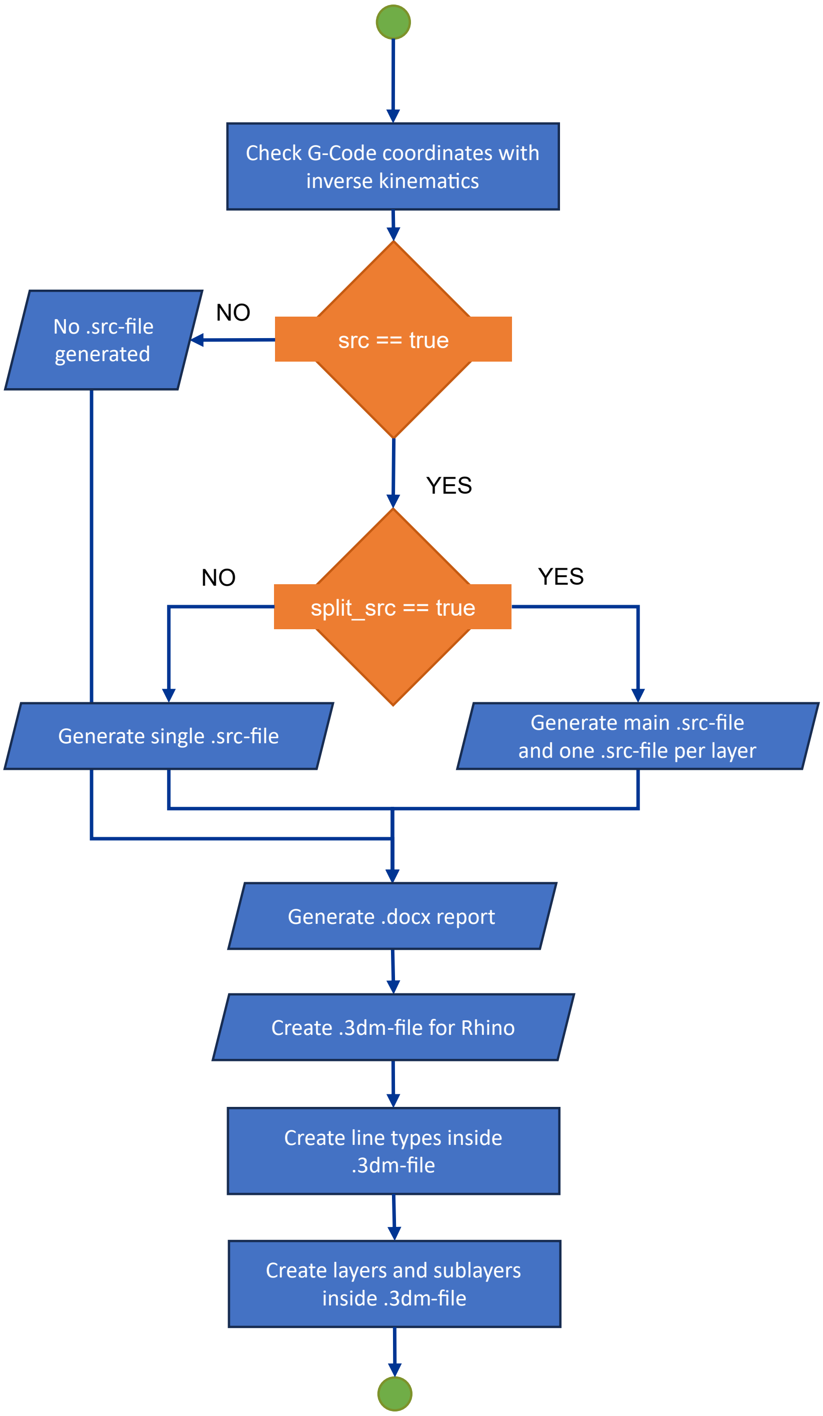

Figure 4.37 Flowchart of *main*-Function (Part 3)

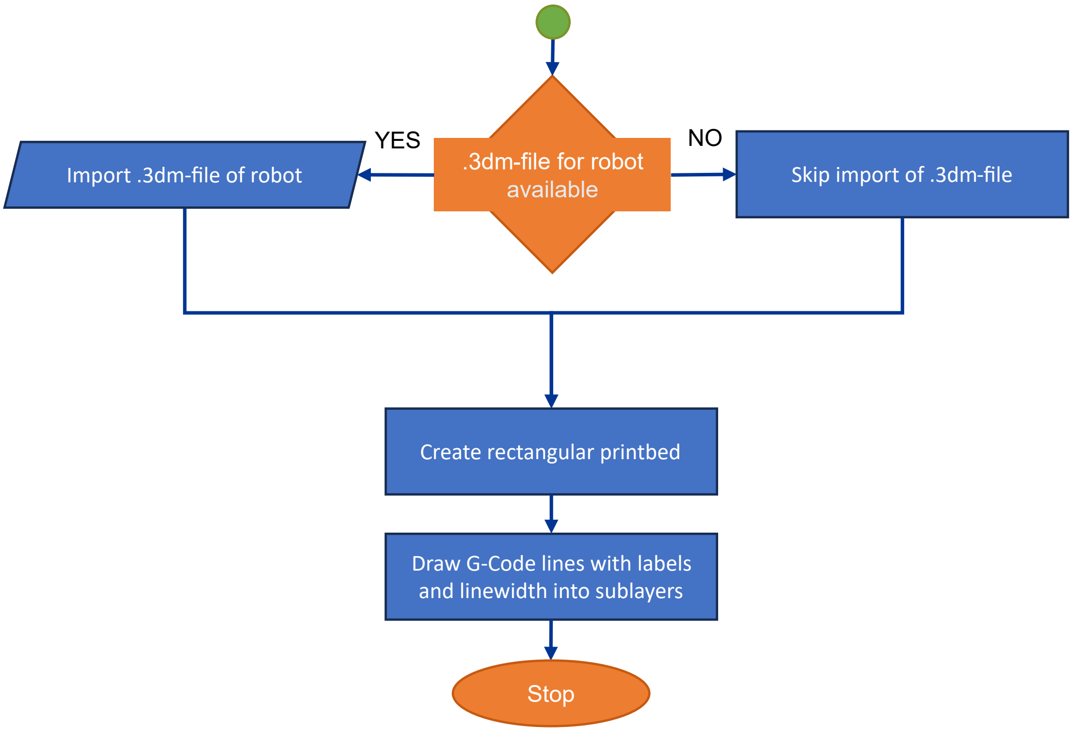

Figure 4.38 Flowchart of *main*-Function (Part 4)

5 Validation and Limitations

5.1 Validation [package: *tests*]

In addition to the actual implementation, validating the program is an essential step in the overall workflow. The goal is to identify and eliminate programming errors using either existing reference solutions or custom examples that have been verified for correctness. The program described in the previous chapters was therefore extensively tested during development, among other methods using the *pytest* library [70].

5.1.1 Validation of Rhino Output

To verify the correct transfer of geometry data, the output in Rhinoceros3D was compared with the dimensions specified in *printer.def.json*. Figure 5.1 shows a comparison between the measured dimensions of the test object in Autodesk Fusion 360 and in Rhinoceros3D after the slicing process. It should be noted that the dimensions measured in Rhino represent only the centerlines of the tool path and do not account for the extrusion width of 25 mm (or 32 mm for the second "finger" from the left).

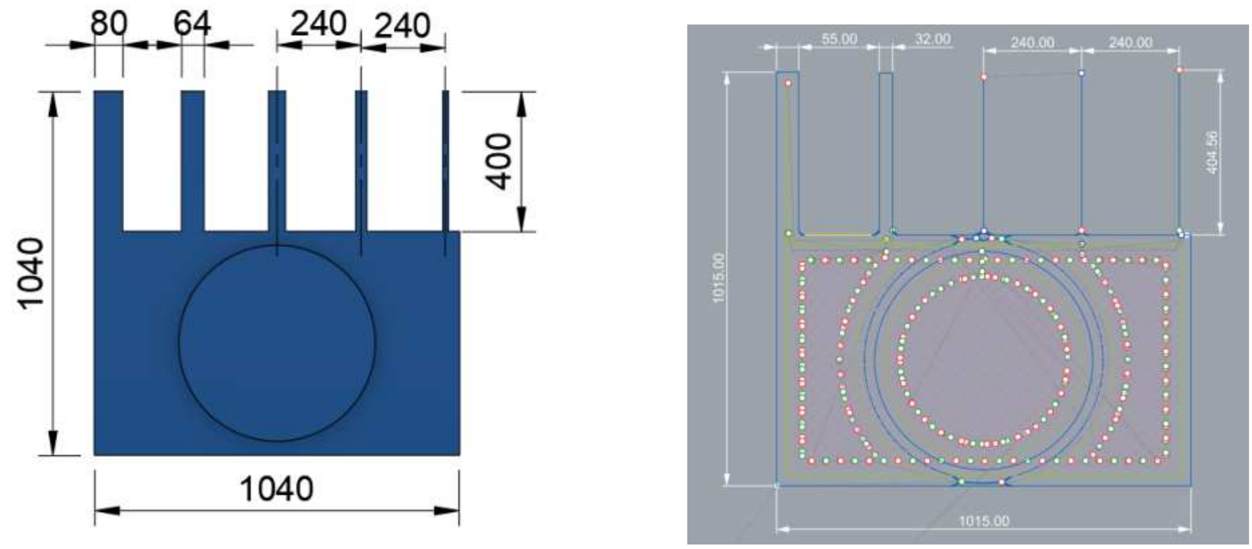

(a) Top View of Test-Object with Measurements from Fusion 360 [11]

(b) Top View of Test-Object with Measurements from Rhinoceros3D [75]

Figure 5.1 Comparison of Measurements for Sliced Test-Object (Scaled 8000 %)

As the comparison shows, the distance of 240 mm between the “fingers” matches exactly. The overall dimensions of the object also correspond to the specifications when accounting for half the extrusion width of 25 mm and 32 mm respectively on each edge. This also applies to the sizing of the individual finger geometries when considering the line width. Only the length of the finger segments shows a minor deviation, which amounts to approximately 1 % compared to the original design geometry. Due to the very close match of all other dimensions, this deviation is attributed to the slicing process itself rather than to the subsequent processing within the program code.

5.1.2 Validation of Robot Kinematics

In addition to the visual inspection of the results in the Rhino file, the kinematic module developed in this work was subjected to comprehensive validation. For this purpose, approximately 23 000 different positions were generated using the RoboDK software [76] for the implemented model of the KUKA KR 340 R3300. For each position, both a forward and an inverse kinematic solution were calculated and stored in a corresponding *.json* file.
The validation process was carried out in two steps:

- **Forward kinematics:** Based on the given joint angles, the position and orientation of the end-effector were computed. The results were then compared to the reference values stored in the test dataset.
- **Inverse kinematics:** Starting from the predefined position and orientation of the end-effector, a homogeneous transformation matrix was constructed. Based on this matrix, the corresponding joint angles were calculated and compared to the list of solutions provided in the test file.

A test case is considered successful for the forward kinematic case, if all computed values match the reference solutions within a defined tolerance. For the inverse kinematic test all calculated solutions need to be clearly identifiable and need to match with the specified tolerance compared to the expected solution set. Table 5.1 provides a summary of the validation test results for the kinematic module.

Table 5.1 Summary of Validation Tests for the Kinematics Module

Test	Passed / Failed	Tolerance
Forward kinematic	23.196 / 4	$\pm 2 \times 10^{-2}$ [deg]
Inverse kinematic	23.200 / 0	$\pm 10^{-2}$ [mm] and [deg]

The failed test cases in the forward kinematics exclusively involve configurations in which the wrist pitch angle is exactly $90°$. This configuration corresponds to the *Gimbal Lock* scenario illustrated in Figure 4.16b, in which no unique solution for the orientation exists. As a result, the computed solution does not match the reference result from RoboDK within the specified tolerance. Such singularities are extremely rare in practical operation and are typically handled internally by the robot's control software. Since the forward kinematics still returns a numerically valid result, the *.src* file is generated even in these cases. The issue is therefore confined to the test definition within the program and is not further addressed. All other test cases passed successfully within the defined tolerance of around 10^{-2} degree or millimeters, which is below the specified accuracy of the robot (see Chapter 2.6.1).

5.2 Limitations

In addition to validating the program's functionality, it is essential to understand its current boundaries and constraints in order to use the application effectively and safely. While several limitations have already been discussed throughout this work, the present chapter provides a concise overview of the most significant restrictions.

- **Validation of input arguments:** At present, only the parameters defined by the user in *setup.json* are validated according to their specified data types. The input values contained in the associated *.def.json* configuration files are not subject to validation. As a result, invalid entries in these files cannot neither be detected nor handled by the program.
- **Robot kinematics:** The application is currently restricted to 6-DOF robots based on the OPW architecture. Alternative joint configurations or other robot types are not supported by the present implementation.
- **Tool frame orientation:** The current version does not support relative rotations between $TOOL and $NULLFRAME. Consequently, tools must be mounted with an orientation that is parallel to the flange coordinate frame.
- **Singularities in forward kinematics:** For pitch angles (rotation about the Y-axis) of exactly $90°$, a singularity occurs. While the computed results mostly agree with those produced by RoboDK, numerical inaccuracies may arise in this configuration. This special case affects only the start and end positions.
- **Singularities in inverse kinematics:** In addition to the already discussed *wrist singularity*, two other singularity types may arise according to [82]. The first is the *shoulder singularity*, which occurs when axes A1 and A6 become collinear. The second is the *elbow singularity*, which results from the alignment of links "c_2" and "c_3" (cf. Figure 4.11) in parallel. The former can be ruled out for the present configuration due to the robot's fixed orientation with respect to the print bed during operation. For the latter, further investigation is currently not required given the existing setup. However, should the arrangement of the robot or print bed change in the future, or should the software be adapted for other configurations, this limitation may need to be reconsidered.
- **Limitations in the selection of slicer arguments:** At present, the *CuraEngine.exe* only processes the most deeply nested parameters from the respective *.def.json* files. Higher-level parameters cannot be used, even though they are generally accepted and handled by the program as documented in [93] and mentioned in the Help section accessible via the `CuraEngine help` command in the command line interface.
- **Incomplete validation of slicer arguments:** The complete set of Cura parameters comprises more than 600 individual entries, many of which are internally cross-referenced or duplicated. It was not feasible within the scope of this work to validate all of these options. Therefor ongoing updates and validation can be documented using the Excel files provided in the `Cura` package of the GitHub project.
- **Import of external *.3dm* files:** When importing external Rhino files, only specific geometry types are supported (Points, Curves, Lines, B-reps, and Meshes). If a file contains unsupported entity types, this may result in warnings or, in some cases, a program interruption.
- **Compatibility with Cura versions:** The program has been specifically developed for use with *Ultimaker Cura 5.8.0*. Using other versions of Cura (either earlier or later) may require adjustments to the program's structure.

- **Software requirement Rhinoceros3D:** During execution, the program accesses Rhinoceros3D in the background. Therefore, a locally installed version of Rhino 8 is required to run the application.
- **Geometric representation of the print path:** To minimize memory consumption and reduce runtime, the print path geometry is not rendered with full geometric fidelity as mentioned in Chapter 4.9 in Rhinoceros3D. As a result, the representation of layer height and the positioning of the printed object on the print bed may significantly deviate from the actual printed geometry.

6 Outlook

While the previous chapter focused on the current limitations of the implementation, this chapter explores potential enhancements and future developments. The aim is to identify opportunities that go beyond the limitations previously described and to outline strategies that could be beneficial for further optimization of the program.
This chapter is intended to serve as an impetus for new ideas and to present perspectives for additional functionalities and possibilities to expand the capabilities of the software.

6.1 Simple Extensions of the Program

Parallel Processes

To reduce program runtime, it would be feasible to parallelize specific sub-processes and distribute them across multiple CPU cores. This approach could be applied, for example, to the kinematic calculations or to the writing of the Rhino file, thereby significantly decreasing execution time for these modules.

Feedrate Input

As described in Chapter 4.4, lines containing only feedrate values are already extracted from the G-code. In future implementations, this information could be used in combination with the feedrate values included in the *general commands*to directly control the travel and print speeds from the G-code itself, rather than specifying it externally in *setup.json*.

6.2 Advanced Extensions of the Program

Calibration of Printing Parameters

In addition to specifying the printing parameters, proper calibration of the printer is essential for achieving consistently high-quality print results. The tests listed in [91] provide an overview of commonly used calibration prints for polymer-based FDM processes. Implementing similar calibration routines tailored to the specific setup described in this work could further enhance print quality and reproducibility. In the long term, an automated calibration procedure based on the available sensors and cameras within the robotic environment may be considered. Ultimately, the goal could be to dynamically and autonomously adjust printing parameters, thereby reducing the manual effort required for setup and monitoring of the process chain.

Graphical User Interface

To simplify input handling and reduce the likelihood of user errors, the implementation of a graphical user interface could be a useful enhancement. The structure of such an interface could follow the layout of Cura's native GUI. In addition to streamlining the input process, it would also significantly facilitate parameter validation compared to the current *.json*-based input format.

Simulation of the Printing Process Using Rhinoceros3D

At present, the printing process can only be followed manually by examining the layer-by-layer geometry rendered in the Rhino file. This visualization is limited to the gradual build-up of the printed object on the print bed.
Although the reachability of individual robot positions is already verified by computing each movement point-by-point, the results are currently used only for simple Boolean checks of reachability.
For future versions of the program, it would be highly beneficial to simulate the complete printing process, including all robotic motion sequences. Therefor it is crucial that the simulated trajectories precisely reflect the actual robotic movements, as any deviation could result in unrealistic or infeasible paths that would not be executable in the real system.
Such a detailed simulation would also enable the extraction of dynamic process variables, such as the actual speed and acceleration of the nozzle. These data could then be used to optimize the control of external components, like robot-pump-interaction by improving the synchronization between material flow and robotic motion.
As a simplified alternative, a so-called *dry-run* could be implemented. In this approach, the generated G-code would be executed without material extrusion in an initial run. During this process, telemetry data such as velocity, position, or acceleration could be recorded. These data could subsequently serve as input parameters for the actual print operation, thereby refining the control of hardware components and reducing process variability.

Non-Planar Slicing

Since the robotic system used is capable of executing complex spatial movements beyond the purely Cartesian motions confined to the X-Y plane of each print layer, more advanced tool path strategies could be implemented from a hardware perspective. On the software side, the so-called *non-planar slicing* method allows for generating print paths that are no longer limited to planar and parallel layer heights. Open-source tools such as the slicer presented in [111] or its more recent extension [15] could serve as the basis for such an implementation.
The main benefit of this approach lies in the ability to eliminate the need for support structures by conforming the printing path to the curvature of the object. This enables the fabrication of complex geometries and undercuts without additional scaffolding (e.g. support). Furthermore, non-planar slicing offers significant potential in the context of load-oriented design, making it a valuable alternative to the conventional layer-by-layer approach currently implemented.

7 Conclusion

The program presented in this work significantly improved the previous software-based workflow for concrete-3D-printing at the Technical University of Munich. By integrating all required process steps, starting with provision of a *.stl* file and ending in the visualization of the generated print path on the computer the sequence of operations is now considerably simplified for the user. Instead of manually executing individual steps of the process chain, the user is only required to input the necessary information once at the beginning of the workflow. All subsequent operations are executed automatically, while erroneous inputs are clearly identified and documented in a transparent manner. This not only improves the overall clarity of the process but also reduces potential sources of error during both setup-phase and execution.

Through the provided documentation on GitHub and the modular structure of the entire program, the prerequisites for future expansion, validation, and improvements by external users are established. Furthermore, any modifications to the software components, such as Rhinoceros3D or Ultimaker Cura can be implemented efficiently by targeting the relevant packages. The serial structure of the `main`-function also facilitates the straightforward integration of additional functionality.

Taken as a whole, the program provides a robust foundation for continued use in future applications. For reliable and flawless use in research or industrial contexts, however, the limitations outlined in Chapter 5.2 must either be resolved or carefully considered. Among the possible enhancements presented in Chapter 6, *non-planar slicing* appears particularly promising, as it would allow for a more advanced exploitation of geometric freedom in 3D-printing with mineral-based materials such as concrete.

A further development of the current software can therefore be regarded as both valuable and worthwhile.

A G-Code Listings

A.1 Prusa Slicer 2.9.2 – G-Code Listing

```
; generated by PrusaSlicer 2.9.2 on 2025-04-14 at 12:06:16 UTC

;

; external perimeters extrusion width = 0.42mm
; perimeters extrusion width = 0.44mm
; infill extrusion width = 0.44mm
; solid infill extrusion width = 0.44mm
; top infill extrusion width = 0.40mm
; first layer extrusion width = 0.42mm

M201 X500 Y500 Z100 E5000 ; sets maximum accelerations, mm/sec^2
M203 X500 Y500 Z10 E60 ; sets maximum feedrates, mm / sec
M204 S500 T1000 ; sets acceleration (S) and retract acceleration (R), mm/sec^2
M205 X8.00 Y8.00 Z0.40 E5.00 ; sets the jerk limits, mm/sec
M205 S0 T0 ; sets the minimum extruding and travel feed rate, mm/sec

; printing object Slicer Test v3.stl id:0 copy 0
; stop printing object Slicer Test v3.stl id:0 copy 0

;TYPE:Custom
G90 ; use absolute coordinates
M83 ; extruder relative mode
M104 S150 ; set temporary nozzle temp to prevent oozing during homing
M140 S0 ; set final bed temp
G4 S30 ; allow partial nozzle warmup
G28 ; home all axis
G1 Z50 F240
G1 X2.0 Y10 F3000
M104 S20 ; set final nozzle temp
M190 S0 ; wait for bed temp to stabilize
M109 S20 ; wait for nozzle temp to stabilize
G1 Z0.28 F240
G92 E0
G1 X2.0 Y140 E10 F1500 ; prime the nozzle
G1 X2.3 Y140 F5000
G92 E0
G1 X2.3 Y10 E10 F1200 ; prime the nozzle
G92 E0
G21 ; set units to millimeters
G90 ; use absolute coordinates
M83 ; use relative distances for extrusion
```

Listing A.1.1 G-Code Generated Using Prusa Slicer [68] (Initialization)

```
; Filament gcode
M107
;LAYER_CHANGE
;Z:0.2
;HEIGHT:0.2
G1 E-5 F3600
G1 Z.2 F9000
; printing object Slicer Test v3.stl id:0 copy 0
G1 X116.331 Y116.704
G1 Z.2
G1 E5 F2400
M204 S500
;TYPE:External perimeter
;WIDTH:0.592344
G1 F1200
G1 X116.055 Y116.724 E.01721
;WIDTH:0.552764
G1 X115.779 Y116.743 E.01596
;WIDTH:0.555403
G1 X115.709 Y116.763 E.00422
;WIDTH:0.597621
```

```
G1 X115.639 Y116.783 E.00457
;WIDTH:0.63984
G1 X115.57 Y116.802 E.00483
;WIDTH:0.682058
G1 X115.5 Y116.822 E.00527
G1 E-3.5 F3600
;WIPE_START
G1 F7200
G1 X115.57 Y116.802 E-.03458
G1 X115.639 Y116.783 E-.03399
G1 X115.709 Y116.763 E-.03458
G1 X115.779 Y116.743 E-.03458
G1 X116.055 Y116.724 E-.13141
G1 X116.331 Y116.704 E-.13144
;WIPE_END
G1 E-1.09942 F3600
G1 X115.5 Y121.481 F9000
G1 E5 F2400
;WIDTH:0.6
G1 F1200
G1 X115.5 Y116.979 E.28384
;WIDTH:0.641029
G1 X115.5 Y116.9 E.00535
;WIDTH:0.682058
G1 X115.5 Y116.822 E.00564
G1 X115.407 Y116.792 E.00707
;WIDTH:0.633492
G1 X115.314 Y116.762 E.00653
;WIDTH:0.584925
G1 X115.221 Y116.732 E.00599
;WIDTH:0.568366
G1 X114.788 Y116.716 E.02577
G1 E-3.5 F3600
;WIPE_START
G1 F7200
G1 X115.221 Y116.732 E-.20582
G1 X115.314 Y116.762 E-.04642
G1 X115.407 Y116.792 E-.04642
G1 X115.5 Y116.822 E-.04642
G1 X115.5 Y116.9 E-.03705
G1 X115.5 Y116.979 E-.03752
G1 X115.5 Y119.253 E-1.08035
;WIPE_END
G1 X118.5 Y121.488 F9000
G1 E5 F2400
;WIDTH:0.400002
G1 F1200
G1 X118.5 Y116.981 E.18214
G1 E-3.5 F3600
;WIPE_START
G1 F7200
G1 X118.5 Y120.139 E-1.5
;WIPE_END
G1 X121.5 Y121.495 F9000
G1 E5 F2400
;WIDTH:0.38292
G1 F1200
G1 X121.5 Y116.979 E.17378
G1 E-3.5 F3600
;WIPE_START
G1 F7200
G1 X121.5 Y120.137 E-1.5
;WIPE_END
G1 X114.813 Y109.281 F9000
G1 E5 F2400
;WIDTH:0.562992
G1 F1200
G1 X115.072 Y109.267 E.01527
;WIDTH:0.534713
G1 X115.331 Y109.253 E.01444
;WIDTH:0.536148
G1 X116.013 Y109.268 E.03808
;WIDTH:0.542128
G1 X116.057 Y109.271 E.00249
G1 E-3.5 F3600
;WIPE_START
G1 F7200
G1 X116.013 Y109.268 E-.02095
G1 X115.331 Y109.253 E-.32403
G1 X115.072 Y109.267 E-.1232
G1 X114.813 Y109.281 E-.1232
;WIPE_END
```

```
G1 E-.90862 F3600
G1 X112.959 Y109.682 F9000
G1 E5 F2400
; TYPE: Perimeter
;WIDTH:0.419999
G1 F1200
G1 X112.363 Y110.23 E.03455
G1 X112.004 Y110.698 E.02517
G1 X111.736 Y111.229 E.02538
G1 X111.516 Y111.724 E.02312
G1 X111.325 Y112.705 E.04265
G1 X111.332 Y113.387 E.02911
G1 X111.458 Y114.08 E.03006
G1 X111.758 Y114.86 E.03566
G1 X111.911 Y115.137 E.0135
G1 X112.204 Y115.58 E.02267
G1 X112.68 Y116.089 E.02974
G1 X113.085 Y116.393 E.02161
G1 X112.64 Y116.465 E.01924
G1 X112.499 Y116.565 E.00738
G1 X112.313 Y116.448 E.00938
G1 X111.263 Y116.318 E.04515
G1 X109.881 Y116.313 E.05898
G1 X109.687 Y116.506 E.01168
G1 X109.687 Y109.686 E.29105
G1 X112.899 Y109.682 E.13708
G1 X113.119 Y110.034 F9000
; TYPE: External perimeter
G1 F1200
G1 X112.662 Y110.459 E.02663
G1 X112.284 Y110.96 E.02678
G1 X111.885 Y111.8 E.03969
G1 X111.702 Y112.705 E.0394
G1 X111.704 Y113.326 E.0265
G1 X111.81 Y113.945 E.0268
G1 X112.145 Y114.805 E.03939
G1 X112.483 Y115.327 E.02654
G1 X112.906 Y115.787 E.02667
G1 X113.379 Y116.142 E.02524
G1 X113.694 Y116.304 E.01512
G1 X114.325 Y116.513 E.02837
;WIDTH:0.469455
G1 X114.479 Y116.581 E.00813
;WIDTH:0.518911
G1 X114.634 Y116.648 E.0091
;WIDTH:0.568366
G1 X114.788 Y116.716 E.01001
G1 X114.588 Y116.739 E.01197
;WIDTH:0.518911
G1 X114.388 Y116.762 E.01085
;WIDTH:0.469455
G1 X114.188 Y116.786 E.00972
;WIDTH:0.419999
G1 X113.291 Y116.753 E.03831
G1 X112.789 Y116.812 E.02157
G1 X112.689 Y116.979 E.00831
G1 X112.689 Y121.474 E.19183
G1 X112.658 Y121.719 E.01054
G1 X112.342 Y121.719 E.01349
G1 X112.311 Y121.486 E.01003
G1 X112.311 Y116.98 E.1923
G1 X112.259 Y116.85 E.00598
G1 X112.144 Y116.793 E.00548
G1 X111.261 Y116.695 E.03791
G1 X109.879 Y116.69 E.05898
;WIDTH:0.42146
G1 X109.689 Y116.878 E.01145
G1 X109.689 Y121.689 E.20611
G1 X109.311 Y121.689 E.01619
G1 X109.31 Y116.118 E.23867
;WIDTH:0.419999
G1 X109.31 Y109.31 E.29054
G1 X113.012 Y109.302 E.15799
;WIDTH:0.446963
G1 X113.527 Y109.284 E.02356
G1 X114.025 Y109.21 E.02302
;WIDTH:0.467444
G1 X114.287 Y109.234 E.01264
;WIDTH:0.515218
G1 X114.55 Y109.258 E.01412
;WIDTH:0.562992
G1 X114.813 Y109.281 E.01554
```

```
G1 X114.783 Y109.295 E.00195
;WIDTH:0.551372
G1 X114.403 Y109.432 E.02324
;WIDTH:0.515765
G1 X114.023 Y109.57 E.02164
;WIDTH:0.480157
G1 X113.642 Y109.708 E.02005
;WIDTH:0.444549
G1 X113.169 Y110.003 E.02534
G1 E-3.5 F3600
;WIPE_START
G1 F7200
G1 X113.119 Y110.034 E-.02794
G1 X112.662 Y110.459 E-.29644
G1 X112.284 Y110.96 E-.29811
G1 X111.885 Y111.8 E-.44172
G1 X111.703 Y112.699 E-.43579
;WIPE_END
G1 X118.018 Y109.669 F9000
G1 E5 F2400
; TYPE: Perimeter
;WIDTH:0.419999
G1 F1200
G1 X118.499 Y109.686 E.02054
G1 X121.313 Y109.687 E.12009
G1 X121.319 Y115.532 E.24944
G1 X121.395 Y116.406 E.03744
G1 X120.972 Y116.347 E.01823
G1 X120.202 Y116.319 E.03288
G1 X119.065 Y116.352 E.04854
G1 X118.451 Y116.43 E.02641
G1 X117.953 Y116.376 E.02138
G1 X118.521 Y115.896 E.03174
G1 X118.899 Y115.443 E.02518
G1 X119.423 Y114.46 E.04754
G1 X119.61 Y113.78 E.0301
G1 X119.68 Y112.783 E.04265
G1 X119.589 Y112.107 E.02911
G1 X119.423 Y111.541 E.02517
G1 X119.29 Y111.267 E.013
G1 X118.899 Y110.558 E.03455
G1 X118.451 Y110.033 E.02945
G1 X118.064 Y109.707 E.02159
G1 X117.981 Y110.133 F9000
; TYPE: External perimeter
G1 F1200
G1 X117.719 Y109.917 E.01449
G1 X117.167 Y109.643 E.0263
G1 X116.602 Y109.458 E.02537
;WIDTH:0.460709
G1 X116.42 Y109.396 E.00909
;WIDTH:0.501419
G1 X116.239 Y109.333 E.00995
;WIDTH:0.542128
G1 X116.057 Y109.271 E.01086
G1 X116.258 Y109.251 E.01141
;WIDTH:0.501419
G1 X116.459 Y109.23 E.01049
;WIDTH:0.460709
G1 X116.659 Y109.21 E.0095
;WIDTH:0.419999
G1 X118.5 Y109.309 E.07868
G1 X121.69 Y109.31 E.13614
G1 X121.696 Y115.511 E.26464
G1 X121.725 Y116.027 E.02206
G1 X121.79 Y116.531 E.02169
G1 X121.79 Y116.79 E.01105
G1 X121.558 Y116.791 E.0099
G1 X121.5 Y116.979 E.0084
G1 X121.449 Y116.795 E.00815
G1 X120.959 Y116.723 E.02114
G1 X120.043 Y116.691 E.03912
G1 X119.141 Y116.723 E.03852
G1 X118.636 Y116.798 E.02179
G1 X118.5 Y116.981 E.00973
;WIDTH:0.419171
G1 X118.401 Y116.81 E.00841
;WIDTH:0.419999
G1 X117.797 Y116.741 E.02594
G1 X116.798 Y116.79 E.04269
;WIDTH:0.459296
G1 X116.69 Y116.77 E.00518
```

```
;WIDTH:0.498593
G1 X116.582 Y116.75 E.00566
;WIDTH:0.53789
G1 X116.474 Y116.731 E.00614
;WIDTH:0.577187
G1 X116.366 Y116.711 E.00664
G1 X116.459 Y116.656 E.00653
;WIDTH:0.53789
G1 X116.553 Y116.6 E.00613
;WIDTH:0.498593
G1 X116.647 Y116.545 E.00562
;WIDTH:0.459296
G1 X116.74 Y116.489 E.00512
;WIDTH:0.419999
G1 X117.195 Y116.346 E.02035
G1 X117.755 Y116.058 E.02687
G1 X118.231 Y115.655 E.02662
G1 X118.63 Y115.17 E.0268
G1 X119.061 Y114.353 E.03942
G1 X119.234 Y113.75 E.02677
G1 X119.306 Y112.829 E.03943
G1 X119.227 Y112.213 E.0265
G1 X119.061 Y111.647 E.02517
G1 X118.609 Y110.799 E.04101
G1 X118.128 Y110.254 E.03102
G1 X118.027 Y110.171 E.00558
G1 E-3.5 F3600
;WIPE_START
G1 F7200
G1 X117.981 Y110.133 E-.02834
G1 X117.719 Y109.917 E-.16129
G1 X117.167 Y109.643 E-.29272
G1 X116.602 Y109.458 E-.2824
G1 X116.42 Y109.396 E-.09133
G1 X116.239 Y109.333 E-.09103
G1 X116.057 Y109.271 E-.09133
G1 X116.258 Y109.251 E-.09595
G1 X116.459 Y109.23 E-.09599
G1 X116.659 Y109.21 E-.09547
G1 X117.025 Y109.23 E-.17415
;WIPE_END
G1 X121.194 Y110.575 F9000
G1 E5 F2400
; TYPE: Solid infill
;WIDTH:0.422094
G1 F1200
G1 X120.596 Y109.977 E.03629
G1 X120.059 Y109.977 E.02304
G1 X121.024 Y110.942 E.05857
G1 X121.025 Y111.478 E.023
G1 X119.523 Y109.977 E.09112
G1 X118.987 Y109.977 E.023
G1 X121.025 Y112.015 E.12368
G1 X121.025 Y112.552 E.02304
G1 X119.481 Y111.007 E.09373
G1 X119.64 Y111.306 E.01453
G1 X119.824 Y111.887 E.02615
G1 X121.026 Y113.089 E.07295
G1 X121.026 Y113.625 E.023
G1 X119.934 Y112.533 E.06627
G1 X119.975 Y112.849 E.01367
G1 X119.955 Y113.09 E.01038
G1 X121.027 Y114.162 E.06506
G1 X121.027 Y114.699 E.02304
G1 X119.914 Y113.586 E.06755
G1 X119.89 Y113.882 E.01274
G1 X119.842 Y114.05 E.0075
G1 X121.028 Y115.235 E.07195
G1 X121.047 Y115.791 E.02387
G1 X119.723 Y114.467 E.08035
G1 X119.638 Y114.698 E.01056
G1 X119.562 Y114.842 E.00699
G1 X120.769 Y116.049 E.07325
G1 X120.214 Y116.03 E.02383
G1 X119.375 Y115.191 E.05092
G1 X119.184 Y115.537 E.01696
G1 X119.683 Y116.036 E.03028
G1 X119.166 Y116.055 E.0222
G1 X118.828 Y115.716 E.02054
G1 E-3.5 F3600
;WIPE_START
G1 F7200
```

```
G1 X119.166 Y116.055 E-.22739
G1 X119.683 Y116.036 E-.24574
G1 X119.184 Y115.537 E-.3352
G1 X119.375 Y115.191 E-.18773
G1 X120.125 Y115.941 E-.50394
;WIPE_END
G1 X112.225 Y110.224 F9000
G1 E5 F2400
;WIDTH:0.427467
G1 F1200
G1 X111.973 Y109.972 E.01551
G1 X111.43 Y109.973 E.02363
G1 X111.864 Y110.407 E.02671
G1 X111.771 Y110.525 E.00654
G1 X111.65 Y110.737 E.01062
G1 X110.887 Y109.974 E.04696
G1 X110.345 Y109.975 E.02359
G1 X111.474 Y111.104 E.06949
G1 X111.297 Y111.471 E.01773
G1 X109.977 Y110.151 E.08124
G1 X109.977 Y110.695 E.02368
G1 X111.183 Y111.901 E.07423
G1 X111.09 Y112.351 E.02
G1 X109.977 Y111.239 E.06847
G1 X109.977 Y111.783 E.02368
G1 X111.044 Y112.849 E.06564
G1 X111.034 Y113.302 E.01972
G1 X111.049 Y113.398 E.00423
G1 X109.977 Y112.327 E.06595
G1 X109.977 Y112.871 E.02368
G1 X111.147 Y114.04 E.07198
G1 X111.465 Y114.902 E.03999
G1 X109.977 Y113.414 E.09159
G1 X109.977 Y113.958 E.02368
G1 X112.14 Y116.121 E.13313
G1 X111.531 Y116.056 E.02666
G1 X109.977 Y114.502 E.09565
G1 X109.977 Y115.046 E.02368
G1 X110.959 Y116.028 E.06044
G1 X110.416 Y116.028 E.02363
G1 X109.808 Y115.42 E.03742
;LAYER_CHANGE
;Z:0.4
;HEIGHT:0.2
;BEFORE_LAYER_CHANGE
G92 E0
;0.4


G1 E-3.5 F3600
;WIPE_START
G1 F7200
G1 X110.416 Y116.028 E-.40842
G1 X110.959 Y116.028 E-.25793
G1 X109.977 Y115.046 E-.65966
G1 X109.977 Y114.68 E-.17399
;WIPE_END
G1 Z.4 F9000
;AFTER_LAYER_CHANGE
;0.4
G1 Z.4
G1 X115.779 Y116.743
G1 E5 F2400
; TYPE: External perimeter
;WIDTH:0.554771
G1 F1500
G1 X115.709 Y116.764 E.00423
;WIDTH:0.595398
G1 X115.639 Y116.785 E.00457
;WIDTH:0.636025
G1 X115.57 Y116.806 E.00484
;WIDTH:0.676652
G1 X115.5 Y116.827 E.00524
G1 E-3.5 F3600
;WIPE_START
G1 F7200
G1 X115.57 Y116.806 E-.03471
G1 X115.639 Y116.785 E-.03426
G1 X115.709 Y116.764 E-.03471
G1 X115.779 Y116.743 E-.03471
;WIPE_END
G1 E-1.36161 F3600
```

```
G1 X115.5 Y121.7 F9000
G1 E5 F2400
;WIDTH:0.638326
G1 F1500
G1 X115.5 Y119.264 E.16415
;WIDTH:0.676652
G1 X115.5 Y116.827 E.17479
G1 X115.399 Y116.805 E.00741
;WIDTH:0.638207
G1 X115.297 Y116.783 E.00703
;WIDTH:0.599761
G1 X115.196 Y116.761 E.00651
;WIDTH:0.561316
G1 X115.095 Y116.739 E.00606
G1 E-3.5 F3600
;WIPE_START
G1 F7200
G1 X115.196 Y116.761 E-.0491
G1 X115.297 Y116.783 E-.0491
G1 X115.399 Y116.805 E-.04956
G1 X115.5 Y116.827 E-.0491
G1 X115.5 Y119.264 E-1.15757
G1 X115.5 Y119.57 E-.14557
;WIPE_END
G1 X118.5 Y121.8 F9000
G1 E5 F2400
;WIDTH:0.4
G1 F1500
G1 X118.5 Y116.979 E.19483
G1 E-3.5 F3600
;WIPE_START
G1 F7200
G1 X118.5 Y120.137 E-1.5
;WIPE_END
G1 X121.5 Y121.9 F9000
G1 E5 F2400
;WIDTH:0.38292
G1 F1500
G1 X121.5 Y116.979 E.18936
G1 E-3.5 F3600
;WIPE_START
G1 F7200
G1 X121.5 Y120.137 E-1.5
;WIPE_END
G1 X114.526 Y109.314 F9000
G1 E5 F2400
;WIDTH:0.627586
G1 F1500
G1 X114.742 Y109.295 E.01435
;WIDTH:0.590813
G1 X114.958 Y109.277 E.01344
;WIDTH:0.55404
G1 X115.173 Y109.259 E.01248
;WIDTH:0.535964
G1 X116.008 Y109.268 E.0466
;WIDTH:0.542126
G1 X116.057 Y109.271 E.00277
G1 E-3.5 F3600
;WIPE_START
G1 F7200
G1 X116.008 Y109.268 E-.02332
G1 X115.173 Y109.259 E-.39665
G1 X114.958 Y109.277 E-.10248
G1 X114.742 Y109.295 E-.10296
G1 X114.526 Y109.314 E-.103
;WIPE_END
G1 E-.77159 F3600
G1 X113.244 Y109.597 F9000
G1 E5 F2400
; TYPE: Perimeter
;WIDTH:0.439999
G1 F1500
G1 X113.254 Y109.597 E.00045
G1 X112.974 Y109.78 E.01503
G1 X112.418 Y110.306 E.0344
G1 X111.96 Y110.948 E.03544
G1 X111.601 Y111.754 E.03965
G1 X111.415 Y112.713 E.0439
G1 X111.422 Y113.381 E.03002
G1 X111.546 Y114.06 E.03102
G1 X111.918 Y114.983 E.04472
G1 X112.44 Y115.718 E.04051
```

```
G1 X112.905 Y116.167 E.02905
G1 X113.239 Y116.403 E.01838
G1 X112.931 Y116.403 E.01384
G1 X112.629 Y116.46 E.01381
G1 X112.5 Y116.549 E.00704
G1 X112.371 Y116.46 E.00704
G1 X112.121 Y116.403 E.01152
G1 X109.979 Y116.403 E.09626
G1 X109.597 Y116.784 E.02425
G1 X109.597 Y109.597 E.32298
G1 X113.184 Y109.597 E.1612
G1 X113.235 Y110.065 F9000
;TYPE:External perimeter
;WIDTH:0.419999
G1 F1500
G1 X112.733 Y110.531 E.02923
G1 X112.257 Y111.205 E.03521
G1 X111.98 Y111.833 E.02929
G1 X111.802 Y112.713 E.03832
G1 X111.804 Y113.318 E.02582
G1 X111.907 Y113.921 E.02611
G1 X112.237 Y114.763 E.03859
G1 X112.709 Y115.44 E.03522
G1 X113.2 Y115.91 E.02901
G1 X113.708 Y116.247 E.02602
G1 X114.471 Y116.562 E.03523
;WIDTH:0.45429
G1 X114.679 Y116.621 E.01007
;WIDTH:0.48858
G1 X114.887 Y116.68 E.01091
;WIDTH:0.52287
G1 X115.095 Y116.739 E.01174
G1 X114.88 Y116.756 E.01172
;WIDTH:0.48858
G1 X114.664 Y116.773 E.01093
;WIDTH:0.45429
G1 X114.449 Y116.79 E.01004
;WIDTH:0.419999
G1 X112.797 Y116.809 E.07051
;WIDTH:0.42146
G1 X112.689 Y116.979 E.00863
G1 X112.689 Y121.789 E.20607
G1 X112.311 Y121.789 E.01619
G1 X112.311 Y116.979 E.20607
G1 X112.252 Y116.843 E.00635
;WIDTH:0.419999
G1 X112.121 Y116.79 E.00603
G1 X109.979 Y116.79 E.09141
;WIDTH:0.45382
G1 X109.899 Y116.853 E.00474
;WIDTH:0.48764
G1 X109.819 Y116.916 E.00513
;WIDTH:0.52146
G1 X109.739 Y116.979 E.00551
G1 X109.739 Y121.739 E.2578
G1 X109.261 Y121.739 E.02589
G1 X109.261 Y116.979 E.2578
G1 X109.244 Y116.66 E.0173
;WIDTH:0.48764
G1 X109.227 Y116.34 E.01613
;WIDTH:0.45382
G1 X109.21 Y116.021 E.01486
;WIDTH:0.419999
G1 X109.21 Y109.21 E.29067
G1 X113.902 Y109.21 E.20024
;WIDTH:0.461517
G1 X114.027 Y109.231 E.006
;WIDTH:0.503034
G1 X114.151 Y109.252 E.00655
;WIDTH:0.544552
G1 X114.276 Y109.272 E.00719
;WIDTH:0.586069
G1 X114.401 Y109.293 E.00779
;WIDTH:0.627586
G1 X114.526 Y109.314 E.00839
G1 X114.482 Y109.339 E.00335
;WIDTH:0.600825
G1 X114.346 Y109.413 E.00978
;WIDTH:0.555619
G1 X114.211 Y109.487 E.00893
;WIDTH:0.510412
G1 X114.075 Y109.561 E.00819
```

```
;WIDTH:0.465206
G1 X113.94 Y109.635 E.00736
;WIDTH:0.419999
G1 X113.286 Y110.034 E.03269
G1 E-3.5 F3600
;WIPE_START
G1 F7200
G1 X113.235 Y110.065 E-.02835
G1 X112.733 Y110.531 E-.32535
G1 X112.257 Y111.205 E-.39194
G1 X111.98 Y111.833 E-.32603
G1 X111.802 Y112.713 E-.42647
G1 X111.802 Y112.717 E-.00186
;WIPE_END
G1 X117.768 Y109.597 F9000
G1 E5 F2400
; TYPE: Perimeter
;WIDTH:0.439999
G1 F1500
G1 X121.403 Y109.597 E.16336
G1 X121.403 Y110.753 E.05195
G1 X121.403 Y116.403 E.25391
G1 X117.766 Y116.403 E.16345
G1 X118.188 Y116.063 E.02435
G1 X118.626 Y115.642 E.0273
G1 X119.056 Y115.031 E.03358
G1 X119.339 Y114.426 E.03002
G1 X119.519 Y113.787 E.02983
G1 X119.584 Y113.289 E.02257
G1 X119.59 Y112.786 E.02261
G1 X119.494 Y112.103 E.031
G1 X119.169 Y111.181 E.04393
G1 X118.81 Y110.592 E.031
G1 X118.233 Y109.953 E.03869
G1 X117.816 Y109.634 E.02359
G1 X116.684 Y109.495 F9000
; TYPE: External perimeter
;WIDTH:0.419999
G1 F1500
G1 X116.603 Y109.458 E.0038
;WIDTH:0.460708
G1 X116.421 Y109.396 E.00909
;WIDTH:0.501417
G1 X116.239 Y109.333 E.00999
;WIDTH:0.542126
G1 X116.057 Y109.271 E.01086
G1 X116.248 Y109.251 E.01085
;WIDTH:0.501417
G1 X116.44 Y109.23 E.01002
;WIDTH:0.460708
G1 X116.631 Y109.21 E.00908
;WIDTH:0.419999
G1 X121.79 Y109.21 E.22017
G1 X121.79 Y110.753 E.06585
G1 X121.79 Y116.79 E.25764
G1 X121.548 Y116.793 E.01033
G1 X121.5 Y116.979 E.0082
;WIDTH:0.404799
G1 X121.467 Y116.842 E.00577
;WIDTH:0.419999
G1 X121.421 Y116.79 E.00296
G1 X118.639 Y116.794 E.11873
G1 X118.5 Y116.979 E.00988
G1 X118.396 Y116.805 E.00865
G1 X118.321 Y116.79 E.00326
G1 X116.544 Y116.79 E.07584
;WIDTH:0.467072
G1 X116.161 Y116.766 E.01842
;WIDTH:0.514144
G1 X115.779 Y116.743 E.02041
G1 X116.169 Y116.648 E.02141
;WIDTH:0.467072
G1 X116.56 Y116.552 E.01933
;WIDTH:0.419999
G1 X117.191 Y116.301 E.02898
G1 X117.68 Y116.001 E.02448
G1 X118.312 Y115.415 E.03678
G1 X118.708 Y114.863 E.02899
G1 X118.968 Y114.317 E.02581
G1 X119.135 Y113.738 E.02572
G1 X119.2 Y113.24 E.02143
G1 X119.206 Y112.833 E.01737
```

```
G1 X119.127 Y112.227 E.02608
G1 X118.835 Y111.377 E.03836
G1 X118.523 Y110.851 E.0261
G1 X117.918 Y110.187 E.03834
G1 X117.422 Y109.828 E.02613
G1 X116.739 Y109.52 E.03197
G1 E-3.5 F3600
;WIPE_START
G1 F7200
G1 X116.684 Y109.495 E-.0287
G1 X116.603 Y109.458 E-.0423
G1 X116.421 Y109.396 E-.09133
G1 X116.239 Y109.333 E-.09148
G1 X116.057 Y109.271 E-.09133
G1 X116.248 Y109.251 E-.09122
G1 X116.44 Y109.23 E-.09174
G1 X116.631 Y109.21 E-.09122
G1 X118.485 Y109.21 E-.88068
;WIPE_END
G1 X121.097 Y112.285 F9000
G1 E5 F2400
; TYPE: Internal infill
;WIDTH:0.44
G1 F3000
G1 X121.097 Y109.903 E.10705
G1 X119.582 Y111.418 E.09629
G1 X119.823 Y112.174 E.03566
G1 X119.9 Y112.851 E.03062
G1 X119.888 Y113.323 E.02122
G1 X119.74 Y114.124 E.03661
G1 X121.097 Y115.518 E.08743
G1 X120.518 Y116.097 E.0368
G1 X118.607 Y116.105 E.08588
G1 X118.914 Y115.765 E.02059
G1 E-3.5 F3600
;WIPE_START
G1 F7200
G1 X118.607 Y116.105 E-.21759
G1 X120.518 Y116.097 E-.90773
G1 X121.076 Y115.54 E-.37468
;WIPE_END
G1 X112.181 Y115.875 F9000
G1 E5 F2400
G1 F3000
G1 X112.447 Y116.168 E.01778
G1 X112.168 Y116.098 E.01293
G1 X110.482 Y116.097 E.07577
G1 X109.903 Y115.518 E.0368
G1 X111.258 Y114.126 E.0873
G1 X111.109 Y113.295 E.03794
G1 X111.109 Y112.707 E.02642
G1 X111.303 Y111.687 E.04666
G1 X111.408 Y111.408 E.0134
G1 X109.903 Y109.903 E.09565
G1 X109.903 Y112.285 E.10705
;LAYER_CHANGE
;Z:0.6
;HEIGHT:0.2
;BEFORE_LAYER_CHANGE
G92 E0
;0.6


G1 E-3.5 F3600
;WIPE_START
G1 F7200
G1 X109.903 Y109.903 E-1.13145
G1 X110.452 Y110.452 E-.36855
;WIPE_END
G1 Z.6 F9000
;AFTER_LAYER_CHANGE
;0.6
G1 Z.6
G1 X115.5 Y121.7
G1 E5 F2400
; TYPE: External perimeter
;WIDTH:0.6
G1 F1500
G1 X115.5 Y116.979 E.29765
G1 E-3.5 F3600
;WIPE_START
G1 F7200
```

```
G1 X115.5 Y120.137 E-1.5
;WIPE_END
G1 X118.5 Y121.8 F9000
G1 E5 F2400
;WIDTH:0.4
G1 F1500
G1 X118.5 Y116.979 E.19483
G1 E-3.5 F3600
;WIPE_START
G1 F7200
G1 X118.5 Y120.137 E-1.5
;WIPE_END
G1 X121.5 Y121.9 F9000
G1 E5 F2400
;WIDTH:0.38292
G1 F1500
G1 X121.5 Y116.979 E.18936
G1 X121.155 Y116.403 F9000
; TYPE: Perimeter
;WIDTH:0.439999
G1 F1500
G1 X118.679 Y116.403 E.11127
G1 X118.563 Y116.415 E.00524
G1 X118.5 Y116.492 E.00447
G1 X118.437 Y116.415 E.00447
G1 X118.321 Y116.403 E.00524
G1 X115.779 Y116.403 E.11424
G1 X115.555 Y116.448 E.01027
G1 X115.5 Y116.531 E.00447
G1 X115.445 Y116.448 E.00447
G1 X115.221 Y116.403 E.01027
G1 X112.879 Y116.403 E.10525
G1 X112.648 Y116.451 E.0106
G1 X112.5 Y116.677 E.01214
G1 X112.352 Y116.451 E.01214
G1 X112.121 Y116.403 E.0106
G1 X109.979 Y116.403 E.09626
G1 X109.597 Y116.784 E.02425
G1 X109.597 Y109.597 E.32298
G1 X121.403 Y109.597 E.53056
G1 X121.403 Y113 E.15293
G1 X121.403 Y116.403 E.15293
G1 X121.215 Y116.403 E.00845
G1 X121.487 Y116.924 F9000
; TYPE: External perimeter
;WIDTH:0.404799
G1 F1500
G1 X121.467 Y116.842 E.00346
;WIDTH:0.419999
G1 X121.421 Y116.79 E.00296
G1 X118.669 Y116.79 E.11745
G1 X118.5 Y116.979 E.01082
G1 X118.359 Y116.794 E.00993
G1 X118.321 Y116.79 E.00163
G1 X115.765 Y116.79 E.10908
;WIDTH:0.465
G1 X115.699 Y116.837 E.00387
;WIDTH:0.51
G1 X115.633 Y116.885 E.00431
;WIDTH:0.555
G1 X115.566 Y116.932 E.00474
;WIDTH:0.6
G1 X115.5 Y116.979 E.00511
G1 X115.449 Y116.935 E.00425
;WIDTH:0.555
G1 X115.397 Y116.892 E.00391
;WIDTH:0.51
G1 X115.346 Y116.848 E.00356
;WIDTH:0.465
G1 X115.295 Y116.805 E.00319
;WIDTH:0.419999
G1 X115.221 Y116.79 E.00322
G1 X112.838 Y116.794 E.1017
;WIDTH:0.42146
G1 X112.689 Y116.979 E.01018
G1 X112.689 Y121.789 E.20607
G1 X112.311 Y121.789 E.01619
G1 X112.311 Y116.979 E.20607
G1 X112.197 Y116.806 E.00888
;WIDTH:0.419999
G1 X112.121 Y116.79 E.00331
G1 X109.979 Y116.79 E.09141
```

```
;WIDTH:0.45382
G1 X109.899 Y116.853 E.00474
;WIDTH:0.48764
G1 X109.819 Y116.916 E.00513
;WIDTH:0.52146
G1 X109.739 Y116.979 E.00551
G1 X109.739 Y121.739 E.2578
G1 X109.261 Y121.739 E.02589
G1 X109.261 Y116.979 E.2578
G1 X109.244 Y116.66 E.0173
;WIDTH:0.48764
G1 X109.227 Y116.34 E.01613
;WIDTH:0.45382
G1 X109.21 Y116.021 E.01486
;WIDTH:0.419999
G1 X109.21 Y109.21 E.29067
G1 X121.79 Y109.21 E.53687
G1 X121.79 Y113 E.16174
G1 X121.79 Y116.79 E.16174
G1 X121.548 Y116.793 E.01033
G1 X121.501 Y116.975 E.00802
G1 E-3.5 F3600
;WIPE_START
G1 F7200
G1 X121.487 Y116.924 E-.02512
G1 X121.467 Y116.842 E-.04009
G1 X121.421 Y116.79 E-.03298
G1 X118.669 Y116.79 E-1.3072
G1 X118.536 Y116.938 E-.09461
;WIPE_END
G1 X119.54 Y115.716 F9000
G1 E5 F2400
M204 S250
; TYPE: Bridge infill
;WIDTH:0.395349
;HEIGHT:0.389872
G1 F1500
G1 X111.702 Y115.716 E.54448
G1 X111.419 Y115.271 E.03663
G1 X119.58 Y115.271 E.56692
G1 X119.797 Y114.826 E.03439
G1 X111.2 Y114.826 E.59721
G1 X111.039 Y114.38 E.03294
G1 X119.962 Y114.38 E.61985
G1 X120.077 Y113.935 E.03193
G1 X110.926 Y113.935 E.63569
G1 X110.856 Y113.49 E.03129
G1 X120.144 Y113.49 E.64521
G1 X120.169 Y113.044 E.03103
G1 X110.829 Y113.044 E.64882
G1 X110.846 Y112.599 E.03094
G1 X120.152 Y112.599 E.64646
G1 X120.092 Y112.154 E.03119
G1 X110.907 Y112.154 E.63805
G1 X111.013 Y111.708 E.03185
G1 X119.989 Y111.708 E.62354
G1 X119.836 Y111.263 E.03269
G1 X111.166 Y111.263 E.60228
G1 X111.369 Y110.818 E.03398
G1 X119.628 Y110.818 E.57373
G1 X119.361 Y110.372 E.03611
G1 X111.64 Y110.372 E.53635
G1 X111.983 Y109.927 E.03903
G1 X119.277 Y109.927 E.50669
M204 S500
G1 X120.539 Y109.722 F9000
; TYPE: Top solid infill
;WIDTH:0.407953
;HEIGHT:0.2
G1 F1800
G1 X121.117 Y110.3 E.03377
G1 X121.117 Y110.816 E.02132
G1 X120.184 Y109.883 E.05451
G1 X119.667 Y109.883 E.02136
G1 X121.117 Y111.333 E.08472
G1 X121.117 Y111.849 E.02132
G1 X120.068 Y110.8 E.06129
G1 X120.235 Y111.187 E.01741
G1 X120.381 Y111.628 E.01919
G1 X121.117 Y112.365 E.04303
G1 X121.117 Y112.881 E.02132
G1 X120.517 Y112.282 E.03503
```

```
G1 X120.567 Y112.848 E.02347
G1 X121.117 Y113.398 E.03213
G1 X121.117 Y113.914 E.02132
G1 X120.556 Y113.352 E.03281
G1 X120.502 Y113.814 E.01922
G1 X121.117 Y114.43 E.03596
G1 X121.117 Y114.946 E.02132
G1 X120.413 Y114.242 E.04113
G1 X120.295 Y114.64 E.01715
G1 X121.117 Y115.463 E.04806
G1 X121.117 Y115.979 E.02132
G1 X120.151 Y115.012 E.05647
G1 X119.984 Y115.361 E.01598
G1 X120.739 Y116.117 E.04414
G1 X120.223 Y116.117 E.02132
G1 X119.795 Y115.689 E.02501
G1 X119.587 Y115.997 E.01535
G1 X119.868 Y116.278 E.01642
G1 E-3.5 F3600
;WIPE_START
G1 F7200
G1 X119.587 Y115.997 E-.18876
G1 X119.795 Y115.689 E-.17654
G1 X120.223 Y116.117 E-.28751
G1 X120.739 Y116.117 E-.2451
G1 X119.984 Y115.361 E-.50751
G1 X120.07 Y115.182 E-.09458
;WIPE_END
G1 X111.515 Y110.136 F9000
G1 E5 F2400
;WIDTH:0.420784
G1 F1800
G1 X111.262 Y109.883 E.0153
G1 X110.728 Y109.883 E.02284
G1 X111.185 Y110.34 E.02764
G1 X110.992 Y110.682 E.01679
G1 X110.193 Y109.883 E.04832
G1 X109.883 Y109.883 E.01326
G1 X109.883 Y110.107 E.00958
G1 X110.822 Y111.046 E.05679
G1 X110.678 Y111.436 E.01778
G1 X109.883 Y110.641 E.04808
G1 X109.883 Y111.175 E.02284
G1 X110.562 Y111.855 E.0411
G1 X110.48 Y112.307 E.01965
G1 X109.883 Y111.71 E.03611
G1 X109.883 Y112.244 E.02284
G1 X110.437 Y112.798 E.03351
G1 X110.442 Y113.338 E.02309
G1 X109.883 Y112.779 E.03381
G1 X109.883 Y113.313 E.02284
G1 X110.522 Y113.952 E.03865
G1 X110.587 Y114.252 E.01313
G1 X110.718 Y114.682 E.01922
G1 X109.883 Y113.847 E.0505
G1 X109.883 Y114.382 E.02288
G1 X111.221 Y115.72 E.08092
G1 X111.504 Y116.12 E.02095
G1 X111.086 Y116.119 E.01788
G1 X109.883 Y114.916 E.07276
G1 X109.883 Y115.45 E.02284
G1 X110.551 Y116.118 E.0404
G1 X110.015 Y116.117 E.02292
G1 X109.722 Y115.824 E.01772
M106 S252.45
;LAYER_CHANGE
;Z:0.8
;HEIGHT:0.2
;BEFORE_LAYER_CHANGE
G92 E0
;0.8


G1 E-3.5 F3600
;WIPE_START
G1 F7200
G1 X110.015 Y116.117 E-.19682
G1 X110.551 Y116.118 E-.2546
G1 X109.883 Y115.45 E-.44873
G1 X109.883 Y114.916 E-.25365
G1 X110.398 Y115.432 E-.3462
;WIPE_END
```

```
G1 Z.8 F9000
;AFTER_LAYER_CHANGE
;0.8
G1 Z.8
G1 X112.908 Y114.29
G1 E5 F2400
; TYPE: Perimeter
;WIDTH:0.439999
G1 F860
G1 X112.833 Y114.118 E.00843
G1 X112.64 Y113.483 E.02983
G1 X112.611 Y112.752 E.03288
G1 X112.685 Y112.3 E.02058
G1 X112.861 Y111.802 E.02374
G1 X113.202 Y111.231 E.02989
G1 X113.375 Y111.039 E.01161
G1 X113.873 Y110.599 E.02986
G1 X114.525 Y110.269 E.03284
G1 X114.959 Y110.151 E.02021
G1 X115.689 Y110.106 E.03287
G1 X116.134 Y110.17 E.0202
G1 X116.811 Y110.415 E.03236
G1 X117.408 Y110.816 E.03232
G1 X117.587 Y110.999 E.0115
G1 X117.885 Y111.365 E.02121
G1 X118.203 Y111.948 E.02984
G1 X118.379 Y112.654 E.0327
G1 X118.386 Y112.925 E.01218
G1 X118.393 Y113.171 E.01106
G1 X118.28 Y113.826 E.02987
G1 X118.118 Y114.248 E.02031
G1 X117.722 Y114.863 E.03287
G1 X117.543 Y115.046 E.0115
G1 X117.028 Y115.465 E.02984
G1 X116.362 Y115.769 E.0329
G1 X116.113 Y115.826 E.01148
G1 X115.452 Y115.9 E.02989
G1 X114.729 Y115.795 E.03283
G1 X114.298 Y115.64 E.02058
G1 X113.84 Y115.376 E.02376
G1 X113.35 Y114.944 E.02936
G1 X112.935 Y114.353 E.03245
G1 X112.932 Y114.345 E.00038
G1 X112.583 Y114.513 F9000
; TYPE: External perimeter
;WIDTH:0.419999
G1 F860
G1 X112.384 Y114.055 E.02131
G1 X112.255 Y113.538 E.02274
G1 X112.222 Y112.728 E.0346
G1 X112.309 Y112.204 E.02267
G1 X112.509 Y111.637 E.02566
G1 X112.889 Y111 E.03165
G1 X113.246 Y110.604 E.02275
G1 X113.663 Y110.272 E.02275
G1 X114.386 Y109.906 E.03458
G1 X114.896 Y109.767 E.02256
G1 X115.705 Y109.717 E.03459
G1 X116.229 Y109.793 E.0226
G1 X116.987 Y110.067 E.0344
G1 X117.657 Y110.517 E.03444
G1 X118.029 Y110.897 E.02269
G1 X118.337 Y111.336 E.02289
G1 X118.569 Y111.816 E.02275
G1 X118.765 Y112.601 E.03453
G1 X118.773 Y112.914 E.01336
G1 X118.781 Y113.199 E.01217
G1 X118.655 Y113.929 E.03161
G1 X118.465 Y114.424 E.02263
G1 X118.027 Y115.106 E.03459
G1 X117.654 Y115.486 E.02272
G1 X117.224 Y115.801 E.02275
G1 X116.487 Y116.137 E.03457
G1 X115.968 Y116.256 E.02272
G1 X115.436 Y116.288 E.02274
G1 X114.634 Y116.173 E.03458
G1 X114.134 Y115.992 E.02269
G1 X113.614 Y115.692 E.02562
G1 X113.06 Y115.204 E.03151
G1 X112.611 Y114.566 E.03329
G1 E-3.5 F3600
;WIPE_START
```

```
G1 F7200
G1 X112.583 Y114.513 E-.02847
G1 X112.384 Y114.055 E-.2372
G1 X112.255 Y113.538 E-.2531
G1 X112.222 Y112.728 E-.38507
G1 X112.309 Y112.204 E-.25231
G1 X112.509 Y111.637 E-.28559
G1 X112.572 Y111.532 E-.05826
;WIPE_END
G1 X114.459 Y110.645 F9000
G1 E5 F2400
; TYPE: Internal infill
;WIDTH:0.44
G1 F860
G1 X114.901 Y110.484 E.02114
G1 X112.977 Y112.407 E.12225
G1 X112.924 Y112.924 E.02336
G1 X115.585 Y115.585 E.16912
G1 X115.415 Y115.585 E.00764
G1 X118.08 Y112.92 E.16937
G1 X118.074 Y112.696 E.01007
G1 X117.995 Y112.38 E.01464
G1 X116.098 Y110.482 E.1206
G1 X115.677 Y110.413 E.01917
G1 X115.095 Y110.449 E.02621
;LAYER_CHANGE
;Z:1
;HEIGHT:0.2
;BEFORE_LAYER_CHANGE
G92 E0
;1


G1 E-3.5 F3600
;WIPE_START
G1 F7200
G1 X115.677 Y110.413 E-.27698
G1 X116.098 Y110.482 E-.20264
G1 X117.617 Y112.001 E-1.02038
;WIPE_END
G1 Z1 F9000
;AFTER_LAYER_CHANGE
;1
G1 Z1
G1 X115.053 Y110.156
G1 E5 F2400
; TYPE: Perimeter
;WIDTH:0.439999
G1 F1397
G1 X115.376 Y110.104 E.0147
G1 X115.904 Y110.129 E.02375
G1 X116.596 Y110.317 E.03223
G1 X117.215 Y110.663 E.03187
G1 X117.694 Y111.107 E.02935
G1 X117.853 Y111.327 E.0122
G1 X118.119 Y111.774 E.02338
G1 X118.337 Y112.401 E.02983
G1 X118.358 Y112.657 E.01154
G1 X118.396 Y113.121 E.02092
G1 X118.295 Y113.766 E.02934
G1 X118.112 Y114.262 E.02376
G1 X117.879 Y114.659 E.02069
G1 X117.437 Y115.155 E.02986
G1 X117.015 Y115.473 E.02375
G1 X116.607 Y115.681 E.02058
G1 X115.901 Y115.872 E.03287
G1 X115.645 Y115.888 E.01153
G1 X114.982 Y115.853 E.02984
G1 X114.294 Y115.636 E.03242
G1 X113.735 Y115.298 E.02936
G1 X113.353 Y114.949 E.02325
G1 X112.935 Y114.354 E.03268
G1 X112.703 Y113.731 E.02988
G1 X112.616 Y113.204 E.024
G1 X112.637 Y112.54 E.02986
G1 X112.843 Y111.839 E.03284
G1 X113.054 Y111.442 E.0202
G1 X113.522 Y110.88 E.03287
G1 X113.873 Y110.599 E.02021
G1 X114.525 Y110.269 E.03284
G1 X114.778 Y110.2 E.01179
G1 X114.994 Y110.165 E.00983
```

```
G1 X114.939 Y109.784 F9000
;TYPE:External perimeter
;WIDTH:0.419999
G1 F1397
G1 X115.364 Y109.716 E.01837
G1 X115.965 Y109.744 E.02568
G1 X116.743 Y109.955 E.0344
G1 X117.445 Y110.348 E.03433
G1 X117.986 Y110.849 E.03147
G1 X118.338 Y111.337 E.02568
G1 X118.57 Y111.819 E.02283
G1 X118.72 Y112.33 E.02273
G1 X118.744 Y112.625 E.01263
G1 X118.786 Y113.135 E.02184
G1 X118.671 Y113.864 E.0315
G1 X118.463 Y114.428 E.02565
G1 X118.194 Y114.887 E.0227
G1 X117.701 Y115.441 E.03165
G1 X117.221 Y115.803 E.02566
G1 X116.746 Y116.044 E.02273
G1 X115.964 Y116.256 E.03458
G1 X115.433 Y116.289 E.02271
G1 X114.903 Y116.234 E.02274
G1 X114.133 Y115.991 E.03446
G1 X113.502 Y115.61 E.03146
G1 X113.061 Y115.206 E.02552
G1 X112.596 Y114.544 E.03453
G1 X112.384 Y114.055 E.02275
G1 X112.254 Y113.534 E.02292
G1 X112.211 Y113 E.02286
G1 X112.254 Y112.469 E.02274
G1 X112.483 Y111.691 E.03461
G1 X112.731 Y111.225 E.02253
G1 X113.249 Y110.602 E.03458
G1 X113.663 Y110.272 E.02259
G1 X114.386 Y109.906 E.03458
G1 X114.676 Y109.827 E.01283
G1 X114.88 Y109.794 E.00882
G1 X116.679 Y110.506 F9000
;TYPE:Top solid infill
;WIDTH:0.414325
G1 F1397
G1 X117.504 Y111.331 E.04904
G1 X117.757 Y111.682 E.01819
G1 X117.94 Y112.061 E.01769
G1 X118.036 Y112.389 E.01437
G1 X116.135 Y110.487 E.11304
G1 X115.86 Y110.413 E.01197
G1 X115.518 Y110.397 E.01439
G1 X118.098 Y112.976 E.15334
G1 X118.109 Y113.11 E.00565
G1 X118.054 Y113.457 E.01477
G1 X115.026 Y110.429 E.18
G1 X114.615 Y110.544 E.01794
G1 X117.949 Y113.878 E.19819
G1 X117.853 Y114.139 E.01169
G1 X117.791 Y114.245 E.00516
G1 X114.266 Y110.72 E.20955
G1 X114.029 Y110.841 E.01119
G1 X113.936 Y110.915 E.005
G1 X117.583 Y114.562 E.2168
G1 X117.335 Y114.84 E.01566
G1 X113.658 Y111.162 E.21861
G1 X113.42 Y111.449 E.01567
G1 X117.056 Y115.085 E.21614
G1 X116.863 Y115.23 E.01015
G1 X116.739 Y115.293 E.00585
G1 X113.207 Y111.762 E.20993
G1 X113.109 Y111.947 E.0088
G1 X113.054 Y112.134 E.00819
G1 X116.369 Y115.449 E.19706
G1 X115.956 Y115.561 E.01799
G1 X112.935 Y112.54 E.17959
G1 X112.887 Y113.018 E.02019
G1 X115.481 Y115.612 E.1542
G1 X115.04 Y115.572 E.01861
G1 X114.859 Y115.515 E.00798
G1 X112.971 Y113.627 E.11223
G1 X113.024 Y113.838 E.00914
G1 X113.186 Y114.213 E.01717
G1 X113.548 Y114.729 E.0265
G1 X114.332 Y115.513 E.04661
```

```
; stop printing object Slicer Test v3.stl id:0 copy 0
G1 E-3.5 F3600
;WIPE_START
G1 F7200;_WIPE
G1 X113.548 Y114.729 E-.52665
G1 X113.186 Y114.213 E-.2994
G1 X113.024 Y113.838 E-.19404
G1 X112.971 Y113.627 E-.10334
G1 X113.532 Y114.188 E-.37657
;WIPE_END
M107
; TYPE: Custom
; Filament-specific end gcode
;END gcode for filament
```

Listing A.1.2 G-Code Generated Using Prusa Slicer [68] (Main)

```
G1 Z3 F600 ; Move print head up
G1 X5 Y193.8 F9000 ; present print
G1 Z71 F600 ; Move print head further up
G1 Z150 F600 ; Move print head further up
M140 S0 ; turn off heatbed
M104 S0 ; turn off temperature
M107 ; turn off fan
M84 X Y E ; disable motors
; objects_info = {"objects":[{"name":"Slicer Test v3.stl id:0 copy 0","polygon
    ":[[122.000,117.000],[121.600,117.000],[121.600,122.000],[121.400,122.000],[121.400,117.000],[118.700
; filament used [mm] = 58.94
; filament used [cm3] = 0.10
; total filament used [g] = 0.00
; total filament cost = 0.00
; total filament used for wipe tower [g] = 0.00
; estimated printing time (normal mode) = 1m 52s
; estimated first layer printing time (normal mode) = 55s

; prusaslicer_config = begin
; arc_fitting = disabled
; autoemit_temperature_commands = 1
; automatic_extrusion_widths = 0
; automatic_infill_combination = 0
; automatic_infill_combination_max_layer_height = 100%
; avoid_crossing_curled_overhangs = 0
; avoid_crossing_perimeters = 0
; avoid_crossing_perimeters_max_detour = 0
; bed_custom_model =
; bed_custom_texture =
; bed_shape = 3x3,228x3,228x228,3x228
; bed_temperature = 0
; bed_temperature_extruder = 0
; before_layer_gcode = ;BEFORE_LAYER_CHANGE\nG92 E0\n;{layer_z}\n\n
; between_objects_gcode =
; binary_gcode = 0
; bottom_fill_pattern = monotonic
; bottom_solid_layers = 1
; bottom_solid_min_thickness = 0
; bridge_acceleration = 250
; bridge_angle = 0
; bridge_fan_speed = 100
; bridge_flow_ratio = 0.95
; bridge_speed = 25
; brim_separation = 0
; brim_type = outer_only
; brim_width = 0
; chamber_minimal_temperature = 0
; chamber_temperature = 0
; color_change_gcode = M600
; colorprint_heights =
; compatible_printers_condition_cummulative = "printer_model=~/(ENDER|CR|SERMOON).*/ and
    nozzle_diameter[0]==0.4";
; complete_objects = 0
; cooling = 1
; cooling_tube_length = 5
; cooling_tube_retraction = 91.5
; default_acceleration = 500
; default_filament_profile = "Generic PLA @CREALITY"
; default_print_profile = "0.16 mm OPTIMAL (0.4 mm nozzle) @CREALITY"
; deretract_speed = 40
; disable_fan_first_layers = 3
; dont_support_bridges = 1
; draft_shield = disabled
```

```
; duplicate_distance = 6
; elefant_foot_compensation = 0.1
; enable_dynamic_fan_speeds = 0
; enable_dynamic_overhang_speeds = 0
; end_filament_gcode = "; Filament-specific end gcode \n;END gcode for filament\n"
; end_gcode = {if max_layer_z < max_print_height}G1 Z{z_offset+min(max_layer_z+2,
    max_print_height)} F600 ; Move print head up{endif}\nG1 X5 Y{print_bed_max[1]*0.85} F{
    travel_speed*60} ; present print\n{if max_layer_z < max_print_height-10}G1 Z{z_offset+
    min(max_layer_z+70, max_print_height-10)} F600 ; Move print head further up{endif}\n{if
    max_layer_z < max_print_height*0.6}G1 Z{max_print_height*0.6} F600 ; Move print head
    further up{endif}\nM140 S0 ; turn off heatbed\nM104 S0 ; turn off temperature\nM107 ;
    turn off fan\nM84 X Y E ; disable motors
; ensure_vertical_shell_thickness = enabled
; external_perimeter_acceleration = 0
; external_perimeter_extrusion_width = 0.42
; external_perimeter_speed = 25
; external_perimeters_first = 0
; extra_loading_move = -2
; extra_perimeters = 0
; extra_perimeters_on_overhangs = 0
; extruder_clearance_height = 20
; extruder_clearance_radius = 20
; extruder_colour = #FCE94F
; extruder_offset = 0x0
; extrusion_axis = E
; extrusion_multiplier = 1
; extrusion_width = 0.44
; fan_always_on = 0
; fan_below_layer_time = 60
; filament_abrasive = 0
; filament_colour = #29B2B2
; filament_cooling_final_speed = 3.4
; filament_cooling_initial_speed = 2.2
; filament_cooling_moves = 4
; filament_cost = 0
; filament_density = 0
; filament_deretract_speed = nil
; filament_diameter = 1.5
; filament_infill_max_crossing_speed = 0
; filament_infill_max_speed = 0
; filament_load_time = 0
; filament_loading_speed = 28
; filament_loading_speed_start = 3
; filament_max_volumetric_speed = 0
; filament_minimal_purge_on_wipe_tower = 15
; filament_multitool_ramming = 0
; filament_multitool_ramming_flow = 10
; filament_multitool_ramming_volume = 10
; filament_notes = ""
; filament_purge_multiplier = 100%
; filament_ramming_parameters = "120 100 6.6 6.8 7.2 7.6 7.9 8.2 8.7 9.4 9.9 10.0| 0.05 6.6
    0.45 6.8 0.95 7.8 1.45 8.3 1.95 9.7 2.45 10 2.95 7.6 3.45 7.6 3.95 7.6 4.45 7.6 4.95
    7.6"
; filament_retract_before_travel = nil
; filament_retract_before_wipe = nil
; filament_retract_layer_change = nil
; filament_retract_length = nil
; filament_retract_length_toolchange = nil
; filament_retract_lift = nil
; filament_retract_lift_above = nil
; filament_retract_lift_below = nil
; filament_retract_restart_extra = nil
; filament_retract_restart_extra_toolchange = nil
; filament_retract_speed = nil
; filament_seam_gap_distance = nil
; filament_settings_id = "My Settings"
; filament_shrinkage_compensation_xy = 0%
; filament_shrinkage_compensation_z = 0%
; filament_soluble = 0
; filament_spool_weight = 0
; filament_stamping_distance = 0
; filament_stamping_loading_speed = 20
; filament_toolchange_delay = 0
; filament_travel_lift_before_obstacle = nil
; filament_travel_max_lift = nil
; filament_travel_ramping_lift = nil
; filament_travel_slope = nil
; filament_type = PLA
; filament_unload_time = 0
; filament_unloading_speed = 90
; filament_unloading_speed_start = 100
; filament_vendor = (Unknown)
```

```
; filament_wipe = nil
; fill_angle = 45
; fill_density = 20%
; fill_pattern = grid
; first_layer_acceleration = 0
; first_layer_acceleration_over_raft = 0
; first_layer_bed_temperature = 0
; first_layer_extrusion_width = 0.42
; first_layer_height = 0.2
; first_layer_infill_speed = 0
; first_layer_speed = 20
; first_layer_speed_over_raft = 30
; first_layer_temperature = 20
; full_fan_speed_layer = 0
; fuzzy_skin = none
; fuzzy_skin_point_dist = 0.8
; fuzzy_skin_thickness = 0.3
; gap_fill_enabled = 1
; gap_fill_speed = 30
; gcode_comments = 0
; gcode_flavor = marlin
; gcode_label_objects = octoprint
; gcode_resolution = 0.0125
; gcode_substitutions =
; high_current_on_filament_swap = 0
; host_type = prusalink
; idle_temperature = nil
; infill_acceleration = 0
; infill_anchor = 600%
; infill_anchor_max = 50
; infill_every_layers = 1
; infill_extruder = 1
; infill_extrusion_width = 0.44
; infill_first = 0
; infill_overlap = 23%
; infill_speed = 50
; interface_shells = 0
; interlocking_beam = 0
; interlocking_beam_layer_count = 2
; interlocking_beam_width = 0.8
; interlocking_boundary_avoidance = 2
; interlocking_depth = 2
; interlocking_orientation = 22.5
; ironing = 0
; ironing_flowrate = 10%
; ironing_spacing = 0.1
; ironing_speed = 20
; ironing_type = top
; layer_gcode = ;AFTER_LAYER_CHANGE\n;{layer_z}
; layer_height = 0.2
; machine_limits_usage = emit_to_gcode
; machine_max_acceleration_e = 5000
; machine_max_acceleration_extruding = 500
; machine_max_acceleration_retracting = 1000
; machine_max_acceleration_travel = 500
; machine_max_acceleration_x = 500
; machine_max_acceleration_y = 500
; machine_max_acceleration_z = 100
; machine_max_feedrate_e = 60
; machine_max_feedrate_x = 500
; machine_max_feedrate_y = 500
; machine_max_feedrate_z = 10
; machine_max_jerk_e = 5
; machine_max_jerk_x = 8
; machine_max_jerk_y = 8
; machine_max_jerk_z = 0.4
; machine_min_extruding_rate = 0
; machine_min_travel_rate = 0
; max_fan_speed = 100
; max_layer_height = 0.32
; max_print_height = 250
; max_print_speed = 100
; max_volumetric_extrusion_rate_slope_negative = 0
; max_volumetric_extrusion_rate_slope_positive = 0
; max_volumetric_speed = 0
; min_bead_width = 85%
; min_fan_speed = 35
; min_feature_size = 25%
; min_layer_height = 0.06
; min_print_speed = 10
; min_skirt_length = 4
; mmu_segmented_region_interlocking_depth = 0
```

```
; mmu_segmented_region_max_width = 0
; multimaterial_purging = 140
; notes =
; nozzle_diameter = 0.4
; nozzle_high_flow = 0
; only_one_perimeter_first_layer = 0
; only_retract_when_crossing_perimeters = 0
; ooze_prevention = 0
; output_filename_format = {input_filename_base}_{print_time}_{digits(layer_height,1,2)}mm_{
    temperature[0]}C_{filament_type[0]}_{printer_model}.gcode
; over_bridge_speed = 0
; overhang_fan_speed_0 = 0
; overhang_fan_speed_1 = 0
; overhang_fan_speed_2 = 0
; overhang_fan_speed_3 = 0
; overhang_speed_0 = 15
; overhang_speed_1 = 15
; overhang_speed_2 = 20
; overhang_speed_3 = 25
; overhangs = 0
; parking_pos_retraction = 92
; pause_print_gcode =
; perimeter_acceleration = 0
; perimeter_extruder = 1
; perimeter_extrusion_width = 0.44
; perimeter_generator = arachne
; perimeter_speed = 40
; perimeters = 2
; physical_printer_settings_id =
; post_process =
; prefer_clockwise_movements = 0
; print_settings_id = 0.20 mm NORMAL (0.4 mm nozzle) @CREALITY
; printer_model = ENDER3
; printer_notes = Don't remove the following keywords! These keywords are used in the "
    compatible printer" condition of the print and filament profiles to link the particular
    print and filament profiles to this printer profile.\nPRINTER_VENDOR_CREALITY\
    nPRINTER_MODEL_ENDER3\nPRINTER_HAS_BOWDEN
; printer_settings_id = Creality Ender-3 (0.4 mm nozzle)
; printer_technology = FFF
; printer_variant = 0.4
; printer_vendor =
; profile_vendor = Creality
; profile_version = 1.0.0
; raft_contact_distance = 0.1
; raft_expansion = 1.5
; raft_first_layer_density = 90%
; raft_first_layer_expansion = 3
; raft_layers = 0
; remaining_times = 0
; resolution = 0
; retract_before_travel = 2
; retract_before_wipe = 70%
; retract_layer_change = 1
; retract_length = 5
; retract_length_toolchange = 1
; retract_lift = 0
; retract_lift_above = 0.2
; retract_lift_below = 0
; retract_restart_extra = 0
; retract_restart_extra_toolchange = 0
; retract_speed = 60
; scarf_seam_entire_loop = 0
; scarf_seam_length = 20
; scarf_seam_max_segment_length = 1
; scarf_seam_on_inner_perimeters = 0
; scarf_seam_only_on_smooth = 1
; scarf_seam_placement = nowhere
; scarf_seam_start_height = 0%
; seam_gap_distance = 15%
; seam_position = nearest
; silent_mode = 0
; single_extruder_multi_material = 0
; single_extruder_multi_material_priming = 0
; skirt_distance = 3
; skirt_height = 2
; skirts = 0
; slice_closing_radius = 0.049
; slicing_mode = regular
; slowdown_below_layer_time = 5
; small_perimeter_speed = 25
; solid_infill_acceleration = 0
; solid_infill_below_area = 0
```

```
; solid_infill_every_layers = 0
; solid_infill_extruder = 1
; solid_infill_extrusion_width = 0.44
; solid_infill_speed = 40
; spiral_vase = 0
; staggered_inner_seams = 0
; standby_temperature_delta = -5
; start_filament_gcode = "; Filament gcode\n"
; start_gcode = G90 ; use absolute coordinates\nM83 ; extruder relative mode\nM104 S{is_nil(idle_temperature[0]) ? 150 : idle_temperature[0]} ; set temporary nozzle temp to prevent oozing during homing\nM140 S{first_layer_bed_temperature[0]} ; set final bed temp\nG4 S30 ; allow partial nozzle warmup\nG28 ; home all axis\nG1 Z50 F240\nG1 X2.0 Y10 F3000\nM104 S{first_layer_temperature[0]} ; set final nozzle temp\nM190 S{first_layer_bed_temperature[0]} ; wait for bed temp to stabilize\nM109 S{first_layer_temperature[0]} ; wait for nozzle temp to stabilize\nG1 Z0.28 F240\nG92 E0\nG1 X2.0 Y140 E10 F1500 ; prime the nozzle\nG1 X2.3 Y140 F5000\nG92 E0\nG1 X2.3 Y10 E10 F1200 ; prime the nozzle\nG92 E0
; support_material = 0
; support_material_angle = 0
; support_material_auto = 1
; support_material_bottom_contact_distance = 0
; support_material_bottom_interface_layers = -1
; support_material_buildplate_only = 0
; support_material_closing_radius = 2
; support_material_contact_distance = 0.15
; support_material_enforce_layers = 0
; support_material_extruder = 0
; support_material_extrusion_width = 0.36
; support_material_interface_contact_loops = 0
; support_material_interface_extruder = 0
; support_material_interface_layers = 2
; support_material_interface_pattern = rectilinear
; support_material_interface_spacing = 0.2
; support_material_interface_speed = 100%
; support_material_pattern = rectilinear
; support_material_spacing = 1
; support_material_speed = 40
; support_material_style = grid
; support_material_synchronize_layers = 0
; support_material_threshold = 40
; support_material_with_sheath = 0
; support_material_xy_spacing = 60%
; support_tree_angle = 40
; support_tree_angle_slow = 25
; support_tree_branch_diameter = 2
; support_tree_branch_diameter_angle = 5
; support_tree_branch_diameter_double_wall = 3
; support_tree_branch_distance = 1
; support_tree_tip_diameter = 0.8
; support_tree_top_rate = 15%
; temperature = 20
; template_custom_gcode =
; thick_bridges = 1
; thin_walls = 0
; thumbnails =
; thumbnails_format = PNG
; toolchange_gcode =
; top_fill_pattern = monotonic
; top_infill_extrusion_width = 0.4
; top_one_perimeter_type = none
; top_solid_infill_acceleration = 0
; top_solid_infill_speed = 30
; top_solid_layers = 1
; top_solid_min_thickness = 0
; travel_acceleration = 0
; travel_lift_before_obstacle = 0
; travel_max_lift = 0
; travel_ramping_lift = 0
; travel_slope = 0
; travel_speed = 150
; travel_speed_z = 0
; use_firmware_retraction = 0
; use_relative_e_distances = 1
; use_volumetric_e = 0
; variable_layer_height = 1
; wall_distribution_count = 1
; wall_transition_angle = 10
; wall_transition_filter_deviation = 25%
; wall_transition_length = 100%
; wipe = 1
; wipe_into_infill = 0
; wipe_into_objects = 0
```

```
; wipe_tower = 0
; wipe_tower_acceleration = 0
; wipe_tower_bridging = 10
; wipe_tower_brim_width = 2
; wipe_tower_cone_angle = 0
; wipe_tower_extra_flow = 100%
; wipe_tower_extra_spacing = 100%
; wipe_tower_extruder = 0
; wipe_tower_no_sparse_layers = 0
; wipe_tower_width = 60
; wiping_volumes_matrix = 0
; wiping_volumes_use_custom_matrix = 0
; xy_size_compensation = 0
; z_offset = 0
; prusaslicer_config = end
```

Listing A.1.3 G-Code generated using Prusa Slicer [68] (Reset)

A.2 OrcaSlicer 2.2.0 – G-Code Listing

```
; HEADER_BLOCK_START
; generated by OrcaSlicer 2.2.0 on 2025-04-14 at 16:23:04
; total layer number: 5
; filament_density: 1.24
; filament_diameter: 1.75
; max_z_height: 1.00
; HEADER_BLOCK_END

; external perimeters extrusion width = 0.45mm
; perimeters extrusion width = 0.45mm
; infill extrusion width = 0.45mm
; solid infill extrusion width = 0.45mm
; top infill extrusion width = 0.40mm
; first layer extrusion width = 0.42mm

; EXECUTABLE_BLOCK_START
M73 P0 R2
M201 X500 Y500 Z100 E5000
M203 X500 Y500 Z10 E60
M204 P500 R1000 T500
M205 X8.00 Y8.00 Z0.40 E5.00 ; sets the jerk limits, mm/sec
; TYPE: Custom
G90 ; use absolute coordinates
M83 ; extruder relative mode
M140 S60 ; set final bed temp
M104 S150 ; set temporary nozzle temp to prevent oozing during homing
G4 S10 ; allow partial nozzle warmup
G28 ; home all axis
G1 Z50 F240
G1 X2 Y10 F3000
M73 P10 R1
M104 S220 ; set final nozzle temp
M190 S60 ; wait for bed temp to stabilize
M109 S220 ; wait for nozzle temp to stabilize
M73 P10 R1
G1 Z0.28 F240
G92 E0
G1 Y140 E10 F1500 ; prime the nozzle
M73 P21 R1
M73 P21 R1
G1 X2.3 F5000
M73 P25 R1
G92 E0
M73 P25 R1
G1 Y10 E10 F1200 ; prime the nozzle
G92 E0
```

Listing A.2.1 G-Code Generated Using Orca Slicer [63] (Initialization)

```
G90
G21
M83 ; use relative distances for extrusion
; filament start gcode
M106 S0
;LAYER_CHANGE
;Z:0.2
```

```
;HEIGHT:0.2
;BEFORE_LAYER_CHANGE
;0.2
G92 E0

G1 E-4 F3600
M73 P30 R1
;_SET_FAN_SPEED_CHANGING_LAYER
; printing object Slicer Test v3.stl id:0 copy 0
M73 P30 R1
G1 Z.6 F9000
G1 X115.895 Y110.906
M73 P31 R1
M73 P31 R1
G1 Z.6
M73 P32 R1
M73 P32 R1
G1 Z.2
G1 E4 F2400
; TYPE: Inner wall
;WIDTH:0.419999
G1 F900
G1 X115.472 Y110.847 E.01312
G1 X114.702 Y110.819 E.0237
G1 X113.565 Y110.852 E.03494
G1 X112.951 Y110.93 E.01901
G1 X112.453 Y110.876 E.0154
G1 X113.021 Y110.396 E.02285
G1 X113.399 Y109.943 E.01814
G1 X113.923 Y108.96 E.03423
G1 X114.11 Y108.28 E.02165
G1 X114.18 Y107.283 E.03071
G1 X114.089 Y106.607 E.02097
G1 X113.923 Y106.041 E.01813
G1 X113.79 Y105.767 E.00935
G1 X113.399 Y105.058 E.02489
G1 X112.951 Y104.533 E.02121
G1 X112.518 Y104.169 E.01739
G1 X112.999 Y104.186 E.01481
G1 X115.813 Y104.187 E.08647
G1 X115.819 Y110.032 E.1796
M73 P33 R1
M73 P33 R1
G1 X115.892 Y110.866 E.02572
G1 X116 Y111.479 F9000
; TYPE: Outer wall
G1 F900
G1 X115.949 Y111.295 E.00585
G1 X115.459 Y111.223 E.01523
G1 X114.543 Y111.191 E.02815
G1 X113.641 Y111.223 E.02773
G1 X113.136 Y111.298 E.01568
G1 X113 Y111.481 E.00701
;WIDTH:0.419168
G1 X112.901 Y111.31 E.00604
;WIDTH:0.419999
G1 X112.297 Y111.241 E.01868
G1 X111.298 Y111.29 E.03075
;WIDTH:0.459296
G1 X111.19 Y111.27 E.00372
;WIDTH:0.498592
G1 X111.082 Y111.25 E.00407
;WIDTH:0.537889
G1 X110.974 Y111.231 E.00442
;WIDTH:0.577185
G1 X110.866 Y111.211 E.00478
G1 X110.959 Y111.156 E.00474
;WIDTH:0.537889
G1 X111.053 Y111.1 E.00439
;WIDTH:0.498592
G1 X111.147 Y111.045 E.00404
;WIDTH:0.459296
G1 X111.24 Y110.989 E.00369
;WIDTH:0.419999
G1 X111.695 Y110.846 E.01466
G1 X112.255 Y110.558 E.01934
G1 X112.731 Y110.155 E.01917
G1 X113.131 Y109.669 E.01932
G1 X113.561 Y108.853 E.02835
M73 P34 R1
M73 P34 R1
G1 X113.734 Y108.25 E.0193
```

```
G1 X113.806 Y107.329 E.02836
G1 X113.727 Y106.713 E.01908
G1 X113.561 Y106.147 E.01813
G1 X113.109 Y105.299 E.02953
G1 X112.628 Y104.754 E.02234
G1 X112.219 Y104.417 E.01628
G1 X111.667 Y104.143 E.01894
G1 X111.102 Y103.958 E.01827
;WIDTH:0.460708
G1 X110.92 Y103.896 E.00654
;WIDTH:0.501417
G1 X110.739 Y103.833 E.00717
;WIDTH:0.542126
G1 X110.557 Y103.771 E.00781
G1 X110.758 Y103.751 E.00821
;WIDTH:0.501417
G1 X110.959 Y103.73 E.00754
;WIDTH:0.460708
G1 X111.159 Y103.71 E.00687
;WIDTH:0.419999
G1 X113 Y103.809 E.05663
G1 X116.19 Y103.81 E.09804
G1 X116.196 Y110.011 E.19054
G1 X116.29 Y111.29 E.0394
M73 P35 R1
M73 P35 R1
G1 X116.058 Y111.291 E.00714
G1 X116.012 Y111.44 E.00479
G1 E-2.8 F3600
;WIPE_START
G1 F900
G1 X115.949 Y111.295 E-.18986
G1 X115.459 Y111.223 E-.59469
G1 X115.113 Y111.211 E-.41545
;WIPE_END
G1 Z.6 F9000
G1 X116 Y115.995 Z.6
G1 Z.2
G1 E4 F2400
;WIDTH:0.38292
G1 F900
G1 X116 Y111.479 E.12513
G1 E-2.8 F3600
M73 P36 R1
;WIPE_START
M73 P36 R1
G1 F900
G1 X116 Y112.479 E-1.2
;WIPE_END
G1 Z.6 F9000
G1 X110.831 Y111.204 Z.6
G1 Z.2
G1 E4 F2400
;WIDTH:0.592342
G1 F900
G1 X110.555 Y111.224 E.0124
;WIDTH:0.552763
G1 X110.279 Y111.243 E.01151
;WIDTH:0.554051
G1 X110.209 Y111.264 E.00303
;WIDTH:0.594918
G1 X110.139 Y111.285 E.00327
;WIDTH:0.635785
G1 X110.07 Y111.306 E.00351
;WIDTH:0.676652
G1 X110 Y111.327 E.00376
G1 E-2.8 F3600
;WIPE_START
G1 F900
G1 X110.07 Y111.306 E-.10332
G1 X110.139 Y111.285 E-.10332
G1 X110.209 Y111.264 E-.10332
G1 X110.279 Y111.243 E-.10332
G1 X110.555 Y111.224 E-.39337
G1 X110.831 Y111.204 E-.39337
;WIPE_END
G1 Z.6 F9000
G1 X110 Y115.981 Z.6
G1 Z.2
M73 P37 R1
M73 P37 R1
G1 E4 F2400
```

```
;WIDTH:0.638326
G1 F900
G1 X110 Y113.654 E.11289
;WIDTH:0.676652
G1 X110 Y111.327 E.12016
G1 X109.899 Y111.305 E.00532
;WIDTH:0.638054
G1 X109.799 Y111.283 E.00499
;WIDTH:0.599455
G1 X109.698 Y111.261 E.00467
;WIDTH:0.560857
G1 X109.598 Y111.239 E.00435
G1 E-2.8 F3600
;WIPE_START
G1 F900
G1 X109.698 Y111.261 E-.12359
G1 X109.799 Y111.283 E-.12359
G1 X109.899 Y111.305 E-.12359
G1 X110 Y111.327 E-.12359
G1 X110 Y111.916 E-.70564
;WIPE_END
G1 Z.6 F9000
G1 X113 Y115.988 Z.6
G1 Z.2
G1 E4 F2400
M73 P38 R1
;WIDTH:0.400002
M73 P38 R1
G1 F900
G1 X113 Y111.481 E.13115
G1 E-2.8 F3600
;WIPE_START
G1 F900
G1 X113 Y112.481 E-1.2
;WIPE_END
G1 Z.6 F9000
G1 X109.313 Y103.781 Z.6
G1 Z.2
G1 E4 F2400
;WIDTH:0.562994
G1 F900
M73 P39 R1
M73 P39 R1
G1 X109.572 Y103.767 E.01101
;WIDTH:0.534714
G1 X109.831 Y103.753 E.01041
;WIDTH:0.536148
G1 X110.513 Y103.768 E.02742
;WIDTH:0.542126
G1 X110.557 Y103.771 E.00179
G1 E-2.8 F3600
;WIPE_START
G1 F900
G1 X110.513 Y103.768 E-.05267
G1 X109.831 Y103.753 E-.81865
G1 X109.572 Y103.767 E-.31173
G1 X109.558 Y103.768 E-.01695
;WIPE_END
G1 Z.6 F9000
G1 X107.094 Y111.006 Z.6
G1 Z.2
G1 E4 F2400
; TYPE: Inner wall
;WIDTH:0.419999
G1 F900
G1 X106.999 Y111.065 E.00342
G1 X106.87 Y110.971 E.00491
G1 X106.312 Y110.876 E.01737
G1 X105.763 Y110.818 E.01698
G1 X104.381 Y110.813 E.04247
G1 X104.187 Y111.006 E.0084
G1 X104.187 Y104.186 E.20956
G1 X107.459 Y104.182 E.10052
M73 P40 R1
M73 P40 R1
G1 X106.863 Y104.729 E.02484
G1 X106.504 Y105.198 E.01814
G1 X106.236 Y105.729 E.01828
G1 X106.016 Y106.224 E.01663
G1 X105.825 Y107.205 E.03071
G1 X105.832 Y107.887 E.02097
G1 X105.958 Y108.581 E.02166
```

```
G1 X106.258 Y109.36 E.02567
G1 X106.411 Y109.637 E.00972
G1 X106.71 Y110.086 E.01655
G1 X107.175 Y110.584 E.02096
G1 X107.584 Y110.893 E.01574
G1 X107.195 Y110.943 E.01203
M73 P41 R1
M73 P41 R1
G1 X107.128 Y110.985 E.00244
G1 X107.289 Y111.312 F9000
;TYPE:Outer wall
G1 F900
G1 X107.189 Y111.479 E.00599
G1 X107.189 Y115.974 E.13812
G1 X107.158 Y116.219 E.00758
G1 X106.842 Y116.219 E.00972
G1 X106.811 Y115.986 E.0072
G1 X106.811 Y111.48 E.13846
G1 X106.71 Y111.313 E.00601
G1 X106.271 Y111.251 E.01363
G1 X105.761 Y111.195 E.01574
G1 X104.379 Y111.19 E.04247
;WIDTH:0.42146
G1 X104.189 Y111.378 E.00826
G1 X104.189 Y116.189 E.1484
G1 X103.811 Y116.189 E.01168
M73 P42 R1
M73 P42 R1
G1 X103.81 Y110.618 E.17184
;WIDTH:0.419999
G1 X103.81 Y103.81 E.20922
G1 X107.512 Y103.802 E.11375
;WIDTH:0.446963
G1 X108.027 Y103.784 E.01697
G1 X108.525 Y103.71 E.01657
M73 P43 R1
;WIDTH:0.467445
M73 P43 R1
G1 X108.778 Y103.738 E.0088
;WIDTH:0.51522
G1 X109.03 Y103.766 E.00979
;WIDTH:0.562994
G1 X109.283 Y103.795 E.01078
;WIDTH:0.551374
G1 X108.903 Y103.932 E.01676
;WIDTH:0.515766
G1 X108.523 Y104.07 E.01558
;WIDTH:0.480158
G1 X108.142 Y104.208 E.01441
;WIDTH:0.444549
G1 X107.619 Y104.534 E.0202
;WIDTH:0.419999
G1 X107.163 Y104.959 E.01914
G1 X106.783 Y105.46 E.01932
G1 X106.385 Y106.3 E.02856
G1 X106.202 Y107.205 E.02836
G1 X106.204 Y107.826 E.01908
G1 X106.31 Y108.445 E.01931
G1 X106.645 Y109.305 E.02836
G1 X106.985 Y109.828 E.01916
G1 X107.466 Y110.338 E.02153
G1 X107.88 Y110.643 E.01581
G1 X108.195 Y110.804 E.01088
G1 X109.043 Y111.084 E.02743
;WIDTH:0.454086
G1 X109.228 Y111.136 E.00643
;WIDTH:0.488172
G1 X109.413 Y111.187 E.00697
;WIDTH:0.522258
G1 X109.598 Y111.239 E.0075
G1 X109.326 Y111.256 E.01065
;WIDTH:0.488172
G1 X109.054 Y111.273 E.00989
;WIDTH:0.454086
G1 X108.782 Y111.29 E.00913
;WIDTH:0.419999
G1 X107.791 Y111.253 E.03047
G1 X107.329 Y111.307 E.01428
G1 E-2.8 F3600
;WIPE_START
G1 F900
G1 X107.189 Y111.479 E-.26622
```

```
G1 X107.189 Y112.257 E-.93378
;WIPE_END
G1 Z.6 F9000
G1 X106.739 Y104.718
M73 P44 R1
M73 P44 R1
G1 Z.6
G1 Z.2
G1 E4 F2400
; TYPE: Bottom surface
;WIDTH:0.42906
G1 F2100
G1 X106.485 Y104.464 E.01132
G1 X105.94 Y104.465 E.01715
G1 X106.378 Y104.902 E.01946
G1 X106.277 Y105.03 E.00509
G1 X106.161 Y105.232 E.00735
G1 X105.395 Y104.466 E.03408
G1 X104.85 Y104.467 E.01715
G1 X105.983 Y105.601 E.05043
G1 X105.806 Y105.969 E.01287
G1 X104.47 Y104.633 E.05945
G1 X104.47 Y105.179 E.01718
G1 X105.691 Y106.4 E.05432
G1 X105.597 Y106.852 E.01454
G1 X104.47 Y105.725 E.05016
G1 X104.47 Y106.271 E.01718
M73 P45 R1
M73 P45 R1
G1 X105.542 Y107.343 E.04771
G1 X105.542 Y107.802 E.01444
G1 X105.557 Y107.905 E.00327
G1 X104.47 Y106.817 E.0484
G1 X104.47 Y107.363 E.01718
G1 X105.658 Y108.551 E.05286
G1 X105.977 Y109.417 E.02902
G1 X104.47 Y107.91 E.06706
G1 X104.47 Y108.456 E.01718
G1 X106.643 Y110.629 E.09672
G1 X106.032 Y110.564 E.01935
G1 X104.47 Y109.002 E.0695
G1 X104.47 Y109.548 E.01718
G1 X105.458 Y110.536 E.04395
G1 X104.912 Y110.536 E.01718
G1 X104.3 Y109.924 E.02721
G1 E-2.8 F3600
;WIPE_START
G1 F2100
G1 X104.912 Y110.536 E-1.03773
G1 X105.047 Y110.536 E-.16227
M73 P46 R1
;WIPE_END
M73 P46 R1
G1 Z.6 F9000
G1 X115.701 Y105.07 Z.6
G1 Z.2
G1 E4 F2400
;WIDTH:0.423234
G1 F2100
G1 X115.101 Y104.47 E.02631
G1 X114.563 Y104.469 E.01667
G1 X115.532 Y105.438 E.04246
G1 X115.532 Y105.977 E.01668
G1 X114.025 Y104.469 E.06606
G1 X113.487 Y104.469 E.01667
G1 X115.533 Y106.515 E.08966
G1 X115.533 Y107.053 E.01668
G1 X113.956 Y105.476 E.06913
G1 X114.193 Y105.957 E.01662
M73 P47 R1
M73 P47 R1
G1 X114.315 Y106.373 E.01346
G1 X115.533 Y107.591 E.05339
G1 X115.534 Y108.13 E.01668
G1 X114.425 Y107.021 E.04859
G1 X114.468 Y107.349 E.01026
G1 X114.448 Y107.582 E.00723
G1 X115.534 Y108.668 E.0476
G1 X115.535 Y109.206 E.01668
G1 X114.407 Y108.079 E.04941
G1 X114.382 Y108.381 E.00939
G1 X114.336 Y108.545 E.00529
```

```
G1 X115.535 Y109.745 E.05258
G1 X115.555 Y110.303 E.0173
G1 X114.216 Y108.963 E.0587
G1 X114.131 Y109.195 E.00765
G1 X114.054 Y109.339 E.00507
G1 X115.272 Y110.557 E.05336
G1 X114.715 Y110.538 E.01727
G1 X113.867 Y109.69 E.03715
G1 X113.675 Y110.036 E.01226
G1 X114.183 Y110.543 E.02223
G1 X113.664 Y110.562 E.0161
G1 X113.318 Y110.217 E.01515
; stop printing object Slicer Test v3.stl id:0 copy 0
M106 S255
;LAYER_CHANGE
;Z:0.4
;HEIGHT:0.2
;BEFORE_LAYER_CHANGE
;0.4
G92 E0

G1 E-2.8 F3600
;WIPE_START
G1 F2100
M73 P48 R1
M73 P48 R1
G1 X113.664 Y110.562 E-.58669
G1 X114.174 Y110.544 E-.61331
;WIPE_END
;_SET_FAN_SPEED_CHANGING_LAYER
; printing object Slicer Test v3.stl id:0 copy 0
G1 Z.8 F9000
G1 X112.354 Y104.132 Z.8
G1 Z.4
G1 E4 F2400
; TYPE: Inner wall
;WIDTH:0.449999
G1 F2077
G1 X115.868 Y104.132 E.11656
G1 X115.868 Y110.868 E.22344
G1 X112.349 Y110.868 E.11672
G1 X112.647 Y110.668 E.01188
M73 P49 R1
M73 P49 R1
G1 X113.208 Y110.102 E.02644
G1 X113.588 Y109.546 E.02234
G1 X113.873 Y108.936 E.02234
G1 X114.057 Y108.264 E.02313
G1 X114.125 Y107.282 E.03265
G1 X114.034 Y106.615 E.02234
G1 X113.837 Y105.971 E.02232
G1 X113.537 Y105.367 E.02236
G1 X113.144 Y104.821 E.02232
G1 X112.743 Y104.412 E.01903
G1 X112.387 Y104.155 E.01455
G1 X110.831 Y103.857 F9000
; TYPE: Outer wall
;WIDTH:0.542128
G1 F2077
G1 X110.557 Y103.771 E.0117
G1 X110.844 Y103.748 E.0117
;WIDTH:0.496064
G1 X111.13 Y103.725 E.01062
;WIDTH:0.449999
G1 X116.275 Y103.725 E.17066
G1 X116.275 Y111.275 E.25045
G1 X116.045 Y111.278 E.00763
G1 X116.023 Y111.378 E.00341
;WIDTH:0.41646
G1 X116 Y111.479 E.00313
;WIDTH:0.4225
G1 X115.97 Y111.334 E.00457
;WIDTH:0.449999
G1 X115.921 Y111.275 E.00253
G1 X113.135 Y111.28 E.09242
G1 X113 Y111.479 E.00798
G1 X112.903 Y111.292 E.00699
G1 X112.821 Y111.275 E.00275
G1 X111.131 Y111.275 E.05608
;WIDTH:0.49338
G1 X110.844 Y111.252 E.01056
;WIDTH:0.536761
```

```
G1 X110.557 Y111.229 E.01158
G1 X110.847 Y111.138 E.01225
;WIDTH:0.49338
G1 X111.138 Y111.046 E.01117
;WIDTH:0.449999
G1 X111.705 Y110.81 E.0204
G1 X112.451 Y110.304 E.02991
M73 P50 R1
M73 P50 R1
G1 X112.874 Y109.868 E.02014
G1 X113.221 Y109.37 E.02014
G1 X113.482 Y108.822 E.02014
G1 X113.651 Y108.23 E.0204
G1 X113.721 Y107.332 E.02991
G1 X113.644 Y106.729 E.02014
G1 X113.47 Y106.148 E.02013
G1 X113.204 Y105.601 E.02017
G1 X112.853 Y105.106 E.02013
G1 X112.421 Y104.671 E.02035
G1 X111.735 Y104.207 E.02749
G1 X111.106 Y103.944 E.02262
;WIDTH:0.496064
G1 X110.87 Y103.869 E.00914
G1 E-2.8 F3600
;WIPE_START
G1 F2400
G1 X110.557 Y103.771 E-.39302
G1 X110.844 Y103.748 E-.34502
G1 X111.13 Y103.725 E-.34502
G1 X111.228 Y103.725 E-.11693
;WIPE_END
G1 Z.8 F9000
G1 X116 Y116.4 Z.8
M73 P50 R0
M73 P50 R0
G1 Z.4
G1 E4 F2400
;WIDTH:0.38292
G1 F2077
G1 X116 Y111.479 E.13635
G1 E-2.8 F3600
M73 P51 R0
;WIPE_START
M73 P51 R0
G1 F2400
G1 X116 Y112.479 E-1.2
;WIPE_END
G1 Z.8 F9000
G1 X110 Y111.332 Z.8
G1 Z.4
G1 E4 F2400
;WIDTH:0.672612
G1 F2077
G1 X110.074 Y111.303 E.00409
;WIDTH:0.623385
G1 X110.148 Y111.273 E.00377
;WIDTH:0.574158
G1 X110.222 Y111.244 E.00345
;WIDTH:0.539606
G1 X110.545 Y111.23 E.01305
G1 X109.331 Y111.22 F9000
;WIDTH:0.560456
G1 F2077
G1 X109.721 Y111.24 E.0165
;WIDTH:0.558581
G1 X109.791 Y111.263 E.00308
;WIDTH:0.596591
G1 X109.861 Y111.286 E.00331
;WIDTH:0.634602
G1 X109.93 Y111.309 E.00354
;WIDTH:0.672612
G1 X110 Y111.332 E.00376
G1 X110 Y111.405 E.00377
;WIDTH:0.636306
G1 X110 Y111.479 E.00355
;WIDTH:0.6
G1 X110 Y116.2 E.21433
G1 E-2.8 F3600
;WIPE_START
G1 F2400
M73 P52 R0
M73 P52 R0
```

```
G1 X110 Y115.2 E-1.2
;WIPE_END
G1 Z.8 F9000
G1 X113 Y116.3 Z.8
G1 Z.4
G1 E4 F2400
;WIDTH:0.4
G1 F2077
G1 X113 Y111.479 E.14029
G1 E-2.8 F3600
;WIPE_START
G1 F2400
G1 X113 Y112.479 E-1.2
;WIPE_END
G1 Z.8 F9000
G1 X110.557 Y103.771 Z.8
G1 Z.4
M73 P53 R0
M73 P53 R0
G1 E4 F2400
;WIDTH:0.542128
G1 F2077
G1 X110.508 Y103.768 E.00198
;WIDTH:0.535964
G1 X109.673 Y103.759 E.03356
;WIDTH:0.554041
G1 X109.458 Y103.777 E.00902
;WIDTH:0.590814
G1 X109.242 Y103.795 E.00967
;WIDTH:0.627586
G1 X109.026 Y103.814 E.01031
G1 E-2.8 F3600
;WIPE_START
G1 F2400
G1 X109.242 Y103.795 E-.25979
G1 X109.458 Y103.777 E-.25979
G1 X109.673 Y103.759 E-.25979
G1 X110.024 Y103.763 E-.42063
;WIPE_END
G1 Z.8 F9000
G1 X104.132 Y111.214 Z.8
G1 Z.4
G1 E4 F2400
; TYPE: Inner wall
;WIDTH:0.449999
G1 F2077
M73 P54 R0
M73 P54 R0
G1 X104.132 Y104.132 E.23493
G1 X107.638 Y104.132 E.11631
G1 X107.386 Y104.302 E.01009
G1 X106.887 Y104.789 E.02313
G1 X106.392 Y105.493 E.02854
G1 X106.288 Y105.702 E.00775
G1 X106.067 Y106.247 E.0195
G1 X105.88 Y107.213 E.03265
G1 X105.891 Y107.906 E.02299
G1 X106.08 Y108.795 E.03014
G1 X106.379 Y109.487 E.02499
G1 X106.763 Y110.063 E.02297
G1 X107.311 Y110.63 E.02616
G1 X107.633 Y110.868 E.0133
G1 X107.236 Y110.885 E.01319
G1 X107 Y111.007 E.00883
G1 X106.886 Y110.928 E.00462
G1 X106.621 Y110.868 E.00898
G1 X104.479 Y110.868 E.07108
G1 X104.16 Y111.186 E.01493
G1 X104.359 Y111.377 F9000
; TYPE: Outer wall
;WIDTH:0.52146
G1 F2077
G1 X104.239 Y111.479 E.00612
G1 X104.239 Y116.239 E.18564
G1 X103.761 Y116.239 E.01866
G1 X103.761 Y111.479 E.18564
G1 X103.743 Y111 E.01867
M73 P55 R0
;WIDTH:0.48573
M73 P55 R0
G1 X103.725 Y110.521 E.01728
;WIDTH:0.449999
```

```
G1 X103.725 Y103.725 E.22545
G1 X108.402 Y103.725 E.15514
;WIDTH:0.494396
G1 X108.558 Y103.747 E.0058
;WIDTH:0.538793
G1 X108.714 Y103.769 E.00637
;WIDTH:0.58319
G1 X108.87 Y103.792 E.00694
;WIDTH:0.627586
G1 X109.026 Y103.814 E.00751
G1 X108.981 Y103.838 E.00242
;WIDTH:0.604692
G1 X108.844 Y103.909 E.00709
;WIDTH:0.566019
G1 X108.706 Y103.98 E.0066
;WIDTH:0.527346
G1 X108.569 Y104.052 E.00612
;WIDTH:0.488673
G1 X108.431 Y104.123 E.00563
;WIDTH:0.449999
G1 X107.665 Y104.598 E.02991
G1 X107.22 Y105.023 E.0204
G1 X106.662 Y105.864 E.03348
G1 X106.465 Y106.329 E.01676
G1 X106.287 Y107.213 E.02991
G1 X106.291 Y107.826 E.02035
G1 X106.456 Y108.638 E.02749
G1 X106.721 Y109.266 E.02262
G1 X107.031 Y109.749 E.01901
G1 X107.655 Y110.388 E.02964
G1 X108.197 Y110.759 E.02176
G1 X108.75 Y111.008 E.02013
;WIDTH:0.486818
G1 X108.943 Y111.079 E.00746
;WIDTH:0.523637
G1 X109.137 Y111.149 E.00807
;WIDTH:0.560456
G1 X109.331 Y111.22 E.00869
G1 X109.288 Y111.226 E.00181
;WIDTH:0.548669
G1 X109.001 Y111.25 E.01187
;WIDTH:0.499334
G1 X108.714 Y111.275 E.01072
;WIDTH:0.449999
G1 X107.379 Y111.275 E.0443
G1 X107.238 Y111.332 E.00504
;WIDTH:0.449612
G1 X107.189 Y111.479 E.00512
;WIDTH:0.42146
G1 X107.189 Y116.289 E.14839
G1 X106.811 Y116.289 E.01168
G1 X106.811 Y111.479 E.14839
;WIDTH:0.449612
G1 X106.762 Y111.332 E.00512
M73 P56 R0
;WIDTH:0.449999
M73 P56 R0
G1 X106.621 Y111.275 E.00504
G1 X104.479 Y111.275 E.07108
;WIDTH:0.48573
G1 X104.389 Y111.351 E.00422
G1 E-2.8 F3600
;WIPE_START
G1 F2400
G1 X104.239 Y111.479 E-.23648
G1 X104.239 Y112.281 E-.96352
;WIPE_END
G1 Z.8 F9000
G1 X106.434 Y110.563
G1 Z.8
G1 Z.4
G1 E4 F2400
; TYPE: Sparse infill
;WIDTH:0.45
G1 F2077
G1 X104.806 Y110.563 E.05401
G1 X104.437 Y110.194 E.01728
G1 X104.437 Y109.806 E.01289
G1 X105.706 Y108.537 E.0595
G1 X105.587 Y107.938 E.02026
G1 X105.574 Y107.209 E.0242
G1 X105.592 Y107.032 E.00588
```

```
G1 X105.769 Y106.18 E.02888
G1 X105.879 Y105.879 E.01062
G1 X104.437 Y104.437 E.06764
G1 X104.437 Y106.066 E.05401
M73 P57 R0
M73 P57 R0
G1 E-3 F3600
;WIPE_START
G1 X104.437 Y105.066 E-1
;WIPE_END
G1 Z.8 F9000
G1 X115.563 Y106.066 Z.8
G1 Z.4
G1 E4 F2400
G1 F2077
G1 X115.563 Y104.437 E.05401
G1 X114.125 Y105.875 E.06746
G1 X114.329 Y106.535 E.02293
G1 X114.435 Y107.354 E.02738
G1 X114.351 Y108.374 E.03394
G1 X114.3 Y108.543 E.00586
M73 P58 R0
M73 P58 R0
G1 X115.563 Y109.806 E.05924
G1 X115.563 Y110.194 E.01289
G1 X115.192 Y110.565 E.01737
G1 X113.564 Y110.572 E.05401
; stop printing object Slicer Test v3.stl id:0 copy 0
;LAYER_CHANGE
;Z:0.6
;HEIGHT:0.2
;BEFORE_LAYER_CHANGE
;0.6
G92 E0

G1 E-3 F3600
;WIPE_START
G1 X114.564 Y110.567 E-1
;WIPE_END
;_SET_FAN_SPEED_CHANGING_LAYER
; printing object Slicer Test v3.stl id:0 copy 0
G1 Z1 F9000
G1 X104.132 Y111.214 Z1
G1 Z.6
G1 E4 F2400
; TYPE: Inner wall
;WIDTH:0.449999
G1 X104.132 Y104.132 E.23492
G1 X115.868 Y104.132 E.3893
M73 P59 R0
M73 P59 R0
G1 X115.868 Y110.868 E.22345
G1 X113.066 Y110.868 E.09295
G1 X113 Y110.949 E.00347
G1 X112.944 Y110.88 E.00295
G1 X112.821 Y110.868 E.0041
G1 F1200
G1 X110.942 Y110.868 E.06233
G1 F840
G1 X110.279 Y110.868 E.02199
G1 X110.042 Y110.916 E.00802
G1 F960
G1 X110 Y110.979 E.00251
G1 X109.958 Y110.916 E.00251
G1 F840
G1 X109.721 Y110.868 E.00802
G1 X109.052 Y110.868 E.02219
M106 S255
G1 F1200
G1 X107.379 Y110.868 E.0555
G1 F2400
G1 X107.134 Y110.919 E.0083
G1 X107 Y111.124 E.00812
G1 X106.866 Y110.919 E.00812
G1 X106.621 Y110.868 E.0083
G1 X104.479 Y110.868 E.07105
M73 P60 R0
M73 P60 R0
G1 X104.16 Y111.186 E.01494
G1 X104.359 Y111.377 F9000
; TYPE: Outer wall
;WIDTH:0.52146
```

```
G1 F2400
G1 X104.239 Y111.479 E.00612
G1 X104.239 Y116.239 E.18564
G1 X103.761 Y116.239 E.01866
G1 X103.761 Y111.479 E.18564
G1 X103.743 Y111 E.01867
;WIDTH:0.48573
G1 X103.725 Y110.521 E.01728
;WIDTH:0.449999
G1 X103.725 Y103.725 E.22545
G1 X116.275 Y103.725 E.41631
G1 X116.275 Y111.275 E.25045
G1 X116.045 Y111.278 E.00763
M73 P61 R0
M73 P61 R0
G1 X116.023 Y111.378 E.00341
;WIDTH:0.41646
G1 X116 Y111.479 E.00313
;WIDTH:0.4225
G1 X115.97 Y111.334 E.00457
;WIDTH:0.449999
G1 X115.921 Y111.275 E.00253
G1 X113.168 Y111.275 E.09133
G1 X113 Y111.479 E.00876
G1 X112.862 Y111.279 E.00803
G1 X110.259 Y111.275 E.08637
;WIDTH:0.4875
G1 X110.194 Y111.326 E.00298
;WIDTH:0.525
G1 X110.129 Y111.377 E.00323
;WIDTH:0.5625
G1 X110.065 Y111.428 E.00348
;WIDTH:0.6
G1 X110 Y111.479 E.00374
G1 X109.95 Y111.432 E.00311
;WIDTH:0.5625
G1 X109.9 Y111.385 E.0029
;WIDTH:0.525
G1 X109.85 Y111.338 E.00269
;WIDTH:0.4875
G1 X109.8 Y111.291 E.00248
;WIDTH:0.449999
G1 X109.721 Y111.275 E.00267
G1 X107.338 Y111.275 E.07905
G1 X107.189 Y111.479 E.00837
;WIDTH:0.42146
G1 X107.189 Y116.289 E.14839
G1 X106.811 Y116.289 E.01168
G1 X106.811 Y111.479 E.14839
;WIDTH:0.449999
G1 X106.703 Y111.292 E.00714
G1 X106.621 Y111.275 E.00277
G1 X104.479 Y111.275 E.07108
;WIDTH:0.48573
G1 X104.389 Y111.351 E.00422
G1 E-2.8 F3600
;WIPE_START
G1 F2400
G1 X104.239 Y111.479 E-.23648
G1 X104.239 Y112.281 E-.96352
;WIPE_END
G1 Z1 F9000
M73 P62 R0
M73 P62 R0
G1 X116 Y116.4 Z1
G1 Z.6
G1 E4 F2400
;WIDTH:0.38292
G1 X116 Y111.479 E.13635
G1 E-2.8 F3600
;WIPE_START
G1 F2400
G1 X116 Y112.479 E-1.2
;WIPE_END
G1 Z1 F9000
G1 X113 Y116.3 Z1
G1 Z.6
M73 P63 R0
M73 P63 R0
G1 E4 F2400
;WIDTH:0.4
G1 X113 Y111.479 E.14029
```

```
G1 E-2.8 F3600
;WIPE_START
G1 F2400
G1 X113 Y112.479 E-1.2
;WIPE_END
G1 Z1 F9000
G1 X110 Y116.2 Z1
G1 Z.6
G1 E4 F2400
;WIDTH:0.6
G1 X110 Y111.479 E.21433
M73 P64 R0
M73 P64 R0
G1 E-2.8 F3600
;WIPE_START
G1 F2400
G1 X110 Y112.479 E-1.2
;WIPE_END
G1 Z1 F9000
G1 X113.873 Y110.58
G1 Z1
G1 Z.6
G1 E4 F2400
; TYPE: Bridge
;WIDTH:0.429646
G1 F1500
G1 X106.351 Y110.577 E.23705
G1 X106.059 Y110.193 E.01519
G1 X113.943 Y110.193 E.24847
M73 P65 R0
M73 P65 R0
G1 X114.18 Y109.807 E.01428
G1 X105.819 Y109.807 E.26347
G1 X105.627 Y109.42 E.01361
G1 X114.37 Y109.42 E.27553
G1 X114.52 Y109.033 E.01307
G1 X105.477 Y109.033 E.285
G1 X105.363 Y108.646 E.0127
M73 P66 R0
M73 P66 R0
G1 X114.634 Y108.646 E.29213
G1 X114.712 Y108.26 E.01244
G1 X105.285 Y108.26 E.2971
G1 X105.238 Y107.873 E.01227
M73 P67 R0
M73 P67 R0
G1 X114.759 Y107.873 E.30001
G1 X114.773 Y107.486 E.0122
G1 X105.224 Y107.486 E.30093
G1 X105.237 Y107.16 E.01028
G1 X105.241 Y107.1 E.00192
G1 X114.756 Y107.1 E.29987
G1 X114.708 Y106.713 E.01228
M73 P68 R0
M73 P68 R0
G1 X105.289 Y106.713 E.29682
G1 X105.37 Y106.326 E.01245
G1 X114.627 Y106.326 E.2917
G1 X114.511 Y105.939 E.01272
G1 X105.486 Y105.939 E.2844
G1 X105.64 Y105.553 E.01311
M73 P69 R0
M73 P69 R0
G1 X114.358 Y105.553 E.27475
G1 X114.165 Y105.166 E.01363
G1 X105.835 Y105.166 E.26249
G1 X106.078 Y104.779 E.01439
G1 X114.132 Y104.779 E.25382
G1 X114.982 Y104.252 F9000
M73 P70 R0
; TYPE: Top surface
;WIDTH:0.421038
M73 P70 R0
G1 F1800
M106 S255
G1 X115.748 Y105.018 E.0334
G1 X115.748 Y105.553 F9000
G1 F1800
G1 X114.447 Y104.252 E.0567
G1 X113.912 Y104.252 F9000
G1 F1800
G1 X115.748 Y106.088 E.08
```

```
G1 X115.748 Y106.622 F9000
G1 F1800
G1 X114.52 Y105.394 E.05352
G1 X114.82 Y106.229 F9000
G1 F1800
G1 X115.748 Y107.157 E.04044
G1 X115.748 Y107.692 F9000
G1 F1800
G1 X114.95 Y106.894 E.03476
G1 X114.985 Y107.463 F9000
G1 F1800
G1 X115.748 Y108.227 E.03328
G1 X115.748 Y108.761 F9000
G1 F1800
G1 X114.962 Y107.975 E.03425
G1 X114.896 Y108.444 F9000
G1 F1800
G1 X115.748 Y109.296 E.03713
G1 X115.748 Y109.831 F9000
M73 P71 R0
M73 P71 R0
G1 F1800
G1 X114.794 Y108.876 E.0416
G1 X114.66 Y109.277 F9000
G1 F1800
G1 X115.748 Y110.366 E.04742
G1 X115.596 Y110.748 F9000
G1 F1800
G1 X114.499 Y109.651 E.04779
G1 X114.315 Y110.001 F9000
G1 F1800
G1 X115.062 Y110.748 E.03255
G1 X114.527 Y110.748 F9000
G1 F1800
G1 X114.107 Y110.329 E.01829
G1 E-2.81299 F3600
;WIPE_START
G1 F1800
G1 X114.527 Y110.748 E-1.18701
;WIPE_END
G1 Z1 F9000
G1 X105.894 Y104.674 Z1
G1 Z.6
G1 E4 F2400
;WIDTH:0.420974
G1 F1800
M73 P72 R0
M73 P72 R0
G1 X105.472 Y104.252 E.01838
G1 X104.938 Y104.252 F9000
G1 F1800
G1 X105.687 Y105.001 E.03265
G1 X105.502 Y105.351 F9000
G1 F1800
G1 X104.403 Y104.252 E.0479
G1 X104.252 Y104.635 F9000
G1 F1800
G1 X105.342 Y105.725 E.0475
G1 X105.208 Y106.126 F9000
G1 F1800
G1 X104.252 Y105.17 E.04168
G1 X104.252 Y105.704 F9000
G1 F1800
G1 X105.105 Y106.558 E.03717
G1 X105.036 Y107.024 F9000
G1 F1800
G1 X104.252 Y106.239 E.03419
G1 X104.252 Y106.774 F9000
G1 F1800
G1 X105.013 Y107.535 E.03317
G1 X105.053 Y108.109 F9000
G1 F1800
G1 X104.252 Y107.308 E.0349
G1 X104.252 Y107.843 F9000
G1 F1800
G1 X105.178 Y108.769 E.04034
G1 X105.483 Y109.609 F9000
G1 F1800
G1 X104.252 Y108.378 E.05366
G1 X104.252 Y108.912 F9000
M73 P73 R0
M73 P73 R0
```

```
G1 F1800
G1 X106.091 Y110.752 E.08014
G1 X105.555 Y110.751 F9000
G1 F1800
G1 X104.252 Y109.447 E.0568
G1 X104.252 Y109.982 F9000
G1 F1800
G1 X105.02 Y110.749 E.03346
; stop printing object Slicer Test v3.stl id:0 copy 0
;LAYER_CHANGE
;Z:0.8
;HEIGHT:0.2
;BEFORE_LAYER_CHANGE
;0.8
G92 E0

G1 E-2.8 F3600
;WIPE_START
G1 F1800
G1 X104.312 Y110.042 E-1.2
;WIPE_END
;_SET_FAN_SPEED_CHANGING_LAYER
; printing object Slicer Test v3.stl id:0 copy 0
G1 Z1.2 F9000
G1 X107.865 Y109.411 Z1.2
G1 Z.8
G1 E4 F2400
; TYPE: Inner wall
;WIDTH:0.449999
G1 F600
G1 X107.591 Y109.052 E.01496
G1 X107.352 Y108.588 E.01732
G1 X107.171 Y107.956 E.02182
M73 P74 R0
M73 P74 R0
G1 X107.135 Y107.512 E.01477
G1 X107.224 Y106.794 E.02402
G1 X107.368 Y106.366 E.01496
G1 X107.62 Y105.909 E.01732
G1 X108.036 Y105.416 E.02141
G1 X108.612 Y104.994 E.02369
G1 X108.842 Y104.889 E.00838
G1 X109.473 Y104.683 E.02201
G1 X109.993 Y104.637 E.01732
G1 X110.647 Y104.709 E.02182
G1 X111.08 Y104.846 E.01505
G1 X111.542 Y105.088 E.01732
G1 X112.05 Y105.5 E.02169
G1 X112.372 Y105.898 E.01699
G1 X112.576 Y106.287 E.01457
G1 X112.739 Y106.69 E.01442
G1 X112.862 Y107.629 E.03142
G1 X112.831 Y107.88 E.00838
G1 X112.737 Y108.317 E.01482
G1 X112.472 Y108.949 E.02275
G1 X112.045 Y109.494 E.02297
G1 X111.663 Y109.823 E.01671
M73 P75 R0
M73 P75 R0
G1 X111.094 Y110.148 E.02173
G1 X110.395 Y110.337 E.02402
G1 X109.945 Y110.365 E.01496
G1 X109.427 Y110.305 E.01732
G1 X108.801 Y110.102 E.02182
G1 X108.413 Y109.885 E.01476
G1 X107.896 Y109.437 E.02269
G1 X107.567 Y109.691 F9000
; TYPE: Outer wall
G1 F600
G1 X107.246 Y109.271 E.01754
G1 X106.972 Y108.739 E.01986
G1 X106.769 Y108.029 E.02449
G1 X106.726 Y107.504 E.01748
G1 X106.825 Y106.702 E.02678
G1 X106.994 Y106.202 E.01754
G1 X107.283 Y105.677 E.01986
G1 X107.757 Y105.116 E.02436
G1 X108.405 Y104.641 E.02668
G1 X108.887 Y104.421 E.01757
G1 X109.401 Y104.281 E.01767
G1 X109.998 Y104.228 E.01986
M73 P76 R0
```

```
M73 P76 R0
G1 X110.731 Y104.309 E.02449
G1 X111.237 Y104.468 E.01757
G1 X111.767 Y104.746 E.01986
G1 X112.34 Y105.21 E.02446
G1 X112.714 Y105.673 E.01976
G1 X113.057 Y106.327 E.02449
G1 X113.205 Y106.833 E.01748
G1 X113.271 Y107.638 E.02678
G1 X113.206 Y108.163 E.01757
G1 X113.056 Y108.676 E.01772
G1 X112.825 Y109.156 E.01768
G1 X112.518 Y109.593 E.01772
G1 X112.144 Y109.975 E.01771
G1 X111.714 Y110.29 E.01771
G1 X111.241 Y110.53 E.01758
G1 X110.462 Y110.741 E.02678
G1 X109.934 Y110.774 E.01754
G1 X109.34 Y110.704 E.01986
G1 X108.637 Y110.477 E.02449
G1 X108.177 Y110.22 E.01748
M73 P77 R0
M73 P77 R0
G1 X107.597 Y109.717 E.02546
G1 E-2.8 F3600
;WIPE_START
G1 F2400
G1 X107.246 Y109.271 E-.6815
G1 X107.048 Y108.887 E-.5185
;WIPE_END
G1 Z1.2 F9000
G1 X108.762 Y105.263
G1 Z1.2
G1 Z.8
G1 E4 F2400
; TYPE: Sparse infill
;WIDTH:0.45
G1 F600
G1 X109.158 Y105.085 E.01439
G1 X107.595 Y106.648 E.07329
G1 X107.523 Y106.862 E.0075
G1 X107.45 Y107.45 E.01967
G1 X110.053 Y110.053 E.12207
M73 P78 R0
M73 P78 R0
G1 X109.943 Y110.057 E.00365
G1 X112.542 Y107.458 E.12192
G1 X112.501 Y106.964 E.01646
G1 X112.41 Y106.653 E.01075
G1 X110.85 Y105.093 E.07316
G1 X110.584 Y105.009 E.00927
G1 X109.99 Y104.944 E.01982
G1 X109.527 Y104.985 E.01542
G1 X109.354 Y105.032 E.00595
; stop printing object Slicer Test v3.stl id:0 copy 0
;LAYER_CHANGE
;Z:1
;HEIGHT:0.2
;BEFORE_LAYER_CHANGE
;1
G92 E0

G1 E-3 F3600
M73 P79 R0
;WIPE_START
M73 P79 R0
G1 X109.527 Y104.985 E-.1793
G1 X109.99 Y104.944 E-.46483
G1 X110.344 Y104.983 E-.35587
;WIPE_END
;_SET_FAN_SPEED_CHANGING_LAYER
; printing object Slicer Test v3.stl id:0 copy 0
G1 Z1.4 F9000
G1 X108.401 Y109.875 Z1.4
G1 Z1
G1 E4 F2400
; TYPE: Inner wall
;WIDTH:0.449999
G1 F911
G1 X107.91 Y109.457 E.0214
G1 X107.741 Y109.241 E.00908
G1 X107.474 Y108.833 E.01617
```

```
G1 X107.22 Y108.195 E.02281
G1 X107.144 Y107.505 E.02301
G1 X107.186 Y107.01 E.01648
G1 X107.366 Y106.372 E.02198
G1 X107.695 Y105.802 E.02182
G1 X108.031 Y105.419 E.01692
G1 X108.612 Y104.994 E.02389
G1 X108.842 Y104.889 E.00838
G1 X109.467 Y104.685 E.02181
G1 X110.123 Y104.64 E.02182
M73 P80 R0
M73 P80 R0
G1 X110.641 Y104.707 E.01732
G1 X111.074 Y104.844 E.01505
G1 X111.65 Y105.161 E.02182
G1 X112.042 Y105.491 E.01699
G1 X112.443 Y106.007 E.02169
G1 X112.559 Y106.241 E.00866
G1 X112.735 Y106.676 E.01555
G1 X112.862 Y107.629 E.03191
G1 X112.831 Y107.88 E.00838
G1 X112.678 Y108.517 E.02173
G1 X112.343 Y109.145 E.02361
G1 X111.867 Y109.673 E.0236
G1 X111.508 Y109.936 E.01475
G1 X110.912 Y110.214 E.02182
G1 X110.648 Y110.278 E.00901
G1 X110.164 Y110.352 E.01622
G1 X109.678 Y110.338 E.01614
G1 X109.038 Y110.198 E.02173
G1 X108.437 Y109.894 E.02236
G1 X108.173 Y110.217 F9000
;TYPE:Outer wall
G1 F911
G1 X107.615 Y109.74 E.02435
G1 X107.245 Y109.269 E.01986
G1 X106.995 Y108.799 E.01767
G1 X106.823 Y108.294 E.01771
G1 X106.737 Y107.766 E.01772
G1 X106.737 Y107.234 E.01768
G1 X106.823 Y106.706 E.01772
G1 X106.994 Y106.204 E.01761
G1 X107.362 Y105.564 E.02449
G1 X107.755 Y105.117 E.01973
G1 X108.405 Y104.641 E.02675
G1 X108.887 Y104.421 E.01757
M73 P81 R0
M73 P81 R0
G1 X109.399 Y104.282 E.01761
G1 X110.136 Y104.231 E.02449
G1 X110.73 Y104.308 E.01986
G1 X111.235 Y104.468 E.01757
G1 X111.882 Y104.823 E.02449
G1 X112.337 Y105.207 E.01976
G1 X112.789 Y105.79 E.02446
G1 X113.056 Y106.325 E.01986
G1 X113.205 Y106.833 E.01755
G1 X113.271 Y107.638 E.02678
G1 X113.206 Y108.163 E.01757
G1 X113.057 Y108.672 E.01758
G1 X112.679 Y109.381 E.02665
G1 X112.141 Y109.977 E.02664
G1 X111.716 Y110.288 E.01747
G1 X111.047 Y110.6 E.02449
G1 X110.465 Y110.741 E.01986
G1 X109.933 Y110.774 E.01767
G1 X109.402 Y110.719 E.01771
G1 X108.891 Y110.58 E.01758
G1 X108.209 Y110.235 E.02535
G1 E-2.8 F3600
;WIPE_START
G1 F2400
G1 X107.615 Y109.74 E-.92763
G1 X107.475 Y109.561 E-.27237
;WIPE_END
G1 Z1.4 F9000
G1 X111.19 Y105.044
M73 P82 R0
M73 P82 R0
G1 Z1.4
G1 Z1
G1 E4 F2400
```

```
; TYPE: Top surface
;WIDTH:0.410992
G1 F911
G1 X112.464 Y106.318 E.05403
G1 X112.696 Y107.071 F9000
G1 F911
G1 X110.425 Y104.8 E.09633
G1 X109.881 Y104.776 F9000
G1 F911
G1 X112.741 Y107.636 E.12128
G1 X112.678 Y108.094 F9000
G1 F911
M73 P83 R0
M73 P83 R0
G1 X109.409 Y104.825 E.13865
G1 X109.008 Y104.944 F9000
G1 F911
G1 X112.556 Y108.492 E.15048
G1 X112.375 Y108.832 F9000
G1 F911
G1 X108.654 Y105.111 E.15781
G1 X108.354 Y105.331 F9000
G1 F911
G1 X112.175 Y109.153 E.16209
G1 X111.928 Y109.426 F9000
M73 P84 R0
M73 P84 R0
G1 F911
G1 X108.065 Y105.563 E.16388
G1 X107.821 Y105.84 F9000
G1 F911
G1 X111.659 Y109.677 E.16277
G1 X111.342 Y109.881 F9000
G1 F911
G1 X107.625 Y106.164 E.15769
G1 X107.447 Y106.507 F9000
M73 P85 R0
M73 P85 R0
G1 F911
G1 X110.987 Y110.047 E.15016
G1 X110.589 Y110.169 F9000
G1 F911
G1 X107.325 Y106.904 E.13847
G1 X107.263 Y107.364 F9000
G1 F911
G1 X110.133 Y110.234 E.12173
G1 X109.588 Y110.209 F9000
M73 P86 R0
M73 P86 R0
G1 F911
G1 X107.295 Y107.916 E.09725
G1 X107.516 Y108.657 F9000
G1 F911
G1 X108.804 Y109.946 E.05466
; stop printing object Slicer Test v3.stl id:0 copy 0
G1 E-2.8 F3600
;WIPE_START
G1 F1800
G1 X108.097 Y109.239 E-1.2
;WIPE_END
M106 S0
; TYPE: Custom
; filament end gcode
```

Listing A.2.2 G-Code Generated Using Orca Slicer [63] (Main)

```
G1 Z3 F600 ; Move print head up
G1 X5 Y176 F9000 ; present print
G1 Z71 F600 ; Move print head further up
M73 P87 R0
M73 P87 R0
G1 Z150 F600 ; Move print head further up
M73 P93 R0
M140 S0 ; turn off heatbed
M104 S0 ; turn off temperature
M107 ; turn off fan
M84 X Y E ; disable motors
M73 P100 R0
; EXECUTABLE_BLOCK_END

; filament used [mm] = 46.37
```

```
; filament used [cm3] = 0.11
; filament used [g] = 0.14
; filament cost = 0.00
; total filament used [g] = 0.14
; total filament cost = 0.00
; total layers count = 5
; estimated printing time (normal mode) = 2m 0s

; CONFIG_BLOCK_START
; accel_to_decel_enable = 1
; accel_to_decel_factor = 50%
; activate_air_filtration = 0
; activate_chamber_temp_control = 0
; adaptive_bed_mesh_margin = 0
; adaptive_pressure_advance = 0
; adaptive_pressure_advance_bridges = 0
; adaptive_pressure_advance_model = "0,0,0\n0,0,0"
; adaptive_pressure_advance_overhangs = 0
; additional_cooling_fan_speed = 70
; alternate_extra_wall = 0
; auxiliary_fan = 0
; bbl_calib_mark_logo = 1
; bbl_use_printhost = 0
; bed_custom_model =
; bed_custom_texture =
; bed_exclude_area = 0x0
; bed_mesh_max = 99999,99999
; bed_mesh_min = -99999,-99999
; bed_mesh_probe_distance = 50,50
; before_layer_change_gcode = ;BEFORE_LAYER_CHANGE\n;[layer_z]\nG92 E0\n
; best_object_pos = 0.5,0.5
; bottom_shell_layers = 1
; bottom_shell_thickness = 0
; bottom_solid_infill_flow_ratio = 1
; bottom_surface_pattern = monotonic
; bridge_acceleration = 50%
; bridge_angle = 0
; bridge_density = 100%
; bridge_flow = 0.95
; bridge_no_support = 0
; bridge_speed = 25
; brim_ears_detection_length = 1
; brim_ears_max_angle = 125
; brim_object_gap = 0
; brim_type = auto_brim
; brim_width = 0
; chamber_temperature = 0
; change_extrusion_role_gcode =
; change_filament_gcode = M600
; close_fan_the_first_x_layers = 1
; complete_print_exhaust_fan_speed = 80
; cool_plate_temp = 60
; cool_plate_temp_initial_layer = 60
; cooling_tube_length = 5
; cooling_tube_retraction = 91.5
; counterbore_hole_bridging = none
; curr_bed_type = High Temp Plate
; default_acceleration = 0
; default_filament_colour = ""
; default_filament_profile = "Creality Generic PLA"
; default_jerk = 0
; default_print_profile = 0.20mm Standard @Creality Ender3
; deretraction_speed = 40
; detect_narrow_internal_solid_infill = 1
; detect_overhang_wall = 1
; detect_thin_wall = 1
; different_settings_to_system = bottom_shell_layers;skirt_loops;sparse_infill_density;
    sparse_infill_pattern;top_shell_layers;top_shell_thickness;;
; disable_m73 = 0
; dont_filter_internal_bridges = disabled
; dont_slow_down_outer_wall = 0
; draft_shield = disabled
; during_print_exhaust_fan_speed = 60
; elefant_foot_compensation = 0.1
; elefant_foot_compensation_layers = 1
; emit_machine_limits_to_gcode = 1
; enable_arc_fitting = 0
; enable_filament_ramming = 1
; enable_long_retraction_when_cut = 0
; enable_overhang_bridge_fan = 1
; enable_overhang_speed = 1
; enable_pressure_advance = 0
```

```
; enable_prime_tower = 0
; enable_support = 0
; enforce_support_layers = 0
; eng_plate_temp = 60
; eng_plate_temp_initial_layer = 60
; ensure_vertical_shell_thickness = ensure_all
; exclude_object = 0
; extra_loading_move = -2
; extra_perimeters_on_overhangs = 0
; extruder_clearance_height_to_lid = 25
; extruder_clearance_height_to_rod = 25
; extruder_clearance_radius = 47
; extruder_colour = #26A69A
; extruder_offset = 0x0
; fan_cooling_layer_time = 100
; fan_kickstart = 0
; fan_max_speed = 100
; fan_min_speed = 100
; fan_speedup_overhangs = 1
; fan_speedup_time = 0
; filament_colour = #26A69A
; filament_cooling_final_speed = 3.4
; filament_cooling_initial_speed = 2.2
; filament_cooling_moves = 4
; filament_cost = 20
; filament_density = 1.24
; filament_diameter = 1.75
; filament_end_gcode = "; filament end gcode \n"
; filament_flow_ratio = 0.98
; filament_ids = GFL99
; filament_is_support = 0
; filament_loading_speed = 28
; filament_loading_speed_start = 3
; filament_max_volumetric_speed = 12
; filament_minimal_purge_on_wipe_tower = 15
; filament_multitool_ramming = 0
; filament_multitool_ramming_flow = 10
; filament_multitool_ramming_volume = 10
; filament_notes = ""
; filament_ramming_parameters = "120 100 6.6 6.8 7.2 7.6 7.9 8.2 8.7 9.4 9.9 10.0| 0.05 6.6
    0.45 6.8 0.95 7.8 1.45 8.3 1.95 9.7 2.45 10 2.95 7.6 3.45 7.6 3.95 7.6 4.45 7.6 4.95
    7.6"
; filament_settings_id = "Creality Generic PLA"
; filament_shrink = 100%
; filament_shrinkage_compensation_z = 100%
; filament_soluble = 0
; filament_stamping_distance = 0
; filament_stamping_loading_speed = 0
; filament_start_gcode = "; filament start gcode\n"
; filament_toolchange_delay = 0
; filament_type = PLA
; filament_unloading_speed = 90
; filament_unloading_speed_start = 100
; filament_vendor = Generic
; filename_format = {input_filename_base}_{filament_type[initial_tool]}_{print_time}.gcode
; filter_out_gap_fill = 0
; first_layer_print_sequence = 0
; flush_into_infill = 0
; flush_into_objects = 0
; flush_into_support = 1
; flush_multiplier = 0
; flush_volumes_matrix = 0
; flush_volumes_vector = 140,140
; full_fan_speed_layer = 0
; fuzzy_skin = none
; fuzzy_skin_first_layer = 0
; fuzzy_skin_point_distance = 0.8
; fuzzy_skin_thickness = 0.3
; gap_fill_target = nowhere
; gap_infill_speed = 30
; gcode_add_line_number = 0
; gcode_comments = 0
; gcode_flavor = marlin
; gcode_label_objects = 1
; has_scarf_joint_seam = 0
; head_wrap_detect_zone =
; high_current_on_filament_swap = 0
; hole_to_polyhole = 0
; hole_to_polyhole_threshold = 0.01
; hole_to_polyhole_twisted = 1
; host_type = octoprint
; hot_plate_temp = 60
```

```
; hot_plate_temp_initial_layer = 60
; idle_temperature = 0
; independent_support_layer_height = 1
; infill_anchor = 400%
; infill_anchor_max = 20
; infill_combination = 0
; infill_combination_max_layer_height = 100%
; infill_direction = 45
; infill_jerk = 9
; infill_wall_overlap = 25%
; initial_layer_acceleration = 0
; initial_layer_infill_speed = 35
; initial_layer_jerk = 9
; initial_layer_line_width = 0.42
; initial_layer_min_bead_width = 85%
; initial_layer_print_height = 0.2
; initial_layer_speed = 15
; initial_layer_travel_speed = 100%
; inner_wall_acceleration = 0
; inner_wall_jerk = 9
; inner_wall_line_width = 0.45
; inner_wall_speed = 40
; interface_shells = 0
; interlocking_beam = 0
; interlocking_beam_layer_count = 2
; interlocking_beam_width = 0.8
; interlocking_boundary_avoidance = 2
; interlocking_depth = 2
; interlocking_orientation = 22.5
; internal_bridge_flow = 1
; internal_bridge_speed = 150%
; internal_solid_infill_acceleration = 100%
; internal_solid_infill_line_width = 0
; internal_solid_infill_pattern = monotonic
; internal_solid_infill_speed = 50
; ironing_angle = -1
; ironing_flow = 15%
; ironing_pattern = zig-zag
; ironing_spacing = 0.1
; ironing_speed = 15
; ironing_type = no ironing
; is_infill_first = 0
; layer_change_gcode =
; layer_height = 0.2
; line_width = 0.45
; long_retractions_when_cut = 0
; machine_end_gcode = {if max_layer_z < printable_height}G1 Z{z_offset+min(max_layer_z+2, printable_height)} F600 ; Move print head up{endif}\nG1 X5 Y{print_bed_max[1]*0.8} F{travel_speed*60} ; present print\n{if max_layer_z < printable_height-10}G1 Z{z_offset+min(max_layer_z+70, printable_height-10)} F600 ; Move print head further up{endif}\n{if max_layer_z < max_print_height*0.6}G1 Z{printable_height*0.6} F600 ; Move print head further up{endif}\nM140 S0 ; turn off heatbed\nM104 S0 ; turn off temperature\nM107 ; turn off fan\nM84 X Y E ; disable motors
; machine_load_filament_time = 0
; machine_max_acceleration_e = 5000,5000
; machine_max_acceleration_extruding = 500,500
; machine_max_acceleration_retracting = 1000,1000
; machine_max_acceleration_travel = 1500,1250
; machine_max_acceleration_x = 500,500
; machine_max_acceleration_y = 500,500
; machine_max_acceleration_z = 100,100
; machine_max_jerk_e = 5,5
; machine_max_jerk_x = 8,8
; machine_max_jerk_y = 8,8
; machine_max_jerk_z = 0.4,0.4
; machine_max_speed_e = 60,60
; machine_max_speed_x = 500,500
; machine_max_speed_y = 500,500
; machine_max_speed_z = 10,10
; machine_min_extruding_rate = 0,0
; machine_min_travel_rate = 0,0
; machine_pause_gcode = M25
; machine_start_gcode = G90 ; use absolute coordinates\nM83 ; extruder relative mode\nM140 S[bed_temperature_initial_layer_single] ; set final bed temp\nM104 S150 ; set temporary nozzle temp to prevent oozing during homing\nG4 S10 ; allow partial nozzle warmup\nG28 ; home all axis\nG1 Z50 F240\nG1 X2 Y10 F3000\nM104 S[nozzle_temperature_initial_layer] ; set final nozzle temp\nM190 S[bed_temperature_initial_layer_single] ; wait for bed temp to stabilize\nM109 S[nozzle_temperature_initial_layer] ; wait for nozzle temp to stabilize\nG1 Z0.28 F240\nG92 E0\nG1 Y140 E10 F1500 ; prime the nozzle\nG1 X2.3 F5000\nG92 E0\nG1 Y10 E10 F1200 ; prime the nozzle\nG92 E0
; machine_tool_change_time = 0
; machine_unload_filament_time = 0
```

```
; make_overhang_printable = 0
; make_overhang_printable_angle = 55
; make_overhang_printable_hole_size = 0
; manual_filament_change = 0
; max_bridge_length = 10
; max_layer_height = 0.36
; max_travel_detour_distance = 0
; max_volumetric_extrusion_rate_slope = 0
; max_volumetric_extrusion_rate_slope_segment_length = 3
; min_bead_width = 85%
; min_feature_size = 25%
; min_layer_height = 0.08
; min_length_factor = 0.5
; min_skirt_length = 0
; min_width_top_surface = 300%
; minimum_sparse_infill_area = 10
; mmu_segmented_region_interlocking_depth = 0
; mmu_segmented_region_max_width = 0
; notes =
; nozzle_diameter = 0.4
; nozzle_height = 2.5
; nozzle_hrc = 0
; nozzle_temperature = 220
; nozzle_temperature_initial_layer = 220
; nozzle_temperature_range_high = 230
; nozzle_temperature_range_low = 190
; nozzle_type = undefine
; nozzle_volume = 0
; only_one_wall_first_layer = 0
; only_one_wall_top = 0
; ooze_prevention = 0
; other_layers_print_sequence = 0
; other_layers_print_sequence_nums = 0
; outer_wall_acceleration = 500
; outer_wall_jerk = 9
; outer_wall_line_width = 0.45
; outer_wall_speed = 40
; overhang_1_4_speed = 0
; overhang_2_4_speed = 20
; overhang_3_4_speed = 15
; overhang_4_4_speed = 10
; overhang_fan_speed = 100
; overhang_fan_threshold = 50%
; overhang_reverse = 0
; overhang_reverse_internal_only = 0
; overhang_reverse_threshold = 50%
; overhang_speed_classic = 0
; parking_pos_retraction = 92
; pellet_flow_coefficient = 0.4157
; pellet_modded_printer = 0
; post_process =
; precise_outer_wall = 0
; precise_z_height = 0
; preferred_orientation = 0
; preheat_steps = 1
; preheat_time = 30
; pressure_advance = 0.02
; prime_tower_brim_width = 3
; prime_tower_width = 60
; prime_volume = 45
; print_compatible_printers = "Creality Ender-3 0.4 nozzle"
; print_flow_ratio = 1
; print_order = default
; print_sequence = by layer
; print_settings_id = 0.20mm Standard @Creality Ender3
; printable_area = 0x0,220x0,220x220,0x220
; printable_height = 250
; printer_model = Creality Ender-3
; printer_notes =
; printer_settings_id = Creality Ender-3 0.4 nozzle
; printer_structure = i3
; printer_technology = FFF
; printer_variant = 0.4
; printhost_authorization_type = key
; printhost_ssl_ignore_revoke = 0
; printing_by_object_gcode =
; purge_in_prime_tower = 1
; raft_contact_distance = 0.1
; raft_expansion = 1.5
; raft_first_layer_density = 90%
; raft_first_layer_expansion = 2
; raft_layers = 0
```

```
; reduce_crossing_wall = 0
; reduce_fan_stop_start_freq = 1
; reduce_infill_retraction = 1
; required_nozzle_HRC = 0
; resolution = 0.012
; retract_before_wipe = 70%
; retract_length_toolchange = 1
; retract_lift_above = 0
; retract_lift_below = 0
; retract_lift_enforce = All Surfaces
; retract_restart_extra = 0
; retract_restart_extra_toolchange = 0
; retract_when_changing_layer = 1
; retraction_distances_when_cut = 18
; retraction_length = 4
; retraction_minimum_travel = 2
; retraction_speed = 60
; role_based_wipe_speed = 1
; rotate_solid_infill_direction = 1
; scan_first_layer = 0
; scarf_angle_threshold = 155
; scarf_joint_flow_ratio = 1
; scarf_joint_speed = 100%
; scarf_overhang_threshold = 40%
; seam_gap = 10%
; seam_position = aligned
; seam_slope_conditional = 0
; seam_slope_entire_loop = 0
; seam_slope_inner_walls = 0
; seam_slope_min_length = 20
; seam_slope_start_height = 0
; seam_slope_steps = 10
; seam_slope_type = none
; silent_mode = 0
; single_extruder_multi_material = 1
; single_extruder_multi_material_priming = 0
; skirt_distance = 2
; skirt_height = 2
; skirt_loops = 0
; skirt_speed = 50
; skirt_start_angle = -135
; skirt_type = combined
; slice_closing_radius = 0.049
; slicing_mode = regular
; slow_down_for_layer_cooling = 1
; slow_down_layer_time = 8
; slow_down_layers = 0
; slow_down_min_speed = 10
; slowdown_for_curled_perimeters = 1
; small_area_infill_flow_compensation = 0
; small_area_infill_flow_compensation_model = 0,0;"\n0.2,0.4444";"\n0.4,0.6145";"\n0.6,0.7059";"\n0.8,0.7619";"\n1.5,0.8571";"\n2,0.8889";"\n3,0.9231";"\n5,0.9520";"\n10,1"
; small_perimeter_speed = 50%
; small_perimeter_threshold = 0
; solid_infill_direction = 45
; solid_infill_filament = 1
; sparse_infill_acceleration = 100%
; sparse_infill_density = 20%
; sparse_infill_filament = 1
; sparse_infill_line_width = 0.45
; sparse_infill_pattern = grid
; sparse_infill_speed = 60
; spiral_mode = 0
; spiral_mode_max_xy_smoothing = 200%
; spiral_mode_smooth = 0
; staggered_inner_seams = 0
; standby_temperature_delta = -5
; start_end_points = 30x-3,54x245
; support_air_filtration = 0
; support_angle = 0
; support_base_pattern = rectilinear
; support_base_pattern_spacing = 0.2
; support_bottom_interface_spacing = 0.5
; support_bottom_z_distance = 0.2
; support_chamber_temp_control = 0
; support_critical_regions_only = 0
; support_expansion = 0
; support_filament = 0
; support_interface_bottom_layers = -1
; support_interface_filament = 0
; support_interface_loop_pattern = 0
; support_interface_not_for_body = 1
```

```
; support_interface_pattern = auto
; support_interface_spacing = 0.2
; support_interface_speed = 80
; support_interface_top_layers = 3
; support_line_width = 0.38
; support_material_interface_fan_speed = -1
; support_multi_bed_types = 0
; support_object_xy_distance = 0.35
; support_on_build_plate_only = 0
; support_remove_small_overhang = 1
; support_speed = 40
; support_style = grid
; support_threshold_angle = 30
; support_top_z_distance = 0.15
; support_type = normal(auto)
; temperature_vitrification = 60
; template_custom_gcode =
; textured_cool_plate_temp = 40
; textured_cool_plate_temp_initial_layer = 40
; textured_plate_temp = 60
; textured_plate_temp_initial_layer = 60
; thick_bridges = 0
; thick_internal_bridges = 1
; thumbnails =
; thumbnails_format = PNG
; time_cost = 0
; time_lapse_gcode =
; timelapse_type = 0
; top_bottom_infill_wall_overlap = 25%
; top_shell_layers = 1
; top_shell_thickness = 0.2
; top_solid_infill_flow_ratio = 1
; top_surface_acceleration = 0
; top_surface_jerk = 9
; top_surface_line_width = 0.4
; top_surface_pattern = monotonicline
; top_surface_speed = 30
; travel_acceleration = 0
; travel_jerk = 12
; travel_slope = 3
; travel_speed = 150
; travel_speed_z = 0
; tree_support_adaptive_layer_height = 1
; tree_support_angle_slow = 25
; tree_support_auto_brim = 1
; tree_support_branch_angle = 40
; tree_support_branch_angle_organic = 40
; tree_support_branch_diameter = 5
; tree_support_branch_diameter_angle = 5
; tree_support_branch_diameter_double_wall = 3
; tree_support_branch_diameter_organic = 2
; tree_support_branch_distance = 5
; tree_support_branch_distance_organic = 1
; tree_support_brim_width = 3
; tree_support_tip_diameter = 0.8
; tree_support_top_rate = 30%
; tree_support_wall_count = 0
; upward_compatible_machine =
; use_firmware_retraction = 0
; use_relative_e_distances = 1
; wall_direction = auto
; wall_distribution_count = 1
; wall_filament = 1
; wall_generator = arachne
; wall_loops = 2
; wall_sequence = inner wall/outer wall
; wall_transition_angle = 10
; wall_transition_filter_deviation = 25%
; wall_transition_length = 100%
; wipe = 1
; wipe_before_external_loop = 0
; wipe_distance = 1
; wipe_on_loops = 0
; wipe_speed = 80%
; wipe_tower_bridging = 10
; wipe_tower_cone_angle = 0
; wipe_tower_extra_flow = 100%
; wipe_tower_extra_spacing = 100%
; wipe_tower_filament = 0
; wipe_tower_max_purge_speed = 90
; wipe_tower_no_sparse_layers = 0
; wipe_tower_rotation_angle = 0
```

```
; wipe_tower_x = 0.000
; wipe_tower_x = 0
; wipe_tower_y = 250.000
; wipe_tower_y = 250
; wiping_volumes_extruders = 70,70,70,70,70,70,70,70,70,70
; xy_contour_compensation = 0
; xy_hole_compensation = 0
; z_hop = 0.4
; z_hop_types = Normal Lift
; z_offset = 0
; first_layer_bed_temperature = 60
; bed_shape = 0x0,220x0,220x220,0x220
; first_layer_temperature = 220
; first_layer_height = 0.200
; CONFIG_BLOCK_END
```

Listing A.2.3 G-Code Generated Using Orca Slicer [63] (Reset)

A.3 Ultimaker Cura 5.8.0 – G-Code Listing

```
;FLAVOR:Marlin
;TIME:78
;Filament used: 0.0294967m
;Layer height: 0.2
;MINX:111.2
;MINY:111.2
;MINZ:0.2
;MAXX:123.8
;MAXY:124.653
;MAXZ:1
;TARGET_MACHINE.NAME:Creality Ender-3
;Generated with Cura_SteamEngine 5.10.0
M140 S50
M105
M190 S50
M104 S200
M105
M109 S200
; Ender 3 Custom Start G-code
G92 E0 ; Reset Extruder
G28 ; Home all axes
G1 Z2.0 F3000 ; Move Z Axis up little to prevent scratching of Heat Bed
G1 X0.1 Y20 Z0.3 F5000.0 ; Move to start position
G1 X0.1 Y200.0 Z0.3 F1500.0 E15 ; Draw the first line
G1 X0.4 Y200.0 Z0.3 F5000.0 ; Move to side a little
G1 X0.4 Y20 Z0.3 F1500.0 E30 ; Draw the second line
G92 E0 ; Reset Extruder
G1 Z2.0 F3000 ; Move Z Axis up little to prevent scratching of Heat Bed
G1 X5 Y20 Z0.3 F5000.0 ; Move over to prevent blob squish
```

Listing A.3.1 G-Code Generated Using Ultimaker Cura [97] (Initialization)

```
M82 ;absolute extrusion mode
G92 E0
G92 E0
G1 F2700 E-5
;LAYER_COUNT:5
;LAYER:0
M107
;MESH:Slicer Test v3.stl
G0 F6000 X111.6 Y118.8 Z0.2
;TYPE:WALL-INNER
G1 F2700 E0
G1 F1200 X112 Y118.4 E0.01881
G1 X114.159 Y118.403 E0.09062
G1 X114.331 Y118.445 E0.09651
G1 X114.5 Y118.558 E0.10327
G1 X114.639 Y118.458 E0.10897
G1 X114.846 Y118.401 E0.11611
G1 X115.209 Y118.399 E0.12818
G1 X114.917 Y118.185 E0.14022
G1 X114.663 Y117.96 E0.15151
G1 X114.447 Y117.734 E0.16191
G1 X114.263 Y117.518 E0.17135
G1 X114.06 Y117.233 E0.18298
G1 X113.867 Y116.902 E0.19573
```

```
G1 X113.724 Y116.602 E0.20678
G1 X113.62 Y116.334 E0.21634
G1 X113.511 Y115.962 E0.22924
G1 X113.447 Y115.634 E0.24035
G1 X113.412 Y115.314 E0.25106
G1 X113.4 Y114.979 E0.26221
G1 X113.415 Y114.638 E0.27356
G1 X113.447 Y114.362 E0.2828
G1 X113.511 Y114.036 E0.29385
G1 X113.603 Y113.712 E0.30505
G1 X113.724 Y113.394 E0.31637
G1 X113.867 Y113.094 E0.32742
G1 X114.06 Y112.767 E0.34005
G1 X114.259 Y112.487 E0.35148
G1 X114.471 Y112.236 E0.36241
G1 X114.663 Y112.036 E0.37163
G1 X114.917 Y111.811 E0.38291
G1 X115.192 Y111.604 E0.39436
G1 X111.601 Y111.601 E0.5138
G1 X111.6 Y118.8 E0.75324
G1 F2700 E-4.24676
G0 F6000 X111.49 Y118.8
G0 X115.937 Y118.586
G0 X116.533 Y117.666
G0 X118.576 Y117.622
G0 X120.5 Y118.437
G1 F2700 E0.75324
G1 F1200 X120.642 Y118.402 E0.7581
G1 X123.4 Y118.4 E0.84983
G1 X123.4 Y111.6 E1.076
G1 X119.81 Y111.6 E1.19541
G1 X120.195 Y111.911 E1.21187
G1 X120.444 Y112.144 E1.22321
G1 X120.669 Y112.399 E1.23452
G1 X120.865 Y112.659 E1.24535
G1 X121.031 Y112.92 E1.25564
G1 X121.267 Y113.351 E1.27198
G1 X121.425 Y113.814 E1.28825
G1 X121.508 Y114.146 E1.29963
G1 X121.564 Y114.466 E1.31044
G1 X121.594 Y114.81 E1.32192
G1 X121.594 Y115.191 E1.3346
G1 X121.565 Y115.523 E1.34568
G1 X121.516 Y115.816 E1.35556
G1 X121.425 Y116.172 E1.36778
G1 X121.269 Y116.635 E1.38403
G1 X121.009 Y117.119 E1.40231
G1 X120.861 Y117.343 E1.41124
G1 X120.673 Y117.597 E1.42175
G1 X120.437 Y117.856 E1.4334
G1 X120.168 Y118.11 E1.44571
G1 X119.804 Y118.399 E1.46116
G1 X120.32 Y118.4 E1.47833
G1 X120.5 Y118.437 E1.48444
G0 F6000 X120.5 Y119
;TYPE:WALL-OUTER
G1 F1200 X120.625 Y118.8 E1.49228
G1 X123.44 Y118.804 E1.58591
G1 F1297.3 X123.5 Y119 E1.59222
G1 X123.56 Y118.804 E1.59852
G1 F1200 X123.8 Y118.8 E1.60651
G1 X123.8 Y111.2 E1.85928
G1 X118.991 Y111.2 E2.01923
G1 F1165 X118.664 Y111.212 E2.03044
G1 F948.6 X118.321 Y111.294 E2.04528
G1 X118.621 Y111.46 E2.05971
G1 F1165 X118.908 Y111.578 E2.07034
G1 F1200 X119.182 Y111.705 E2.08038
G1 X119.44 Y111.85 E2.09022
G1 X119.697 Y112.023 E2.10053
G1 X119.924 Y112.205 E2.11021
G1 X120.146 Y112.41 E2.12026
G1 X120.342 Y112.63 E2.13006
G1 X120.529 Y112.875 E2.14031
G1 X120.673 Y113.099 E2.14916
G1 X120.906 Y113.531 E2.16549
G1 X121.051 Y113.96 E2.18055
G1 X121.122 Y114.254 E2.19061
G1 X121.172 Y114.551 E2.20063
G1 X121.196 Y114.843 E2.21037
G1 X121.196 Y115.157 E2.22082
G1 X121.17 Y115.457 E2.23083
```

```
G1 X121.122 Y115.747 E2.24061
G1 X121.046 Y116.044 E2.2508
G1 X120.906 Y116.46 E2.2654
G1 X120.675 Y116.899 E2.2819
G1 X120.52 Y117.132 E2.29121
G1 X120.353 Y117.357 E2.30053
G1 X120.134 Y117.594 E2.31126
G1 X119.915 Y117.8 E2.32126
G1 X119.682 Y117.988 E2.33122
G1 X119.428 Y118.154 E2.34131
G1 X119.184 Y118.294 E2.35067
G1 X118.894 Y118.424 E2.36124
G1 X118.605 Y118.529 E2.37147
G1 X118.309 Y118.609 E2.38166
G1 F1048 X117.911 Y118.742 E2.39764
G1 X118.326 Y118.799 E2.4136
G1 F1200 X120.378 Y118.805 E2.48185
G1 X120.5 Y119 E2.4895
G1 X120.5 Y123.8 E2.64915
G1 F2700 E-2.35085
G0 F6000 X119.635 Y123.8
G0 X118.465 Y123.7
G0 X117.5 Y123.7
G1 F2700 E2.64915
G1 F781.8 X117.5 Y122.079 E2.73191
G1 F747.7 X117.5 Y120.458 E2.81844
G1 F716.4 X117.5 Y118.837 E2.90875
G1 F800 X117.214 Y118.742 E2.92378
G1 F890.5 X116.824 Y118.719 E2.94129
G0 F6000 X117.5 Y118.836
G1 F800 X117.751 Y118.747 E2.95458
G1 F930.2 X117.911 Y118.742 E2.96145
G1 F2700 E-2.03855
G0 F6000 X119.063 Y118.586
G0 X123.5 Y119
G1 F2700 E2.96145
G1 F1411.8 X123.5 Y123.9 E3.09997
G1 F2700 E-1.90003
G0 F6000 X122.735 Y123.9
G0 X121.353 Y124.653
G0 X116.547 Y124.653
G0 X115.565 Y123.8
G0 X114.7 Y123.8
G1 F2700 E3.09997
G1 F1200 X114.7 Y119 E3.25962
G1 X114.758 Y118.858 E3.26472
G1 X114.882 Y118.8 E3.26928
G1 X116.167 Y118.8 E3.31202
G1 F1165 X116.483 Y118.788 E3.32285
G1 F975.6 X116.824 Y118.719 E3.33708
G1 X116.515 Y118.578 E3.35098
G1 F1165 X115.953 Y118.363 E3.37159
G1 F1200 X115.701 Y118.235 E3.38099
G1 X115.43 Y118.066 E3.39161
G1 X115.18 Y117.883 E3.40192
G1 X114.951 Y117.683 E3.41203
G1 X114.751 Y117.474 E3.42165
G1 X114.567 Y117.258 E3.43109
G1 X114.379 Y116.989 E3.44201
G1 X114.227 Y116.728 E3.45205
G1 X114.097 Y116.457 E3.46205
G1 X113.993 Y116.189 E3.47161
G1 X113.903 Y115.884 E3.48219
G1 X113.846 Y115.599 E3.49185
G1 X113.812 Y115.297 E3.50196
G1 X113.8 Y114.995 E3.51201
G1 X113.813 Y114.684 E3.52237
G1 X113.845 Y114.408 E3.53161
G1 X113.907 Y114.1 E3.54206
G1 X113.993 Y113.807 E3.55221
G1 X114.097 Y113.539 E3.56178
G1 X114.227 Y113.268 E3.57177
G1 X114.379 Y113.01 E3.58173
G1 X114.566 Y112.743 E3.59257
G1 X114.759 Y112.513 E3.60256
G1 X114.951 Y112.313 E3.61178
G1 X115.194 Y112.102 E3.62249
G1 X115.444 Y111.92 E3.63277
G1 X115.7 Y111.766 E3.64271
G1 X115.972 Y111.626 E3.65288
G1 F1162.2 X116.515 Y111.417 E3.67286
G1 F973.6 X116.816 Y111.28 E3.68642
```

```
G1 X116.484 Y111.214 E3.7003
G1 F1162.2 X116.194 Y111.201 E3.71026
G1 F1200 X111.201 Y111.201 E3.87633
G1 X111.2 Y118 E4.10247
G1 F1066.7 X111.25 Y119 E4.13993
G1 F960 X111.25 Y123.75 E4.33741
G1 X111.75 Y123.75 E4.3582
G1 X111.75 Y119 E4.55568
G1 F1066.7 X112 Y118.8 E4.56766
G1 F1200 X114.12 Y118.801 E4.63818
G1 X114.242 Y118.858 E4.64265
G1 X114.3 Y119 E4.64776
G1 X114.3 Y123.8 E4.8074
G1 X114.7 Y123.8 E4.82071
G1 F2700 E-0.17929
G0 F6000 X116.816 Y111.28
G1 F2700 E4.82071
G1 F892.2 X117.126 Y111.258 E4.83461
G1 F944.9 X117.433 Y111.25 E4.84758
G1 F948.6 X117.867 Y111.256 E4.86585
G1 F872.7 X118.321 Y111.294 E4.88668
G1 F2700 E-0.11332
G0 F6000 X118.138 Y112.238
G0 X119.818 Y116.633
G0 X120.748 Y118.043
;TYPE:SKIN
G1 F2700 E4.88668
G1 F1200 X120.954 Y117.819 E4.8968
G1 X121.169 Y117.527 E4.90886
G1 X121.339 Y117.271 E4.91908
G1 X121.602 Y116.769 E4.93793
G1 X121.766 Y116.285 E4.95493
G1 X121.87 Y115.875 E4.969
G1 X121.918 Y115.581 E4.97891
G1 X121.951 Y115.219 E4.991
G1 X121.956 Y114.843 E5.0035
G1 X121.92 Y114.411 E5.01792
G1 X121.869 Y114.121 E5.02772
G1 X121.762 Y113.691 E5.04245
G1 X121.602 Y113.219 E5.05903
G1 X121.344 Y112.743 E5.07704
G1 X121.17 Y112.465 E5.08795
G1 X120.951 Y112.178 E5.09995
G1 X120.76 Y111.96 E5.10959
G1 X123.04 Y111.96 E5.18543
G1 X123.04 Y118.04 E5.38765
G1 X120.748 Y118.043 E5.46388
G0 F6000 X121.44 Y117.48
G1 F1200 X121.801 Y117.841 E5.48086
G0 F6000 X122.366 Y117.84
G1 F1200 X121.644 Y117.119 E5.5148
G0 F6000 X121.822 Y116.731
G1 F1200 X122.84 Y117.749 E5.56268
G0 F6000 X122.84 Y117.183
G1 F1200 X121.965 Y116.308 E5.60384
G0 F6000 X122.076 Y115.853
G1 F1200 X122.84 Y116.617 E5.63977
G0 F6000 X122.84 Y116.052
G1 F1200 X122.139 Y115.35 E5.67277
G0 F6000 X122.152 Y114.798
G1 F1200 X122.84 Y115.486 E5.70513
G0 F6000 X122.84 Y114.92
G1 F1200 X122.078 Y114.159 E5.74095
G0 F6000 X122.84 Y114.355
G1 F1200 X121.868 Y113.383 E5.78667
G0 F6000 X122.84 Y113.223
G1 F1200 X121.777 Y112.16 E5.83667
G0 F6000 X121.221 Y112.17
G1 F1200 X122.84 Y113.789 E5.91282
G0 F6000 X123.3 Y113.789
G0 X123.3 Y112.658
G0 X122.84 Y112.658
G1 F1200 X122.342 Y112.16 E5.93625
G1 F2700 E0.93625
G0 F6000 X122.342 Y111.7
G0 X120.332 Y111.786
G0 X121.168 Y113.589
G0 X120.147 Y113.984
G0 X115.922 Y117.355
G0 X114.235 Y118.044
G1 F2700 E5.93625
G1 F1200 X111.96 Y118.04 E6.01191
```

```
G1 X111.96 Y111.96 E6.21414
G1 X114.225 Y111.963 E6.28947
G1 X113.983 Y112.25 E6.30196
G1 X113.727 Y112.617 E6.31684
G1 X113.538 Y112.943 E6.32937
G1 X113.295 Y113.471 E6.34871
G1 X113.155 Y113.951 E6.36534
G1 X113.084 Y114.324 E6.37796
G1 X113.052 Y114.656 E6.38906
G1 X113.04 Y114.967 E6.39941
G1 X113.052 Y115.327 E6.41139
G1 X113.093 Y115.714 E6.42433
G1 X113.155 Y116.032 E6.43511
G1 X113.307 Y116.564 E6.45351
G1 X113.539 Y117.051 E6.47145
G1 X113.727 Y117.383 E6.48414
G1 X113.927 Y117.671 E6.49581
G1 X114.235 Y118.044 E6.51189
G0 F6000 X114.662 Y118.107
G0 X114.539 Y118.334
G0 X112.749 Y118.301
G0 X112.75 Y117.841
G1 F1200 X112.16 Y117.251 E6.53965
G0 F6000 X112.16 Y116.685
G1 F1200 X113.317 Y117.843 E6.59409
G0 F6000 X113.636 Y117.595
G1 F1200 X112.16 Y116.12 E6.66349
G0 F6000 X112.16 Y115.554
G1 F1200 X113.071 Y116.465 E6.70634
G0 F6000 X112.892 Y115.721
G1 F1200 X112.16 Y114.988 E6.7408
G0 F6000 X112.16 Y114.423
G1 F1200 X112.846 Y115.108 E6.77304
G0 F6000 X112.861 Y114.558
G1 F1200 X112.16 Y113.857 E6.80602
G0 F6000 X112.16 Y113.291
G1 F1200 X112.932 Y114.063 E6.84233
G0 F6000 X113.046 Y113.612
G1 F1200 X112.16 Y112.726 E6.884
G0 F6000 X112.16 Y112.16
G1 F1200 X113.201 Y113.201 E6.93297
G0 F6000 X113.381 Y112.815
G1 F1200 X112.726 Y112.161 E6.96375
G0 F6000 X113.292 Y112.161
G1 F1200 X113.592 Y112.461 E6.97787
;MESH:NONMESH
G0 F300 X113.592 Y112.461 Z0.4
G0 F6000 X113.968 Y112.726
G0 X113.294 Y115.696
G0 X114.699 Y118.257
G0 X111.785 Y118.436
G0 X111.786 Y118.144
G0 X111.49 Y118.8
G0 X111.6 Y118.8
;TIME_ELAPSED:22.884674
;LAYER:1
;note -- min layer time used
M106 S85
; TYPE: WALL-INNER
;MESH:Slicer Test v3.stl
G1 F1201.7 X112 Y118.4 E6.99668
G1 X114.159 Y118.403 E7.06849
G1 X114.331 Y118.445 E7.07438
G1 X114.5 Y118.558 E7.08114
G1 X114.639 Y118.458 E7.08683
G1 X114.846 Y118.401 E7.09398
G1 X115.209 Y118.399 E7.10605
G1 X114.917 Y118.185 E7.11809
G1 X114.663 Y117.96 E7.12938
G1 X114.447 Y117.734 E7.13977
G1 X114.263 Y117.518 E7.14921
G1 X114.06 Y117.233 E7.16085
G1 X113.867 Y116.902 E7.17359
G1 X113.724 Y116.602 E7.18465
G1 X113.62 Y116.334 E7.19421
G1 X113.511 Y115.962 E7.2071
G1 X113.447 Y115.634 E7.21822
G1 X113.412 Y115.314 E7.22892
G1 X113.4 Y114.979 E7.24007
G1 X113.415 Y114.638 E7.25142
G1 X113.447 Y114.362 E7.26067
G1 X113.511 Y114.036 E7.27172
```

```
G1 X113.603 Y113.712 E7.28292
G1 X113.724 Y113.394 E7.29423
G1 X113.867 Y113.094 E7.30529
G1 X114.06 Y112.767 E7.31792
G1 X114.259 Y112.487 E7.32934
G1 X114.471 Y112.236 E7.34027
G1 X114.663 Y112.036 E7.34949
G1 X114.917 Y111.811 E7.36078
G1 X115.192 Y111.604 E7.37223
G1 X111.601 Y111.601 E7.49166
G1 X111.6 Y118.8 E7.7311
G1 F2700 E2.7311
G0 F7500 X111.49 Y118.8
G0 X115.937 Y118.586
G0 X116.533 Y117.666
G0 X118.576 Y117.622
G0 X119.063 Y118.586
G0 X120.534 Y118.127
G0 X120.5 Y118.437
G1 F2700 E7.7311
G1 F1201.7 X120.642 Y118.402 E7.73597
G1 X123.4 Y118.4 E7.8277
G1 X123.4 Y111.6 E8.05387
G1 X119.81 Y111.6 E8.17327
G1 X120.195 Y111.911 E8.18973
G1 X120.444 Y112.144 E8.20107
G1 X120.669 Y112.399 E8.21239
G1 X120.865 Y112.659 E8.22321
G1 X121.031 Y112.92 E8.2335
G1 X121.267 Y113.351 E8.24985
G1 X121.425 Y113.814 E8.26612
G1 X121.508 Y114.146 E8.2775
G1 X121.564 Y114.466 E8.2883
G1 X121.594 Y114.81 E8.29979
G1 X121.594 Y115.191 E8.31246
G1 X121.565 Y115.523 E8.32355
G1 X121.516 Y115.816 E8.33343
G1 X121.425 Y116.172 E8.34565
G1 X121.269 Y116.635 E8.3619
G1 X121.009 Y117.119 E8.38017
G1 X120.861 Y117.343 E8.3891
G1 X120.673 Y117.597 E8.39961
G1 X120.437 Y117.856 E8.41127
G1 X120.168 Y118.11 E8.42357
G1 X119.804 Y118.399 E8.43903
G1 X120.32 Y118.4 E8.45619
G1 X120.5 Y118.437 E8.4623
G0 F7500 X120.5 Y119
;TYPE:WALL-OUTER
G1 F1201.7 X120.5 Y123.8 E8.62195
G1 F2700 E3.62195
G0 F7500 X121.365 Y123.8
G0 X122.735 Y123.9
G0 X123.5 Y123.9
G1 F2700 E8.62195
G1 F1413.7 X123.5 Y119 E8.76048
G1 F2700 E3.76048
G0 F7500 X123.5 Y118.49
G0 X120.5 Y118.49
G0 X120.5 Y119
G1 F2700 E8.76048
G1 F1201.7 X120.625 Y118.8 E8.76833
G1 X123.44 Y118.804 E8.86195
G1 F1299.1 X123.469 Y118.9 E8.86504
G1 X123.5 Y119 E8.86826
G1 X123.531 Y118.9 E8.87148
G1 X123.56 Y118.804 E8.87457
G1 F1201.7 X123.8 Y118.8 E8.88255
G1 X123.8 Y111.2 E9.13533
G1 X118.991 Y111.2 E9.29527
G1 F1166.7 X118.664 Y111.212 E9.30648
G1 F949.9 X118.321 Y111.294 E9.32132
G1 X118.621 Y111.46 E9.33575
G1 F1166.7 X118.908 Y111.578 E9.34638
G1 F1201.7 X119.182 Y111.705 E9.35642
G1 X119.44 Y111.85 E9.36627
G1 X119.697 Y112.023 E9.37657
G1 X119.924 Y112.205 E9.38625
G1 X120.146 Y112.41 E9.3963
G1 X120.342 Y112.63 E9.4061
G1 X120.529 Y112.875 E9.41635
G1 X120.673 Y113.099 E9.42521
```

```
G1 X120.906 Y113.531 E9.44153
G1 X121.051 Y113.96 E9.45659
G1 X121.122 Y114.254 E9.46665
G1 X121.172 Y114.551 E9.47667
G1 X121.196 Y114.843 E9.48641
G1 X121.196 Y115.157 E9.49686
G1 X121.17 Y115.457 E9.50687
G1 X121.122 Y115.747 E9.51665
G1 X121.046 Y116.044 E9.52685
G1 X120.906 Y116.46 E9.54145
G1 X120.675 Y116.899 E9.55794
G1 X120.52 Y117.132 E9.56725
G1 X120.353 Y117.357 E9.57657
G1 X120.134 Y117.594 E9.5873
G1 X119.915 Y117.8 E9.5973
G1 X119.682 Y117.988 E9.60726
G1 X119.428 Y118.154 E9.61735
G1 X119.184 Y118.294 E9.62671
G1 X118.894 Y118.424 E9.63728
G1 X118.605 Y118.529 E9.64751
G1 X118.309 Y118.609 E9.65771
G1 F1049.5 X117.911 Y118.742 E9.67369
G1 X118.326 Y118.799 E9.68964
G1 F1201.7 X120.378 Y118.805 E9.75789
G1 X120.5 Y119 E9.76554
G1 F2700 E4.76554
G0 F7500 X120.5 Y118.49
G0 X119.063 Y118.586
G0 X117.911 Y118.742
G1 F2700 E9.76554
G1 F931.5 X117.751 Y118.747 E9.77241
G1 F801.1 X117.5 Y118.836 E9.7857
G0 F7500 X116.824 Y118.719
G1 F891.8 X117.214 Y118.742 E9.8032
G1 F801.1 X117.5 Y118.836 E9.81822
G1 F717.4 X117.5 Y120.457 E9.90853
G1 F748.7 X117.5 Y122.078 E9.99506
G1 F782.9 X117.5 Y123.699 E10.07782
G1 F2700 E5.07782
G0 F7500 X116.535 Y123.699
G0 X115.565 Y123.8
G0 X114.7 Y123.8
G1 F2700 E10.07782
G1 F1201.7 X114.7 Y119 E10.23747
G1 X114.758 Y118.858 E10.24257
G1 X114.882 Y118.8 E10.24713
G1 X116.167 Y118.8 E10.28987
G1 F1166.7 X116.483 Y118.788 E10.3007
G1 F977 X116.824 Y118.719 E10.31493
G1 X116.515 Y118.578 E10.32883
G1 F1166.7 X115.953 Y118.363 E10.34944
G1 F1201.7 X115.701 Y118.235 E10.35884
G1 X115.43 Y118.066 E10.36946
G1 X115.18 Y117.883 E10.37977
G1 X114.951 Y117.683 E10.38988
G1 X114.751 Y117.474 E10.3995
G1 X114.567 Y117.258 E10.40894
G1 X114.379 Y116.989 E10.41986
G1 X114.227 Y116.728 E10.4299
G1 X114.097 Y116.457 E10.4399
G1 X113.993 Y116.189 E10.44946
G1 X113.903 Y115.884 E10.46004
G1 X113.846 Y115.599 E10.4697
G1 X113.812 Y115.297 E10.47981
G1 X113.8 Y114.995 E10.48986
G1 X113.813 Y114.684 E10.50022
G1 X113.845 Y114.408 E10.50946
G1 X113.907 Y114.1 E10.51991
G1 X113.993 Y113.807 E10.53006
G1 X114.097 Y113.539 E10.53963
G1 X114.227 Y113.268 E10.54962
G1 X114.379 Y113.01 E10.55958
G1 X114.566 Y112.743 E10.57042
G1 X114.759 Y112.513 E10.58041
G1 X114.951 Y112.313 E10.58963
G1 X115.194 Y112.102 E10.60034
G1 X115.444 Y111.92 E10.61062
G1 X115.7 Y111.766 E10.62056
G1 X115.972 Y111.626 E10.63073
G1 F1163.8 X116.515 Y111.417 E10.65071
G1 F975 X116.816 Y111.28 E10.66427
G1 X116.484 Y111.214 E10.67815
```

```
G1 F1163.8 X116.194 Y111.201 E10.68811
G1 F1201.7 X111.201 Y111.201 E10.85418
G1 X111.2 Y118 E11.08032
G1 F1068.2 X111.25 Y119 E11.11778
G1 F961.3 X111.25 Y123.75 E11.31526
G1 X111.75 Y123.75 E11.33605
G1 X111.75 Y119 E11.53353
G1 F1068.2 X112 Y118.8 E11.54551
G1 F1201.7 X114.12 Y118.801 E11.61603
G1 X114.242 Y118.858 E11.6205
G1 X114.3 Y119 E11.62561
G1 X114.3 Y123.8 E11.78525
G1 X114.7 Y123.8 E11.79856
G1 F2700 E6.79856
G0 F7500 X116.816 Y111.28
G1 F2700 E11.79856
G1 F893.4 X117.126 Y111.258 E11.81246
G1 F946.2 X117.433 Y111.25 E11.82543
G1 F949.9 X117.867 Y111.256 E11.8437
G1 F873.9 X118.321 Y111.294 E11.86453
G1 F2700 E6.86453
G0 F7500 X119.063 Y111.414
G0 X121.008 Y112.334
G0 X120.92 Y112.4
;TYPE:FILL
G1 F2700 E11.86453
G1 F1201.7 X122.598 Y112.4 E11.92034
G0 F7500 X122.8 Y112.2
G1 F1201.7 X123.32 Y111.68 E11.9448
G0 F7500 X123.32 Y112.006
G1 F1201.7 X122.993 Y111.68 E11.96016
G0 F7500 X122.993 Y111.91
G0 X121.645 Y113.501
G0 X121.426 Y113.573
G1 F1201.7 X122.8 Y112.2 E12.02476
G1 X122.8 Y117.142 E12.18913
G1 X123.32 Y117.663 E12.21362
G0 F7500 X123.056 Y117.6
G1 F1201.7 X120.92 Y117.6 E12.28466
G0 F7500 X121.007 Y117.667
G0 X122.335 Y118.09
G0 X122.335 Y118.322
G1 F1201.7 X123.32 Y117.337 E12.33099
G0 F7500 X122.8 Y117.142
G1 F1201.7 X121.572 Y115.915 E12.38873
G1 F2700 E7.38873
G0 F7500 X121.799 Y115.972
G0 X121.168 Y116.411
G0 X120.147 Y116.016
G0 X115.556 Y117.062
G0 X114.808 Y117.862
G0 X113.986 Y117.662
G0 X114.075 Y117.6
G1 F2700 E12.38873
G1 F1201.7 X111.944 Y117.6 E12.45961
G0 F7500 X111.681 Y117.662
G1 F1201.7 X112.4 Y116.942 E12.49345
G0 F7500 X111.68 Y117.337
G1 F1201.7 X112.664 Y118.321 E12.53973
G0 F7500 X112.664 Y118.09
G0 X113.199 Y115.966
G0 X113.421 Y115.922
G1 F1201.7 X112.4 Y116.942 E12.58774
G1 X112.4 Y112.401 E12.73877
G1 X111.681 Y111.681 E12.77261
G0 F7500 X111.681 Y112.005
G1 F1201.7 X112.005 Y111.681 E12.78785
G0 F7500 X112.401 Y112.4
G1 F1201.7 X114.076 Y112.4 E12.84356
G0 F7500 X113.987 Y112.337
G0 X113.36 Y113.49
G0 X113.571 Y113.571
G1 F1201.7 X112.4 Y112.401 E12.89862
G1 F2700 E7.89862
;MESH:NONMESH
G0 F300 X112.4 Y112.401 Z0.6
G0 F7500 X113.584 Y114.68
G0 X114.665 Y115
G0 X117.441 Y117.834
G0 X117.5 Y118.535
;TIME_ELAPSED:39.150134
;LAYER:2
```

```
M106 S170
;TYPE:WALL-INNER
;MESH:Slicer Test v3.stl
G1 F2700 E12.89862
G1 F1500 X117.553 Y118.452 E12.9019
G1 X117.732 Y118.403 E12.90807
G1 X120.424 Y118.403 E12.99761
G1 X120.5 Y118.498 E13.00165
G1 X120.575 Y118.403 E13.00568
G1 X123.4 Y118.4 E13.09964
G1 X123.4 Y111.6 E13.32581
G1 X111.6 Y111.6 E13.71828
G1 X111.6 Y118.8 E13.95775
G1 X112 Y118.4 E13.97656
G1 X114.169 Y118.403 E14.0487
G1 X114.351 Y118.455 E14.055
G1 X114.5 Y118.688 E14.0642
G1 X114.649 Y118.455 E14.0734
G1 X114.831 Y118.403 E14.07969
G1 X117.268 Y118.403 E14.16075
G1 X117.447 Y118.452 E14.16692
G1 X117.5 Y118.535 E14.1702
G0 F9000 X117.5 Y119
;TYPE:WALL-OUTER
G1 F1000 X117.5 Y123.7 E14.40468
G1 F2700 E9.40468
G0 F9000 X118.465 Y123.7
G0 X119.635 Y123.8
G0 X120.5 Y123.8
G1 F2700 E14.40468
G1 F1500 X120.5 Y119 E14.56433
G1 F2700 E9.56433
G0 F9000 X120.5 Y118.49
G0 X123.5 Y118.49
G0 X123.5 Y119
G1 F2700 E14.56433
G1 F1764.7 X123.5 Y123.9 E14.70286
G1 F2700 E9.70286
G0 F9000 X122.735 Y123.9
G0 X122.747 Y119.653
G0 X117.5 Y119
G1 F2700 E14.70286
G1 F1200 X117.737 Y118.8 E14.71575
G1 F1500 X120.345 Y118.805 E14.80249
G1 X120.5 Y119 E14.81078
G1 X120.655 Y118.805 E14.81906
G1 X123.44 Y118.804 E14.91169
G1 F1621.6 X123.5 Y119 E14.918
G1 X123.56 Y118.804 E14.9243
G1 F1500 X123.8 Y118.8 E14.93229
G1 X123.8 Y111.2 E15.18507
G1 X111.2 Y111.2 E15.60414
G1 X111.2 Y118 E15.83031
G1 F1333.3 X111.25 Y119 E15.86778
G1 F1200 X111.25 Y123.75 E16.06526
G1 X111.75 Y123.75 E16.08605
G1 X111.75 Y119 E16.28353
G1 F1333.3 X112 Y118.8 E16.29551
G1 F1500 X114.174 Y118.802 E16.36782
G1 X114.3 Y119 E16.37562
G1 X114.3 Y123.8 E16.53527
G1 X114.7 Y123.8 E16.54857
G1 X114.7 Y119 E16.70822
G1 X114.827 Y118.801 E16.71607
G1 X117.263 Y118.8 E16.7971
G1 F1200 X117.5 Y119 E16.80999
G0 F9000 X117.5 Y118.094
;TYPE:SKIN
G1 F1500 X117.495 Y118.095 E16.81016
G1 X117.214 Y118.04 E16.81968
G1 X114.795 Y118.045 E16.90014
G1 X114.477 Y118.13 E16.91109
G1 X114.245 Y118.042 E16.91934
G1 X111.96 Y118.04 E16.99534
G1 X111.96 Y111.96 E17.19756
G1 X123.04 Y111.96 E17.56608
G1 X123.04 Y118.04 E17.7683
G1 X117.73 Y118.04 E17.94492
G1 X117.5 Y118.094 E17.95277
G0 F9000 X117.56 Y118.348
G0 X115.081 Y118.403
G0 X112.749 Y118.3
```

```
G0 X112.749 Y117.84
G1 F1500 X112.16 Y117.251 E17.98048
G0 F9000 X112.16 Y116.685
G1 F1500 X113.315 Y117.841 E18.03483
G0 F9000 X113.882 Y117.841
G1 F1500 X112.16 Y116.12 E18.1158
G0 F9000 X112.16 Y115.554
G1 F1500 X114.517 Y117.911 E18.22667
G0 F9000 X115.019 Y117.847
G1 F1500 X112.16 Y114.988 E18.36115
G0 F9000 X112.16 Y114.423
G1 F1500 X115.583 Y117.846 E18.52216
G0 F9000 X116.147 Y117.844
G1 F1500 X112.16 Y113.857 E18.70969
G0 F9000 X112.16 Y113.291
G1 F1500 X116.712 Y117.843 E18.9238
G0 F9000 X117.284 Y117.85
G1 F1500 X112.16 Y112.726 E19.16482
G0 F9000 X112.16 Y112.16
G1 F1500 X117.841 Y117.841 E19.43204
G0 F9000 X118.406 Y117.841
G1 F1500 X112.726 Y112.16 E19.69923
G0 F9000 X113.291 Y112.16
G1 F1500 X118.972 Y117.841 E19.96645
G0 F9000 X119.537 Y117.84
G1 F1500 X113.857 Y112.16 E20.23362
G0 F9000 X114.423 Y112.16
G1 F1500 X120.103 Y117.84 E20.50079
G0 F9000 X120.668 Y117.84
G1 F1500 X114.988 Y112.16 E20.76796
G0 F9000 X115.554 Y112.16
G1 F1500 X121.233 Y117.839 E21.03508
G0 F9000 X121.799 Y117.839
G1 F1500 X116.12 Y112.16 E21.3022
G0 F9000 X116.685 Y112.16
G1 F1500 X122.365 Y117.839 E21.56935
G0 F9000 X122.84 Y117.749
G1 F1500 X117.251 Y112.16 E21.83224
G0 F9000 X117.817 Y112.16
G1 F1500 X122.84 Y117.183 E22.0685
G0 F9000 X122.84 Y116.617
G1 F1500 X118.382 Y112.16 E22.27817
G0 F9000 X118.948 Y112.16
G1 F1500 X122.84 Y116.052 E22.46124
G0 F9000 X122.84 Y115.486
G1 F1500 X119.514 Y112.16 E22.61768
G0 F9000 X120.079 Y112.16
G1 F1500 X122.84 Y114.92 E22.74753
G0 F9000 X122.84 Y114.355
G1 F1500 X120.645 Y112.16 E22.85078
G0 F9000 X121.211 Y112.16
G1 F1500 X122.84 Y113.789 E22.9274
G0 F9000 X122.84 Y113.223
G1 F1500 X121.777 Y112.16 E22.9774
G0 F9000 X122.342 Y112.16
G1 F1500 X122.84 Y112.658 E23.00082
;MESH:NONMESH
G0 F300 X122.84 Y112.658 Z0.8
G0 F9000 X123.3 Y112.658
G0 X123.228 Y118.228
G0 X117.607 Y118.337
G0 X117.5 Y117.888
;TIME_ELAPSED:57.168930
;LAYER:3
;note -- min layer time used
M106 S255
;TYPE:WALL-INNER
;MESH:Slicer Test v3.stl
G1 F600 X117.67 Y117.892 E23.00648
G1 X118.262 Y117.809 E23.02636
G1 X118.813 Y117.583 E23.04617
G1 X119.298 Y117.287 E23.06507
G1 X119.727 Y116.854 E23.08534
G1 X120.001 Y116.464 E23.10119
G1 X120.202 Y116.045 E23.11665
G1 X120.308 Y115.724 E23.12789
G1 X120.4 Y115.215 E23.1451
G1 X120.376 Y114.643 E23.16414
G1 X120.332 Y114.381 E23.17298
G1 X120.204 Y113.955 E23.18777
G1 X119.997 Y113.528 E23.20355
G1 X119.726 Y113.141 E23.21927
```

```
G1 X119.321 Y112.733 E23.23839
G1 X118.928 Y112.469 E23.25413
G1 X118.458 Y112.252 E23.27135
G1 X117.779 Y112.102 E23.29448
G1 X117.207 Y112.114 E23.31351
G1 X116.62 Y112.223 E23.33337
G1 X116.087 Y112.464 E23.35282
G1 X115.582 Y112.808 E23.37315
G1 X115.113 Y113.332 E23.39654
G1 X114.836 Y113.85 E23.41607
G1 X114.684 Y114.301 E23.4319
G1 X114.611 Y114.77 E23.44769
G1 X114.611 Y115.229 E23.46296
G1 X114.684 Y115.699 E23.47878
G1 X114.836 Y116.146 E23.49448
G1 X115.113 Y116.664 E23.51402
G1 X115.512 Y117.11 E23.53392
G1 X115.974 Y117.48 E23.55361
G1 X116.517 Y117.727 E23.57345
G1 X117.078 Y117.879 E23.59278
G1 X117.5 Y117.888 E23.60682
G0 F9000 X117.5 Y118.294
;TYPE:WALL-OUTER
G1 F600 X117.695 Y118.292 E23.6133
G1 X117.972 Y118.261 E23.62257
G1 X118.236 Y118.216 E23.63148
G1 X118.494 Y118.145 E23.64038
G1 X118.74 Y118.054 E23.64911
G1 X118.993 Y117.941 E23.65832
G1 X119.227 Y117.809 E23.66726
G1 X119.449 Y117.662 E23.67611
G1 X119.655 Y117.493 E23.68498
G1 X119.857 Y117.303 E23.6942
G1 X120.034 Y117.111 E23.70288
G1 X120.2 Y116.892 E23.71202
G1 X120.347 Y116.666 E23.72099
G1 X120.471 Y116.429 E23.72989
G1 X120.576 Y116.188 E23.73863
G1 X120.697 Y115.822 E23.75145
G1 X120.773 Y115.402 E23.76565
G1 X120.796 Y115.127 E23.77483
G1 X120.796 Y114.861 E23.78367
G1 X120.773 Y114.593 E23.79262
G1 X120.706 Y114.19 E23.80621
G1 X120.577 Y113.809 E23.81959
G1 X120.471 Y113.572 E23.82822
G1 X120.343 Y113.326 E23.83745
G1 X120.196 Y113.099 E23.84644
G1 X120.034 Y112.885 E23.85537
G1 X119.857 Y112.693 E23.86405
G1 X119.656 Y112.503 E23.87325
G1 X119.445 Y112.334 E23.88224
G1 X119.227 Y112.188 E23.89097
G1 X118.993 Y112.059 E23.89986
G1 X118.739 Y111.941 E23.90917
G1 X118.495 Y111.852 E23.91781
G1 X118.236 Y111.784 E23.92672
G1 X117.97 Y111.735 E23.93571
G1 X117.695 Y111.704 E23.94492
G1 X117.433 Y111.701 E23.95363
G1 X117.165 Y111.716 E23.96256
G1 X116.893 Y111.757 E23.97171
G1 X116.636 Y111.814 E23.98047
G1 X116.38 Y111.893 E23.98938
G1 X116.123 Y111.999 E23.99862
G1 X115.891 Y112.115 E24.00725
G1 X115.657 Y112.262 E24.01644
G1 X115.441 Y112.421 E24.02536
G1 X115.238 Y112.594 E24.03423
G1 X115.053 Y112.786 E24.0431
G1 X114.875 Y112.999 E24.05233
G1 X114.721 Y113.216 E24.06118
G1 X114.589 Y113.447 E24.07003
G1 X114.468 Y113.692 E24.07912
G1 X114.374 Y113.945 E24.0881
G1 X114.295 Y114.205 E24.09714
G1 X114.246 Y114.46 E24.10577
G1 X114.212 Y114.737 E24.11505
G1 X114.201 Y115.003 E24.12391
G1 X114.212 Y115.263 E24.13256
G1 X114.246 Y115.537 E24.14175
G1 X114.295 Y115.795 E24.15048
```

```
G1 X114.374 Y116.051 E24.15939
G1 X114.468 Y116.304 E24.16837
G1 X114.589 Y116.549 E24.17746
G1 X114.721 Y116.78 E24.18631
G1 X114.875 Y116.997 E24.19516
G1 X115.053 Y117.21 E24.20439
G1 X115.238 Y117.402 E24.21326
G1 X115.442 Y117.575 E24.22215
G1 X115.657 Y117.738 E24.23113
G1 X115.89 Y117.88 E24.2402
G1 X116.123 Y117.997 E24.24888
G1 X116.381 Y118.103 E24.25815
G1 X116.633 Y118.182 E24.26694
G1 X116.893 Y118.243 E24.27582
G1 X117.164 Y118.28 E24.28492
G1 X117.433 Y118.295 E24.29388
G1 X117.5 Y118.294 E24.29611
G0 F9000 X117.5 Y117.527
;TYPE:SKIN
G1 F600 X117.122 Y117.516 E24.30868
G1 X116.536 Y117.357 E24.32888
G1 X116.084 Y117.109 E24.34603
G1 X115.755 Y116.842 E24.36012
G1 X115.41 Y116.456 E24.37734
G1 X115.169 Y116.004 E24.39437
G1 X115.031 Y115.603 E24.40848
G1 X114.968 Y115.204 E24.42191
G1 X114.968 Y114.792 E24.43562
G1 X115.031 Y114.393 E24.44905
G1 X115.169 Y113.992 E24.46316
G1 X115.406 Y113.544 E24.48002
G1 X115.766 Y113.143 E24.49794
G1 X116.173 Y112.82 E24.51522
G1 X116.729 Y112.569 E24.53551
G1 X117.241 Y112.472 E24.55284
G1 X117.744 Y112.461 E24.56958
G1 X118.263 Y112.576 E24.58726
G1 X118.657 Y112.739 E24.60144
G1 X119.07 Y112.99 E24.61751
G1 X119.446 Y113.373 E24.63536
G1 X119.687 Y113.715 E24.64928
G1 X119.865 Y114.077 E24.6627
G1 X120.009 Y114.566 E24.67965
G1 X120.039 Y115.186 E24.7003
G1 X119.957 Y115.626 E24.71518
G1 X119.865 Y115.909 E24.72508
G1 X119.687 Y116.278 E24.73871
G1 X119.393 Y116.693 E24.75562
G1 X118.988 Y117.054 E24.77367
G1 X118.657 Y117.256 E24.78656
G1 X118.159 Y117.457 E24.80443
G1 X117.64 Y117.531 E24.82186
G1 X117.5 Y117.527 E24.82652
G0 F9000 X117.469 Y117.787
G0 X118.214 Y117.654
G0 X118.741 Y117.439
G0 X119.116 Y117.211
G0 X119.547 Y116.829
G0 X119.726 Y116.576
G0 X120.221 Y115.641
G0 X119.766 Y115.559
G1 F600 X118.056 Y117.269 E24.90695
G0 F9000 X117.433 Y117.326
G1 F600 X119.826 Y114.934 E25.01949
G0 F9000 X119.761 Y114.433
G1 F600 X116.935 Y117.259 E25.15242
G0 F9000 X116.512 Y117.116
G1 F600 X119.611 Y114.017 E25.29818
G0 F9000 X119.403 Y113.66
G1 F600 X116.154 Y116.909 E25.45101
G0 F9000 X115.849 Y116.648
G1 F600 X119.145 Y113.352 E25.60604
G0 F9000 X118.844 Y113.087
G1 F600 X115.582 Y116.349 E25.75948
G0 F9000 X115.384 Y115.981
G1 F600 X118.483 Y112.883 E25.90522
G0 F9000 X118.063 Y112.736
G1 F600 X115.231 Y115.569 E26.03845
G0 F9000 X115.169 Y115.065
G1 F600 X117.569 Y112.665 E26.15134
G0 F9000 X116.935 Y112.733
G1 F600 X115.226 Y114.442 E26.23173
```

```
;MESH:NONMESH
G0 F300 X115.226 Y114.442 Z1
G0 F9000 X114.775 Y114.371
G0 X114.771 Y115.215
G0 X114.84 Y115.66
G0 X114.984 Y116.081
G0 X115.243 Y116.57
G0 X115.623 Y116.993
G0 X115.974 Y117.275
G0 X116.366 Y117.494
G0 X117.469 Y117.787
G0 X117.5 Y117.888
;TIME_ELAPSED:68.095268
;LAYER:4
;note -- min layer time used
; TYPE: WALL-INNER
;MESH:Slicer Test v3.stl
G1 F600 X117.67 Y117.892 E26.23738
G1 X118.262 Y117.809 E26.25726
G1 X118.813 Y117.583 E26.27707
G1 X119.298 Y117.287 E26.29597
G1 X119.727 Y116.854 E26.31624
G1 X120.001 Y116.464 E26.3321
G1 X120.202 Y116.045 E26.34755
G1 X120.308 Y115.724 E26.3588
G1 X120.4 Y115.215 E26.376
G1 X120.376 Y114.643 E26.39504
G1 X120.332 Y114.381 E26.40388
G1 X120.204 Y113.955 E26.41867
G1 X119.997 Y113.528 E26.43446
G1 X119.726 Y113.141 E26.45017
G1 X119.321 Y112.733 E26.46929
G1 X118.928 Y112.469 E26.48504
G1 X118.458 Y112.252 E26.50225
G1 X117.779 Y112.102 E26.52538
G1 X117.207 Y112.114 E26.54441
G1 X116.62 Y112.223 E26.56427
G1 X116.087 Y112.464 E26.58373
G1 X115.582 Y112.808 E26.60405
G1 X115.113 Y113.332 E26.62744
G1 X114.836 Y113.85 E26.64698
G1 X114.684 Y114.301 E26.6628
G1 X114.611 Y114.77 E26.67859
G1 X114.611 Y115.229 E26.69386
G1 X114.684 Y115.699 E26.70968
G1 X114.836 Y116.146 E26.72538
G1 X115.113 Y116.664 E26.74492
G1 X115.512 Y117.11 E26.76482
G1 X115.974 Y117.48 E26.78451
G1 X116.517 Y117.727 E26.80435
G1 X117.078 Y117.879 E26.82368
G1 X117.5 Y117.888 E26.83772
G0 F9000 X117.5 Y118.294
; TYPE: WALL-OUTER
G1 F600 X117.695 Y118.292 E26.84421
G1 X117.972 Y118.261 E26.85348
G1 X118.236 Y118.216 E26.86238
G1 X118.494 Y118.145 E26.87128
G1 X118.74 Y118.054 E26.88001
G1 X118.993 Y117.941 E26.88922
G1 X119.227 Y117.809 E26.89816
G1 X119.449 Y117.662 E26.90702
G1 X119.655 Y117.493 E26.91588
G1 X119.857 Y117.303 E26.9251
G1 X120.034 Y117.111 E26.93379
G1 X120.2 Y116.892 E26.94293
G1 X120.347 Y116.666 E26.95189
G1 X120.471 Y116.429 E26.96079
G1 X120.576 Y116.188 E26.96953
G1 X120.697 Y115.822 E26.98235
G1 X120.773 Y115.402 E26.99655
G1 X120.796 Y115.127 E27.00573
G1 X120.796 Y114.861 E27.01458
G1 X120.773 Y114.593 E27.02352
G1 X120.706 Y114.19 E27.03711
G1 X120.577 Y113.809 E27.05049
G1 X120.471 Y113.572 E27.05912
G1 X120.343 Y113.326 E27.06835
G1 X120.196 Y113.099 E27.07734
G1 X120.034 Y112.885 E27.08627
G1 X119.857 Y112.693 E27.09496
G1 X119.656 Y112.503 E27.10416
```

```
G1 X119.445 Y112.334 E27.11315
G1 X119.227 Y112.188 E27.12187
G1 X118.993 Y112.059 E27.13076
G1 X118.739 Y111.941 E27.14008
G1 X118.495 Y111.852 E27.14871
G1 X118.236 Y111.784 E27.15762
G1 X117.97 Y111.735 E27.16662
G1 X117.695 Y111.704 E27.17582
G1 X117.433 Y111.701 E27.18454
G1 X117.165 Y111.716 E27.19346
G1 X116.893 Y111.757 E27.20261
G1 X116.636 Y111.814 E27.21137
G1 X116.38 Y111.893 E27.22028
G1 X116.123 Y111.999 E27.22952
G1 X115.891 Y112.115 E27.23815
G1 X115.657 Y112.262 E27.24734
G1 X115.441 Y112.421 E27.25626
G1 X115.238 Y112.594 E27.26514
G1 X115.053 Y112.786 E27.274
G1 X114.875 Y112.999 E27.28324
G1 X114.721 Y113.216 E27.29209
G1 X114.589 Y113.447 E27.30093
G1 X114.468 Y113.692 E27.31002
G1 X114.374 Y113.945 E27.319
G1 X114.295 Y114.205 E27.32804
G1 X114.246 Y114.46 E27.33667
G1 X114.212 Y114.737 E27.34596
G1 X114.201 Y115.003 E27.35481
G1 X114.212 Y115.263 E27.36347
G1 X114.246 Y115.537 E27.37265
G1 X114.295 Y115.795 E27.38138
G1 X114.374 Y116.051 E27.3903
G1 X114.468 Y116.304 E27.39927
G1 X114.589 Y116.549 E27.40836
G1 X114.721 Y116.78 E27.41721
G1 X114.875 Y116.997 E27.42606
G1 X115.053 Y117.21 E27.43529
G1 X115.238 Y117.402 E27.44416
G1 X115.442 Y117.575 E27.45306
G1 X115.657 Y117.738 E27.46203
G1 X115.89 Y117.88 E27.47111
G1 X116.123 Y117.997 E27.47978
G1 X116.381 Y118.103 E27.48905
G1 X116.633 Y118.182 E27.49784
G1 X116.893 Y118.243 E27.50672
G1 X117.164 Y118.28 E27.51582
G1 X117.433 Y118.295 E27.52478
G1 X117.5 Y118.294 E27.52701
G0 F9000 X117.5 Y117.527
;TYPE:SKIN
G1 F600 X117.122 Y117.516 E27.53959
G1 X116.536 Y117.357 E27.55978
G1 X116.084 Y117.109 E27.57693
G1 X115.755 Y116.842 E27.59102
G1 X115.41 Y116.456 E27.60824
G1 X115.169 Y116.004 E27.62528
G1 X115.031 Y115.603 E27.63938
G1 X114.968 Y115.204 E27.65282
G1 X114.968 Y114.792 E27.66652
G1 X115.031 Y114.393 E27.67996
G1 X115.169 Y113.992 E27.69406
G1 X115.406 Y113.544 E27.71092
G1 X115.766 Y113.143 E27.72884
G1 X116.173 Y112.82 E27.74612
G1 X116.729 Y112.569 E27.76641
G1 X117.241 Y112.472 E27.78374
G1 X117.744 Y112.461 E27.80048
G1 X118.263 Y112.576 E27.81816
G1 X118.657 Y112.739 E27.83234
G1 X119.07 Y112.99 E27.84842
G1 X119.446 Y113.373 E27.86627
G1 X119.687 Y113.715 E27.88018
G1 X119.865 Y114.077 E27.8936
G1 X120.009 Y114.566 E27.91055
G1 X120.039 Y115.186 E27.9312
G1 X119.957 Y115.626 E27.94609
G1 X119.865 Y115.909 E27.95598
G1 X119.687 Y116.278 E27.96961
G1 X119.393 Y116.693 E27.98652
G1 X118.988 Y117.054 E28.00457
G1 X118.657 Y117.256 E28.01747
G1 X118.159 Y117.457 E28.03533
```

```
G1 X117.64 Y117.531 E28.05277
G1 X117.5 Y117.527 E28.05742
G0 F9000 X116.595 Y117.161
G1 F600 X115.35 Y115.915 E28.11601
G0 F9000 X115.168 Y115.168
G1 F600 X117.322 Y117.322 E28.21733
G0 F9000 X117.863 Y117.297
G1 F600 X115.196 Y114.63 E28.34277
G0 F9000 X115.314 Y114.183
G1 F600 X118.31 Y117.179 E28.4837
G0 F9000 X118.695 Y116.998
G1 F600 X115.497 Y113.8 E28.63412
G0 F9000 X115.736 Y113.474
G1 F600 X119.02 Y116.757 E28.78857
G0 F9000 X119.303 Y116.475
G1 F600 X116.023 Y113.194 E28.94287
G0 F9000 X116.352 Y112.958
G1 F600 X119.533 Y116.139 E29.0925
G0 F9000 X119.708 Y115.748
G1 F600 X116.743 Y112.783 E29.23196
G0 F9000 X117.208 Y112.682
G1 F600 X119.816 Y115.291 E29.35466
G0 F9000 X119.816 Y114.725
G1 F600 X117.762 Y112.671 E29.45127
G0 F9000 X118.588 Y112.931
G1 F600 X119.553 Y113.896 E29.49666
;TIME_ELAPSED:78.759930
G1 F2700 E24.49666
M140 S0
M107
G91 ;Relative positioning
```

Listing A.3.2 G-Code Generated Using Ultimaker Cura [97] (Main)

```
G1 E-2 F2700 ;Retract a bit
G1 E-2 Z0.2 F2400 ;Retract and raise Z
G1 X5 Y5 F3000 ;Wipe out
G1 Z10 ;Raise Z more
G90 ;Absolute positioning

G1 X0 Y235 ;Present print
M106 S0 ;Turn-off fan
M104 S0 ;Turn-off hotend
M140 S0 ;Turn-off bed

M84 X Y E ;Disable all steppers but Z

M82 ;absolute extrusion mode
M104 S0
;End of Gcode
;SETTING_3 {"global_quality": "[general]\\nversion = 4\\nname = Standard Quality
;SETTING_3  #2\\ndefinition = creality_ender3\\n\\n[metadata]\\ntype = quality_c
;SETTING_3 hanges\\nquality_type = standard\\nsetting_version = 25\\n\\n[values]
;SETTING_3 \\nadhesion_type = none\\n\\n", "extruder_quality": ["[general]\\nver
;SETTING_3 sion = 4\\nname = Standard Quality #2\\ndefinition = creality_ender3\
;SETTING_3 \n\\n[metadata]\\ntype = quality_changes\\nquality_type = standard\\n
;SETTING_3 setting_version = 25\\nposition = 0\\n\\n[values]\\nfill_outline_gaps
;SETTING_3  = True\\ninfill_pattern = grid\\ninitial_bottom_layers = 1\\ntop_lay
;SETTING_3 ers = 1\\n\\n"]}
```

Listing A.3.3 G-Code Generated Using Ultimaker Cura [97] (Reset)

B Fixed Arguments for Cura

Listing B.1 Fixed arguments specified in *preset_arguments.py*

```
    preset = {
        "machine_name": machine_name,  # match "id" from Robot.setup.json
        "machine_width": bed_size["X"],  # match "bed_size" from Robot.setup.json
        "machine_depth": bed_size["Y"],  # match "bed_size" from Robot.setup.json
        "machine_height": bed_size["Z"],  # match "bed_size" from Robot.setup.json
        "machine_show_variants": False,  # allows only one variant of machine
        "machine_start_gcode": "",  # no custom G-Code possible for start sequence
        "machine_end_gcode": "",  # no custom G-Code possible for end sequence
        "machine_center_is_zero": False,  # to fix origin to print bed corner matching $BASE
        "machine_extruder_start_code": "",  # no custom G-Code possible for extruder start
        "machine_extruder_end_code": "",  # no custom G-Code possible for extruder stop
        "machine_g_code_flavor": "RepRap (Marlin/Sprinter)",  # Fixed to Marlin as specified
        "material_guid": "",
        "material_type": "",  # no material specified
        "material_brand": "",
        "machine_shape": "rectangular",  # circular shape not compatible with Rhino implementation and Report
        "machine_extruder_count": 1,  # no dual extruder possible
        "extruders_enabled_count": 0,
        "machine_firmware_retract": False,  # No G10 or G11 commands to specify retractions
        "initial_layer_line_width_factor": 100,  # line width for layer 0 fixed to 100 %
        "ironing_enabled": False,  # not possible to differentiate between surface and ironing; therefor disabled
        "roofing_layer_count": "0",  # unresolved issue if not specified here
        "wall_0_material_flow": flow[
            "wall_outer"
        ],  # to match "linetype_flow" input from Pump.setup.json
        "wall_x_material_flow": flow[
            "wall_inner"
        ],  # to match "linetype_flow" input from Pump.setup.json
        "wall_0_material_flow_roofing": flow[
            "wall_outer"
        ],  # to match "linetype_flow" input from Pump.setup.json
        "wall_x_material_flow_roofing": flow[
            "wall_inner"
        ],  # to match "linetype_flow" input from Pump.setup.json
        "skin_material_flow": flow[
            "surface"
        ],  # to match "linetype_flow" input from Pump.setup.json
```

```
        "roofing_material_flow": flow[
            "surface"
        ],  # to match "linetype_flow" input from Pump.setup.json
        "infill_material_flow": flow[
            "infill"
        ],  # to match "linetype_flow" input from Pump.setup.json
        "skirt_brim_material_flow": flow[
            "curb"
        ],  # to match "linetype_flow" input from Pump.setup.json
        "support_material_flow": flow[
            "support"
        ],  # to match "linetype_flow" input from Pump.setup.json
        "support_roof_material_flow": flow[
            "support"
        ],  # to match "linetype_flow" input from Pump.setup.json
        "support_bottom_material_flow": flow[
            "support"
        ],  # to match "linetype_flow" input from Pump.setup.json
        "prime_tower_flow": 100,  # as default flow for not specified line types is 100% and prime tower has not been tested
        "material_flow_layer_0": 100,  # flow for layer 0 fixed to 100%; no bed adhesion problems for concrete 3D-printing
        "retraction_enable": pump_retract,  # to match "retract" input from Pump.setup.json
        "retraction_hop_enabled": False,  # could disturb layer_height calculation; therefor deactivated
        "layer_0_z_overlap": 0,  # could disturb layer_height calculation; therefor deactivated
        "wipe_hop_enable": False,  # could disturb layer_height calculation; therefor deactivated
        "mesh_rotation_matrix": scaling,  # calculated for "cura_scaling" from Cura.setup.json via module scaling_matrix.py
        "filament_diameter": filament_dia,  # to match "filament_diameter" input from Pump.setup.json and recalculate E-value correctly
    }
```

C List of Usable and Validated Commands from *printer.def.json* With Comments

Parent Key	Key	Description	Unit	Type	Value	Usable	Comment
machine_settings	machine_name	The name of your 3D printer model.		str	Unknown	yes	setup.json [Robot.id]
machine_settings	machine_show_variants	Whether to show the different variants of this machine, which are described in separate json files.		bool	False	fixed	
machine_settings	machine_start_gcode	G-code commands to be executed at the very start - separated by \n.		str		fixed	
machine_settings	machine_end_gcode	G-code commands to be executed at the very end - separated by \n.		str		fixed	
machine_settings	material_guid	GUID of the material. This is set automatically.		str		fixed	
machine_settings	material_type	The type of material used.		str		fixed	
machine_settings	material_brand	The brand of material used.		str		fixed	
machine_settings	material_diameter	Adjusts the diameter of the filament used. Match this value with the diameter of the used filament.	mm	float	25	yes	setup.json [Pump.filament_diameter]
machine_settings	material_bed_temp_wait	Whether to insert a command to wait until the build plate temperature is reached at the start.		bool	True	no	
machine_settings	material_print_temp_wait	Whether to wait until the nozzle temperature is reached at the start.		bool	True	no	
machine_settings	material_print_temp_prepend	Whether to include nozzle temperature commands at the start of the gcode. When the start_gcode already contains nozzle temperature commands Cura frontend will automatically disable this setting.		bool	True	no	
machine_settings	material_bed_temp_prepend	Whether to include build plate temperature commands at the start of the gcode. When the start_gcode already contains build plate temperature commands Cura frontend will automatically disable this setting.		bool	True	no	
machine_settings	machine_width	The width (X-direction) of the printable area.		float	1200	yes	setup.json [Robot.bed_size ("X")]
machine_settings	machine_depth	The depth (Y-direction) of the printable area.		float	4500	yes	setup.json [Robot.bed_size ("Y")]
machine_settings	machine_height	The height (Z-direction) of the printable area.		float	2000	yes	setup.json [Robot.bed_size ("Z")]
machine_settings	machine_shape	The shape of the build plate without taking unprintable areas into account.		key	rectangular	fixed	only rectangular possible
machine_settings	machine_buildplate_type	The material of the build plate installed on the printer.		key	aluminum	no	
machine_settings	machine_heated_bed	Whether the machine has a heated build plate present.		bool	False	no	
machine_settings	machine_heated_build_volume	Whether the machine is able to stabilize the build volume temperature.		bool	False	no	
machine_settings	machine_always_write_active_tool	Write active tool after sending temp commands to inactive tool. Required for Dual Extruder printing with Smoothie or other firmware with modal tool commands.		bool	False	no	
machine_settings	machine_center_is_zero	Whether the X/Y coordinates of the zero position of the printer is at the center of the printable area.		bool	False	yes	
machine_settings	machine_extruder_count	Number of extruder trains. An extruder train is the combination of a feeder, bowden tube, and nozzle.		int	1	fixed	only singel extruder possible
machine_settings	extruders_enabled_count	Number of extruder trains that are enabled; automatically set in software		int	1	fixed	only singel extruder possible
machine_settings	machine_nozzle_tip_outer_diameter	The outer diameter of the tip of the nozzle.	mm	float	30	yes	for collision avoidance
machine_settings	machine_nozzle_head_distance	The height difference between the tip of the nozzle and the lowest part of the print head.	mm	float	10	yes	for collision avoidance
machine_settings	machine_nozzle_expansion_angle	The angle between the horizontal plane and the conical part right above the tip of the nozzle.	°	int	45	yes	for collision avoidance

machine_settings	machine_heat_zone_length	The distance from the tip of the nozzle in which heat from the nozzle is transferred to the filament.	mm	float	16	no	
machine_settings	machine_nozzle_temp_enabled	Whether to control temperature from Cura. Turn this off to control nozzle temperature from outside of Cura.		bool	True	no	
machine_settings	machine_nozzle_heat_up_speed	The speed (°C/s) by which the nozzle heats up averaged over the window of normal printing temperatures and the standby temperature.	°C/s	float	2	no	
machine_settings	machine_nozzle_cool_down_speed	The speed (°C/s) by which the nozzle cools down averaged over the window of normal printing temperatures and the standby temperature.	°C/s	float	2	no	
machine_settings	machine_min_cool_heat_time_window	The minimal time an extruder has to be inactive before the nozzle is cooled. Only when an extruder is not used for longer than this time will it be allowed to cool down to the standby temperature.	s	float	50	no	
machine_settings	machine_gcode_flavor	The type of g-code to be generated.		key	RepRap (Marlin/Sprinter)	fixed	fixed to Marlin
machine_settings	machine_firmware_retract	Whether to use firmware retract commands (G10/G11) instead of using the E property in G1 commands to retract the material.		bool	False	fixed	
machine_settings	machine_extruders_share_heater	Whether the extruders share a single heater rather than each extruder having its own heater.		bool	False	no	
machine_settings	machine_extruders_share_nozzle	Whether the extruders share a single nozzle rather than each extruder having its own nozzle. When set to true, it is expected that the printer-start gcode script properly sets up all extruders in an initial retraction state that is known and mutually compatible (either zero or one filament not retracted); in that case the initial retraction status is described, per extruder, by the 'machine_extruders_shared_nozzle_initial_retraction' parameter.		bool	False	no	
machine_settings	machine_extruders_shared_nozzle_initial_retraction	How much the filament of each extruder is assumed to have been retracted from the shared nozzle tip at the completion of the printer-start gcode script; the value should be equal to or greater than the length of the common part of the nozzle's ducts.	mm	float	0	no	
machine_settings	machine_disallowed_areas	A list of polygons with areas the print head is not allowed to enter.		list[float]	[]	yes	
machine_settings	nozzle_disallowed_areas	A list of polygons with areas the nozzle is not allowed to enter.		list[float]	[]	yes	
machine_settings	machine_head_with_fans_polygon	The shape of the print head. These are coordinates relative to the position of the print head, which is usually the position of its first extruder. The dimensions left and in front of the print head must be negative coordinates.		list[float]	[[-150, 150], [150, 150], [150, -150], [-150, -150]]	yes	
machine_settings	gantry_height	The height difference between the tip of the nozzle and the gantry system (X and Y axes).		float	99999999999	yes	
machine_settings	machine_nozzle_id	The nozzle ID for an extruder train, such as "AA 0.4" and "BB 0.8".		str	unknown	no	for multi-head configurations
machine_settings	machine_nozzle_size	The inner diameter of the nozzle. Change this setting when using a non-standard nozzle size.	mm	float	25	yes	
machine_settings	machine_use_extruder_offset_to_offset_coords	Apply the extruder offset to the coordinate system. Affects all extruders.		bool	True	yes	

machine_settings	extruder_prime_pos_z	The Z coordinate of the position where the nozzle primes at the start of printing.	mm	float	0	possibly	priming not tested
machine_settings	extruder_prime_pos_abs	Make the extruder prime position absolute rather than relative to the last-known location of the head.		bool	False	possibly	
machine_settings	machine_max_feedrate_x	The maximum speed for the motor of the X-direction.	mm/s	float	2000	no	speed set in .src file (not taken from G-Code)
machine_settings	machine_max_feedrate_y	The maximum speed for the motor of the Y-direction.	mm/s	float	2000	no	speed set in .src file (not taken from G-Code)
machine_settings	machine_max_feedrate_z	The maximum speed for the motor of the Z-direction.	mm/s	float	2000	no	speed set in .src file (not taken from G-Code)
machine_settings	machine_max_feedrate_e	The maximum speed of the filament.	mm/s	float	2000	no	speed set in .src file (not taken from G-Code)
machine_settings	machine_max_acceleration_x	Maximum acceleration for the motor of the X-direction	mm/s²	float	9000	no	
machine_settings	machine_max_acceleration_y	Maximum acceleration for the motor of the Y-direction.	mm/s²	float	9000	no	
machine_settings	machine_max_acceleration_z	Maximum acceleration for the motor of the Z-direction.	mm/s²	float	100	no	
machine_settings	machine_max_acceleration_e	Maximum acceleration for the motor of the filament.	mm/s²	float	10000	no	
machine_settings	machine_acceleration	The default acceleration of print head movement.	mm/s²	float	4000	no	
machine_settings	machine_max_jerk_xy	Default jerk for movement in the horizontal plane.	mm/s	float	20	no	
machine_settings	machine_max_jerk_z	Default jerk for the motor of the Z-direction.	mm/s	float	20	no	
machine_settings	machine_max_jerk_e	Default jerk for the motor of the filament.	mm/s	float	5	no	
machine_settings	machine_steps_per_mm_x	How many steps of the stepper motor will result in one millimeter of movement in the X direction.		float	1	no	
machine_settings	machine_steps_per_mm_y	How many steps of the stepper motor will result in one millimeter of movement in the Y direction.		float	1	no	
machine_settings	machine_steps_per_mm_z	How many steps of the stepper motor will result in one millimeter of movement in the Z direction.		float	1	no	
machine_settings	machine_steps_per_mm_e	How many steps of the stepper motors will result in moving the feeder wheel by one millimeter around its circumference.		float	1	no	for calculation of steps in X3G format https://github.com/Ultimaker/Cura/issues/5756
machine_settings	machine_endstop_positive_direction_x	Whether the endstop of the X axis is in the positive direction (high X coordinate) or negative (low X coordinate).		bool	False	no	
machine_settings	machine_endstop_positive_direction_y	Whether the endstop of the Y axis is in the positive direction (high Y coordinate) or negative (low Y coordinate).		bool	False	no	
machine_settings	machine_endstop_positive_direction_z	Whether the endstop of the Z axis is in the positive direction (high Z coordinate) or negative (low Z coordinate).		bool	True	no	
machine_settings	machine_minimum_feedrate	The minimal movement speed of the print head.	mm/s	float	0	no	speed set in .src file (not taken from G-Code)
machine_settings	machine_feeder_wheel_diameter	The diameter of the wheel that drives the material in the feeder.	mm	float	10	no	
machine_settings	machine_scale_fan_speed_zero_to_one	Scale the fan speed to be between 0 and 1 instead of between 0 and 256.		bool	False	no	
resolution	layer_height	The height of each layer in mm. Higher values produce faster prints in lower resolution, lower values produce slower prints in higher resolution.	mm	float	15	yes	
resolution	layer_height_0	The height of the initial layer in mm. A thicker initial layer makes adhesion to the build plate easier.	mm	float	15	yes	

wall_line_width	wall_line_width_0	Width of the outermost wall line. By lowering this value, higher levels of detail can be printed.	mm	float	25	yes	
wall_line_width	wall_line_width_x	Width of a single wall line for all wall lines except the outermost one.	mm	float	25	yes	
line_width	skin_line_width	Width of a single top/bottom line.	mm	float	25	yes	
line_width	infill_line_width	Width of a single infill line.	mm	float	25	yes	
line_width	skirt_brim_line_width	Width of a single skirt or brim line.	mm	float	25	yes	
line_width	support_line_width	Width of a single support structure line.	mm	float	25	yes	
support_interface _line_width	support_roof_line_width	Width of a single support roof line.	mm	float	25	yes	
support_interface _line_width	support_bottom_line_width	Width of a single support floor line.	mm	float	25	yes	
line_width	prime_tower_line_width	Width of a single prime tower line.	mm	float	25	possibly	
resolution	initial_layer_line_width_factor	Multiplier of the line width on the first layer. Increasing this could improve bed adhesion.	%	float	100	fixed	
wall_extruder_nr	wall_0_extruder_nr	The extruder train used for printing the outer wall. This is used in multi-extrusion.		int	0	no	
wall_extruder_nr	wall_x_extruder_nr	The extruder train used for printing the inner walls. This is used in multi-extrusion.		int	0	no	
wall_thickness	wall_line_count	The number of walls. When calculated by the wall thickness, this value is rounded to a whole number.		int	2	yes	
shell	wall_transition_length	When transitioning between different numbers of walls as the part becomes thinner, a certain amount of space is allotted to split or join the wall lines.	mm	float	25	yes	
shell	wall_distribution_count	The number of walls, counted from the center, over which the variation needs to be spread. Lower values mean that the outer walls don't change in width.		int	1	yes	
shell	wall_transition_angle	When to create transitions between even and odd numbers of walls. A wedge shape with an angle greater than this setting will not have transitions and no walls will be printed in the center to fill the remaining space. Reducing this setting reduces the number and length of these center walls, but may leave gaps or overextrude.	°	float	10	yes	
shell	wall_transition_filter_distance	If it would be transitioning back and forth between different numbers of walls in quick succession, don't transition at all. Remove transitions if they are closer together than this distance.	mm	float	100	yes	
shell	wall_transition_filter_deviation	Prevent transitioning back and forth between one extra wall and one less. This margin extends the range of line widths which follow to [Minimum Wall Line Width - Margin, 2 * Minimum Wall Line Width + Margin]. Increasing this margin reduces the number of transitions, which reduces the number of extrusion starts/stops and travel time. However, large line width variation can lead to under- or overextrusion problems.	mm	float	0.1	yes	
shell	wall_0_wipe_dist	Distance of a travel move inserted after the outer wall, to hide the Z seam better.	mm	float	12.5	yes	

shell	wall_0_inset	Inset applied to the path of the outer wall. If the outer wall is smaller than the nozzle, and printed after the inner walls, use this offset to get the hole in the nozzle to overlap with the inner walls instead of the outside of the model.	mm	float	0	yes	
shell	optimize_wall_printing_order	Optimize the order in which walls are printed so as to reduce the number of retractions and the distance travelled. Most parts will benefit from this being enabled but some may actually take longer so please compare the print time estimates with and without optimization. First layer is not optimized when choosing brim as build plate adhesion type.		bool	True	yes	
shell	inset_direction	Determines the order in which walls are printed. Printing outer walls earlier helps with dimensional accuracy, as faults from inner walls cannot propagate to the outside. However printing them later allows them to stack better when overhangs are printed. When there is an uneven amount of total innner walls, the 'center last line' is always printed last.		key	outside_in	yes	
shell	alternate_extra_perimeter	Prints an extra wall at every other layer. This way infill gets caught between these extra walls, resulting in stronger prints.		bool	False	yes	
min_wall_line_width	min_even_wall_line_width	The minimum line width for normal polygonal walls. This setting determines at which model thickness we switch from printing a single thin wall line, to printing two wall lines. A higher Minimum Even Wall Line Width leads to a higher maximum odd wall line width. The maximum even wall line width is calculated as Outer Wall Line Width + 0.5 * Minimum Odd Wall Line Width.	mm	float	25	yes	
min_wall_line_width	min_odd_wall_line_width	The minimum line width for middle line gap filler polyline walls. This setting determines at which model thickness we switch from printing two wall lines, to printing two outer walls and a single central wall in the middle. A higher Minimum Odd Wall Line Width leads to a higher maximum even wall line width. The maximum odd wall line width is calculated as 2 * Minimum Even Wall Line Width.	mm	float	25	yes	
shell	fill_outline_gaps	Print pieces of the model which are horizontally thinner than the nozzle size.		bool	True	yes	
shell	min_feature_size	Minimum thickness of thin features. Model features that are thinner than this value will not be printed, while features thicker than the Minimum Feature Size will be widened to the Minimum Wall Line Width.	mm	float	15	yes	
shell	min_bead_width	Width of the wall that will replace thin features (according to the Minimum Feature Size) of the model. If the Minimum Wall Line Width is thinner than the thickness of the feature, the wall will become as thick as the feature itself.	mm	float	12.5	yes	
shell	xy_offset	Amount of offset applied to all polygons in each layer. Positive values can compensate for too big holes; negative values can compensate for too small holes.	mm	float	0	yes	

shell	xy_offset_layer_0	Amount of offset applied to all polygons in the first layer. A negative value can compensate for squishing of the first layer known as "elephant's foot".	mm	float	0	yes	
shell	hole_xy_offset	When greater than zero, the Hole Horizontal Expansion is the amount of offset applied to all holes in each layer. Positive values increase the size of the holes, negative values reduce the size of the holes. When this setting is enabled it can be further tuned with Hole Horizontal Expansion Max Diameter.	mm	float	0	yes	
shell	hole_xy_offset_max_diameter	When greater than zero, the Hole Horizontal Expansion is gradually applied on small holes (small holes are expanded more). When set to zero the Hole Horizontal Expansion will be applied to all holes. Holes larger than the Hole Horizontal Expansion Max Diameter are not expanded.	mm	float	0	yes	
shell	z_seam_type	Starting point of each path in a layer. When paths in consecutive layers start at the same point a vertical seam may show on the print. When aligning these near a user specified location, the seam is easiest to remove. When placed randomly the inaccuracies at the paths' start will be less noticeable. When taking the shortest path the print will be quicker.		key	sharpest_corner	yes	
shell	z_seam_on_vertex	Place the z-seam on a polygon vertex. Switching this off can place the seam between vertices as well. (Keep in mind that this won't override the restrictions on placing the seam on an unsupported overhang.)		bool	False	yes	
z_seam_position	z_seam_x	The X coordinate of the position near where to start printing each part in a layer.	mm	float	100	yes	
z_seam_position	z_seam_y	The Y coordinate of the position near where to start printing each part in a layer.	mm	float	100	yes	
shell	z_seam_corner	Control whether corners on the model outline influence the position of the seam. None means that corners have no influence on the seam position. Hide Seam makes the seam more likely to occur on an inside corner. Expose Seam makes the seam more likely to occur on an outside corner. Hide or Expose Seam makes the seam more likely to occur at an inside or outside corner. Smart Hiding allows both inside and outside corners, but chooses inside corners more frequently, if appropriate.		key	z_seam_corner_inner	yes	
shell	z_seam_relative	When enabled, the z seam coordinates are relative to each part's centre. When disabled, the coordinates define an absolute position on the build plate.		bool	False	yes	
top_bottom	roofing_extruder_nr	The extruder train used for printing the top most skin. This is used in multi-extrusion.		int	0	no	
roofing_layer_count	roofing_line_width	Width of a single line of the areas at the top of the print.	mm	float	25	yes	
roofing_layer_count	roofing_pattern	The pattern of the top most layers.		key	lines	yes	

roofing_layer_count	roofing_monotonic	Print top surface lines in an ordering that causes them to always overlap with adjacent lines in a single direction. This takes slightly more time to print, but makes flat surfaces look more consistent.		bool	True	yes	
roofing_layer_count	roofing_angles	A list of integer line directions to use when the top surface skin layers use the lines or zig zag pattern. Elements from the list are used sequentially as the layers progress and when the end of the list is reached, it starts at the beginning again. The list items are separated by commas and the whole list is contained in square brackets. Default is an empty list which means use the traditional default angles (45 and 135 degrees).		list[float]	[45, 135]	yes	
top_bottom	top_bottom_extruder_nr	The extruder train used for printing the top and bottom skin. This is used in multi-extrusion.		int	0	no	
top_thickness	top_layers	The number of top layers. When calculated by the top thickness, this value is rounded to a whole number.		int	3	yes	
bottom_thickness	bottom_layers	The number of bottom layers. When calculated by the bottom thickness, this value is rounded to a whole number.		int	3	yes	
bottom_thickness	initial_bottom_layers	The number of initial bottom layers, from the build-plate upwards. When calculated by the bottom thickness, this value is rounded to a whole number.		int	3	yes	
top_bottom	top_bottom_pattern	The pattern of the top/bottom layers.		str	lines	yes	
top_bottom	top_bottom_pattern_0	The pattern on the bottom of the print on the first layer.		str	lines	yes	
top_bottom	connect_skin_polygons	Connect top/bottom skin paths where they run next to each other. For the concentric pattern enabling this setting greatly reduces the travel time, but because the connections can happen midway over infill this feature can reduce the top surface quality.		bool	False	yes	
top_bottom	skin_monotonic	Print top/bottom lines in an ordering that causes them to always overlap with adjacent lines in a single direction. This takes slightly more time to print, but makes flat surfaces look more consistent.		bool	False	yes	
top_bottom	skin_angles	A list of integer line directions to use when the top/bottom layers use the lines or zig zag pattern. Elements from the list are used sequentially as the layers progress and when the end of the list is reached, it starts at the beginning again. The list items are separated by commas and the whole list is contained in square brackets. Default is an empty list which means use the traditional default angles (45 and 135 degrees).		list[float]	[ ]	yes	
top_bottom	small_skin_width	Small top/bottom regions are filled with walls instead of the default top/bottom pattern. This helps to avoids jerky motions. Off for the topmost (air-exposed) layer by default (see 'Small Top/Bottom On Surface').	mm	float	1	yes	

top_bottom	small_skin_on_surface	Enable small (up to 'Small Top/Bottom Width') regions on the topmost skinned layer (exposed to air) to be filled with walls instead of the default pattern.		bool	False	yes	
top_bottom	skin_no_small_gaps_heuristic	When the model has small vertical gaps of only a few layers, there should normally be skin around those layers in the narrow space. Enable this setting to not generate skin if the vertical gap is very small. This improves printing time and slicing time, but technically leaves infill exposed to the air.		bool	False	yes	
top_bottom	skin_outline_count	Replaces the outermost part of the top/bottom pattern with a number of concentric lines. Using one or two lines improves roofs that start on infill material.		int	1	yes	
top_bottom	ironing_enabled	Go over the top surface one additional time, but this time extruding very little material. This is meant to melt the plastic on top further, creating a smoother surface. The pressure in the nozzle chamber is kept high so that the creases in the surface are filled with material.		bool	False	fixed	due to no possibility to determine the ironing layer for flow calculation
top_bottom	ironing_only_highest_layer	Only perform ironing on the very last layer of the mesh. This saves time if the lower layers don't need a smooth surface finish.		bool	True	no	
top_bottom	ironing_pattern	The pattern to use for ironing top surfaces.		key	zigzag	no	
top_bottom	ironing_monotonic	Print ironing lines in an ordering that causes them to always overlap with adjacent lines in a single direction. This takes slightly more time to print, but makes flat surfaces look more consistent.		bool	False	no	
top_bottom	ironing_line_spacing	The distance between the lines of ironing.	mm	float	7.5	no	
top_bottom	ironing_flow	The amount of material, relative to a normal skin line, to extrude during ironing. Keeping the nozzle filled helps filling some of the crevices of the top surface, but too much results in overextrusion and blips on the side of the surface.	%	float	10	no	
top_bottom	ironing_inset	A distance to keep from the edges of the model. Ironing all the way to the edge of the mesh may result in a jagged edge on your print.	mm	float	12.5	no	
top_bottom	speed_ironing	The speed at which to pass over the top surface.	mm/s	float	200	no	
top_bottom	acceleration_ironing	The acceleration with which ironing is performed.	mm/s²	float	3000	no	
top_bottom	jerk_ironing	The maximum instantaneous velocity change while performing ironing.	mm/s	float	20	no	
skin_overlap	skin_overlap_mm	Adjust the amount of overlap between the walls and (the endpoints of) the skin-centerlines. A slight overlap allows the walls to connect firmly to the skin. Note that, given an equal skin and wall line-width, any value over half the width of the wall may already cause any skin to go past the wall, because at that point the position of the nozzle of the skin-extruder may already reach past the middle of the wall.	mm	float	1	yes	

skin_preshrink	top_skin_preshrink	The largest width of top skin areas which are to be removed. Every skin area smaller than this value will disappear. This can help in limiting the amount of time and material spent on printing top skin at slanted surfaces in the model.	mm	float	1	yes	
skin_preshrink	bottom_skin_preshrink	The largest width of bottom skin areas which are to be removed. Every skin area smaller than this value will disappear. This can help in limiting the amount of time and material spent on printing bottom skin at slanted surfaces in the model.	mm	float	1	yes	
expand_skins_expand_distance	top_skin_expand_distance	The distance the top skins are expanded into the infill. Higher values makes the skin attach better to the infill pattern and makes the walls on the layer above adhere better to the skin. Lower values save amount of material used.	mm	float	1	yes	
expand_skins_ expand_distance	bottom_skin_expand_distance	The distance the bottom skins are expanded into the infill. Higher values makes the skin attach better to the infill pattern and makes the skin adhere better to the walls on the layer below. Lower values save amount of material used.	mm	float	1	yes	
max_skin_angle _for_expansion	min_skin_width_for_expansion	Skin areas narrower than this are not expanded. This avoids expanding the narrow skin areas that are created when the model surface has a slope close to the vertical.	mm	float	0	yes	
infill	infill_extruder_nr	The extruder train used for printing infill. This is used in multi-extrusion.		int	0	no	
infill_sparse_density	infill_line_distance	Distance between the printed infill lines. This setting is calculated by the infill density and the infill line width.	mm	float	2	yes	
infill	infill_pattern	The pattern of the infill material of the print. The line and zig zag infill swap direction on alternate layers, reducing material cost. The grid, triangle, tri-hexagon, cubic, octet, quarter cubic, cross and concentric patterns are fully printed every layer. Gyroid, cubic, quarter cubic and octet infill change with every layer to provide a more equal distribution of strength over each direction. Lightning infill tries to minimize the infill, by only supporting the ceiling of the object.		key	grid	yes	
infill	zig_zaggify_infill	Connect the ends where the infill pattern meets the inner wall using a line which follows the shape of the inner wall. Enabling this setting can make the infill adhere to the walls better and reduce the effects of infill on the quality of vertical surfaces. Disabling this setting reduces the amount of material used.		bool	False	yes	
infill	connect_infill_polygons	Connect infill paths where they run next to each other. For infill patterns which consist of several closed polygons, enabling this setting greatly reduces the travel time.		bool	True	yes	

infill	infill_angles	A list of integer line directions to use. Elements from the list are used sequentially as the layers progress and when the end of the list is reached, it starts at the beginning again. The list items are separated by commas and the whole list is contained in square brackets. Default is an empty list which means use the traditional default angles (45 and 135 degrees for the lines and zig zag patterns and 45 degrees for all other patterns).		list[float]	[ ]	yes	
infill	infill_offset_x	The infill pattern is moved this distance along the X axis.	mm	float	0	yes	
infill	infill_offset_y	The infill pattern is moved this distance along the Y axis.	mm	float	0	yes	
infill	infill_randomize_start_location	Randomize which infill line is printed first. This prevents one segment becoming the strongest, but it does so at the cost of an additional travel move.		bool	False	yes	
infill	infill_multiplier	Convert each infill line to this many lines. The extra lines do not cross over each other, but avoid each other. This makes the infill stiffer, but increases print time and material usage.		int	1	yes	
infill	infill_wall_line_count	Add extra walls around the infill area. Such walls can make top/bottom skin lines sag down less which means you need less top/bottom skin layers for the same quality at the cost of some extra material. This feature can combine with the Connect Infill Polygons to connect all the infill into a single extrusion path without the need for travels or retractions if configured right.		int	0	yes	
infill	sub_div_rad_add	An addition to the radius from the center of each cube to check for the boundary of the model, as to decide whether this cube should be subdivided. Larger values lead to a thicker shell of small cubes near the boundary of the model.	mm	float	25	possibly	
infill_overlap	infill_overlap_mm	The amount of overlap between the infill and the walls. A slight overlap allows the walls to connect firmly to the infill.	mm	float	2.5	yes	
infill	infill_wipe_dist	Distance of a travel move inserted after every infill line, to make the infill stick to the walls better. This option is similar to infill overlap, but without extrusion and only on one end of the infill line.	mm	float	2.5	yes	
infill	infill_sparse_thickness	The thickness per layer of infill material. This value should always be a multiple of the layer height and is otherwise rounded.	mm	float	15	yes	
infill	gradual_infill_steps	Number of times to reduce the infill density by half when getting further below top surfaces. Areas which are closer to top surfaces get a higher density, up to the Infill Density.		int	0	yes	
infill	gradual_infill_step_height	The height of infill of a given density before switching to half the density.	mm	float	1.5	yes	

infill	infill_before_walls	Print the infill before printing the walls. Printing the walls first may lead to more accurate walls, but overhangs print worse. Printing the infill first leads to sturdier walls, but the infill pattern might sometimes show through the surface.		bool	True	yes	
infill	min_infill_area	Don't generate areas of infill smaller than this (use skin instead).	mm²	float	0	yes	
infill	infill_support_enabled	Print infill structures only where tops of the model should be supported. Enabling this reduces print time and material usage, but leads to ununiform object strength.		bool	False	yes	
infill	infill_support_angle	The minimum angle of internal overhangs for which infill is added. At a value of 0° objects are totally filled with infill, 90° will not provide any infill.	°	float	40	yes	
skin_edge_ support_thickness	skin_edge_support_layers	The number of infill layers that supports skin edges.		int	4	yes	
lightning_infill_ support_angle	lightning_infill_overhang_angle	Determines when a lightning infill layer has to support the model above it. Measured in the angle given the thickness.	°	float	40	yes	
lightning_infill_ support_angle	lightning_infill_prune_angle	The endpoints of infill lines are shortened to save on material. This setting is the angle of overhang of the endpoints of these lines.	°	float	40	yes	
lightning_infill_ support_angle	lightning_infill_straightening_angle	The infill lines are straightened out to save on printing time. This is the maximum angle of overhang allowed across the length of the infill line.	°	float	40	yes	
material	default_material_print_temperature	The default temperature used for printing. This should be the "base" temperature of a material. All other print temperatures should use offsets based on this value	°C	float	20	no	
material	build_volume_temperature	The temperature of the environment to print in. If this is 0, the build volume temperature will not be adjusted.	°C	float	0	no	
material	material_print_temperature	The temperature used for printing.	°C	float	20	no	
material	material_print_temperature_layer_0	The temperature used for printing the first layer.	°C	float	20	no	
material	material_initial_print_temperature	The minimal temperature while heating up to the Printing Temperature at which printing can already start.	°C	float	20	no	
material	material_final_print_temperature	The temperature to which to already start cooling down just before the end of printing.	°C	float	20	no	
material	material_extrusion_cool_down_speed	The extra speed by which the nozzle cools while extruding. The same value is used to signify the heat up speed lost when heating up while extruding.	°C/s	float	1	no	
material	default_material_bed_temperature	The default temperature used for the heated build plate. This should be the "base" temperature of a build plate. All other print temperatures should use offsets based on this value	°C	float	20	no	
material	material_bed_temperature	The temperature used for the heated build plate. If this is 0, the build plate is left unheated.	°C	float	20	no	
material	material_bed_temperature_layer_0	The temperature used for the heated build plate at the first layer. If this is 0, the build plate is left unheated during the first layer.	°C	float	20	no	
material	material_adhesion_tendency	Surface adhesion tendency.		int	10	no	

material	material_surface_energy	Surface energy.	%	int	100	no	
material_shrinkage_percentage	material_shrinkage_percentage_xy	To compensate for the shrinkage of the material as it cools down, the model will be scaled with this factor in the XY-direction (horizontally).	%	float	100	yes	
material_shrinkage_percentage	material_shrinkage_percentage_z	To compensate for the shrinkage of the material as it cools down, the model will be scaled with this factor in the Z-direction (vertically).	%	float	100	yes	
material	material_crystallinity	Is this material the type that breaks off cleanly when heated (crystalline), or is it the type that produces long intertwined polymer chains (non-crystalline)?		bool	False	no	
material	material_anti_ooze_retracted_position	How far the material needs to be retracted before it stops oozing.	mm	float	0	no	
material	material_anti_ooze_retraction_speed	How fast the material needs to be retracted during a filament switch to prevent oozing.	mm/s	float	250	no	
material	material_break_preparation_retracted_position	How far the filament can be stretched before it breaks, while heated.	mm	float	0	no	
material	material_break_preparation_speed	How fast the filament needs to be retracted just before breaking it off in a retraction.	mm/s	float	250	no	
material	material_break_preparation_temperature	The temperature used to purge material, should be roughly equal to the highest possible printing temperature.	°C	float	20	no	
material	material_break_retracted_position	How far to retract the filament in order to break it cleanly.	mm	float	0	no	
material	material_break_speed	The speed at which to retract the filament in order to break it cleanly.	mm/s	float	250	no	
material	material_break_temperature	The temperature at which the filament is broken for a clean break.	°C	float	20	no	
material	material_flush_purge_speed	How fast to prime the material after switching to a different material.		float	50	no	
material	material_flush_purge_length	How much material to use to purge the previous material out of the nozzle (in length of filament) when switching to a different material.		float	100	no	
material	material_end_of_filament_purge_speed	How fast to prime the material after replacing an empty spool with a fresh spool of the same material.		float	50	no	
material	material_end_of_filament_purge_length	How much material to use to purge the previous material out of the nozzle (in length of filament) when replacing an empty spool with a fresh spool of the same material.		float	100	no	
material	material_maximum_park_duration	How long the material can be kept out of dry storage safely.		float	300	no	
material	material_no_load_move_factor	A factor indicating how much the filament gets compressed between the feeder and the nozzle chamber, used to determine how far to move the material for a filament switch.		float	0.940860215	no	
wall_material_flow	wall_0_material_flow	Flow compensation on the outermost wall line.	%	float	100	yes	setup.json [Pump.linetype_flow ("wall_outer")]
wall_material_flow	wall_x_material_flow	Flow compensation on wall lines for all wall lines except the outermost one.	%	float	100	yes	setup.json [Pump.linetype_flow ("wall_inner")]
wall_material_flow	wall_0_material_flow_roofing	Flow compensation on the top surface outermost wall line.	%	float	100	no	setup.json [Pump.linetype_flow ("wall_outer")]
wall_material_flow	wall_x_material_flow_roofing	Flow compensation on top surface wall lines for all wall lines except the outermost one.	%	float	100	no	setup.json [Pump.linetype_flow ("wall_inner")]
material_flow	skin_material_flow	Flow compensation on top/bottom lines.	%	float	100	partially	setup.json [Pump.linetype_flow ("surface")]
material_flow	roofing_material_flow	Flow compensation on lines of the areas at the top of the print.	%	float	100	partially	setup.json [Pump.linetype_flow ("surface")]

material_flow	infill_material_flow	Flow compensation on infill lines.	%	float	100	yes	setup.json [Pump.linetype_flow ("infill")]
material_flow	skirt_brim_material_flow	Flow compensation on skirt or brim lines.	%	float	100	yes	setup.json [Pump.linetype_flow ("curb")]
material_flow	support_material_flow	Flow compensation on support structure lines.	%	float	100	yes	setup.json [Pump.linetype_flow ("support")]
support_interface _material_flow	support_roof_material_flow	Flow compensation on support roof lines.	%	float	100	no	setup.json [Pump.linetype_flow ("support")]
support_interface _material_flow	support_bottom_material_flow	Flow compensation on support floor lines.	%	float	100	no	setup.json [Pump.linetype_flow ("support")]
material_flow	prime_tower_flow	Flow compensation on prime tower lines.	%	float	100	no	Multi-material not supported
material	material_flow_layer_0	Flow compensation for the first layer: the amount of material extruded on the initial layer is multiplied by this value.	%	float	100	fixed	
material	wall_x_material_flow_layer_0	Flow compensation on wall lines for all wall lines except the outermost one, but only for the first layer	%	float	100	no	setup.json [Pump.linetype_flow ("wall_outer")]
material	wall_0_material_flow_layer_0	Flow compensation on the outermost wall line of the first layer.	%	float	100	no	setup.json [Pump.linetype_flow ("wall_inner")]
material	skin_material_flow_layer_0	Flow compensation on bottom lines of the first layer	%	float	100	no	setup.json [Pump.linetype_flow ("surface")]
material	material_standby_temperature	The temperature of the nozzle when another nozzle is currently used for printing.	°C	float	20	no	
material	material_is_support_material	Is this material typically used as a support material during printing.		bool	False	no	
speed_print	speed_infill	The speed at which infill is printed.	mm/s	float	60	no	
speed_wall	speed_wall_0	The speed at which the outermost walls are printed. Printing the outer wall at a lower speed improves the final skin quality. However, having a large difference between the inner wall speed and the outer wall speed will affect quality in a negative way.	mm/s	float	30	no	
speed_wall	speed_wall_x	The speed at which all inner walls are printed. Printing the inner wall faster than the outer wall will reduce printing time. It works well to set this in between the outer wall speed and the infill speed.	mm/s	float	60	no	
speed_wall	speed_wall_0_roofing	The speed at which the top surface outermost wall is printed.	mm/s	float	30	no	
speed_wall	speed_wall_x_roofing	The speed at which the top surface inner walls are printed.	mm/s	float	60	no	
speed_print	speed_roofing	The speed at which top surface skin layers are printed.	mm/s	float	25	no	
speed_print	speed_topbottom	The speed at which top/bottom layers are printed.	mm/s	float	30	no	
speed_support	speed_support_infill	The speed at which the infill of support is printed. Printing the infill at lower speeds improves stability.	mm/s	float	60	no	
speed_support_ interface	speed_support_roof	The speed at which the roofs of support are printed. Printing them at lower speeds can improve overhang quality.	mm/s	float	40	no	
speed_support_ interface	speed_support_bottom	The speed at which the floor of support is printed. Printing it at lower speed can improve adhesion of support on top of your model.	mm/s	float	40	no	
speed_print	speed_prime_tower	The speed at which the prime tower is printed. Printing the prime tower slower can make it more stable when the adhesion between the different filaments is suboptimal.	mm/s	float	60	no	
speed	speed_travel	The speed at which travel moves are made.	mm/s	float	120	no	

speed_layer_0	speed_print_layer_0	The speed of printing for the initial layer. A lower value is advised to improve adhesion to the build plate.	mm/s	float	30	no	
speed_layer_0	speed_travel_layer_0	The speed of travel moves in the initial layer. A lower value is advised to prevent pulling previously printed parts away from the build plate. The value of this setting can automatically be calculated from the ratio between the Travel Speed and the Print Speed.	mm/s	float	60	no	
speed	skirt_brim_speed	The speed at which the skirt and brim are printed. Normally this is done at the initial layer speed, but sometimes you might want to print the skirt or brim at a different speed.	mm/s	float	30	no	
speed	speed_z_hop	The speed at which the vertical Z movement is made for Z Hops. This is typically lower than the print speed since the build plate or machine's gantry is harder to move.	mm/s	float	10	no	
speed	speed_slowdown_layers	The first few layers are printed slower than the rest of the model, to get better adhesion to the build plate and improve the overall success rate of prints. The speed is gradually increased over these layers.		int	2	no	
speed	speed_equalize_flow_width_factor	Extrusion width based correction factor on the speed. At 0% the movement speed is kept constant at the Print Speed. At 100% the movement speed is adjusted so that the flow (in mm^3/s) is kept constant, i.e. lines half the normal Line Width are printed twice as fast and lines twice as wide are printed half as fast. A value larger than 100% can help to compensate for the higher pressure required to extrude wide lines.	%	float	100	no	
speed	acceleration_enabled	Enables adjusting the print head acceleration. Increasing the accelerations can reduce printing time at the cost of print quality.		bool	False	no	
speed	acceleration_travel_enabled	Use a separate acceleration rate for travel moves. If disabled, travel moves will use the acceleration value of the printed line at their destination.		bool	True	no	
acceleration_print	acceleration_infill	The acceleration with which infill is printed.	mm/s^2	float	3000	no	
acceleration_wall	acceleration_wall_0	The acceleration with which the outermost walls are printed.	mm/s^2	float	3000	no	
acceleration_wall	acceleration_wall_x	The acceleration with which all inner walls are printed.	mm/s^2	float	3000	no	
acceleration_wall	acceleration_wall_0_roofing	The acceleration with which the top surface outermost walls are printed.	mm/s^2	float	3000	no	
acceleration_wall	acceleration_wall_x_roofing	The acceleration with which the top surface inner walls are printed.	mm/s^2	float	3000	no	
acceleration_print	acceleration_roofing	The acceleration with which top surface skin layers are printed.	mm/s^2	float	3000	no	
acceleration_print	acceleration_topbottom	The acceleration with which top/bottom layers are printed.	mm/s^2	float	3000	no	
acceleration_support	acceleration_support_infill	The acceleration with which the infill of support is printed.	mm/s^2	float	3000	no	
acceleration_support _interface	acceleration_support_roof	The acceleration with which the roofs of support are printed. Printing them at lower acceleration can improve overhang quality.	mm/s^2	float	3000	no	

acceleration_support _interface	acceleration_support_bottom	The acceleration with which the floors of support are printed. Printing them at lower acceleration can improve adhesion of support on top of your model.	mm/s^2	float	3000	no	
acceleration_print	acceleration_prime_tower	The acceleration with which the prime tower is printed.	mm/s^2	float	3000	no	
speed	acceleration_travel	The acceleration with which travel moves are made.	mm/s^2	float	5000	no	
acceleration_layer_0	acceleration_print_layer_0	The acceleration during the printing of the initial layer.	mm/s^2	float	3000	no	
acceleration_layer_0	acceleration_travel_layer_0	The acceleration for travel moves in the initial layer.	mm/s^2	float	3000	no	
speed	acceleration_skirt_brim	The acceleration with which the skirt and brim are printed. Normally this is done with the initial layer acceleration, but sometimes you might want to print the skirt or brim at a different acceleration.	mm/s^2	float	3000	no	
speed	jerk_enabled	Enables adjusting the jerk of print head when the velocity in the X or Y axis changes. Increasing the jerk can reduce printing time at the cost of print quality.		bool	False	no	
speed	jerk_travel_enabled	Use a separate jerk rate for travel moves. If disabled, travel moves will use the jerk value of the printed line at their destination.		bool	True	no	
jerk_print	jerk_infill	The maximum instantaneous velocity change with which infill is printed.	mm/s	float	20	no	
jerk_wall	jerk_wall_0	The maximum instantaneous velocity change with which the outermost walls are printed.	mm/s	float	20	no	
jerk_wall	jerk_wall_x	The maximum instantaneous velocity change with which all inner walls are printed.	mm/s	float	20	no	
jerk_wall	jerk_wall_0_roofing	The maximum instantaneous velocity change with which the top surface outermost walls are printed.	mm/s	float	20	no	
jerk_wall	jerk_wall_x_roofing	The maximum instantaneous velocity change with which the top surface inner walls are printed.	mm/s	float	20	no	
jerk_print	jerk_roofing	The maximum instantaneous velocity change with which top surface skin layers are printed.	mm/s	float	20	no	
jerk_print	jerk_topbottom	The maximum instantaneous velocity change with which top/bottom layers are printed.	mm/s	float	20	no	
jerk_support	jerk_support_infill	The maximum instantaneous velocity change with which the infill of support is printed.	mm/s	float	20	no	
jerk_support_ interface	jerk_support_roof	The maximum instantaneous velocity change with which the roofs of support are printed.	mm/s	float	20	no	
jerk_support_ interface	jerk_support_bottom	The maximum instantaneous velocity change with which the floors of support are printed.	mm/s	float	20	no	
jerk_print	jerk_prime_tower	The maximum instantaneous velocity change with which the prime tower is printed.	mm/s	float	20	no	
speed	jerk_travel	The maximum instantaneous velocity change with which travel moves are made.	mm/s	float	30	no	
jerk_layer_0	jerk_print_layer_0	The maximum instantaneous velocity change during the printing of the initial layer.	mm/s	float	20	no	
jerk_layer_0	jerk_travel_layer_0	The acceleration for travel moves in the initial layer.	mm/s	float	20	no	
speed	jerk_skirt_brim	The maximum instantaneous velocity change with which the skirt and brim are printed.	mm/s	float	20	no	
travel	retraction_enable	Retract the filament when the nozzle is moving over a non-printed area.		bool	True	yes	

travel	retract_at_layer_change	Retract the filament when the nozzle is moving to the next layer.		bool	False	yes	
travel	retraction_amount	The length of material retracted during a retraction move.	mm	float	100	yes	
retraction_speed	retraction_retract_speed	The speed at which the filament is retracted during a retraction move.	mm/s	float	25	no	
retraction_speed	retraction_prime_speed	The speed at which the filament is primed during a retraction move.	mm/s	float	25	no	
travel	retraction_extra_prime_amount	Some material can ooze away during a travel move, which can be compensated for here.	mm^3	float	0	no	
travel	retraction_min_travel	The minimum distance of travel needed for a retraction to happen at all. This helps to get fewer retractions in a small area.	mm	float	50	yes	
travel	retraction_count_max	This setting limits the number of retractions occurring within the minimum extrusion distance window. Further retractions within this window will be ignored. This avoids retracting repeatedly on the same piece of filament, as that can flatten the filament and cause grinding issues.		int	5	yes	
travel	retraction_extrusion_window	The window in which the maximum retraction count is enforced. This value should be approximately the same as the retraction distance, so that effectively the number of times a retraction passes the same patch of material is limited.	mm	float	50	yes	
travel	retraction_combing	Combing keeps the nozzle within already printed areas when traveling. This results in slightly longer travel moves but reduces the need for retractions. If combing is off, the material will retract and the nozzle moves in a straight line to the next point. It is also possible to avoid combing over top/bottom skin areas or to only comb within the infill.		key	all	yes	
travel	retraction_combing_max_distance	When greater than zero, combing travel moves that are longer than this distance will use retraction. If set to zero, there is no maximum and combing moves will not use retraction.	mm	float	0	yes	
travel	travel_retract_before_outer_wall	Always retract when moving to start an outer wall.		bool	False	yes	
travel	travel_avoid_other_parts	The nozzle avoids already printed parts when traveling. This option is only available when combing is enabled.		bool	True	yes	
travel	travel_avoid_supports	The nozzle avoids already printed supports when traveling. This option is only available when combing is enabled.		bool	False	yes	
travel	travel_avoid_distance	The distance between the nozzle and already printed parts when avoiding during travel moves.	mm	float	5	yes	
travel	layer_start_x	The X coordinate of the position near where to find the part to start printing each layer.	mm	float	0	yes	
travel	layer_start_y	The Y coordinate of the position near where to find the part to start printing each layer.	mm	float	0	yes	
travel	retraction_hop_enabled	Whenever a retraction is done, the build plate is lowered to create clearance between the nozzle and the print. It prevents the nozzle from hitting the print during travel moves, reducing the chance to knock the print from the build plate.		bool	False	fixed	due to layer height calculation a z-hop can not be enabled

travel	retraction_hop_only_when_collides	Only perform a Z Hop when moving over printed parts which cannot be avoided by horizontal motion by Avoid Printed Parts when Traveling.		bool	False	no	
travel	retraction_hop	The height difference when performing a Z Hop.	mm	float	1	no	
travel	retraction_hop_after_extruder_switch	After the machine switched from one extruder to the other, the build plate is lowered to create clearance between the nozzle and the print. This prevents the nozzle from leaving oozed material on the outside of a print.		bool	True	no	
travel	retraction_hop_after_extruder_switch_height	The height difference when performing a Z Hop after extruder switch.	mm	float	1	no	
cooling	cool_fan_enabled	Enables the print cooling fans while printing. The fans improve print quality on layers with short layer times and bridging / overhangs.		bool	True	no	
cool_fan_speed	cool_fan_speed_min	The speed at which the fans spin before hitting the threshold. When a layer prints faster than the threshold, the fan speed gradually inclines towards the maximum fan speed.	%	float	100	no	
cool_fan_speed	cool_fan_speed_max	The speed at which the fans spin on the minimum layer time. The fan speed gradually increases between the regular fan speed and maximum fan speed when the threshold is hit.	%	float	100	no	
cooling	cool_min_layer_time_fan_speed_max	The layer time which sets the threshold between regular fan speed and maximum fan speed. Layers that print slower than this time use regular fan speed. For faster layers the fan speed gradually increases towards the maximum fan speed.	s	float	10	no	
cooling	cool_fan_speed_0	The speed at which the fans spin at the start of the print. In subsequent layers the fan speed is gradually increased up to the layer corresponding to Regular Fan Speed at Height.	%	float	0	no	
cool_fan_full_at_height	cool_fan_full_layer	The layer at which the fans spin on regular fan speed. If regular fan speed at height is set, this value is calculated and rounded to a whole number.		int	2	no	
cooling	cool_min_layer_time	The minimum time spent in a layer. This forces the printer to slow down, to at least spend the time set here in one layer. This allows the printed material to cool down properly before printing the next layer. Layers may still take shorter than the minimal layer time if Lift Head is disabled and if the Minimum Speed would otherwise be violated.	s	float	5	no	
cooling	cool_min_speed	The minimum print speed, despite slowing down due to the minimum layer time. When the printer would slow down too much, the pressure in the nozzle would be too low and result in bad print quality.	mm/s	float	10	no	
cooling	cool_lift_head	When the minimum speed is hit because of minimum layer time, lift the head away from the print and wait the extra time until the minimum layer time is reached.		bool	False	no	
cooling	cool_min_temperature	Gradually reduce to this temperature when printing at reduced speeds because of minimum layer time.	°C	float	0	no	

cooling	cool_during_extruder_switch	<html>Whether to activate the cooling fans during a nozzle switch. This can help reducing oozing by cooling the nozzle faster: - Unchanged: keep the fans as they were previously - Only last extruder: turn on the fan of the last used extruder, but turn the others off (if any). This is useful if you have completely separate extruders. - All fans: turn on all fans during nozzle switch. This is useful if you have a single cooling fan, or multiple fans that stay close to each other. </html>		key	unchanged	no	
support	support_enable	Generate structures to support parts of the model which have overhangs. Without these structures, such parts would collapse during printing.		bool	False	possibly	
support_extruder_nr	support_infill_extruder_nr	The extruder train to use for printing the infill of the support. This is used in multi-extrusion.		int	0	no	
support_extruder_nr	support_extruder_nr_layer_0	The extruder train to use for printing the first layer of support infill. This is used in multi-extrusion.		int	0	no	
support_interface_extruder_nr	support_roof_extruder_nr	The extruder train to use for printing the roofs of the support. This is used in multi-extrusion.		int	0	no	
support_interface_extruder_nr	support_bottom_extruder_nr	The extruder train to use for printing the floors of the support. This is used in multi-extrusion.		int	0	no	
support	support_structure	Chooses between the techniques available to generate support. "Normal" support creates a support structure directly below the overhanging parts and drops those areas straight down. "Tree" support creates branches towards the overhanging areas that support the model on the tips of those branches, and allows the branches to crawl around the model to support it from the build plate as much as possible.		key	normal	possibly	
support	support_tree_angle	The maximum angle of the branches while they grow around the model. Use a lower angle to make them more vertical and more stable. Use a higher angle to be able to have more reach.	°	float	60	possibly	
support	support_tree_branch_diameter	The diameter of the thinnest branches of tree support. Thicker branches are more sturdy. Branches towards the base will be thicker than this.	mm	float	5	possibly	
support	support_tree_max_diameter	The diameter of the widest branches of tree support. A thicker trunk is more sturdy; a thinner trunk takes up less space on the build plate.	mm	float	25	possibly	
support	support_tree_branch_diameter_angle	The angle of the branches' diameter as they gradually become thicker towards the bottom. An angle of 0 will cause the branches to have uniform thickness over their length. A bit of an angle can increase stability of the tree support.	°	float	7	possibly	
support_z_seam_away_from_model	support_z_seam_min_distance	The distance between the model and its support structure at the z-axis seam.	mm	float	50	possibly	
support	support_type	Adjusts the placement of the support structures. The placement can be set to touching build plate or everywhere. When set to everywhere the support structures will also be printed on the model.		key	everywhere	possibly	

support	support_tree_angle_slow	The preferred angle of the branches, when they do not have to avoid the model. Use a lower angle to make them more vertical and more stable. Use a higher angle for branches to merge faster.	°	float	50	possibly	
support	support_tree_max_diameter_increase_by_merges_when_support_to_model	The most the diameter of a branch that has to connect to the model may increase by merging with branches that could reach the buildplate. Increasing this reduces print time, but increases the area of support that rests on model	mm	float	1	possibly	
support	support_tree_min_height_to_model	How tall a branch has to be if it is placed on the model. Prevents small blobs of support. This setting is ignored when a branch is supporting a support roof.	mm	float	50	possibly	
support	support_tree_bp_diameter	Diameter every branch tries to achieve when reaching the buildplate. Improves bed adhesion.	mm	float	50	possibly	
support	support_tree_top_rate	Adjusts the density of the support structure used to generate the tips of the branches. A higher value results in better overhangs, but the supports are harder to remove. Use Support Roof for very high values or ensure support density is similarly high at the top.	%	float	15	possibly	
support	support_tree_tip_diameter	The diameter of the top of the tip of the branches of tree support.	mm	float	25	possibly	
support	support_tree_limit_branch_reach	Limit how far each branch should travel from the point it supports. This can make the support more sturdy, but will increase the amount of branches (and because of that material usage/print time)		bool	True	possibly	
support	support_tree_branch_reach_limit	A recomendation to how far branches can move from the points they support. Branches can violate this value to reach their destination (buildplate or a flat part of the model). Lowering this value will make the support more sturdy, but increase the amount of branches (and because of that material usage/print time)	mm	float	30	possibly	
support	support_tree_rest_preference	The preferred placement of the support structures. If structures can't be placed at the preferred location, they will be place elsewhere, even if that means placing them on the model.		key	buildplate	possibly	
support	support_angle	The minimum angle of overhangs for which support is added. At a value of 0° all overhangs are supported, 90° will not provide any support.	°	float	50	possibly	
support	support_pattern	The pattern of the support structures of the print. The different options available result in sturdy or easy to remove support.		key	zigzag	possibly	
support	support_wall_count	The number of walls with which to surround support infill. Adding a wall can make support print more reliably and can support overhangs better, but increases print time and material used.		int	1	possibly	
support_interface_wall_count	support_roof_wall_count	The number of walls with which to surround support interface roof. Adding a wall can make support print more reliably and can support overhangs better, but increases print time and material used.		int	0	possibly	

support_interface_wall_count	support_bottom_wall_count	The number of walls with which to surround support interface floor. Adding a wall can make support print more reliably and can support overhangs better, but increases print time and material used.		int	0	possibly	
support	zig_zaggify_support	Connect the ends of the support lines together. Enabling this setting can make your support more sturdy and reduce underextrusion, but it will cost more material.		bool	False	possibly	
support	support_connect_zigzags	Connect the ZigZags. This will increase the strength of the zig zag support structure.		bool	True	possibly	
support_infill_rate	support_line_distance	Distance between the printed support structure lines. This setting is calculated by the support density.	mm	float	25	possibly	
support_infill_rate	support_initial_layer_line_distance	Distance between the printed initial layer support structure lines. This setting is calculated by the support density.	mm	float	25	possibly	
support	support_infill_density_multiplier_initial_layer	Multiplier for the infill on the initial layers of the support. Increasing this may help for bed adhesion.		int	1	possibly	
support	support_infill_angles	A list of integer line directions to use. Elements from the list are used sequentially as the layers progress and when the end of the list is reached, it starts at the beginning again. The list items are separated by commas and the whole list is contained in square brackets. Default is an empty list which means use the default angle 0 degrees.		list[int]	[ ]	possibly	
support	support_brim_enable	Generate a brim within the support infill regions of the first layer. This brim is printed underneath the support, not around it. Enabling this setting increases the adhesion of support to the build plate.		bool	True	possibly	
support_brim_width	support_brim_line_count	The number of lines used for the support brim. More brim lines enhance adhesion to the build plate, at the cost of some extra material.		int	3	possibly	
support_z_distance	support_top_distance	Distance from the top of the support to the print.	mm	float	5	possibly	
support_z_distance	support_bottom_distance	Distance from the print to the bottom of the support. Note that this is rounded up to the next layer height.	mm	float	5	possibly	
support	support_xy_distance	Distance of the support structure from the print in the X/Y directions.	mm	float	40	possibly	
support	support_xy_overrides_z	Whether the Support X/Y Distance overrides the Support Z Distance or vice versa. When X/Y overrides Z the X/Y distance can push away the support from the model, influencing the actual Z distance to the overhang. We can disable this by not applying the X/Y distance around overhangs.		key	z_overrides_xy	possibly	
support	support_xy_distance_overhang	Distance of the support structure from the overhang in the X/Y directions.	mm	float	12.5	possibly	
support	support_bottom_stair_step_height	The height of the steps of the stair-like bottom of support resting on the model. A low value makes the support harder to remove, but too high values can lead to unstable support structures. Set to zero to turn off the stair-like behaviour.	mm	float	0	possibly	

support	support_bottom_stair_step_width	The maximum width of the steps of the stair-like bottom of support resting on the model. A low value makes the support harder to remove, but too high values can lead to unstable support structures.	mm	float	5	possibly	
support	support_bottom_stair_step_min_slope	The minimum slope of the area for stair-stepping to take effect. Low values should make support easier to remove on shallower slopes, but really low values may result in some very counter-intuitive results on other parts of the model.	°	float	10	possibly	
support	support_join_distance	The maximum distance between support structures in the X/Y directions. When separate structures are closer together than this value, the structures merge into one.	mm	float	2	possibly	
support	support_offset	Amount of offset applied to all support polygons in each layer. Positive values can smooth out the support areas and result in more sturdy support.	mm	float	50	possibly	
support	support_infill_sparse_thickness	The thickness per layer of support infill material. This value should always be a multiple of the layer height and is otherwise rounded.	mm	float	15	possibly	
support	gradual_support_infill_steps	Number of times to reduce the support infill density by half when getting further below top surfaces. Areas which are closer to top surfaces get a higher density, up to the Support Infill Density.		int	0	possibly	
support	gradual_support_infill_step_height	The height of support infill of a given density before switching to half the density.	mm	float	1	possibly	
support	minimum_support_area	Minimum area size for support polygons. Polygons which have an area smaller than this value will not be generated.	mm²	float	0	possibly	
support_interface_ enable	support_roof_enable	Generate a dense slab of material between the top of support and the model. This will create a skin between the model and support.		bool	False	possibly	
support_interface_ enable	support_bottom_enable	Generate a dense slab of material between the bottom of the support and the model. This will create a skin between the model and support.		bool	False	possibly	
support_interface_ height	support_roof_height	The thickness of the support roofs. This controls the amount of dense layers at the top of the support on which the model rests.	mm	float	1	possibly	
support_interface_ height	support_bottom_height	The thickness of the support floors. This controls the number of dense layers that are printed on top of places of a model on which support rests.	mm	float	1	possibly	
support_roof_ density	support_roof_line_distance	Distance between the printed support roof lines. This setting is calculated by the Support Roof Density, but can be adjusted separately.	mm	float	25	possibly	
support_bottom_ density	support_bottom_line_distance	Distance between the printed support floor lines. This setting is calculated by the Support Floor Density, but can be adjusted separately.	mm	float	25	possibly	
support_interface_ pattern	support_roof_pattern	The pattern with which the roofs of the support are printed.		key	concentric	possibly	
support_interface_ pattern	support_bottom_pattern	The pattern with which the floors of the support are printed.		key	concentric	possibly	
minimum_interface_ area	minimum_roof_area	Minimum area size for the roofs of the support. Polygons which have an area smaller than this value will be printed as normal support.	mm²	float	1	possibly	

minimum_interface_ area	minimum_bottom_area	Minimum area size for the floors of the support. Polygons which have an area smaller than this value will be printed as normal support.	mm^2	float	1	possibly	
support_interface_ offset	support_roof_offset	Amount of offset applied to the roofs of the support.	mm	float	0	possibly	
support_interface_ offset	support_bottom_offset	Amount of offset applied to the floors of the support.	mm	float	0	possibly	
support	support_interface_priority	How support interface and support will interact when they overlap. Currently only implemented for support roof.		key	interface_area_ overwrite_support_area	possibly	
support_interface_ angles	support_roof_angles	A list of integer line directions to use. Elements from the list are used sequentially as the layers progress and when the end of the list is reached, it starts at the beginning again. The list items are separated by commas and the whole list is contained in square brackets. Default is an empty list which means use the default angles (alternates between 45 and 135 degrees if interfaces are quite thick or 90 degrees).		list[int]	[ ]	possibly	
support_interface_ angles	support_bottom_angles	A list of integer line directions to use. Elements from the list are used sequentially as the layers progress and when the end of the list is reached, it starts at the beginning again. The list items are separated by commas and the whole list is contained in square brackets. Default is an empty list which means use the default angles (alternates between 45 and 135 degrees if interfaces are quite thick or 90 degrees).		list[int]	[ ]	possibly	
support	support_fan_enable	When enabled, the print cooling fan speed is altered for the skin regions immediately above the support.		bool	False	no	
support	support_supported_skin_fan_speed	Percentage fan speed to use when printing the skin regions immediately above the support. Using a high fan speed can make the support easier to remove.	%	float	100	no	
support	support_use_towers	Use specialized towers to support tiny overhang areas. These towers have a larger diameter than the region they support. Near the overhang the towers' diameter decreases, forming a roof.		bool	True	possibly	
support	support_tower_diameter	The diameter of a special tower.	mm	float	3	possibly	
support	support_tower_maximum_supported_diameter	Maximum diameter in the X/Y directions of a small area which is to be supported by a specialized support tower.	mm	float	3	possibly	
support	support_tower_roof_angle	The angle of a rooftop of a tower. A higher value results in pointed tower roofs, a lower value results in flattened tower roofs.	°	int	65	possibly	
support	support_mesh_drop_down	Make support everywhere below the support mesh, so that there's no overhang in the support mesh.		bool	True	possibly	
support	support_meshes_present	There are support meshes present in the scene. This setting is controlled by Cura.		bool	False	possibly	
platform_adhesion	prime_blob_enable	Whether to prime the filament with a blob before printing. Turning this setting on will ensure that the extruder will have material ready at the nozzle before printing. Printing Brim or Skirt can act like priming too, in which case turning this setting off saves some time.		bool	False	possibly	

platform_adhesion	extruder_prime_pos_x	The X coordinate of the position where the nozzle primes at the start of printing.	mm	float	0	possibly	
platform_adhesion	extruder_prime_pos_y	The Y coordinate of the position where the nozzle primes at the start of printing.	mm	float	0	possibly	
platform_adhesion	adhesion_type	Different options that help to improve both priming your extrusion and adhesion to the build plate. Brim adds a single layer flat area around the base of your model to prevent warping. Raft adds a thick grid with a roof below the model. Skirt is a line printed around the model, but not connected to the model.		key	none	partially	none, skirt, brim tested raft not tested and adjusted
adhesion_extruder_nr	skirt_brim_extruder_nr	The extruder train to use for printing the skirt or brim. This is used in multi-extrusion.		int	0	no	
adhesion_extruder_nr	raft_base_extruder_nr	The extruder train to use for printing the first layer of the raft. This is used in multi-extrusion.		int	0	no	
adhesion_extruder_nr	raft_interface_extruder_nr	The extruder train to use for printing the middle layer of the raft. This is used in multi-extrusion.		int	0	no	
adhesion_extruder_nr	raft_surface_extruder_nr	The extruder train to use for printing the top layer(s) of the raft. This is used in multi-extrusion.		int	0	no	
platform_adhesion	skirt_line_count	Multiple skirt lines help to prime your extrusion better for small models. Setting this to 0 will disable the skirt.		int	5	yes	
platform_adhesion	skirt_height	Printing the innermost skirt line with multiple layers makes it easy to remove the skirt.		int	1	yes	
platform_adhesion	skirt_gap	The horizontal distance between the skirt and the first layer of the print. This is the minimum distance. Multiple skirt lines will extend outwards from this distance.	mm	float	20	yes	
platform_adhesion	skirt_brim_minimal_length	The minimum length of the skirt or brim. If this length is not reached by all skirt or brim lines together, more skirt or brim lines will be added until the minimum length is reached. Note: If the line count is set to 0 this is ignored.	mm	float	250	yes	
brim_width	brim_line_count	The number of lines used for a brim. More brim lines enhance adhesion to the build plate, but also reduces the effective print area.		int	10	yes	
platform_adhesion	brim_gap	The horizontal distance between the first brim line and the outline of the first layer of the print. A small gap can make the brim easier to remove while still providing the thermal benefits.	mm	float	5	yes	
platform_adhesion	brim_replaces_support	Enforce brim to be printed around the model even if that space would otherwise be occupied by support. This replaces some regions of the first layer of support by brim regions.		bool	True	yes	
platform_adhesion	brim_location	Print a brim on the outside of the model, inside, or both. Depending on the model, this helps reducing the amount of brim you need to remove afterwards, while ensuring a proper bed adhesion.		key	outside	yes	
platform_adhesion	brim_inside_margin	A brim around a model may touch an other model where you don't want it. This removes all brim within this distance from brimless models.	mm	float	75	yes	
platform_adhesion	brim_smart_ordering	Swap print order of the innermost and second innermost brim lines. This improves brim removal.		bool	True	yes	

raft_margin	raft_base_margin	If the raft base is enabled, this is the extra raft area around the model which is also given a raft. Increasing this margin will create a stronger raft while using more material and leaving less area for your print.	mm	float	15	possibly	
raft_margin	raft_interface_margin	If the raft middle is enabled, this is the extra raft area around the model which is also given a raft. Increasing this margin will create a stronger raft while using more material and leaving less area for your print.	mm	float	15	possibly	
raft_margin	raft_surface_margin	If the raft top is enabled, this is the extra raft area around the model which is also given a raft. Increasing this margin will create a stronger raft while using more material and leaving less area for your print.	mm	float	15	possibly	
raft_remove_ inside_corners	raft_base_remove_inside_corners	Remove inside corners from the raft base, causing the raft to become convex.		bool	False	possibly	
raft_remove_ inside_corners	raft_interface_remove_inside_corners	Remove inside corners from the raft middle part, causing the raft to become convex.		bool	False	possibly	
raft_remove_ inside_corners	raft_surface_remove_inside_corners	Remove inside corners from the raft top part, causing the raft to become convex.		bool	False	possibly	
raft_smoothing	raft_base_smoothing	This setting controls how much inner corners in the raft base outline are rounded. Inward corners are rounded to a semi circle with a radius equal to the value given here. This setting also removes holes in the raft outline which are smaller than such a circle.	mm	float	5	possibly	
raft_smoothing	raft_interface_smoothing	This setting controls how much inner corners in the raft middle outline are rounded. Inward corners are rounded to a semi circle with a radius equal to the value given here. This setting also removes holes in the raft outline which are smaller than such a circle.	mm	float	5	possibly	
raft_smoothing	raft_surface_smoothing	This setting controls how much inner corners in the raft top outline are rounded. Inward corners are rounded to a semi circle with a radius equal to the value given here. This setting also removes holes in the raft outline which are smaller than such a circle.	mm	float	5	possibly	
platform_adhesion	raft_airgap	The gap between the final raft layer and the first layer of the model. Only the first layer is raised by this amount to lower the bonding between the raft layer and the model. Makes it easier to peel off the raft.	mm	float	0	possibly	
platform_adhesion	layer_0_z_overlap	Make the first and second layer of the model overlap in the Z direction to compensate for the filament lost in the airgap. All models above the first model layer will be shifted down by this amount. It may be noted that sometimes the second layer is printed below initial layer because of this setting. This is intended behavior	mm	float	0	fixed	due to layer height calculation layer shift in z direction is not possible
platform_adhesion	raft_base_thickness	Layer thickness of the base raft layer. This should be a thick layer which sticks firmly to the printer build plate.	mm	float	18	possibly	

platform_adhesion	raft_base_line_width	Width of the lines in the base raft layer. These should be thick lines to assist in build plate adhesion.	mm	float	25	possibly	
platform_adhesion	raft_base_line_spacing	The distance between the raft lines for the base raft layer. Wide spacing makes for easy removal of the raft from the build plate.	mm	float	50	possibly	
raft_base_ infill_overlap	raft_base_infill_overlap_mm	The amount of overlap between the infill and the walls of the raft base. A slight overlap allows the walls to connect firmly to the infill.	mm	float	0	possibly	
platform_adhesion	raft_interface_layers	The number of layers between the base and the surface of the raft. These comprise the main thickness of the raft. Increasing this creates a thicker, sturdier raft.		int	1	possibly	
platform_adhesion	raft_interface_thickness	Layer thickness of the middle raft layer.	mm	float	15	possibly	
platform_adhesion	raft_interface_line_width	Width of the lines in the middle raft layer. Making the second layer extrude more causes the lines to stick to the build plate.	mm	float	30	possibly	
platform_adhesion	raft_interface_line_spacing	The distance between the raft lines for the middle raft layer. The spacing of the middle should be quite wide, while being dense enough to support the top raft layers.	mm	float	50	possibly	
platform_adhesion	raft_interface_z_offset	When printing the first layer of the raft interface, translate by this offset to customize the adhesion between base and interface. A negative offset should improve the adhesion.	mm	float	0	possibly	
raft_interface_ infill_overlap	raft_interface_infill_overlap_mm	The amount of overlap between the infill and the walls of the raft interface. A slight overlap allows the walls to connect firmly to the infill.	mm	float	0	possibly	
platform_adhesion	raft_surface_layers	The number of top layers on top of the 2nd raft layer. These are fully filled layers that the model sits on. 2 layers result in a smoother top surface than 1.		int	2	possibly	
platform_adhesion	raft_surface_thickness	Layer thickness of the top raft layers.	mm	float	15	possibly	
platform_adhesion	raft_surface_line_width	Width of the lines in the top surface of the raft. These can be thin lines so that the top of the raft becomes smooth.	mm	float	25	possibly	
platform_adhesion	raft_surface_line_spacing	The distance between the raft lines for the top raft layers. The spacing should be equal to the line width, so that the surface is solid.	mm	float	25	possibly	
platform_adhesion	raft_surface_z_offset	When printing the first layer of the raft surface, translate by this offset to customize the adhesion between interface and surface. A negative offset should improve the adhesion.	mm	float	0	possibly	
platform_adhesion	raft_surface_monotonic	Print raft top surface lines in an ordering that causes them to always overlap with adjacent lines in a single direction. This takes slightly more time to print, but makes the surface look more consistent, which is also visible on the model bottom surface.		bool	False	possibly	
raft_surface_ infill_overlap	raft_surface_infill_overlap_mm	The amount of overlap between the infill and the walls of the raft surface. A slight overlap allows the walls to connect firmly to the infill.	mm	float	0	possibly	
raft_wall_count	raft_base_wall_count	The number of contours to print around the linear pattern in the base layer of the raft.		int	1	possibly	
raft_wall_count	raft_interface_wall_count	The number of contours to print around the linear pattern in the middle layers of the raft.		int	0	possibly	

raft_wall_count	raft_surface_wall_count	The number of contours to print around the linear pattern in the top layers of the raft.		int	0	possibly	
raft_speed	raft_base_speed	The speed at which the base raft layer is printed. This should be printed quite slowly, as the volume of material coming out of the nozzle is quite high.	mm/s	float	15	no	
raft_speed	raft_interface_speed	The speed at which the middle raft layer is printed. This should be printed quite slowly, as the volume of material coming out of the nozzle is quite high.	mm/s	float	15	no	
raft_speed	raft_surface_speed	The speed at which the top raft layers are printed. These should be printed a bit slower, so that the nozzle can slowly smooth out adjacent surface lines.	mm/s	float	20	no	
raft_acceleration	raft_base_acceleration	The acceleration with which the base raft layer is printed.	mm/s²	float	3000	no	
raft_acceleration	raft_interface_acceleration	The acceleration with which the middle raft layer is printed.	mm/s²	float	3000	no	
raft_acceleration	raft_surface_acceleration	The acceleration with which the top raft layers are printed.	mm/s²	float	3000	no	
raft_jerk	raft_base_jerk	The jerk with which the base raft layer is printed.	mm/s	float	20	no	
raft_jerk	raft_interface_jerk	The jerk with which the middle raft layer is printed.	mm/s	float	20	no	
raft_jerk	raft_surface_jerk	The jerk with which the top raft layers are printed.	mm/s	float	20	no	
raft_fan_speed	raft_base_fan_speed	The fan speed for the base raft layer.	%	float	0	no	
raft_fan_speed	raft_interface_fan_speed	The fan speed for the middle raft layer.	%	float	0	no	
raft_fan_speed	raft_surface_fan_speed	The fan speed for the top raft layers.	%	float	0	no	
raft_flow	raft_base_flow	The amount of material, relative to a normal extrusion line, to extrude during raft base printing. Having an increased flow may improve adhesion and raft structural strength.	%	float	100	yes	setup.json [Pump.linetype_flow ("support")]
raft_flow	raft_interface_flow	The amount of material, relative to a normal extrusion line, to extrude during raft interface printing. Having an increased flow may improve adhesion and raft structural strength.	%	float	100	no	set by raft_base_flow
raft_flow	raft_surface_flow	The amount of material, relative to a normal extrusion line, to extrude during raft surface printing. Having an increased flow may improve adhesion and raft structural strength.	%	float	100	no	set by raft_base_flow
dual	prime_tower_enable	Print a tower next to the print which serves to prime the material after each nozzle switch.		bool	False	no	
dual	prime_tower_mode	<html>How to generate the prime tower: - Normal: create a bucket in which secondary materials are primed - Interleaved: create a prime tower as sparse as possible. This will save time and filament, but is only possible if the used materials adhere to each other </html>		key	normal	no	
dual	prime_tower_size	The width of the prime tower.	mm	float	20	no	
dual	prime_tower_min_volume	The minimum volume for each layer of the prime tower in order to purge enough material.	mm³	float	6	no	
dual	prime_tower_max_bridging_distance	The maximum length of the branches which may be printed over the air.	mm	float	5	no	

dual	prime_tower_min_shell_thickness	The minimum thickness of the prime tower shell. You may increase it to make the prime tower stronger.	mm	float	25	no	
dual	prime_tower_position_x	The x coordinate of the position of the prime tower.	mm	float	200	no	
dual	prime_tower_position_y	The y coordinate of the position of the prime tower.	mm	float	200	no	
dual	prime_tower_wipe_enabled	After printing the prime tower with one nozzle, wipe the oozed material from the other nozzle off on the prime tower.		bool	True	no	
dual	prime_tower_brim_enable	By enabling this setting, your prime-tower will get a brim, even if the model doesn't. If you want a sturdier base for a high tower, you can increase the base height.		bool	False	no	
dual	prime_tower_base_size	The width of the prime tower brim/base. A larger base enhances adhesion to the build plate, but also reduces the effective print area.	mm	float	50	no	
dual	prime_tower_base_height	The height of the prime tower base. Increasing this value will result in a more sturdy prime tower because the base will be wider. If this setting is too low, the prime tower will not have a sturdy base.	mm	float	0	no	
dual	prime_tower_base_curve_magnitude	The magnitude factor used for the slope of the prime tower base. If you increase this value, the base will become slimmer. If you decrease it, the base will become thicker.		float	4	no	
dual	prime_tower_raft_base_line_spacing	The distance between the raft lines for the unique prime tower raft layer. Wide spacing makes for easy removal of the raft from the build plate.	mm	float	50	no	
dual	ooze_shield_enabled	Enable exterior ooze shield. This will create a shell around the model which is likely to wipe a second nozzle if it's at the same height as the first nozzle.		bool	False	possibly	
dual	ooze_shield_angle	The maximum angle a part in the ooze shield will have. With 0 degrees being vertical, and 90 degrees being horizontal. A smaller angle leads to less failed ooze shields, but more material.	°	float	60	possibly	
dual	ooze_shield_dist	Distance of the ooze shield from the print, in the X/Y directions.	mm	float	2	possibly	
dual	switch_extruder_retraction_amount	The amount of retraction when switching extruders. Set to 0 for no retraction at all. This should generally be the same as the length of the heat zone.	mm	float	20	no	
switch_extruder_ retraction_speeds	switch_extruder_retraction_speed	The speed at which the filament is retracted during a nozzle switch retract.	mm/s	float	20	no	
switch_extruder_ retraction_speeds	switch_extruder_prime_speed	The speed at which the filament is pushed back after a nozzle switch retraction.	mm/s	float	20	no	
dual	switch_extruder_extra_prime_amount	Extra material to prime after nozzle switching.	mm^3	float	0	no	
meshfix	meshfix_union_all	Ignore the internal geometry arising from overlapping volumes within a mesh and print the volumes as one. This may cause unintended internal cavities to disappear.		bool	True	yes	
meshfix	meshfix_union_all_remove_holes	Remove the holes in each layer and keep only the outside shape. This will ignore any invisible internal geometry. However, it also ignores layer holes which can be viewed from above or below.		bool	False	yes	

meshfix	meshfix_extensive_stitching	Extensive stitching tries to stitch up open holes in the mesh by closing the hole with touching polygons. This option can introduce a lot of processing time.		bool	False	yes	
meshfix	meshfix_keep_open_polygons	Normally Cura tries to stitch up small holes in the mesh and remove parts of a layer with big holes. Enabling this option keeps those parts which cannot be stitched. This option should be used as a last resort option when everything else fails to produce proper g-code.		bool	False	yes	
meshfix	multiple_mesh_overlap	Make meshes which are touching each other overlap a bit. This makes them bond together better.	mm	float	0.5	yes	
meshfix	carve_multiple_volumes	Remove areas where multiple meshes are overlapping with each other. This may be used if merged dual material objects overlap with each other.		bool	True	yes	
meshfix	alternate_carve_order	Switch to which mesh intersecting volumes will belong with every layer, so that the overlapping meshes become interwoven. Turning this setting off will cause one of the meshes to obtain all of the volume in the overlap, while it is removed from the other meshes.		bool	True	yes	
meshfix	remove_empty_first_layers	Remove empty layers beneath the first printed layer if they are present. Disabling this setting can cause empty first layers if the Slicing Tolerance setting is set to Exclusive or Middle.		bool	True	yes	
meshfix	meshfix_maximum_resolution	The minimum size of a line segment after slicing. If you increase this, the mesh will have a lower resolution. This may allow the printer to keep up with the speed it has to process g-code and will increase slice speed by removing details of the mesh that it can't process anyway.	mm	float	0.5	yes	
meshfix	meshfix_maximum_travel_resolution	The minimum size of a travel line segment after slicing. If you increase this, the travel moves will have less smooth corners. This may allow the printer to keep up with the speed it has to process g-code, but it may cause model avoidance to become less accurate.	mm	float	1	yes	
meshfix	meshfix_maximum_deviation	The maximum deviation allowed when reducing the resolution for the Maximum Resolution setting. If you increase this, the print will be less accurate, but the g-code will be smaller. Maximum Deviation is a limit for Maximum Resolution, so if the two conflict the Maximum Deviation will always be held true.	mm	float	0.025	yes	
meshfix	meshfix_maximum_extrusion_area_deviation	The maximum extrusion area deviation allowed when removing intermediate points from a straight line. An intermediate point may serve as width-changing point in a long straight line. Therefore, if it is removed, it will cause the line to have a uniform width and, as a result, lose (or gain) a bit of extrusion area. If you increase this you may notice slight under- (or over-) extrusion in between straight parallel walls, as more intermediate width-changing points will be allowed to be removed. Your print will be less accurate, but the g-code will be smaller.	μm²	float	50000	yes	

meshfix	meshfix_fluid_motion_enabled	When enabled tool paths are corrected for printers with smooth motion planners. Small movements that deviate from the general tool path direction are smoothed to improve fluid motions.		bool	True	yes	
meshfix	meshfix_fluid_motion_shift_distance	Distance points are shifted to smooth the path	mm	float	0.1	yes	
meshfix	meshfix_fluid_motion_small_distance	Distance points are shifted to smooth the path	mm	float	0.01	yes	
meshfix	meshfix_fluid_motion_angle	If a toolpath-segment deviates more than this angle from the general motion it is smoothed.	°	float	15	yes	
blackmagic	print_sequence	Whether to print all models one layer at a time or to wait for one model to finish, before moving on to the next. One at a time mode is possible if a) only one extruder is enabled and b) all models are separated in such a way that the whole print head can move in between and all models are lower than the distance between the nozzle and the X/Y axes.		key	all_at_once	yes	
blackmagic	user_defined_print_order_enabled	Allows you to order the object list to manually set the print sequence. First object from the list will be printed first.		bool	False	yes	
blackmagic	infill_mesh	Use this mesh to modify the infill of other meshes with which it overlaps. Replaces infill regions of other meshes with regions for this mesh. It's suggested to only print one Wall and no Top/Bottom Skin for this mesh.		bool	False	yes	
blackmagic	infill_mesh_order	Determines the priority of this mesh when considering multiple overlapping infill meshes. Areas where multiple infill meshes overlap will take on the settings of the mesh with the highest rank. An infill mesh with a higher rank will modify the infill of infill meshes with lower rank and normal meshes.		int	0	yes	
blackmagic	cutting_mesh	Limit the volume of this mesh to within other meshes. You can use this to make certain areas of one mesh print with different settings and with a whole different extruder.		bool	False	yes	
blackmagic	mold_enabled	Print models as a mold, which can be cast in order to get a model which resembles the models on the build plate.		bool	False	possibly	
blackmagic	mold_width	The minimal distance between the outside of the mold and the outside of the model.	mm	float	5	possibly	
blackmagic	mold_roof_height	The height above horizontal parts in your model which to print mold.	mm	float	0.5	possibly	
blackmagic	mold_angle	The angle of overhang of the outer walls created for the mold. 0° will make the outer shell of the mold vertical, while 90° will make the outside of the model follow the contour of the model.	°	float	40	possibly	
blackmagic	support_mesh	Use this mesh to specify support areas. This can be used to generate support structure.		bool	False	possibly	
blackmagic	anti_overhang_mesh	Use this mesh to specify where no part of the model should be detected as overhang. This can be used to remove unwanted support structure.		bool	False	possibly	

blackmagic	magic_mesh_surface_mode	Treat the model as a surface only, a volume, or volumes with loose surfaces. The normal print mode only prints enclosed volumes. "Surface" prints a single wall tracing the mesh surface with no infill and no top/bottom skin. "Both" prints enclosed volumes like normal and any remaining polygons as surfaces.		key	normal	yes	
blackmagic	magic_spiralize	Spiralize smooths out the Z move of the outer edge. This will create a steady Z increase over the whole print. This feature turns a solid model into a single walled print with a solid bottom. This feature should only be enabled when each layer only contains a single part.		bool	False	yes	
blackmagic	smooth_spiralized_contours	Smooth the spiralized contours to reduce the visibility of the Z seam (the Z seam should be barely visible on the print but will still be visible in the layer view). Note that smoothing will tend to blur fine surface details.		bool	True	yes	
blackmagic	relative_extrusion	Use relative extrusion rather than absolute extrusion. Using relative E-steps makes for easier post-processing of the g-code. However, it's not supported by all printers and it may produce very slight deviations in the amount of deposited material compared to absolute E-steps. Irrespective of this setting, the extrusion mode will always be set to absolute before any g-code script is output.		bool	False	yes	
experimental	slicing_tolerance	Vertical tolerance in the sliced layers. The contours of a layer are normally generated by taking cross sections through the middle of each layer's thickness (Middle). Alternatively each layer can have the areas which fall inside of the volume throughout the entire thickness of the layer (Exclusive) or a layer has the areas which fall inside anywhere within the layer (Inclusive). Inclusive retains the most details, Exclusive makes for the best fit and Middle stays closest to the original surface.		key	middle	yes	
experimental	infill_enable_travel_optimization	When enabled, the order in which the infill lines are printed is optimized to reduce the distance travelled. The reduction in travel time achieved very much depends on the model being sliced, infill pattern, density, etc. Note that, for some models that have many small areas of infill, the time to slice the model may be greatly increased.		bool	False	yes	
experimental	material_flow_temp_graph	Data linking material flow (in mm3 per second) to temperature (degrees Celsius).	[[mm^3,°C]]	str	[[3.5, 200],[7.0, 240]]	no	
experimental	minimum_polygon_circumference	Polygons in sliced layers that have a circumference smaller than this amount will be filtered out. Lower values lead to higher resolution mesh at the cost of slicing time. It is meant mostly for high resolution SLA printers and very tiny 3D models with a lot of details.	mm	float	1	yes	

experimental	interlocking_enable	At the locations where models touch, generate an interlocking beam structure. This improves the adhesion between models, especially models printed in different materials.		bool	False	possibly	
experimental	interlocking_beam_width	The width of the interlocking structure beams.	mm	float	0.8	possibly	
experimental	interlocking_orientation	The height of the beams of the interlocking structure, measured in number of layers. Less layers is stronger, but more prone to defects.	°	float	22.5	possibly	
experimental	interlocking_beam_layer_count	The height of the beams of the interlocking structure, measured in number of layers. Less layers is stronger, but more prone to defects.		int	2	possibly	
experimental	interlocking_depth	The distance from the boundary between models to generate interlocking structure, measured in cells. Too few cells will result in poor adhesion.		int	2	possibly	
experimental	interlocking_boundary_avoidance	The distance from the outside of a model where interlocking structures will not be generated, measured in cells.		int	2	possibly	
experimental	support_skip_some_zags	Skip some support line connections to make the support structure easier to break away. This setting is applicable to the Zig Zag support infill pattern.		bool	False	yes	
support_skip_ zag_per_mm	support_zag_skip_count	Skip one in every N connection lines to make the support structure easier to break away.		int	5	yes	
experimental	draft_shield_enabled	This will create a wall around the model, which traps (hot) air and shields against exterior airflow. Especially useful for materials which warp easily.		bool	False	yes	
experimental	draft_shield_dist	Distance of the draft shield from the print, in the X/Y directions.	mm	float	10	yes	
experimental	draft_shield_height_limitation	Set the height of the draft shield. Choose to print the draft shield at the full height of the model or at a limited height.		key	full	yes	
experimental	draft_shield_height	Height limitation of the draft shield. Above this height no draft shield will be printed.	mm	float	10	yes	
experimental	conical_overhang_enabled	Change the geometry of the printed model such that minimal support is required. Steep overhangs will become shallow overhangs. Overhanging areas will drop down to become more vertical.		bool	False	yes	
experimental	conical_overhang_angle	The maximum angle of overhangs after the they have been made printable. At a value of 0° all overhangs are replaced by a piece of model connected to the build plate, 90° will not change the model in any way.	°	float	50	yes	
experimental	conical_overhang_hole_size	The maximum area of a hole in the base of the model before it's removed by Make Overhang Printable. Holes smaller than this will be retained. A value of 0 mm^2 will fill all holes in the models base.	mm^2	float	0	yes	
experimental	coasting_enable	Coasting replaces the last part of an extrusion path with a travel path. The oozed material is used to print the last piece of the extrusion path in order to reduce stringing.		bool	False	possibly	
experimental	coasting_volume	The volume otherwise oozed. This value should generally be close to the nozzle diameter cubed.	mm^3	float	15625	possibly	

experimental	coasting_min_volume	The smallest volume an extrusion path should have before allowing coasting. For smaller extrusion paths, less pressure has been built up in the bowden tube and so the coasted volume is scaled linearly. This value should always be larger than the Coasting Volume.	mm³	float	625	possibly	
experimental	coasting_speed	The speed by which to move during coasting, relative to the speed of the extrusion path. A value slightly under 100% is advised, since during the coasting move the pressure in the bowden tube drops.	%	float	90	no	
experimental	cross_infill_pocket_size	The size of pockets at four-way crossings in the cross 3D pattern at heights where the pattern is touching itself.	mm	float	2	yes	
experimental	cross_infill_density_image	The file location of an image of which the brightness values determine the minimal density at the corresponding location in the infill of the print.		str		possibly	
experimental	cross_support_density_image	The file location of an image of which the brightness values determine the minimal density at the corresponding location in the support.		str		possibly	
experimental	support_conical_enabled	Make support areas smaller at the bottom than at the overhang.		bool	False	yes	
experimental	support_conical_angle	The angle of the tilt of conical support. With 0 degrees being vertical, and 90 degrees being horizontal. Smaller angles cause the support to be more sturdy, but consist of more material. Negative angles cause the base of the support to be wider than the top.	°	float	30	yes	
experimental	support_conical_min_width	Minimum width to which the base of the conical support area is reduced. Small widths can lead to unstable support structures.	mm	float	5	yes	
experimental	magic_fuzzy_skin_enabled	Randomly jitter while printing the outer wall, so that the surface has a rough and fuzzy look.		bool	False	possibly	
experimental	magic_fuzzy_skin_outside_only	Jitter only the parts' outlines and not the parts' holes.		bool	False	possibly	
experimental	magic_fuzzy_skin_thickness	The width within which to jitter. It's advised to keep this below the outer wall width, since the inner walls are unaltered.	mm	float	5	possibly	
magic_fuzzy_skin _point_density	magic_fuzzy_skin_point_dist	The average distance between the random points introduced on each line segment. Note that the original points of the polygon are discarded, so a high smoothness results in a reduction of the resolution. This value must be higher than half the Fuzzy Skin Thickness.	mm	float	10	possibly	
experimental	flow_rate_max_extrusion_offset	The maximum distance in mm to move the filament to compensate for changes in flow rate.	mm	float	0	no	
experimental	flow_rate_extrusion_offset_factor	How far to move the filament in order to compensate for changes in flow rate, as a percentage of how far the filament would move in one second of extrusion.	%	float	100	no	
experimental	adaptive_layer_height_enabled	Adaptive layers computes the layer heights depending on the shape of the model.		bool	False	possibly	adaptive layer height not tested
experimental	adaptive_layer_height_variation	The maximum allowed height different from the base layer height.	mm	float	10	possibly	

experimental	adaptive_layer_height_variation_step	The difference in height of the next layer height compared to the previous one.	mm	float	1	possibly	
experimental	adaptive_layer_height_threshold	Target horizontal distance between two adjacent layers. Reducing this setting causes thinner layers to be used to bring the edges of the layers closer together.	mm	float	12.5	possibly	
experimental	wall_overhang_angle	Walls that overhang more than this angle will be printed using overhanging wall settings. When the value is 90, no walls will be treated as overhanging. Overhang that gets supported by support will not be treated as overhang either.	°	float	90	yes	
experimental	seam_overhang_angle	Try to prevent seams on walls that overhang more than this angle. When the value is 90, no walls will be treated as overhanging.	°	float	90	yes	
experimental	wall_overhang_speed_factor	Overhanging walls will be printed at this percentage of their normal print speed.	%	float	100	yes	
experimental	bridge_settings_enabled	Detect bridges and modify print speed, flow and fan settings while bridges are printed.		bool	False	yes	
experimental	bridge_wall_min_length	Unsupported walls shorter than this will be printed using the normal wall settings. Longer unsupported walls will be printed using the bridge wall settings.	mm	float	5	yes	
experimental	bridge_skin_support_threshold	If a skin region is supported for less than this percentage of its area, print it using the bridge settings. Otherwise it is printed using the normal skin settings.	%	float	50	yes	
experimental	bridge_sparse_infill_max_density	Maximum density of infill considered to be sparse. Skin over sparse infill is considered to be unsupported and so may be treated as a bridge skin.	%	float	0	yes	
experimental	bridge_wall_coast	This controls the distance the extruder should coast immediately before a bridge wall begins. Coasting before the bridge starts can reduce the pressure in the nozzle and may produce a flatter bridge.	%	float	100	yes	
experimental	bridge_wall_speed	The speed at which the bridge walls are printed.	mm/s	float	15	no	
experimental	bridge_wall_material_flow	When printing bridge walls, the amount of material extruded is multiplied by this value.	%	float	50	yes	setup.json [Pump.linetype_flow ("bridge")]
experimental	bridge_skin_speed	The speed at which bridge skin regions are printed.	mm/s	float	15	no	
experimental	bridge_skin_material_flow	When printing bridge skin regions, the amount of material extruded is multiplied by this value.	%	float	60	yes	setup.json [Pump.linetype_flow ("bridge")]
experimental	bridge_skin_density	The density of the bridge skin layer. Values less than 100 will increase the gaps between the skin lines.	%	float	100	yes	
experimental	bridge_fan_speed	Percentage fan speed to use when printing bridge walls and skin.	%	float	100	no	
experimental	bridge_enable_more_layers	If enabled, the second and third layers above the air are printed using the following settings. Otherwise, those layers are printed using the normal settings.		bool	True	no	
experimental	bridge_skin_speed_2	Print speed to use when printing the second bridge skin layer.	mm/s	float	25	no	
experimental	bridge_skin_material_flow_2	When printing the second bridge skin layer, the amount of material extruded is multiplied by this value.	%	float	100	no	

experimental	bridge_skin_density_2	The density of the second bridge skin layer. Values less than 100 will increase the gaps between the skin lines.	%	float	75	no	
experimental	bridge_fan_speed_2	Percentage fan speed to use when printing the second bridge skin layer.	%	float	0	no	
experimental	bridge_skin_speed_3	Print speed to use when printing the third bridge skin layer.	mm/s	float	15	no	
experimental	bridge_skin_material_flow_3	When printing the third bridge skin layer, the amount of material extruded is multiplied by this value.	%	float	110	no	
experimental	bridge_skin_density_3	The density of the third bridge skin layer. Values less than 100 will increase the gaps between the skin lines.	%	float	80	no	
experimental	bridge_fan_speed_3	Percentage fan speed to use when printing the third bridge skin layer.	%	float	0	no	
experimental	clean_between_layers	Whether to include nozzle wipe G-Code between layers (maximum 1 per layer). Enabling this setting could influence behavior of retract at layer change. Please use Wipe Retraction settings to control retraction at layers where the wipe script will be working.		bool	False	no	
experimental	max_extrusion_before_wipe	Maximum material that can be extruded before another nozzle wipe is initiated. If this value is less than the volume of material required in a layer, the setting has no effect in this layer, i.e. it is limited to one wipe per layer.	mm^3	float	10	no	
experimental	wipe_retraction_enable	Retract the filament when the nozzle is moving over a non-printed area.		bool	True	yes	
experimental	wipe_retraction_amount	Amount to retract the filament so it does not ooze during the wipe sequence.	mm	float	1	no	
experimental	wipe_retraction_extra_prime_amount	Some material can ooze away during a wipe travel moves, which can be compensated for here.	mm^3	float	0	no	
wipe_retraction_ speed	wipe_retraction_retract_speed	The speed at which the filament is retracted during a wipe retraction move.	mm/s	float	3	no	
wipe_retraction_ speed	wipe_retraction_prime_speed	The speed at which the filament is primed during a wipe retraction move.	mm/s	float	2	no	
experimental	wipe_pause	Pause after the unretract.	s	float	0	no	
experimental	wipe_hop_enable	When wiping, the build plate is lowered to create clearance between the nozzle and the print. It prevents the nozzle from hitting the print during travel moves, reducing the chance to knock the print from the build plate.		bool	True	possibly	could interfere with layer height calculation
experimental	wipe_hop_amount	The height difference when performing a Z Hop.	mm	float	1	possibly	could interfere with layer height calculation
experimental	wipe_hop_speed	Speed to move the z-axis during the hop.	mm/s	float	10	no	
experimental	wipe_brush_pos_x	X location where wipe script will start.	mm	float	100	no	
experimental	wipe_repeat_count	Number of times to move the nozzle across the brush.		int	5	no	
experimental	wipe_move_distance	The distance to move the head back and forth across the brush.	mm	float	20	no	
small_hole_max_size	small_feature_max_length	Feature outlines that are shorter than this length will be printed using Small Feature Speed.	mm	float	0	yes	
experimental	small_feature_speed_factor	Small features will be printed at this percentage of their normal print speed. Slower printing can help with adhesion and accuracy.	%	float	50	no	

experimental	small_feature_speed_factor_0	Small features on the first layer will be printed at this percentage of their normal print speed. Slower printing can help with adhesion and accuracy.	%	float	50	no	
experimental	material_alternate_walls	Alternate wall directions every other layer and inset. Useful for materials that can build up stress, like for metal printing.		bool	False	yes	
experimental	group_outer_walls	Outer walls of different islands in the same layer are printed in sequence. When enabled the amount of flow changes is limited because walls are printed one type at a time, when disabled the number of travels between islands is reduced because walls in the same islands are grouped.		bool	True	yes	
ppr	ppr_enable	Enable print process reporting for setting threshold values for possible fault detection.		bool	False	no	
ppr	flow_warn_limit	Limit on the flow warning for detection.	%	float	15	no	
ppr	flow_anomaly_limit	Limit on flow anomaly for detection.	%	float	25	no	
ppr	print_temp_warn_limit	Limit on Print temperature warning for detection.	°C	float	3	no	
ppr	print_temp_anomaly_limit	Limit on Print Temperature anomaly for detection.	°C	float	7	no	
ppr	bv_temp_warn_limit	Limit on Build Volume Temperature warning for detection.	°C	float	7.5	no	
ppr	bv_temp_anomaly_limit	Limit on Build Volume temperature Anomaly for detection.	°C	float	10	no	
command_line_ settings	center_object	Whether to center the object on the middle of the build platform (0,0), instead of using the coordinate system in which the object was saved.		bool	True	yes	
command_line_ settings	mesh_position_x	Offset applied to the object in the x direction.		float	0	yes	
command_line_ settings	mesh_position_y	Offset applied to the object in the y direction.		float	0	yes	
command_line_ settings	mesh_position_z	Offset applied to the object in the z direction. With this you can perform what was used to be called 'Object Sink'.		float	0	yes	
command_line_ settings	mesh_rotation_matrix	Transformation matrix to be applied to the model when loading it from file.		str	[[1,0,0], [0,1,0], [0,0,1]]	yes	setup.json [Slicer.cura ("cura_scaling")]

D List of Usable and Validated Commands from *extruder.def.json* With Comments

Parent Key	Key	Description	Unit	Type	Value	Usable	Comment
machine_settings	extruder_nr	The extruder train used for printing. This is used in multi-extrusion.			0	no	
machine_settings	extruder_prime_pos_z	The Z coordinate of the position where the nozzle primes at the start of printing.	mm	float	0	possibly	
machine_settings	machine_extruder_cooling_fan_number	The number of the print cooling fan associated with this extruder. Only change this from the default value of 0 when you have a different print cooling fan for each extruder.		int	0	no	
machine_settings	machine_extruder_end_code	End g-code to execute when switching away from this extruder.		str		no	
machine_settings	machine_extruder_end_code_duration	The time it takes to execute the end g-code, when switching away from this extruder.		float	0	no	
machine_settings	machine_extruder_end_pos_abs	Make the extruder ending position absolute rather than relative to the last-known location of the head.		bool	False	no	
machine_settings	machine_extruder_end_pos_x	The x-coordinate of the ending position when turning the extruder off.	mm	float	0	no	
machine_settings	machine_extruder_end_pos_y	The y-coordinate of the ending position when turning the extruder off.	mm	float	0	no	
machine_settings	machine_extruder_start_code	Start g-code to execute when switching to this extruder.		str		no	
machine_settings	machine_extruder_start_code_duration	The time it'll take to execute the start g-code, when switching to this extruder.		float	0	no	
machine_settings	machine_extruder_start_pos_abs	Make the extruder starting position absolute rather than relative to the last-known location of the head.		bool	False	no	
machine_settings	machine_extruder_start_pos_x	The x-coordinate of the starting position when turning the extruder on.	mm	float	0	no	
machine_settings	machine_extruder_start_pos_y	The y-coordinate of the starting position when turning the extruder on.	mm	float	0	no	
machine_settings	machine_nozzle_id	The nozzle ID for an extruder train, such as "AA 0.4" and "BB 0.8".		str	unknown	no	
machine_settings	machine_nozzle_offset_x	The x-coordinate of the offset of the nozzle.	mm	float	0	possibly	
machine_settings	machine_nozzle_offset_y	The y-coordinate of the offset of the nozzle.	mm	float	0	possibly	
machine_settings	machine_nozzle_size	The inner diameter of the nozzle. Change this setting when using a non-standard nozzle size.	mm	float	25	yes	

material	material_diameter	Adjusts the diameter of the filament used. Match this value with the diameter of the used filament.	mm	float	25	fixed	
platform_adhesion	extruder_prime_pos_x	The X coordinate of the position where the nozzle primes at the start of printing.	mm	float	0	possibly	
platform_adhesion	extruder_prime_pos_y	The Y coordinate of the position where the nozzle primes at the start of printing.	mm	float	0	possibly	

Bibliography

[1] 3D Printhuset A/S. *D-Shape: Besøgsrapport*. Visit Report. Visit date: April 6, 2016. Visited company: Monolite UK (Dinitech SpA). Copenhagen, Denmark: 3D Printhuset A/S, 2016. URL: http://3dprintetbyggeri.dk/pdf/bes%C3%B8gsrapporter/D-Shape.pdf.

[2] 3D Systems, Inc. *3D Systems – Additive Manufacturing Solutions*. Accessed: 8 April 2025. n.d. URL: https://www.3dsystems.com/.

[3] ABB Robotics. *ABB Robotics and Porsche Consulting collaborate to automate the construction industry*. Accessed: 20 Mai 2025. 2023. URL: https://new.abb.com/news/de/detail/107956/prsrl-abb-robotics-and-porsche-consulting-collaborate-to-automate-the-construction-industry.

[4] Acrome. *The Basics of the Stewart Platform*. Accessed: 9 April 2025. 2024. URL: https://acrome.net/post/the-basics-of-the-stewart-platform.

[5] F. A. Adnan et al. "Real-time slicing algorithm for Stereolithography (STL) CAD model applied in additive manufacturing industry". In: *IOP Conference Series: Materials Science and Engineering*. Vol. 342. IOP Publishing, 2018. DOI: 10.1088/1757-899X/342/1/012016. URL: https://doi.org/10.1088/1757-899X/342/1/012016.

[6] Hyejin Ahn. *Computer-aided design — Week 6*. Accessed: 13 April 2025. 2020. URL: https://fabacademy.org/2020/labs/waag/students/hyejin-ahn/week6.html.

[7] Alessandro Ranellucci. *Slic3r: Open Source 3D Printing Toolbox*. Accessed: 19 April 2025. 2025. URL: https://slic3r.org/.

[8] Alberto Alvares, Efrain Rodriguez, and Cristhian Riaño Jaimes. "Development of the Linear Delta Robot for Additive Manufacturing". In: *2018 International Conference on Control, Decision and Information Technologies (CoDIT)*. Accessed: 3 April 2025. 2018, pp. 187–192. DOI: 10.1109/CoDIT.2018.8394869. URL: https://doi.org/10.1109/CoDIT.2018.8394869.

[9] Robert McNeel Associates. *Rhino.Inside*. Version 0.6.0, Available at GitHub: https://github.com/mcneel/rhino.inside. 2021. URL: https://pypi.org/project/rhinoinside/.

[10] Autodesk. *The History of 3D Printing: From the 80s to Today*. Accessed: 3 April 2025. 2023. URL: https://www.autodesk.com/design-make/articles/history-of-3d-printing.

[11] Autodesk Inc. *Fusion 360 – Integrated CAD, CAM, and CAE Software*. Accessed: 8 April 2025. Autodesk Inc. 2024. URL: https://www.autodesk.com/products/fusion-360/overview.

[12] Bayerische Ingenieurekammer-Bau. *3D-Druck: Recycelbare Brücke ohne Armierungsstahl und Mörtel*. Accessed: 20 Mai 2025. 2021. URL: https://www.bayika.de/de/aktuelles/meldungen/2021-07-30_3D-Druck-Recycelbare-Bruecke-ohne-Armierungsstahl-und-Moertel.php.

[13] Bayerische Ingenieurekammer-Bau. *Deutschland braucht 400 Milliarden Euro für Infrastruktur*. Accessed: 20 Mai 2025. 2024. URL: https://www.bayika.de/de/aktuelles/meldungen/2024-11-08_Deutschland-braucht-400-Milliarden-Euro-fuer-Infrastruktur.php.

[14] BCN3D Technologies. *What is Infill?* Accessed: 13 April 2025. 2023. URL: https://support.bcn3d.com/knowledge/infill.

[15] Joshua Bird. *S4 Slicer*. URL: https://github.com/jyjblrd/S4_Slicer.

[16] Mathias Brandstötter, Arthur Angerer, and Michael Hofbaur. "An Analytical Solution of the Inverse Kinematics Problem of Industrial Serial Manipulators with an Ortho-parallel Basis and a Spherical Wrist". In: *Proceedings of the Austrian Robotics Workshop 2014 (Revised Version)*. 22–23 May, 2014. Linz, Austria, 2014.

[17] Bundesanstalt für Straßenwesen (BASt). *Zustandsbewertung der Brücken im Zuge von Bundesfernstraßen*. Accessed: 20 Mai 2025. 2025. URL: https://www.bast.de/DE/Ingenieurbau/Fachthemen/brueckenstatistik/bruecken_hidden_node.html.

[18] COBOD International A/S. *COBOD - World leader in 3D construction printing solutions*. Accessed: 27 April 2025. 2025. URL: https://cobod.com/.

[19] Collaborative Research Centre TRR 277. *Additive Manufacturing in Construction (TRR277)*. Accessed: 2 April 2025. 2025. URL: https://amc-trr277.de/.

[20] StackExchange Community. *How is the E argument calculated for a given G1 command?* Accessed: 29 April 2025. 2018. URL: https://3dprinting.stackexchange.com/questions/6289/how-is-the-e-argument-calculated-for-a-given-g1-command.

[21] Dr. D-Flo. *How to Build a 3D Printer – Extruder*. Accessed: 12 April 2025. 2023. URL: https://www.drdflo.com/pages/Guides/How-to-Build-a-3D-Printer/Extruder.html.

[22] DB InfraGO AG. *InfraGO-Zustandsbericht*. Accessed: 20 Mai 2025. 2024. URL: https://www.dbinfrago.com/web/unternehmen/zielbild-infrastruktur/InfraGO-Zustandsbericht-12636112.

[23] J. Denavit and R. S. Hartenberg. "A Kinematic Notation for Lower-Pair Mechanisms Based on Matrices". In: *Journal of Applied Mechanics* 22.2 (1955), pp. 215–221. ISSN: 0021-8936. DOI: 10.1115/1.4011045. URL: https://doi.org/10.1115/1.4011045.

[24] James Diebel. *Representing Attitude: Euler Angles, Unit Quaternions, and Rotation Vectors*. Tech. rep. Technical Report. Stanford, California, USA: Stanford University, 2006. URL: https://www.astro.rug.nl/software/kapteyn-beta/_downloads/attitude.pdf.

[25] Kathrin Dörfler et al. "Advancing construction in existing contexts: Prospects and barriers of 3D printing with mobile robots for building maintenance and repair". In: *Cement and Concrete Research* 186 (2024), p. 107656. ISSN: 0008-8846. DOI: 10.1016/j.cemconres.2024.107656. URL: https://www.sciencedirect.com/science/article/pii/S0008884624002370.

[26] Eindhoven University of Technology. *3D Concrete Printing – Structural Engineering and Design Research Group*. Accessed: 3 April 2025. 2025. URL: https://www.tue.nl/en/research/research-groups/structural-engineering-and-design/3d-concrete-printing.

[27] Khaled Elashry and Ruairi Glynn. "An Approach to Automated Construction Using Adaptive Programing". In: Springer, 2014, pp. 51–66. ISBN: 978-3-319-04662-4. DOI: 10.1007/978-3-319-04663-1_4.

[28] ETH Zürich, Departement Bau, Umwelt und Geomatik. *Departement Bau, Umwelt und Geomatik – ETH Zürich*. Accessed: 4 April 2025. 2025. URL: https://baug.ethz.ch/.

[29] Fischer Holding GmbH Co. KG. *Baubot – Produktivität und Sicherheit durch Digitalisierung und Automatisierung*. https://www.fischer.de/de-de/produkte/innovationen/baubot. Accessed: 15 April 2025. 2025.

[30] Formlabs. *Vergleich der 3D-Drucktechnologien: FDM, SLA und SLS*. Accessed: 4 April 2025. 2025. URL: https://formlabs.com/de/blog/3D-drucktechnologie-vergleich-fdm-sla-sls/.

[31] PERI GmbH. *MAXIMO – Wandschalung für schnelles Schalen*. Accessed: 26 April 2025. 2024. URL: https://www.peri.de/produkte/maximo-wandschalung-fuer-schnelles-schalen.html#vorteile (visited on 04/13/2025).

[32] Hauptverband der Deutschen Bauindustrie e.V. *Produktivität im Bauhauptgewerbe*. Accessed: 20 Mai 2025. 2023. URL: https://www.bauindustrie.de/zahlen-fakten/publikationen/brancheninfo-bau/produktivitaet-im-bauhauptgewerbe.

[33] Hideo Kodama. *JPS56144478A*. 1980. URL: https://patents.google.com/patent/US4041476A/en (visited on 04/02/2025).

[34] Hilti AG. *Semi-autonomer Baustellenroboter Jaibot*. Accessed: 15 April 2025. 2025. URL: https://www.hilti.de/content/hilti/E3/DE/de/business/business/productivity/semi-autonomer-baustellenroboter-jaibot.html.

[35] Andreas Huber. *Technische Mechanik 3 – Dynamik*. 1st ed. Springer Vieweg Berlin, Heidelberg, 2024. ISBN: 978-3-662-68665-2. DOI: 10.1007/978-3-662-68666-9. URL: https://doi.org/10.1007/978-3-662-68666-9.

[36] ICON Technology, Inc. *ICON - Intelligent Machines Building Humanity's Future*. Accessed: 27 April 2025. 2025. URL: https://iconbuild.com/.

[37] Redaktion ingenieur.de. *Deutschlands bröckelnde Brücken: Der Weg aus der Krise*. Accessed: 20 Mai 2025. 2023. URL: https://www.ingenieur.de/technik/fachbereiche/bau/deutschlands-broeckelnde-bruecken-der-weg-aus-der-krise/.

[38] Instatiq GmbH. *Instatiq – Plan, Print, Progress*. Accessed: 17 April 2025. 2024. URL: https://instatiq.com/.

[39] Behrokh Khoshnevis. "Automated construction by contour crafting—related robotics and information technologies". In: *Automation in Construction* 13.1 (2004). The best of ISARC 2002, pp. 5–19. ISSN: 0926-5805. DOI: https://doi.org/10.1016/j.autcon.2003.08.012. URL: https://www.sciencedirect.com/science/article/pii/S0926580503000736.

[40] Harald Kloft, Norman Hack, and Hendrik Lindemann. "Shotcrete 3D Printing (SC3DP) - 3D-Drucken von großformatigen Betonbauteilen". In: *Deutsche BauZeitschrift* 1 (Feb. 2019), pp. 54–57.

[41] KUKA AG. *KUKA System Software 8.3 V4. Operating and Programming Instructions for System Integrators*. Internal documentation, not publicly available. 2015.

[42] KUKA AG. *Datenblatt KR 340 R3300*. https://www.kuka.com/-/media/kuka-downloads/imported/8350ff3ca11642998dbdc81dcc2ed44c/0000233240_de.pdf. Accessed: 3 April 2025. 2020.

[43] KUKA AG. *Robotersysteme – Produkte und Lösungen*. Accessed: 8 April 2025. n.d. URL: https://www.kuka.com/de-de/produkte-leistungen/robotersysteme.

[44] Ena Lloret-Fritschi et al. "From Smart Dynamic Casting to a Growing Family of Digital Casting Systems". In: *Cement and Concrete Research* 134 (Aug. 2020). Accessed: 3 April 2025. DOI: 10.1016/j.cemconres.2020.106071. URL: https://doi.org/10.1016/j.cemconres.2020.106071.

[45] Dirk Lowke et al. "Particle-bed 3D printing in concrete construction – Possibilities and challenges". In: *Cement and Concrete Research* 112 (2018), pp. 50–65. DOI: https://doi.org/10.1016/j.cemconres.2018.05.018. URL: https://www.sciencedirect.com/science/article/pii/S000888461731267X.

[46] Guowei Ma, Li Wang, and Yuyan Ju. "State-of-the-art of 3D printing technology of cementitious material—An emerging technique for construction". In: *Science China Technological Sciences* 61.4 (2018). Accessed: 5 April 2025, pp. 475–495. DOI: 10.1007/s11431-016-9077-7. URL: https://doi.org/10.1007/s11431-016-9077-7.

[47] Marlin Firmware. *Marlin 3D Printer Firmware*. https://marlinfw.org/. Accessed: 8 April 2025. 2024.

[48] Marlin Firmware. *Marlin G-code Documentation*. Accessed: 8 April 2025. 2025. URL: https://marlinfw.org/meta/gcode/.

[49] Matplotlib Development Team. *Matplotlib - Visualization with Python*. Version 3.9.2, Accessed: 29 April 2025. 2025. URL: https://matplotlib.org/.

[50] McKinsey Global Institute. *Reinventing Construction Through a Productivity Revolution*. Tech. rep. Accessed: 20 Mai 2025. McKinsey & Company, Feb. 2017. URL: https://www.mckinsey.com/capabilities/operations/our-insights/reinventing-construction-through-a-productivity-revolution.

[51] V. Mechtcherine et al. "Extrusion-based additive manufacturing with cement-based materials – Production steps, processes, and their underlying physics: A review". In: *Cement and Concrete Research* 132 (2020). DOI: https://doi.org/10.1016/j.cemconres.2020.106037. URL: https://www.sciencedirect.com/science/article/pii/S0008884619317132.

[52] Viktor Mechtcherine and Venkatesh Naidu Nerella. "3-D-Druck mit Beton: Sachstand, Entwicklungstendenzen, Herausforderungen". In: *Bautechnik* 95.4 (2018), pp. 275–287. DOI: https://doi.org/10.1002/bate.201800001. eprint: https://onlinelibrary.wiley.com/doi/pdf/10.1002/bate.201800001. URL: https://onlinelibrary.wiley.com/doi/abs/10.1002/bate.201800001.

[53] Viktor Mechtcherine et al. "Large-scale digital concrete construction – CONPrint3D concept for on-site, monolithic 3D-printing". In: *Automation in Construction* 107 (2019). ISSN: 0926-5805. DOI: https://doi.org/10.1016/j.autcon.2019.102933. URL: https://www.sciencedirect.com/science/article/pii/S0926580519304601.

[54] Valeria Montjoy. *Infographic: The Evolution of 3D Printing in Architecture Since 1939*. Accessed: 3 April 2025. 2023. URL: https://www.archdaily.com/1005043/infographic-the-evolution-of-3d-printing-in-architecture-since-1939.

[55] Shawn Moylan et al. "An Additive Manufacturing Test Artifact". In: *Journal of Research of the National Institute of Standards and Technology* 119 (2014), pp. 429–459. DOI: 10.6028/jres.119.017. URL: https://doi.org/10.6028/jres.119.017.

[56] Richard M. Murray, Zexiang Li, and S. Shankar Sastry. *A Mathematical Introduction to Robotic Manipulation*. Accessed: 8 April 2025. Boca Raton: CRC Press, 1994. URL: https://www.ce.cit.tum.de/fileadmin/w00cgn/rm/pdf/murray-li-sastry-94-complete.pdf.

[57] Pooyan Nayyeri, Kourosh Zareinia, and Habiba Bougherara. "Planar and nonplanar slicing algorithms for fused deposition modeling technology: a critical review". In: *The International Journal of Advanced Manufacturing Technology* 119.5 (2022), pp. 2785–2810. ISSN: 1433-3015. DOI: 10.1007/s00170-021-08347-x. URL: https://doi.org/10.1007/s00170-021-08347-x.

[58] Saeed B. Niku. *Introduction to Robotics: Analysis, Control, Applications*. 3rd. 528 pages. Wiley, 2019. ISBN: 978-1-119-52760-2.

[59] Deutsches Institut für Normung. *DIN 66025: Programmieren numerisch gesteuerter Werkzeugmaschinen - Zeichencodierte Steuerungssätze*. Beuth Verlag, Berlin. 1982.

[60] Deutsches Institut für Normung. *DIN EN ISO/ASTM 52900:2022-03 – Additive manufacturing – General principles – Terminology*. Beuth Verlag, Berlin. Accessed: 3 April 2025. 2022. URL: https://www.dinmedia.de/en/standard/din-en-iso-astm-52900/344258696.

[61] Open Continuum Robotics. *Continuum Robotics 101*. Accessed: 12 April 2025. Oct. 2022. URL: https://www.opencontinuumrobotics.com/101/2022/10/21/cr-intro.html.

[62] OpenAI. *ChatGPT (GPT-4o)*. Accessed: 21 April 2025. 2025. URL: https://chat.openai.com/.

[63] OrcaSlicer Community. *OrcaSlicer – Powerful and Open-Source Slicer for FDM and Resin 3D Printers*. Version 2.2.0. Accessed: 8 April 2025. 2025. URL: https://orca-slicer.com/.

[64] Zoran Pandilov and Vladimir Dukovski. “Comparison of the Characteristics between Serial and Parallel Robots”. In: *Acta Technica Corviniensis – Bulletin of Engineering* 7.1 (2014), pp. 23–28. ISSN: 2067-3809.

[65] PFT - Technische Förderanlagen GmbH. *PFT HM 24 – Der clevere Mischer für Sack- und Silowaren*. Accessed: 8 April 2025. 2025. URL: https://www.pft.net/de/mischen-foerdern/durchlaufmischer/fuer-sackware/hm-24.html.

[66] PFT - Technische Förderanlagen GmbH. *PFT SWING L – Förderpumpe für pastöse Materialien*. Accessed: 12 April 2025. 2025. URL: https://www.pft.net/de/230v-technik/foerderpumpen/swing-l/.

[67] Prusa Research. *Printer Troubleshooting*. Accessed: 12 April 2025. 2025. URL: https://help.prusa3d.com/category/printer-troubleshooting_227.

[68] Prusa Research. *PrusaSlicer – Open-Source Slicer Software*. Version 2.9.2. Accessed: 8 April 2025. 2025. URL: https://www.prusa3d.com/de/page/prusaslicer_424/.

[69] Putzmeister. *InstaTIQ – Putzmeister Robotic Arm for 3D Concrete Printing*. Accessed: 11 April 2025. 2025. URL: https://bauma.putzmeister.com/de/instatiq.

[70] pytest Development Team. *pytest - Simple powerful testing with Python*. Version 8.3.4, Accessed: 29 April 2025. 2025. URL: https://pypi.org/project/pytest/.

[71] Python Software Foundation. *Python Programming Language, Version 3.12*. https://www.python.org/. Version 3.12, Accessed: 17 April 2025. 2025.

[72] R. Rao. *What are Robot Gantries? Types, Applications, Advantages, Selection Criteria, and more*. Accessed: 11 April 2025. 2023. URL: https://www.wevolver.com/article/gantry-robot.

[73] Prusa Research. *Extrusion stopped mid-print (heat creep)*. 2022. URL: https://help.prusa3d.com/article/extrusion-stopped-mid-print-heat-creep_1948 (visited on 04/11/2025).

[74] Research Nester. *Marktanalyse und Prognose des 3D-Drucks im Bauwesen – Trends, Chancen und Zukunftsausblick bis 2036*. Accessed: 20 Mai 2025. 2024. URL: https://www.researchnester.com/de/reports/3d-printing-construction-market/4593.

[75] Robert McNeel & Associates. *Rhinoceros 3D - Modeling Tools for Designers*. Version 8, Accessed: 29 April 2025. 2025. URL: https://www.rhino3d.com/de/.

[76] RoboDK Software S.L. *RoboDK - Simulation and Programming for Industrial Robots*. Accessed: 27 April 2025. 2025. URL: https://robodk.com/de/.

[77] Robotplace. *Apis Cor 3D Printing System*. Accessed: 8 April 2025. no date. URL: https://robotplace.io/product/apis-cor-3d-printing-system/.

[78] SciPy Community. *SciPy - Fundamental algorithms for scientific computing in Python*. Version 1.15.2, Accessed: 29 April 2025. 2025. URL: https://scipy.org/.

[79] Pshtiwan Shakor et al. “Review of binder jetting 3D printing in the construction industry”. In: *Progress in Additive Manufacturing* 7 (2022). Published: 21 January 2022, pp. 643–669. DOI: 10.1007/s40964-021-00248-9. URL: https://link.springer.com/article/10.1007/s40964-021-00248-9.

[80] Shenzhen Creality 3D Technology Co., Ltd. *Creality – Official Website of 3D Printers and Accessories*. Accessed: 8 April 2025. 2025. URL: https://www.creality.com/.

[81] Tharmalingam Sivarupan et al. “A review on the progress and challenges of binder jet 3D printing of sand moulds for advanced casting”. In: *Additive Manufacturing* 40 (2021), p. 101889. ISSN: 2214-8604. DOI: https://doi.org/10.1016/j.addma.2021.101889. URL: https://www.sciencedirect.com/science/article/pii/S2214860421000543.

[82] RoboDK Software S.L. *Robot Singularities: What Are They and How to Beat Them*. Accessed: 15 Mai 2025. 2022. URL: https://robodk.com/blog/robot-singularities/.

[83] Gregory G. Slabaugh. *Computing Euler Angles from a Rotation Matrix*. No publication date provided; Accessed: 22 April 2025. n.d. URL: https://eecs.qmul.ac.uk/~gslabaugh/publications/euler.pdf.

[84] Steve Canny. *python-docx: Create and update Microsoft Word .docx files*. Version 0.2.4, Accessed: 29 April 2025. 2025. URL: https://pypi.org/project/python-docx/.

[85] Steve Scott Crump. *US5121329A*. 1989. URL: https://patents.google.com/patent/US5121329A/en (visited on 04/02/2025).

[86] Straits Research. *Marktgröße, Marktanteil und Trendanalyse für 3D-Druck im Bauwesen*. 2025. URL: https://straitsresearch.com/report/3d-printing-construction-market.

[87] Stratasys Ltd. *3D-Drucker Übersicht*. Accessed: 2 April 2025. 2025. URL: https://www.stratasys.com/de/3d-printers/.

[88] Julius Sustarevas, Dimitrios Kanoulas, and Simon Julier. "Autonomous Mobile 3D Printing of Large-Scale Trajectories". In: *2022 IEEE/RSJ International Conference on Intelligent Robots and Systems (IROS)*. 2022. DOI: 10.1109/IROS47612.2022.9982274.

[89] Tagesschau.de. *Ein Haus in 140 Stunden*. Accessed: 20 Mai 2025. 2024. URL: https://www.tagesschau.de/wirtschaft/digitales/3d-drucker-groesstes-haus-europas-100.html.

[90] Peter Guthrie Tait. "On the Rotation of a Rigid Body about a Fixed Point". In: *Proceedings of the Royal Society of Edinburgh* 6 (1868), pp. 430–434. URL: https://zenodo.org/record/2093148/files/article.pdf.

[91] Teaching Tech. *3D Printer Calibration Guide*. Accessed: 27 April 2025. 2025. URL: https://teachingtechyt.github.io/calibration.html.

[92] Tuong Phuoc Tho and Truong Thinh Nguyen. "Using a Cable-Driven Parallel Robot with Applications in 3D Concrete Printing". In: *Applied Sciences* 11.2 (2021), p. 563. DOI: 10.3390/app11020563. URL: https://doi.org/10.3390/app11020563.

[93] Ultimaker. *CuraEngine Command Line Reference*. Accessed: 28 April 2025. 2020. URL: https://manpages.ubuntu.com/manpages/focal/en/man1/CuraEngine.1.html.

[94] Ultimaker. *The Complete History of 3D Printing*. Accessed: 1 April 2025. 2023. URL: https://ultimaker.com/de/learn/the-complete-history-of-3d-printing/.

[95] Ultimaker. *Ultimaker Cura User Manual*. 2023. URL: https://support.ultimaker.com.

[96] Ultimaker. *CuraEngine Wiki: Slicing Overview*. Accessed: 27 April 2025. 2025. URL: https://github.com/Ultimaker/CuraEngine/wiki/Slicing.

[97] Ultimaker. *Ultimaker Cura – Advanced 3D Printing Slicer Software*. Version Version 5.10.0. Accessed: 8 April 2025. 2025. URL: https://ultimaker.com/de/software/ultimaker-cura/.

[98] Ultimaker Community User. *Python or Bash Cura Interface?* Forum post, Accessed: 26 April 2025. 2019. URL: https://community.ultimaker.com/topic/30295-python-or-bash-cura-interface/.

[99] Universal Robots. *What Is Robotic Arm Design?* Accessed: 6 April 2025. n.d. URL: https://www.universal-robots.com/in/blog/robotic-arm-design/.

[100] K. Vasilic. "Additive Fertigung im Betonbau: aktueller Stand". In: *Beton- und Stahlbetonbau* 115.11 (2020). Accessed: 3 April 2025, pp. 1006–1012. DOI: 10.1002/best.202000079. URL: https://doi.org/10.1002/best.202000079.

[101] Verified Market Reports. *Globaler Markt für 3D -Drucker des Bauwesens nach Typ (Beton, Metall), nach Anwendung (Gebäude, Infrastruktur), nach geografischem Umfang und Prognose*. Accessed: 20 Mai 2025. 2025. URL: https://www.verifiedmarketreports.com/de/product/construction-3d-printing-market/.

[102] W3Schools. *Python RegEx*. Accessed: 17 April 2025. 2025. URL: https://www.w3schools.com/python/python_regex.asp.

[103] WASP - World's Advanced Saving Project. *Concrete 3D Printer - Delta WASP 3MT CONCRETE*. Accessed: 5 April 2025. 2025. URL: https://www.3dwasp.com/en/concrete-3d-printer-delta-wasp-3mt-concrete/.

[104] Daniel Weger. "Additive Fertigung von Betonstrukturen mit der Selective Paste Intrusion – SPI". Accessed: 3 April 2025. Ph.D. thesis. Technische Universität München, 2020. URL: https://mediatum.ub.tum.de/doc/1540336/document.pdf.

[105] Thomas Wehrli. "Wie William E. Urschel mit der Mauerbaumaschine in die Zukunft fuhr". In: *Baublatt* 21 (2021). Accessed: 2 April 2025, pp. 44–47. URL: https://www.baublatt.ch/file/1376/BB_2121_Urschel_0001.pdf.

[106] Wiliam E Urschel. *US2339892A*. Accessed: 3 April 2025. 1941. URL: https://patents.google.com/patent/US2339892A/en.

[107] Institut der deutschen Wirtschaft Köln. *Wohnungsbedarf: Jährlich müssten 372.600 Wohnungen gebaut werden*. Accessed: 3 Mai 2025. 2024. URL: https://www.iwkoeln.de/presse/pressemitteilungen/jaehrlich-muessten-372600-wohnungen-gebaut-werden.html.

[108] Shaun Wu. *6-Axis Gantry Robot*. Accessed: 8 April 2025. 2019. URL: https://shaunwu25.github.io/2019/06/15/6-Axis-Gantry-Robot.html.

[109] Wyn Kelly Swainson. *US4041476A*. 1971. URL: https://patents.google.com/patent/US4041476A/en (visited on 04/02/2025).

[110] Julian Zeitlhöfler. "Nominal and Observation-Based Attitude Realization for Precise Orbit Determination of the Jason Satellites". PhD thesis. Technical University of Munich, 2019.

[111] Tianyu Zhang et al. "S3-Slicer: A General Slicing Framework for Multi-Axis 3D Printing". In: *ACM Trans. Graph.* 41.6 (2022). Software implementation available at https://github.com/zhangty019/S3_DeformFDM. ISSN: 0730-0301. DOI: 10.1145/3550454.3555516. URL: https://doi.org/10.1145/3550454.3555516.